ISSN No. 2231-3273

INTERNATIONAL JOURNAL OF ENGINEERING SCIENCES AND MANAGEMENT

A Bi-annual Research Journal of

DRONACHARYA
College of Engineering
GREATER NOIDA, U.P., INDIA

Volume I | Issue II | July-Dec 2011

ISSN No. 2231-3273

INTERNATIONAL JOURNAL OF ENGINEERING SCIENCES AND MANAGEMENT

Volume I | Issue II | July-Dec 2011

ISSN No. 2231-3273

INTERNATIONAL JOURNAL OF ENGINEERING SCIENCES AND MANAGEMENT

A Bi-annual Research Journal of
DRONACHARYA
COLLEGE OF ENGINEERING
GREATER NOIDA, U.P., INDIA

Volume I Issue II July-Dec 2011

INTERNATIONAL JOURNAL OF ENGINEERING SCIENCES AND MANAGEMENT

Editorial Information:
For details please write to the Executive Editor, International Journal of Engineering Sciences and Management,
Dronacharya College of Engineering, B-27 Knowledge Park-III, Gautam Budh Nagar,
Greater Noida (U.P)

Telephones:
Landline: 0120-2323851, 2323852, 2323854, 2323855
Mobile : 09312247845, 09910380107

Telefax:
0120-2323853

E-mail.:
advisor.r&d@gnoida.dronacharya.info
principal@gnoida.dronacharya.info
info@dronacharya.info

Website:
www.dronacharya.info

ADVISORY BOARD

FROM THE DESK OF EXECUTIVE EDITOR

Dear Readers,

Welcome to the second issue of the first volume of our research Journal: International Journal of Engineering Sciences and Management (ISSN: 2231-3273). We received many congratulatory messages and accolades from across the globe for the debutant issue of this journal. We sincerely hope that, with the support and contribution of acclaimed experts from the respective research disciplines, the past, present as well as the future issues will contribute in achieving an appreciably high "impact factor" in the research areas of Engineering Sciences and Management.

As you would see in the current issue, we have added four Faculty colleagues from Our College (Dronacharya College of Engineering, Greater Noida) as "Associate Editors" and Dr. Sivakumar Ramasamy from the University of Akron, USA, as one of the Editors for our Journal. It is sincerely hoped that their welcome addition to our Editorial Team will help us in improving the quality and versatility of our Journal. Similarly we are privileged to include the name of Prof. (Dr.) Shailendra Palvia from Long Island University, USA, as an honorary member of our Advisory Board.

Like the earlier issue of our Journal, we received a large number of quality research papers from across the length and breadth of India and abroad for consideration of publication for the current issue of our journal. After a painstaking job by the Reviewers and the members of Editorial Board, we could accept eighteen research papers for this issue. We hope that you will enjoy going through some of these papers depending on your area of interest.

I, as an Executive Editor, wish to place on record, my deepest gratitude for all the members of "Governing Council", "Advisory Board", "Editorial Board" and the Principal of our College for their unstinted support in all aspects for the growth of our Institution including the publication of this Journal.

Further, we wish to thank all those authors who submitted their papers for consideration of publication in our Journal, irrespective of their acceptance or otherwise, and request a similar cooperation from them and all the readers for the future issues.

We shall be grateful and delighted to receive comments about the current issue from you.

Wishing you a thought-provoking and happy reading.

Sincerely,

Prof. (Dr.) Jai Paul Dudeja
Executive Editor

July 2011

CONTENTS

1 The Influence Of Heat Treatment On Microstructure And Hardness Of A Hot Rolled Alloy Steel
T. S. Srivatsan, B.Nurudeen, A.Prakash and M. Petraroli

8 Failure Investigation Of Radiator Supporting Bracket For Structural Vibration Problems Using Operational Modal Analysis, Operating Deflection Shapes And Finite Element Analysis.
Milind D. Kandalkar and Prof. Narendra K. Chhapkhane

18 Deformation of Al-5Zn-1Mg in The Temperature Range of 303- 673K
Rijesh M, James Valder, Geethalakshmi K and A O Surendranathan

23 The impact toughness and fracture behavior of four high strength steels: Role of processing
T. S. Srivatsan, K. Manigandan and Thomas Quick

37 High Performance Low Power Flip-flop By Using Conditional Discharge Technique
Jyoti Kohar, Ankit Malik and Vijeta

42 Mathematical Modelling Of Solar-Based-Inverter With Maximum Power Point Tracking
Ch.Venketeswara Rao, Dr.S.S.Tulasi Ram, Dr.B. Brahmaiah and Prof B.J.J. Raju

50 Design and FPGA Implementation of Feed Forward Neural Network for FIR Filter
Mohammed Waseem*, M.S. Suma* and Cyril Prasanna Raj P*

57 Use Of 3-D HSV Histogram Equalization And Adaptive Hsv Segementation For Content Based Image Retrieval
Ms. Venu Shah, Ms. Archana Choudhary and Prof. Kavita Tewari

62 A Smart Temperature Measuring Technique Using Thermistor
Santhosh K V and Dr. B K Roy

69 Transmission Rate Of Non-cooperative Routing In Ad Hoc Network
K.Vanisree, V.S.K.Reddy and MJC Prasad

78 Computation Of RCS With TLM Method Using Second Order Higdons Boundary Operators
R.Srinivasa.Rao and Dr.PV Subbaiah

83 Code Optimization during processing of Hamming codes in a Data communication system
Rina Choudhary

88 A Simple Algorithm For Fast Detection And Quantification Of Voltage Deviations Using Space Vectors
P. Meena, Dr. K. Uma Rao and Dr. Ravishankar Deekshit

99 Secure Security Access: An Approach To Counter Hacking
Rajesh Kumar and Neelam Ruhil

103 An S-mesh Based Protocol For Peer – To – Peer Streaming To Serve Dynamic Groups
Mr. V. Maruthi Prasad and Mr. V. Raghavendra Prasad

113 Metrics For Measuring The Understandability Of Object-oriented Design Quality
Devpriya Soni

120 Analytical Study Of Auto Run Worm Killer: A Strategic Approach
Aradhana Goutam, Dr. Raj Kamal and Dr. (Mrs.) Maya Ingle

126 Models of Employee Engagement: An Elucidation
G. Swetha and Dr. D. Pradeep Kumar

142 Guidelines for Authors
International Journal Of Engineering Sciences And Management

THE INFLUENCE OF HEAT TREATMENT ON MICROSTRUCTURE AND HARDNESS OF A HOT ROLLED ALLOY STEEL

T. S. Srivatsan
Department of Mechanical Engineering,
The University of Akron, Akron, Ohio 44325-3903
E-mail: tsrivatsan@uakron.edu

B.Nurudeen
Department of Mechanical Engineering,
The University of Akron, Akron, Ohio 44325-3903

A.Prakash
Department of Mechanical Engineering,
The University of Akron, Akron, Ohio 44325-3903

M. Petraroli
Timken Research
The Timken Company, Canton, Ohio 44706-0930, USA

ABSTRACT

In this research paper, the specific influence of quenching and tempering on microstructure and hardness of alloy steel that was hot rolled is presented and discussed. The chosen alloy steel is an economically affordable and viable choice for energy-critical application, such as pressure vessels, for the purpose of storing compressed natural gas. Three samples of the alloy steel were taken from a stock that was in the hot rolled plus quench and tempered condition. The samples were prepared for optical microscopy examination using standard metallographic procedures and then examined in a low magnification light optical microscope. Both microhardness and macro-hardness measurements were made across the polished surfaces of the three samples of the alloy steel. The microhardness and macrohardness values of the alloy steel were consistent through the width of the test specimen. The intrinsic influence of alloy steel composition and secondary processing, i.e., quenching and tempering, on microstructural development and its resultant influence on hardness is presented. The role of microstructure in governing the hardness of the alloy steel is briefly discussed.

Keywords: *Alloy steel, microstructure, microhardness, macrohardness, defects.*

1. INTRODUCTION

The metal steel has over the years spanning the last three decades grown both in stature and strength to be safely categorized as the material that is the back bone of modern day engineering. The metal is noted and put to effective use on account of its high elastic modulus of 200 GPa (30 MPsi) coupled with a fracture toughness and temperature stability that by far exceeds the values of high strength metal-based composites (MMCs) and even the competing high strength aluminum alloys. In light of the recent global energy crisis and its impact on industrial production coupled with the growing importance and emphasis given to clean air initiatives, the number of movable vehicles powered by compressed natural gas (CNG) is increasing at a noticeably rapid pace [1,2]. This requirement has necessitated the need for pressure vessels, which are not only low in weight but also offers a combination of good fracture toughness and acceptable fatigue resistance. Through the years and even up to the present time period in excess of ninety percent of on-board cylinders used for the storage of compressed natural gas are made from high strength steel [3].

Prevailing US government standards and even international standards, such as: ISO 11439, control and regulate the CNG cylinders, which are put to use on board a vessel [2]. The standards have safely categorized the cylinders into four different types.

(a) Type I is an all metal cylinder that is essentially made from AISI 4140 type low alloy steel.

(b) Type II is about 10% to 20% lighter and made of thinner wall 4140 steel but is circumferentially reinforced in the cylindrical section by a composite made of E-glass fiber embedded in a glass matrix.

(c) Type III and Type IV cylinders are fully wrapped with carbon fiber reinforced epoxy based composites.

The material that is often a preferred choice and used for the Type I and Type II pressure vessels, i.e., alloy steel 4140, is the focus of this research study.

Alloy steel (AISI 4140) is a medium carbon chromium-molybdenum steel that finds use in those applications where strength and impact toughness are both required and can be achieved through tempering [4]. Gradual refinements in chemical composition coupled with processing techniques spanning both primary processing and secondary processing have enabled this steel to have a microstructure that offers acceptable fatigue strength and good wear resistance, while it can be chosen and safely used at temperatures as high as 480^{o} C making it a viable choice for critically stressed applications [5]. This steel is frequently used in the quenched and tempered condition in which tempering between 230^{o}C to 370^{o}C is not recommended primarily with the purpose of avoiding blue brittleness [5] or a one-step temper embrittlement [6]. Tempering in this temperature range, i.e., 230^{o}C to 370^{o}C, would cause the yield strength of steel to reach an ultra high strength level, i.e., a minimum yield strength of 1380 MPa (200 Ksi), which makes the steel easily susceptible to embrittlement by gaseous hydrogen [4]. The mechanism of hydrogen embrittlement (HE) is independent of the source of hydrogen, while the kinetics of interaction with the material will tend to vary in a given environment [7]. The embrittlement of this Cr-Mo steel can occur in the presence of hydrogen gas at pressures below one atmosphere [8] or even in ambient air [27 C] at slow strain rates [9]. Thus, it is recommended that alloy steel 4140 be tempered at a temperature higher than 370^{o}C with a concomitant reduction in strength and hardness only with the objective of lowering the tendency for hydrogen embrittlement during actual service.

In this paper, we present the results of a recent study aimed at understanding the specific influence of quenching and tempering on microstructural development and hardness of alloy steel 4140. The alloy steel was chosen in the quenched and tempered condition of hot rolled bar stock. This was done with the objective of establishing intrinsic microstructural influences on hardness of the steel.

2. MATERIAL

The material used in this study was 0.625 inch (15.9 mm) diameter hot rolled and quenched and tempered AISI 4140 steel. The steel was tempered at 400^{o}C immediately following quenching. The chemical composition of the steel is given in Table 1. While carbon is required for the formation of martensite and also enabling to determine the hardness of martensite and the alloy steel, a number of other elements are known for their intrinsic ability to improve the hardenability of steel. This is made possible by retarding the nucleation rate of bainite. The element molybdenum is effective in increasing hardenability while concurrently resisting softening during tempering. Chromium is slightly less effective at increasing hardenability while being very effective at improving the corrosion resistance of the steel. The trace amount of silicon that is present serves to increase the hardness of ferrite thereby enabling in increasing the oxidation resistance of the steel while also being an effective deoxidizer. Overall, the high carbon content in combination with the presence of chromium and molybdenum results in the precipitation and presence of carbides that contributes to improving the creep resistance of the steel. Besides the overall hardening that is achieved by the addition of carbon to iron, the presence of alloying elements serves to improve the hardenability of the steel. The steel was acquired from the manufacturer in the hot rolled and quenched and tempered condition as bar stock 15.9 mm in diameter.

3. EXPERIMENTAL PROCEDURES

3.1 MICROSTRUCTURAL CHARACTERIZATION Samples were cut from the top end, mid-section and tail sections of the as-received hot rolled plus quench and tempered bar stock. The samples are referred to as Sample # 1, Sample # 2 and Sample # 3. An initial characterization of the microstructure of the as-provided material i.e., Sample -1, Sample -2, and Sample -3, was done using a low magnification optical microscope. The three samples that were cut from the as-received stock of the alloy steel 4140 were mounted in bakelite. The mounted samples were then wet ground on progressively finer grades of silicon carbide impregnated emery paper using copious amounts of water both as a lubricant and as a coolant. Subsequently, the ground samples were mechanically polished using five-micron diamond solution. Fine polishing to a perfect mirror-like finish of the surface of alloy steel sample was achieved using one-micron diamond solution as the lubricant. The polished samples were subsequently etched using nital reagent, i.e., a solution mixture of 5-ml of nitric acid (HNO_3) and 85 ml of water (H_2O). The polished and etched surfaces of the alloy steel samples were observed in an optical microscope and photographed using standard bright field illumination technique.

3.2 DETERMINATION OF HARDNESS A basic mechanical property of a material is its hardness. The hardness test is an important and widely used test for the purpose of quickly evaluating the mechanical properties of monolithic metals, their alloy counterparts, and even composite materials based on metal matrices. Hardness can be aptly defined as the resistance offered by the material to indentation, i.e., permanent deformation and cracking [10]. A direct measurement of hardness is a simple yet very useful technique for characterizing the base-line mechanical properties while concurrently investigating, establishing and rationalizing the role and contribution of intrinsic microstructural constituents. The hardness test is simple, easy and can be essentially categorized as being non-destructive [11]. In this study, the Vickers (H_V) micro-hardness measurements were made on a Suntech microhardness tester using an indentation load of 200 grams, a dwell time of 11 seconds, with the aid of a Vickers tool indenter. The indenter (made of diamond) has a square-base pyramidal geometry with an included angle of 136 degrees. The indenter rests for a specified length of time on the polished surface of the test specimen. The machine makes an indent, or impression, on the polished surface of the sample whose diagonal size was measured using a low magnification optical microscope. The area of the impression is directly proportional to the load used and a load independent hardness number can be found. The Vickers hardness number (H_V) is the ratio of applied load to the surface area of the indent. According to the Vickers prescription $H_V = 1.8544\ P/d^2$. At least fifteen indents were made edge-to-edge across the polished surface of each test specimen of the alloy steel samples in the fully annealed condition, and the result is reported as the average value in units of kg/mm^2.

The macrohardness measurements (R_C) were made on a Rockwell hardness machine using an indentation load of 150 Kgf, a minor load of 10 Kgf, 120 degree diamond cone, a dwell time of 10 seconds and the value read on the 'C' scale. The macrohardness tests were also done on the polished surface of the alloy steel test specimen. All the three chosen samples of the alloy steel i.e., Sample #1, Sample #2, and Sample #3, were examined for both microhardness and macro-hardness measurements. The results of the microhardness and macro-hardness tests are summarized in **Table 2**.

4. RESULTS AND DISCUSSION

4.1. MICROSTRUCTURE The microstructure of the candidate alloy steel sample, i.e., 4140 hot rolled plus quenched and tempered, for this study is an important factor that essentially determines its hardness, tensile properties, fracture toughness, fatigue resistance and resultant fracture behavior. The optical micrographs of the three chosen samples of alloy steel are shown in **Figures 1-3** at different magnifications. The three figures reveal the microstructure of alloy steel to be essentially similar with minimal to no difference in the nature, volume fraction, morphology, size and distribution of the intrinsic microstructural constituents. The microstructure of all the three samples essentially comprised of carbon rich (dark regions) and carbon-depleted (light regions) zones. High magnification observation in the dark carbon-rich region revealed fine martensite while the carbon-depleted region was essentially covered with ferrite grains of non-uniform size. In all the three samples examined the volume fraction of the carbon-rich regions was far more noticeable than the carbon-depleted region. The carbon-rich regions are enriched not only by carbon but also the other alloying elements present in this steel. Isolated and randomly distributed MnS particles were present in the carbon-rich regions but could not be easily identified at the allowable magnifications of the optical microscope.

Table 1: Nominal chemical composition of Alloy Steel 4140
(in weight percent)

C	Cr	Mn	Mo	P	S	Si	Iron
0.40	1.0	0.85	0.20	0.03	0.02	0.25	Balance

4.2 HARDNESS TESTS Microhardness measurements were made with care and precision from edge-to-edge of the polished surface of the three samples of hot rolled plus quench and tempered alloy steel 4140. Fifteen measurements were made at different locations on the polished surface of each specimen to gather detailed information regarding spatial variability of hardness. All of the measurements were made with accuracy and precision across the center of the test sample that is mounted in bakelite in order to gather information on spatial variability of hardness while concurrently minimizing contributions from location of the indent. The spatial variability was noticeably less pronounced and the measured microhardness was observed to be uniform throughout each of the three samples of alloy steel 4140. Making measurements on the polished surface of the sample facilitates in reducing spread in the measured hardness values. The microhardness measured provides a measure of the effect of strengthening arising from the presence of intrinsic microstructural phases and/or micro-constituents and the concurrent weakening resulting from the presence of microscopic microstructural defects, such as, microscopic cracks and microscopic voids.

(a) Sample # 1 revealed an average microhardness value of 248.9 kg/mm^2 with the independent values being fairly consistent through the alloy-steel microstructure.

(b) Sample # 2 taken from the center of the quench and tempered bar stock revealed an average micro-hardness value of 242.67 Kg/mm^2, which is marginally lower than Sample # 1, within the limits of experimental error. This is ascribed to the presence of fine intrinsic microstructural defects, such as, microscopic cracks and microscopic voids, in the interior of the hot rolled plus quench and tempered 4140 bar stock.

(c) Sample # 3 revealed an average microhardness value of 250 kg/mm^2, with the independent values being consistent through the alloy test sample from edge-to-edge. The average microhardness of this sample is similar to the average microhardness of Sample # 1 taken from the top end of the alloy steel bar stock.

The average microhardness values of the three samples (Sample #1, Sample # 2 and Sample # 3) are shown in the bar graph in **Figure 4.**

The macrohardness values based on Rockwell C scale, made across the width of each polished sample taken from either end of the hot rolled plus quench and tempered rod stock, gave an average value of 82 kg/mm^2 ($HR_C = 22.69$) for Sample # 1 and Sample # 3 ($HR_C = 22.46$) and a marginally lower value of 81 kg/mm^2 ($HR_C = 21.59$) for Sample #2 taken from the center of the rod stock. All measurements made across the width of the polished surface of the samples. The macrohardness values of the three samples are shown in **Figure 5** and compared with the corresponding microhardness value of each sample. The noticeably observed lower value of macrohardness of the alloy steel 4140 when compared to its microhardness is ascribed to the physical presence and distribution of a healthy population of fine microscopic defects not easily resolvable in a low magnification optical microscope. The bar graph representation does reveal the intrinsic influence of microstructural effects spanning both defects and microstructural phases or micro-constituents on both microhardness, i.e., local hardness, and macro-hardness, i.e., global hardness of the chosen alloy steel.

Table 2: Summary of Hardness Test Results (Average value based on 15 independent measurements)

Sample No.	Microhardness Average		Microhardness	
	(Kg/mm^2)	**H_V (Gpa)**	**Average HR_C**	**Average (Kg/mm^2)**
Sample #1	248.93	2.44	22.69	82
Sample #2	242.67	2.38	21.59	81
Sample #3	250.40	2.46	22.56	82

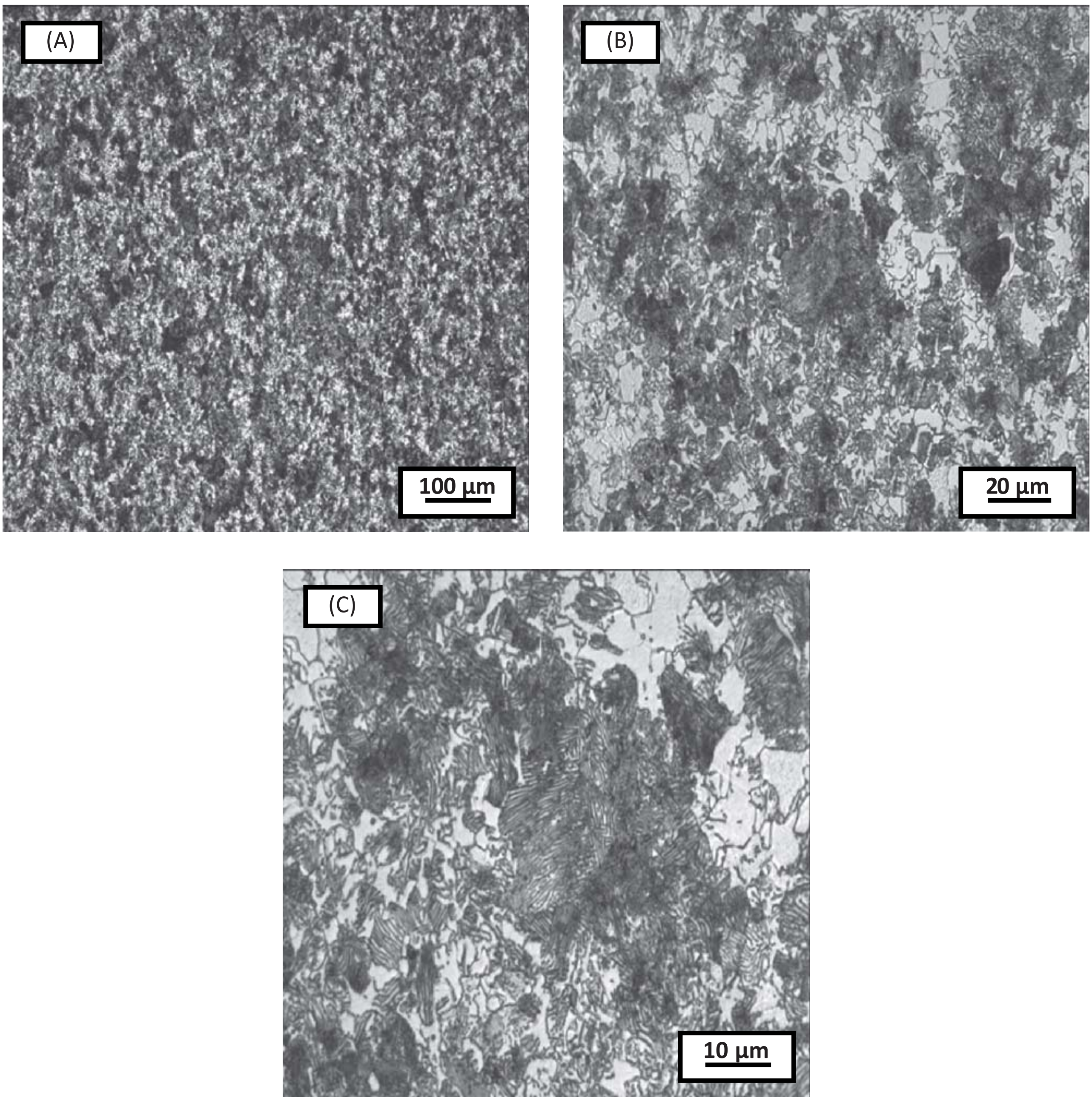

Figure 1: Optical micrographs of Sample #1 of alloy steel 4140 (annealed) at the different magnifications showing the key microstructural constituents and grain size.

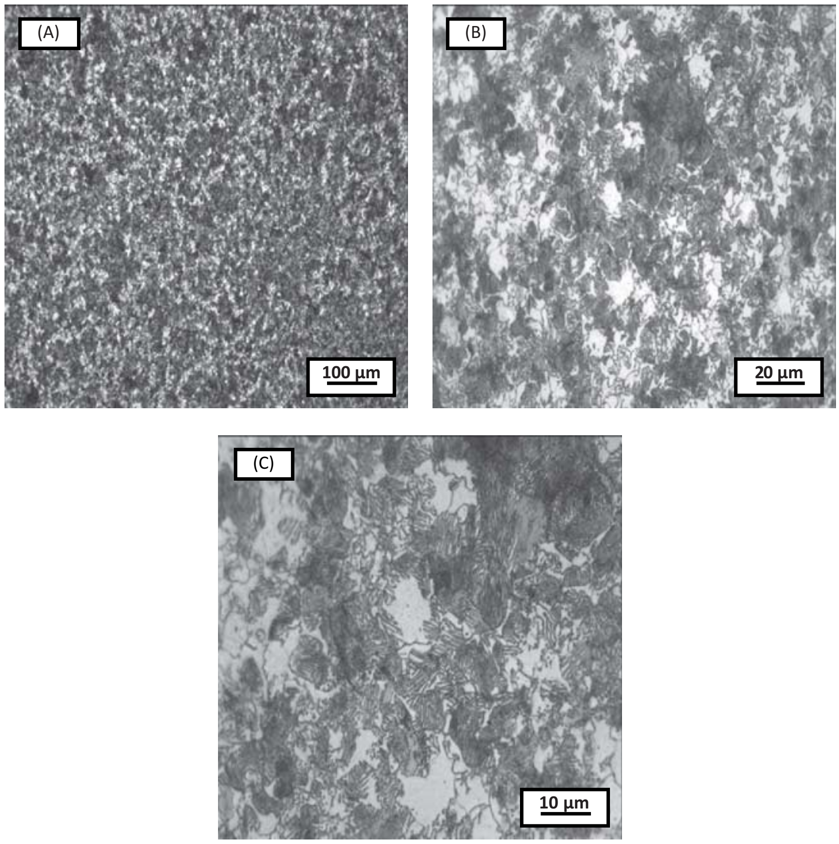

Figure 2: Optical micrographs of Sample #2 of alloy steel 4140 (annealed) at the different magnifications showing the key microstructural constituents and grain size.

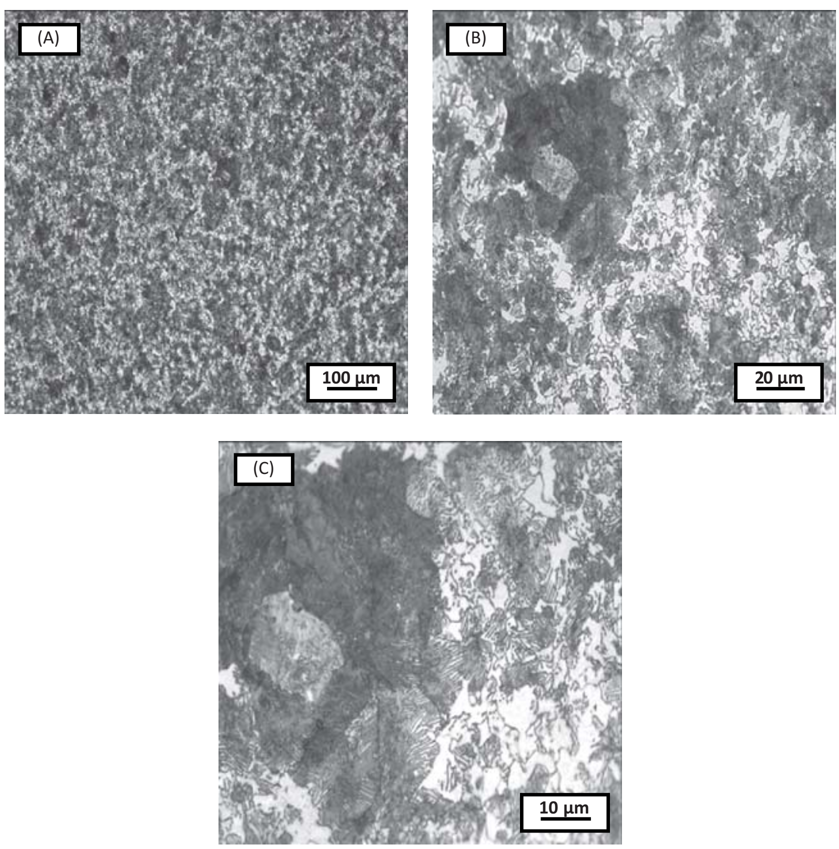

Figure 3: Optical micrographs of Sample #3 of alloy steel 4140 (annealed) at the different magnifications showing the key microstructural constituents and grain size.

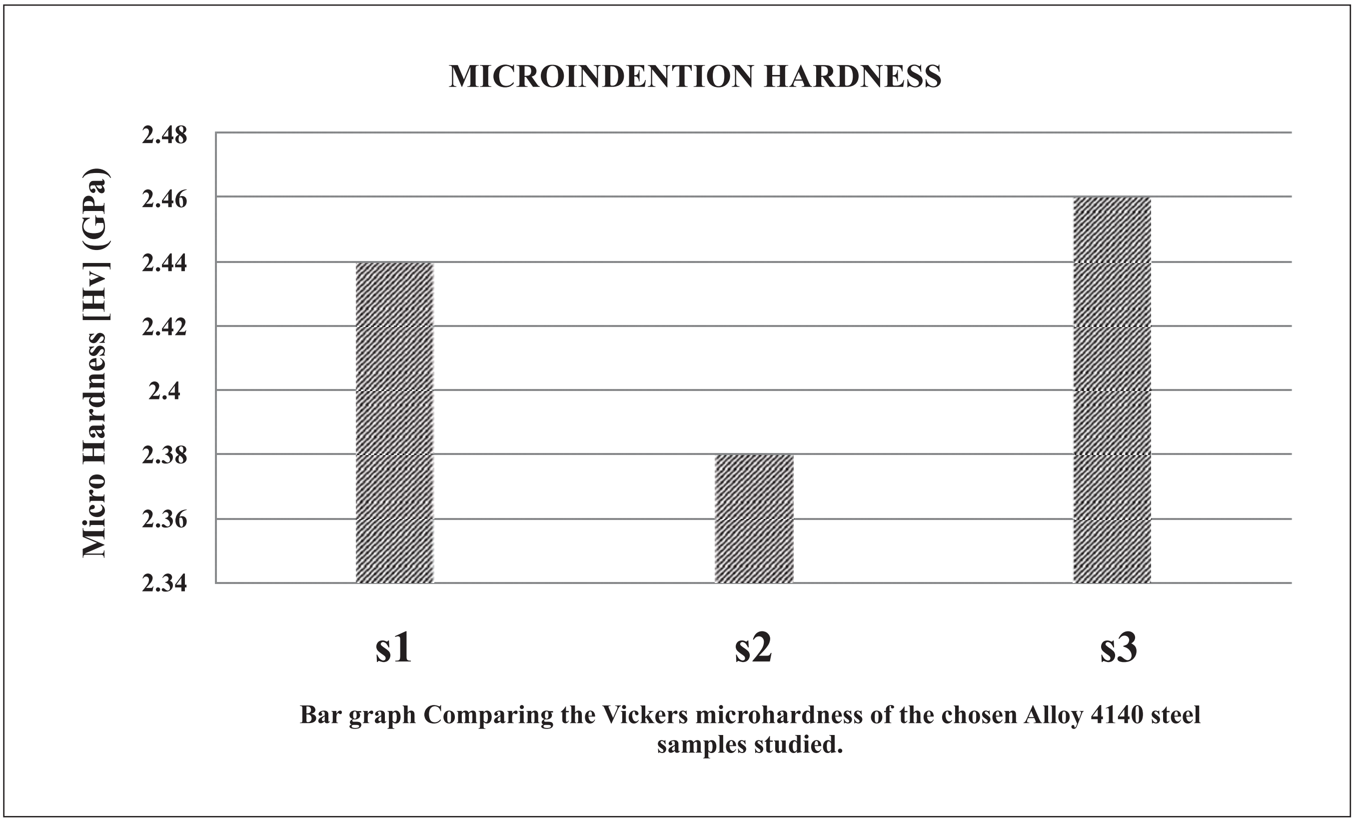

Figure 4. Bar graph comparing the Vickers microhardness of the three chosen samples of alloy steel 4140.

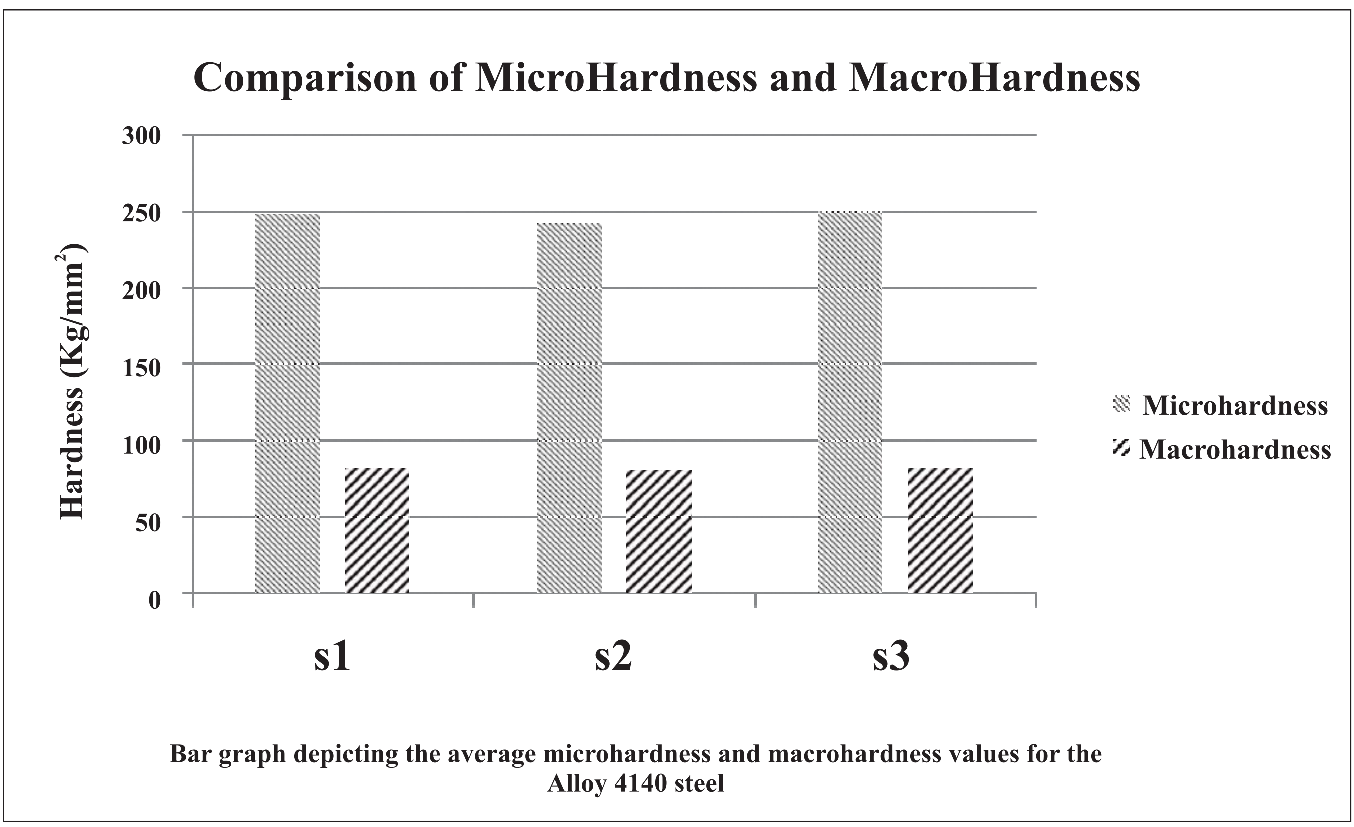

Figure 5. Bar graph comparing the average microhardness and macrohardness values of the three chosen samples of alloy steel 4140.

5. CONCLUSIONS

A careful study of the influence of microstructural development and hardness of alloy steel 4140 in the hot rolled plus quench and tempered condition provides the following key findings:

1. The microstructure of alloy steel was found to essentially similar through its length and thickness with minimal to no difference in the nature, volume fraction, morphology, size and distribution of the intrinsic microstructural constituents.

2. The microstructure of the alloy steel samples revealed a combination of carbon-rich (dark regions) and carbon-depleted (light regions) zones. Higher magnification observation in the dark carbon-rich zone revealed fine martensite while the carbon-depleted zone was essentially covered with a population of ferrite grains of non-uniform size.

3. In the samples examined the volume fraction of the carbon-rich regions was far more noticeable than the carbon-depleted region.

4. The spatial variability was noticeably less pronounced and the measured microhardness was observed to be uniform throughout each of the three samples of alloy steel 4140.

5. The microhardness measured provides a measure of the effect of strengthening arising from the presence of intrinsic microstructural phases or micro-constituent, and a concurrent weakening resulting from the presence of microscopic microstructural defects such as microscopic cracks and microscopic voids.

6. The macrohardness values based on Rockwell C scale, made across the width of the polished sample, gave an average value of 82 kg/mm^2 ($HR_C = 22.69$). The observed lower value of macrohardness of the alloy steel 4140 when compared to its microhardness is ascribed to the physical presence and distribution of a healthy population of fine microscopic defects.

REFERENCES

1. Metals Handbook: Properties and Selection: "Classification and Designation of Carbon and Low Alloy Steels," Tenth Edition, ASM International, Materials Park, Ohio, USA, 1990.

2. B.P. Somerday: "Low Alloy Ferritic Steels Tempered Fe-Cr-Mo Alloys,": in Hydrogen Compatibility of Materials, *editors:* C. San Marchi and B. P. Somerday, Sandia National Laboratories, Alburque, New Mexico, USA.

3. A.W. Loginow and E. H. Phelps: Steels for Hydrogen Pressure Vessels, <u>Corrosion</u> Vol. 31, 1975, pp. 404-412.

4. J.H. Chuang, L.W. Troy and C. Chen: *International Journal of Fatigue,* Vol. 20, No. 7, 1998, pp. 531-536.

5. T.V. Philips and T. J. McCaffrey: "Ultrahigh Strength Steels, in *Metals Handbook, Vol. 1,* Tenth Edition, ASM International, Materials Park, Ohio, USA, 1990, pp. 430-440.

6. W.C. Leslie: *The Physical Metallurgy of Steels*, McGraw Hill Publishers, New York, 1981, pp. 236-242.

7. H.K. Birbaum: Hydrogen Related Failure Mechanisms in Materials, Symposium of TMS, TMS-AIME, Warrendale, PA, USA, 1979, pp. 320-360.

8. D.P. Williams and H. G. Nelson: *Metallurgical Transactions,* Vol. 1, 1970, pp. 63-68.

9. L.W. Tray, W.B. Huang, Y.M. Li and C. Chen: *Journal of Materials Engineering and Performance,* Vol. 6, 1997, pp. 177-181.

10. D.R. Askeland and P.P.; Phulke: *The Science and Engineering of Materials*, Fifth Edition, Thompson Publishers, USA, 2005, pp. 520.

11. G.E. Dieter: *Mechanical Metallurgy*, Third Edition, 1986, McGraw Hill Publishers, pp. 400-410.

FAILURE INVESTIGATION OF RADIATOR SUPPORTING BRACKET FOR STRUCTURAL VIBRATION PROBLEMS USING OPERATIONAL MODAL ANALYSIS, OPERATING DEFLECTION SHAPES AND FINITE ELEMENT ANALYSIS.

Milind D. Kandalkar
Faculty of Mechanical Engineering Department,
Rajarambapu Institute of Technology, Sakhrale (Islampur),
Dist. Sangli – 415414, Maharashtra, India.
E-mail: milindkandalkar@gmail.com
Mobile No. 09960735140

Prof. Narendra K. Chhapkhane
Faculty of Mechanical Engineering Department,
Rajarambapu Institute of Technology, Sakhrale (Islampur),
Dist. Sangli – 415414, Maharashtra, India.
E-mail: nkchap@yahoo.co.in
Mobile No. 09970700868

ABSTRACT

This paper discusses three popular parts of modern day structural dynamics technology; the experimental portion which is referred to as operational modal analysis (OMA), operating deflection shapes (ODS) and the analytical portion which is referred to as Finite Element Analysis (FEA) or Finite Element Modeling (FEM) contained CATIA and ANSYS. It discusses how experimental and analytical methods are used to solve structure vibration problems and the importance of using modal parameters to link testing and analysis. Finally, it shows how structural modification techniques are used as a complement to both methods and how all of the tools may be combined on a radiator supporting bracket problem.

Keywords: *Operational modal analysis, Operating deflection shapes, Finite Element Analysis, Structural dynamics.*

Short Title: *Operational modal analysis (OMA), Operating deflection shapes (ODS), Finite Element Analysis (FEA).*

1. INTRODUCTION

Vibration problems in structures or operating machinery often involve the excitation of structural resonances or modes of vibration. Many types of machinery and equipment have been encountered severe resonance related vibration problems during operation.

Operational modal analysis (OMA) is a procedure which allows extracting modal parameters of structures from measured responses to unknown excitation arising in operating conditions. Modal analysis is a method to describe a structure in terms of its natural characteristics which are the frequency, damping and mode shapes – its dynamic properties.

An Operating Deflection Shapes (ODS) is the motion of one point relative to all others. It shows the deflection of a structure at a particular frequency and also specifies the motion of two or more points to define a shape. ODS analysis is used for determination of the vibration pattern of a structure under given operating conditions. Vibration measurements performed at different points and directions on the structure and the vibration pattern can be shown as an animated geometry model of the structure or listed in a shape table.

Analytical FEA is an integrated collection of modeling and analysis tools designed to be used by the experimentalist. It includes the facility to quickly build simple small scale finite element models and solve them for natural frequencies and mode shapes.

It is the intent of this paper to report on how virtually any design or testing engineer can take advantage of recent advances in computer technology and software developments which allow him to easily use a system capable of offering advanced experimental methods as well as analytical methods in the same basic framework.

2. TEST CONFIGURATION AND SPECIFICATION

The engine used in the study is three cylinders inline four stroke diesel engine (genset) connected to alternator and eddy current type dynamometer for loading. The loading can be changed without stopping the engine and without altering the combustion chamber geometry by specially designed arrangement and should be kept in 1500 RPM rotating speed.

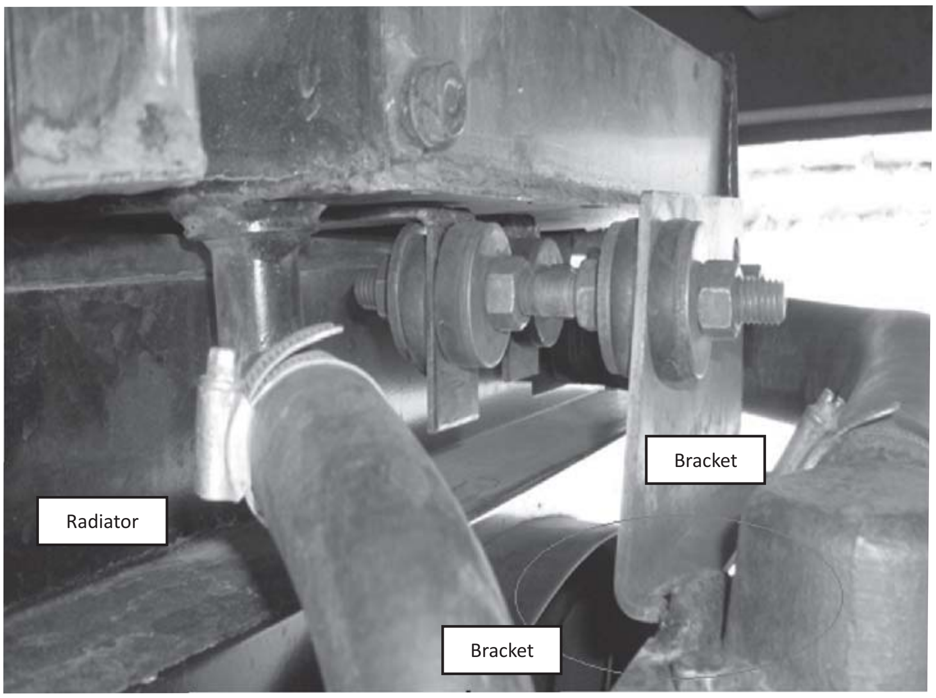

Figure 1. Radiator bracket assemblies.

The component is a fabricated bracket used to support radiator of diesel engine. Presently bracket is failing on the field. The main objective of this paper is to do failure investigation and establish testing process, which would eliminate its failure on the field.

2.1 VIBRATION MEASUREMENT HARDWARE When performing vibration testing, the instrumentation required depends on application, location and purpose. Instrumentation for Operational modal analysis and operating deflection shapes analysis method two single axial accelerometer, data acquisition system called as front end and pc software licenses should be used.
Accelerometer Details: Manufacturer – Endevco, Type – 752A12, Sensitivity – 10.64 mV/m/s2 (104.3 mV/g), Application – Specially used for modal analysis.
Data acquisition system: Made – Bruel & Kjaer, Type – 3050-B-060 LanXI, Module – 6 channel, Frequency range – 51.2 KHz.

2.2 TEST PROCEDUR E The main procedure to perform dissertation work is as follows:

Step 1 – To find out forcing frequency by actual vibration measurements on the engine.

Step 2 – Simulate same operating condition on the Shaker table and carry out OMA & ODS measurement.

Step 3 – To avoid resonance by shifting natural frequency of the bracket (try to modify existing bracket) in FEA.

As often happens with experimental methods, there is no such thing as the 'right way' to perform a modal test. The basic setup of modal test is:

- An excitation mechanism (shaker);
- A number of transducers (typically accelerometers) to measure the structure's response;

3. VIBRATION MEASUREMENTS IN FULL LOAD CONDITION

The radiator supporting bracket is bolted to the engine top surface. The most of the vibration are transferred from cylinder head to bracket directly. There is no provision to damped excessive vibration transferred from cylinder head to bracket. The radiator bottom side is mounted on the canopy base plate and top side is connected to supporting bracket through stray rod.

This test method covers the use of two single axial accelerometer, data acquisition & data processing analyzer and FFT software for the determination of the vibration level in full load condition of the engine.

The vibration data have collected during full load running condition from rocker cover and radiator top surface of the genset. The maximum vibration amplitude of approximately 11m/s2 (193 um) peak was detected in the axial direction on the rocker cover at l.5x engine firing frequency 37.5 Hz under operating speed of 1500 rpm (25 Hz), as shown in Figure 2. However, The maximum vibration amplitude of approximately 8.5m/s2 (149 um) peak was detected in the axial direction on the radiator top at l.5x engine firing frequency 37.5 Hz under operating speed of 1500 rpm (25 Hz), as shown in figure 3.

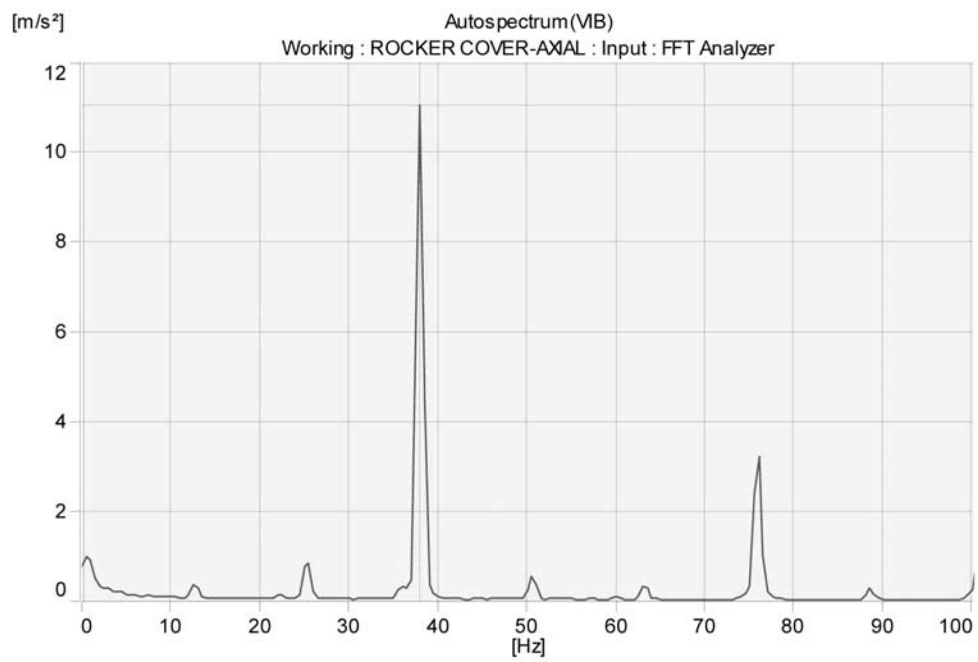

Figure 2. Vibration spectrum (FFT) measurement on rocker cover in axial direction.

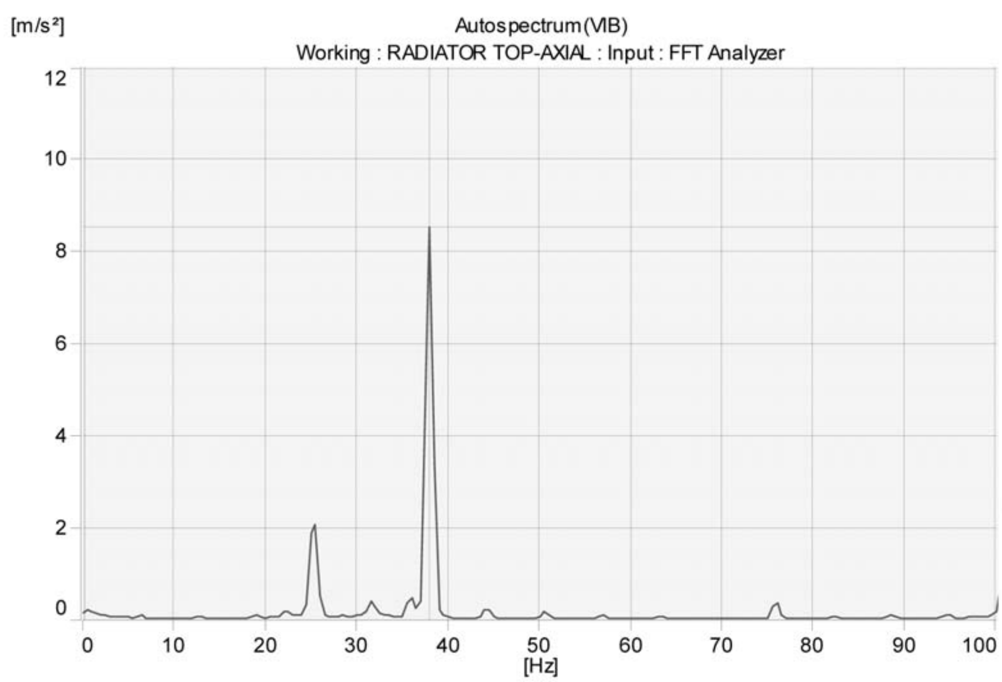

Figure 3. Vibration spectrum (FFT) measurement on radiator top in axial direction.

The vibration data showing first peak at 12.5 Hz i.e 0.5 order (camshaft rotation frequency), second peak at 25 Hz i.e. 1 order (flywheel rotation frequency), third peak at 37.5 Hz i.e. 1.5 order (firing frequency) and rest of the peaks are harmonics. From vibration data it is clear that maximum vibration created due to the engine firing cycle and occurred on 37.5 Hz in an axial direction only. Therefore 37.5 Hz is the dominating frequency. From above vibration data it is clear that maximum excitation occurred in an axial direction only and the failure in a bracket occurred due to the axial vibration.

4. OPERATIONAL MODAL ANALYSIS

The excitation technique used for component under test (radiator supporting bracket) is shaker excitation. The dimension of shaker table is 130*100 mm. To made real vibration condition on shaker table, the radiator assembly with stray rod and bracket are mounted on the table, trying to simulate actual condition. For this setup, fabricate a robust fixture by using mild steel C-channels and angles combination. To comply with real operating condition, deliver a harmonic excitation to the fixture in such a way that radiator supporting bracket accelerate at 11m/s2 at 37.5Hz.

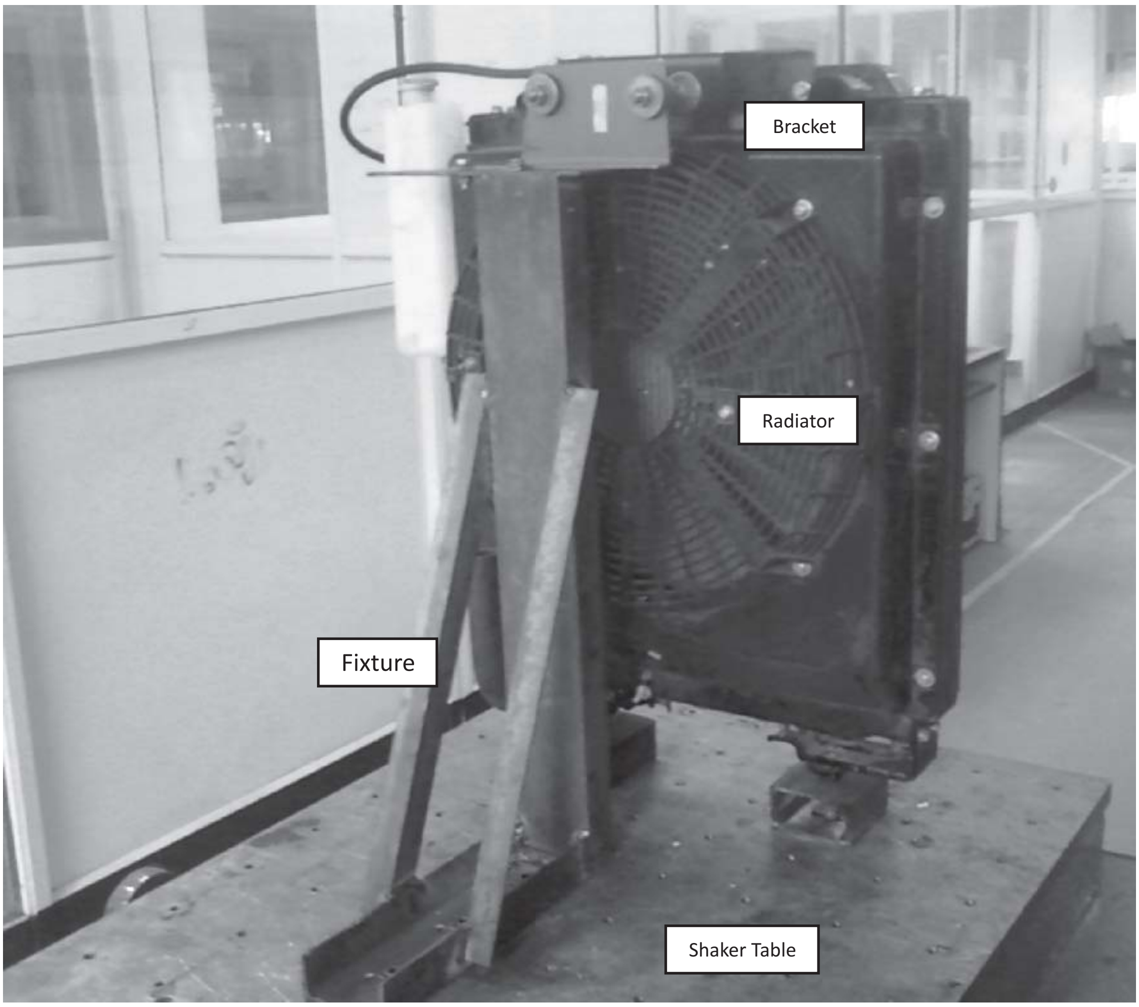

Figure 4. Experimental setup of radiator supporting bracket assembly mounted on shaker table.

The radiator supporting bracket geometry i.e. CAD model is directly imported into the OMA geometry window. After import geometry, the next step is to assign measurements location. For this structure, one location which is bottom side of bracket assign for reference accelerometer and 18 locations on the plate assign for roving response accelerometer measurement. In transducer list blue color accelerometer is reference accelerometer.

Here structure is very thin, therefore frequency span selected is up to 1.6 kHz and sampling frequency is 244.1us selected. The final frequency domain data which get would be the average of 43 measurement data set of one location.

Table 1. shows unmodified radiator supporting bracket curve fit frequency domain decomposition modes, natural frequencies and damping ratios. From table it is reveled that dominated mode is occurred at 37.51Hz and 0.9198% damping ratio i.e underdamped system. It is clear that natural frequency exactly matches with excitation frequency i.e. 37.5Hz and resonance occurred. Due to resonance radiator bracket fails on the field after undergone some excitation cycles.

Table 1. Radiator supporting bracket natural frequencies & damping ratios.

CFDD MODE	FREQUENCY (Hz)	DAMPING RATIO (%)
MODE 1	37.51	0.9198
MODE 2	100.3	1.002
MODE 3	167.6	0.8355
MODE 4	266.5	1.062
MODE 5	373.8	0.7384
MODE 6	551.2	0.8512
MODE 7	750.3	0.2314
MODE 8	868	0.3496
MODE 9	1499	0.8657

5. OPERATING DEFLECTION SHAPES

The ODS is a thorough "artificial excitation signature" vibration test performed on the entire unit structure that usually includes data collection on electrodynamic shaker, the associated attachment i.e. radiator assembly mounted on fixture and supported by using nut & bolt, while the unit is operating under its real dynamic condition (within typical operating range condition), in order to capture the overall motion at known frequency i.e. 37.5 Hz.

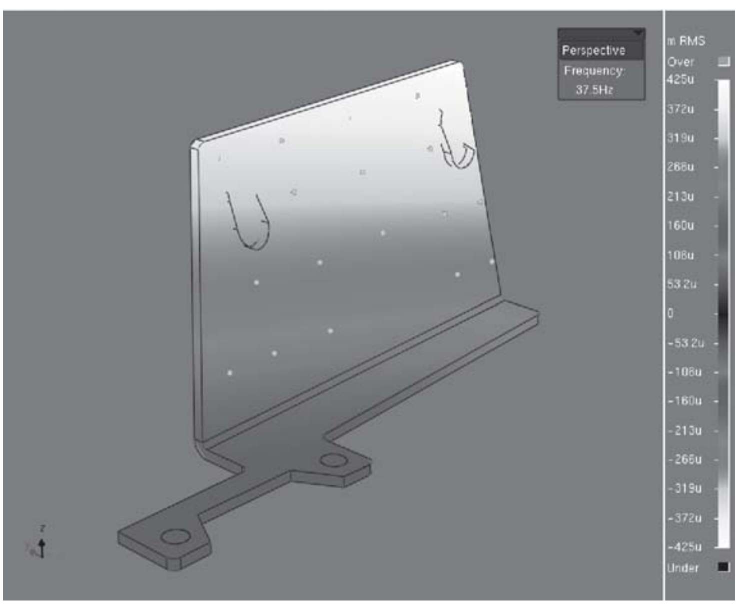

Figure 5. Mode shape at 37.5 Hz & respective displacement values.

The resulting vibration animation describes in exaggerated motion/deformation (but consistently scaled) the bracket motion at the selected frequency in order to easily identity for example the "weakest" location of the bracket.

6. FINITE ELEMENT ANALYSIS

Once the OMA and the ODS animation are created and analyzed at particular frequency, an FEA model is constructed and animated to match the problematic frequencies and the mode shapes. The FEA model incorporates the actual dimensions of the radiator supporting bracket and is typically constructed in CATIA software and analyzed in ANSYS software.

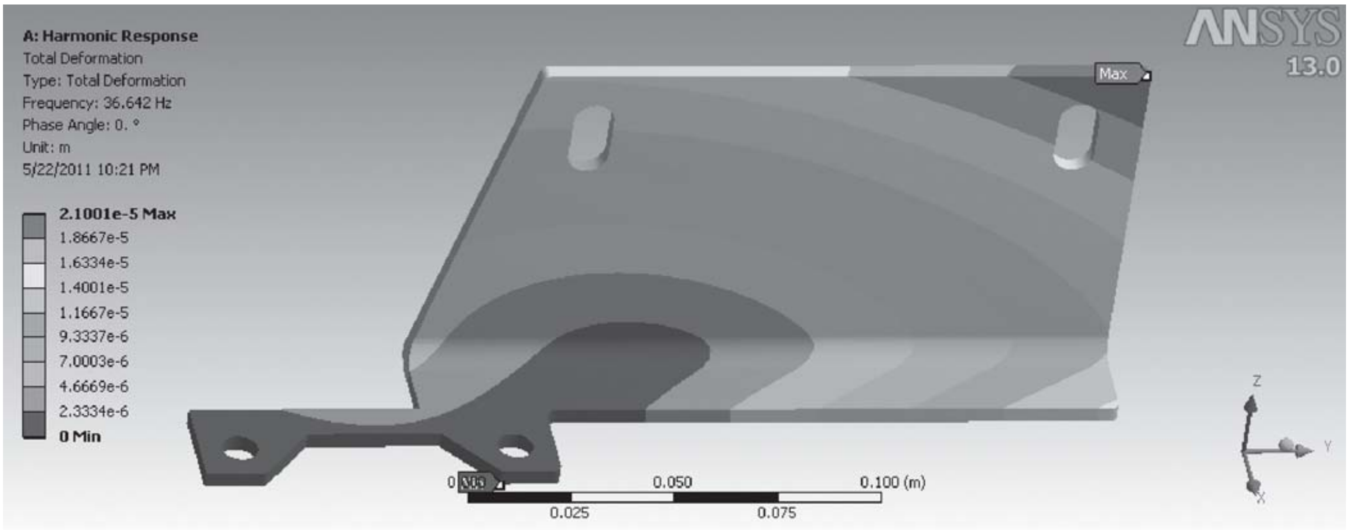

Figure 6. Total deformation of radiator supporting bracket at 36.642 Hz.

Mode	Frequency
1	36.642
2	102.12
3	357.36
4	541.72
5	776.15
6	1414.5

Table 2. Ansys radiator supporting bracket natural frequencies.

7. ANALYTICAL RESULTS MODIFICATIONS

The level of vibration in a structure can be attenuated by reducing either the excitation or the response of the structure to that excitation or both. It is sometimes possible at the design stage to reduce the exciting force or motion by changing the equipment responsible by relocating it within the structure or by isolating it from the structure so that the generated vibration is not transmitted to the supports. The structural response can be altered by changing the mass or stiffness of the structure by moving the source of excitation to another location or by increasing the damping in the structure.

On the basis of the results got experimentally and verified analytically, it is concluded that the bracket failed due to resonance. Hence, the first task was to modify the bracket in such a way that the natural frequency shifts to other location. Thus based on the analysis, the best two modifications are listed below.

The first modification is 60mm by 80mm elliptical hole bracket. This bracket will be useful to modify the existing bracket which has to be supplied to the existing customer with genset. After carry out modification in existing bracket, we will eliminate failure of the bracket on the field.

7.1 60MM BY 80MM ELLIPTICAL HOLE BRACKET

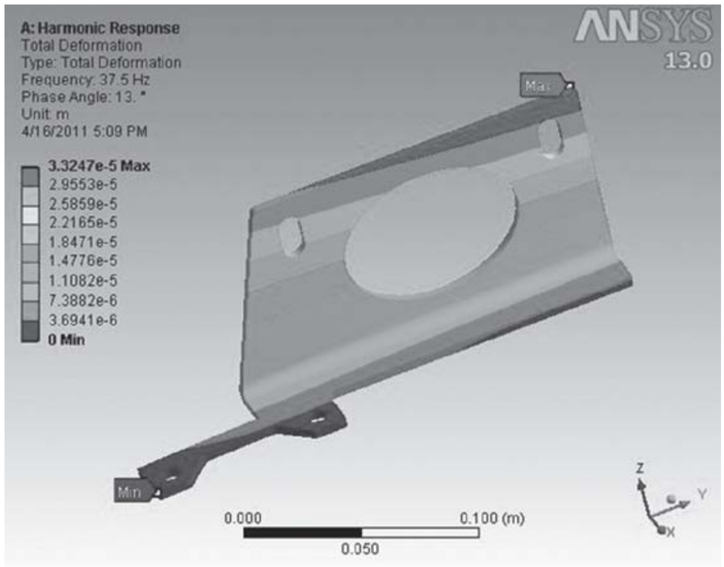

Figure 7. Total deformation of 60mm by 80mm elliptical hole bracket at 44.999Hz natural frequency.

7.2 TRIANGULAR BASE PLATE BRACKET

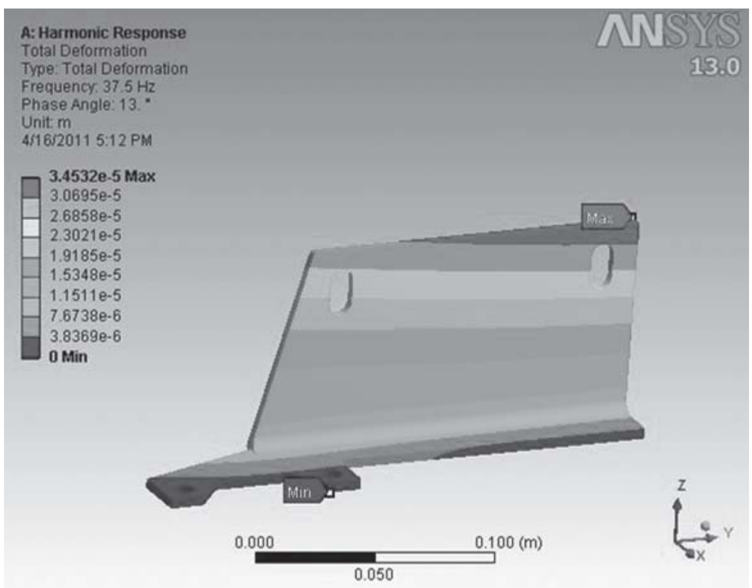

Figure 8. Total deformation of triangular base plate at 46.443Hz natural frequency.

Table 3. Ansys analysis comparison results.

Bracket names	**Total Deformation**		**Equivalent Stress(Mpa)**	
	Max	Min	Max	Min
Original Bracket	2.10e-5	0	3.37e7	199.07
Bracket 60-80	3.32e-5	0	6.55e6	511.01
Triangular bracket	3.45e-5	0	7.92e6	736.42

8. CONCLUSION

Table 4. Comparison of experimental result with analytical result

MODES	EXPERIMENTAL FREQUENCY (Hz)	ANALYTICAL FREQUENCY (Hz)
MODE 1	37.51	36.642
MODE 2	100.3	102.12
MODE 3	167.6	-
MODE 4	266.5	-
MODE 5	373.8	357.36
MODE 6	551.2	541.72
MODE 7	750.3	776.15
MODE 8	868	-
MODE 9	1499	1414.5

Table 4. gives comparison of experimental results with analytical predicted values of original radiator supporting bracket. The experimental results show more modes than analytical analysis. It reveals that there is 3.18% average deviation between the actual measured and analytical predicted value.

From table 1. it is revealed that dominated mode is occurred at 37.51Hz and 0.9198% damping ratio i.e underdamped system. It is clear that natural frequency exactly matches with excitation frequency i.e. 37.5Hz and resonance occurred. Due to resonance radiator bracket fails on the field after undergone some excitation cycles.

After doing analytical analysis it is clear that the maximum stresses i.e.3.3751e7 Pa occurred between two holes of thin base plate area (mounting location of the bracket on the engine). The deformation mentioned area exactly matched with the field failed bracket.

It is reveal that the mode shape of experimentally obtained resonance frequency 37.51 Hz is match with analytically predicted 36.642 Hz natural frequency (Figure 5 & Figure 6).

It is clear that the both modifications will be helpful for failure troubleshooting of the bracket due to vibration. Out of this the 60mm by 80mm elliptical hole bracket will give best result with less material and longer life.

9. APPLICATIONS OF OPERATIONAL MODAL ANALYSIS AND OPERATING DEFLECTION SHAPES

Modal analysis provides an excellent basis for interpreting the behavior of structures in their operating environments. For example, the numerical prediction of forced response allows investigating various scenarios using a virtual dynamic model acquired from test. This is standard practice in the aerospace industry and is an airworthiness requirement to demonstrate the safe operation of aircraft.

1. DAMAGE DETECTION: A major research area in the field of modal analysis is that of damage detection. As structures age, damage will inevitably accumulate. The goal of damage detection techniques is to determine the severity of the damage and to provide guidance on how the usability may have been compromised.

Traditionally, vibration signatures and orbit plots have been the preferred tools for detecting and diagnosing machinery unbalance. Although these tools may be effective when used by an expert, operational deflection shape (ODS) analysis offers a simpler, more straightforward approach for fault detection. Unbalance is more easily characterized by a visual as well as a numerical comparison of a machine's ODS when compared with its baseline ODS.

To identify the crack, contours of the normalized frequency in terms of the normalized crack depth and location are plotted. The intersection of contours with the constant modal natural frequency planes is used to relate the crack location and depth.

2. MODEL UPDATING: The area of damage detection is linked to the model updating. Both processes require the determination of the location of sites which are inappropriately modeled either through structural failure or through inadequate parametric representation. In both areas, the ability to locate these sites is frequently hampered by a lack of experimental data. Two issues need to be resolved. Firstly, the vibration response measurement must be sensitive to the location of the damage site. For instance, if the response of a mode does not exercise the strain energy in the region of the site of interest, there will be no shift in its dynamic properties.

Secondly, the solution may not be unique. An observed shift in modal properties can usually be attributed to more than one location on the structure.

3. Structural modification and control: However well intentioned and thought-out a structural design may be, it is inevitable that structures will occasionally not perform within the desired dynamic response envelope. Resonances may be misplaced or the demands on the structure may simply have been changed. In either case, modifications to the structure are required to bring its dynamic response to within desired tolerances. Two approaches are appropriate and are covered: structural modification and active control.

10. FUTURE SCOPE

The vibration data have been capture by using single axial accelerometer on reference and response position. If tri-axial accelerometer will be used on a reference and response position to carry out vibration measurements in all three directions in place of single axis, the mode shapes obtained from experimental analysis will be much more accurate and the notification of problem area will be much clearer to understand.

On the basis of above instrumentation the current results can be further modified, optimized and improved to get accurate analysis result close to actual test result over large frequency range.

REFERENCES

1. Maki M. Onari & Paul A. Boyadjis, *Solving Structural Vibration Problems Using Operating Deflection Shape and Finite Element Analysis*. *Proceeding of the twenty-fifth international pumps user symposium, 2009 p.85-102.*

2. Brian J. Schwarz & Mark H. Richardson, *Introduction to Operating Deflection Shapes*. CSI Reliability Week, Orlando, FL, 1999 p. 1-7.

3. Havard Vold, Brian Schwarz & Mark Richardson, *Measuring Operating Deflection Shapes under Non-stationary Conditions*. IMAC XVIII, 2000 p.7-10.4.44.

4. ***Bor-tsuen Wang, Determination of Mode Shapes from Operational Deflection Shape. Journal of Sound and Vibration*, p.1-24.**

5. ***Mark H. Richardson,*** *Is It a Mode Shape, or an Operating Deflection Shape?* Sound & Vibration Magazine 30th Anniversary Issue, 1997 p.1-11.

6. Havard Vold, Brian Schwarz & Mark Richardson, *Display Operating Deflection Shapes from Non-stationary Data*. Journal of Sound and Vibration, 2000 p.1- 4.

7. Brian Schwarz & Mark Richardson, *Measurements Required for Displaying Operating Deflection Shapes*, IMAC XXII, 2004 p.26-29.

8. George Fox Lang & Dave Snyder, Understanding *the Physics of Electro dynamics Shaker Performance*. Journal of Sound and Vibration 2001 p.1-9.

9. Paulo S. Varoto & Leopoldo P. R. de Oliveira, *Interaction between a Vibration Exciter and the Structure under Test*. Journal of Sound and Vibration 2002 p.20-25.

10 Dave Cloutier & Dr. Peter Avitabile, *Shaker/Stinger Effects on Measured Frequency Response Functions*. IMAC 27 Orlando, Florida 2008 p.1-7.

11. Application Notes 243-3, *The Fundamentals of Modal Testing*. Agilent Technologies, USA 2000 p.1-56.

12. Peter Avitabile, *Experimental Modal Analysis*. Journal of Sound and Vibration, 2001 p.1- 11.

13. Thomas G.Carne & George H.James, *The inception of OMA in the development of modal testing technology for wind turbines*. Mechanical Systems and Signal Processing 2010 p.1-14.

14. R.Pintelon, B.Peeters & P.Guillaume, *Continuous-time operational modal analysis in the presence of harmonic disturbances*. Mechanical Systems and Signal Processing 22, 2008, p.1017–1035.

15. J.M.W. Brownjohn, Filipe Magalhaes, Elsa Caetano & Alvaro Cunha, *Ambient vibration re-testing and operational modal analysis of the Humber Bridge*. Engineering Structures, 2010 p.1-16.

16. D. Hanson, R.B. Randall, J. Antoni, T.P. Waters, D.J. Thompson & R.A.J. Ford, *Cyclostationarity and the cepstrum for operational modal analysis of MIMO systems—Part II: Obtaining scaled mode shapes through finite element model updating*. Mechanical Systems and Signal Processing 21, 2007 p.2459–2473.

17. Lingmi Zhang, Tong Wang &YukioTamura, *A frequency–spatial domain decomposition (FSDD) method for operational modal analysis*. Mechanical Systems and Signal Processing, 2009 p.1-13.

18. H. Nahvi & M. Jabbari, *Crack detection in beams using experimental modal data and finite element model*. International Journal of Mechanical Sciences 47, 2005 p.1477–1497.

19. Svend Gade & Nis B. Møller & Henrik Herlufsen, *Modal Parameters from a Wind Turbine Wing by Operational Modal Analysis*. The 32nd International Congress and Exposition on Noise Control Engineering Jeju International Convention Center, Seogwipo, Korea, 2003 p.1-8.

20. Paolo L.Gatti and Vittorio Ferrari, *Applied Structural and Mechanical Vibrations Theory, methods and measuring Instrumentation*. Taylor & Francis e-Library, 2003, Ch 4 & 13.

21. S. Graham Kelly, *Fundamentals of Mechanical Vibration*. McGraw Hill, second edition, 2000, Ch 3.

22. Cyril M. Harris & Allan G. Piersol, *Harris' Shock and Vibration Handbook*. McGraw Hill, Fifth edition, 2002, Ch 2 & 22.

23. C. E Beards, *Structural Vibration: Analysis and Damping*. John Wiley &Sons Inc.1996, Ch 2.

24. James Taylor, *The Vibration Analysis Handbook*. First edition, Ch 1.

25. Clarence W. de Silva, *Vibration and Shock Handbook*. Taylor & Francis Group, LLC, 2005, Ch. 15.

26. Clarence W. de Silva, *Vibration-Fundamentals and Practice*. CRC Press, 2000, Ch. 4 & 5.the 60mm by 80mm elliptical hole bracket will give best result with less material and longer life.

DEFORMATION OF Al-5Zn-1Mg IN THE TEMPERATURE RANGE OF 303- 673K

Rijesh M
Department of Metallurgical and Materials Engineering,
National Institute of Technology Karnataka Surathkal,
Srinivasanagar P.O 575025, India

James Valder
Department of Metallurgical and Materials Engineering,
National Institute of Technology Karnataka Surathkal,
Srinivasanagar P.O 575025, India
Email:jamesvalder@gmail.com

A O Surendranathan
Department of Metallurgical and Materials Engineering,
National Institute of Technology Karnataka Surathkal,
Srinivasanagar P.O 575025, India

Geethalakshmi K
Department of Mechanical Engineering,
P C College of Engineering, Verna,
Goa, 403722, India

ABSTRACT

Compression testing of Al-5Zn-1Mg alloy was done at different temperatures from 303 K to 673 K. Graphite is used as a lubricant. Dynamic strain aging was observed to occur in the temperature range of 573-673K. Below 373 K flow stresses were high. Therefore warm working is preferred for Al-5Zn-1Mg alloy in between 373 K and 573 K. This will ensure lesser forces and adequate plasticity.

Keywords: *Compression, Temperature, Dynamic strain aging, Warm working, Al-5Zn-1Mg*

1. INTRODUCTION

The Al-Zn-Mg alloy has gathered a wide acceptance in fabrication of light weight structures where a high strength to weight ratio is an important criteria for application. The characteristics of ternary Al-Zn-Mg alloys are influenced by the high solid solubility of both Zn and Mg. In the ternary system, matrix compositions for invariant reactions are at such high Zn and Mg levels that non equilibrium melting is rarely encountered. For commercial compositions, solvous temperatures are generally low in compositions to those in other heat treatable alloy systems [1]. Extrusion is the manufacturing process by which such structural alloys are formed. Extrusion is an important metal working process in which all the stresses are compressive. [2]. Warm working [3] is gaining prominence since one can realize the advantages and minimize the disadvantages of both cold and hot working. Compression tests are essential to characterize the flow properties of the alloy at the different temperatures used in warm working [4]. Hence the present study has been carried out to study the behaviour of Al-5Zn-1Mg alloy in the various temperatures between room temperature(303K) and 673K, by means of axysymmetric compression test.

2. EXPERIMENTAL INVESTIGATION

The alloys are made by melting aluminium rods and alloying it with Zn and Mg. As cast material is in the form of cylinders and from these cylinders, compression test samples (axysymmetric) of height 37.5 mm and diameter 25 mm ($h_0/d_0 = 1.5$) were machined and annealed in a resistance furnace at 573 K. Samples were lubricated with graphite and heated in a resistance furnace. Temperatures selected for study were 303, 373, 473, 573 and 673 K. The specimens were tested in compression using a 40T universal testing machine. The velocity of ram was 3.3×10^{-4} m/s. The schematic set up is shown in Fig.1.

Traditionally, in finding the solutions of material strength coefficient and strain hardening constant, the material testing is firstly done to acquire force stroke diagram, the engineering stress and engineering strain from which yield strength is found by 0.1% offset method, which are then converted to the true stress and true strain(Fig.2) & log-log plots (Fig.3), respectively. Finally, they are substituted in the conducted formula. As the stress is considered to be a function of the strain, the flow stress formula can be expressed to $\sigma = K\varepsilon^n$ where *K* denotes the material strength coefficient and n denotes the strain hardening exponent [5]. Strength coefficient and strain hardening exponent were determined at various temperatures and plotted as shown in Fig. 4 and 5.

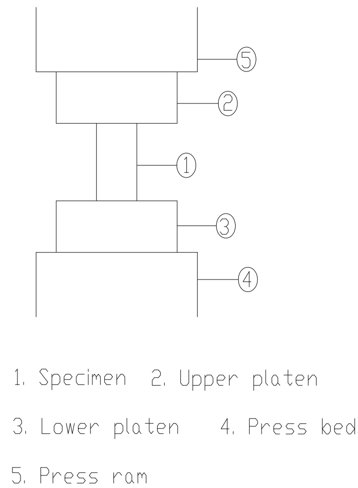

Fig.1. Schematic set up of Compression testing.

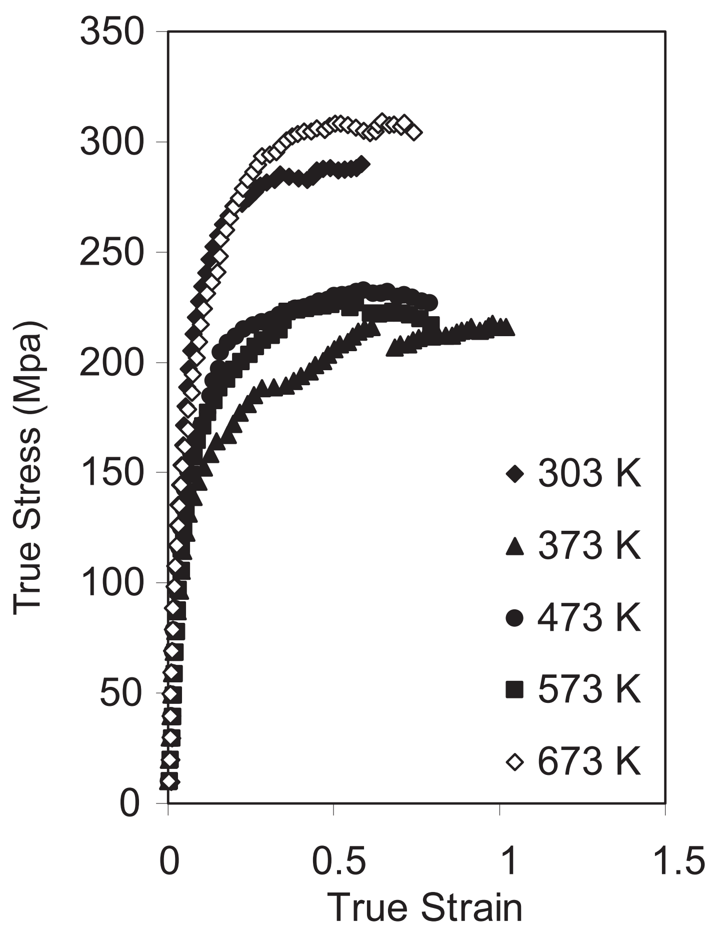

Fig.2. Plot of true stress against true strain at different temperatures

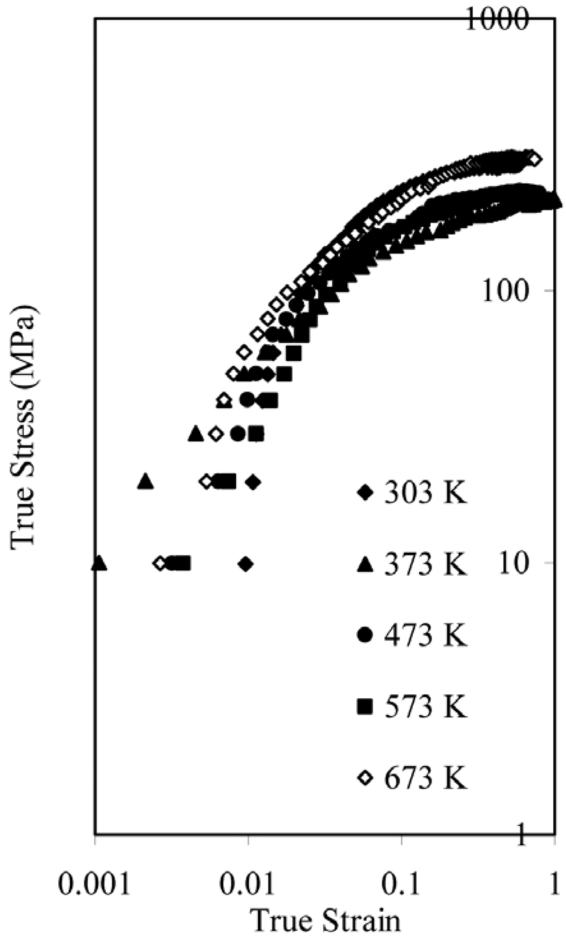

Fig.3. Log-Log plot of true stress and true strain

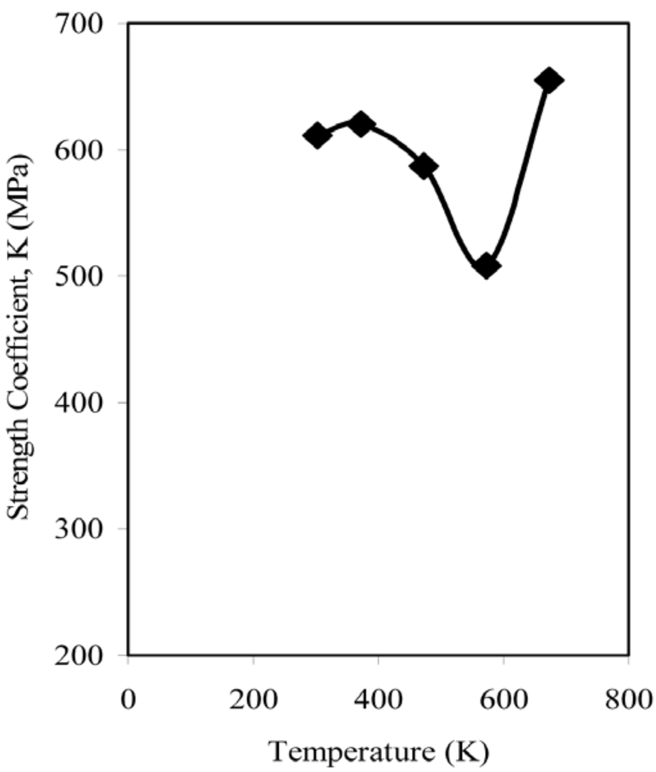

Fig.4. Plot of strength coefficient against temperature

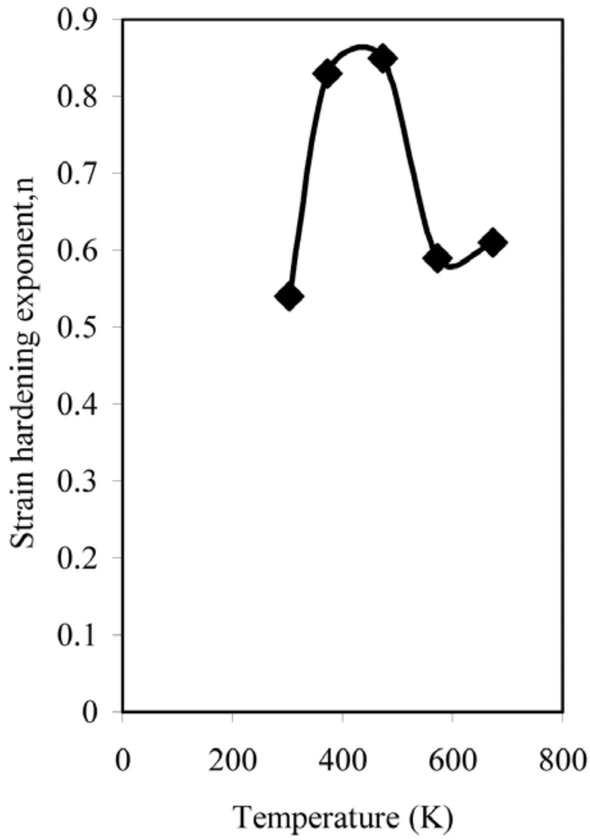

Fig.5. Plot of strain hardening exponent against temperature

3. RESULTS AND DISCUSSION

The stress- strain curve and log- log plot of stress and strain at different temperatures doesn't show a conventional expected line. The sample tested at 673 K took maximum stress to flow where as at 373 K it took the least. Flow stress at 473 and 573 K are less and they are comparable to 373 K. Flow stress for room temperature is high as expected but less than that of 673 K as seen in Fig.2. The material shows a double "n" behaviour as seen in Fig.3. Strength coefficient and strain hardening exponent at different temperatures are contained in Table.1. Strength coefficient increases first as temperature increased upto 373 K and then decreases as temperature goes to 573K and again increases from 573-673 K as shown in Fig.4. Corresponding behaviour of strain hardening exponent is shown in Fig.5. It increased upto 373 K, decreased upto 573 K and then increased upto 673 K. Strain hardening exponent is a very important parameter for the metal forming process. The higher its value, the greater will be the resistance of material and more force will be needed to form [6]. It controls the amount of uniform plastic strain the material can undergo during a compression test before strain localization, sets in leading to failure. As a result, a high coefficient facilitates complex-forming operations without premature failure [7][1]

Table.1. Strength coefficient and strain hardening exponent at different temperatures

Temperature (K)	Strength coefficient, K (MPa)	Strain hardening exponent, n
303	611	0.54
373	620	0.83
473	587	0.85
573	508	0.59
673	655	0.61

Dynamic strain aging occurs in the temperature range of 573-673 K as indicated by rise in K and n in Figs 4 & 5. Dynamic strain aging increases the flow stress and decreases the ductility [8]. Dynamic strain aging is totally undesirable during mechanical processing. Therefore this temperature range should be avoided while working Al-5Zn-1Mg alloy. Below the recrystallisation temperature and above room temperature warm working is to be done to maximize the advantages and minimize the disadvantages of both hot and cold working .at very low temperatures the stresses will be high and ductility low[9]. The adiabatic temperature rise is higher at lower temperature and lesser at higher temperature at a given strain. This can also be taken as an advantage if processing is done at medium temperature in the warm working temperature range.

4. CONCLUSION

From the above results it can be concluded that Al-5Zn-1Mg alloy can be mechanically processed economically and with ease in between 373 K and 573 K. It can be done with graphite as a lubricant. This will ensure lesser forces; adequate plasticity, minimization of embrittlement and less wear & tear of dies.

REFERENCES

1. Hatch J.E., "Aluminium-Properties and Physical Metallurgy", American Society for Metals, Ohio, USA, 1985, 50-52.
2. K. Laue and H.Stenger, ASM, Ohio, 1976, pp 2-5.
3. K. Lange, Hand book of Metal Forming, McGraw Hill, New York, 1985, Chapter 15 pp 1-95.
4. A. Taylan, S. Venugopal and V. Seetharaman, J. of Materials Processing Technology, Elsevier, 21, 1990.
5. *Zone-Ching Lina*, *Chang-Cheng Chenb*, *Hsin-Ho Wanga*, "The determination of material strength coefficient and strain hardening constant by inverse method", journal of materials processing technology 209 (2009) 2393–2401.
6. *Luis Fernando Folle, Sergio Eglan Silveira Netto, Lirio Schaeffer,* "Analysis of the manufacturing process of beverage cans using aluminum alloy"; Journal of materials processing technology 205 (2008), pp 347–352.
7. R. Ebrahimi and N. Pardis "Determination of strain-hardening exponent using double compression test" Materials science and Engineering-A, Volume 518, issues 1-2, 2009, pp 56-60.
8. R. E. Reed Hill and Reza Abbaschean, Physical Metallurgy Principles, PWS Publishing, Boston, 1994, pp 294-298.
9. G. E. Dieter and D. Bacon, Mechanical Metallurgy, McGraw Hill, London, pp530.

THE IMPACT TOUGHNESS AND FRACTURE BEHAVIOR OF FOUR HIGH STRENGTH STEELS: ROLE OF PROCESSING

T. S. Srivatsan
Email: tsrivatsan@uakron.edu
Division of Materials Science and Engineering
Department of Mechanical Engineering,
The University of Akron,
Akron, Ohio 44325-3903, USA

K. Manigandan
Division of Materials Science and Engineering
Department of Mechanical Engineering,
The University of Akron,
Akron, Ohio 44325-3903, USA

Thomas Quick
Department of Geology,
The University of Akron,
Akron, Ohio 44325-3903, USA

ABSTRACT

In this paper the influence of alloy chemistry and secondary processing on impact toughness, quantified using the Charpy V-notch test, and fracture behavior of four high strength steels is presented and discussed. The role of composition in synergism with secondary processing in establishing microstructural development and resultant intrinsic features is presented. The conjoint influence of composition, secondary-processing and microstructural features in governing impact fracture toughness is presented and discussed. The impact fracture behavior of the steels at the two extreme temperatures used in this study is also briefly discussed. The macroscopic and contributing microscopic mechanisms governing Charpy impact toughness and final fracture behavior of the chosen high strength steels are detailed in light of composition, intrinsic microstructural effects and nature of loading.

Keywords: *High strength steels, composition, microstructure, impact toughness, fracture behavior*

1. INTRODUCTION

The search for newer materials that can offer improved properties over the existing counterparts is a never ending process. This has arisen from the challenging requirements for new, improved and high performance materials with the gradual evolution of technology. A few of the characteristics desired in a high strength material for possible selection and potential use for both performance-critical and non-performance-critical applications include enhanced durability, a high strength-to-weight (σ/ρ) ratio, adequate damage tolerance capability, acceptable efficiency, reliability, relative ease of manufacturing and overall cost effectiveness [1-3]. A viable way to effectively compromise strength over ductility or building a perfect balance between the two is what most manufacturers of metals and alloys have been trying to achieve through the years, i.e., since the early 1970's. The steels chosen for this particular study were no exception.

High strength steels are often protected from corrosion by a sacrificial metallic coating [4]. This increases the risk of failure due to embrittlement by hydrogen. Depending on ally chemistry and nature of environment embrittlement by hydrogen can occur in few different ways. Over the years, efforts have been made to suppress embrittlement and failure from occurring. Regardless of the material chosen, several factors are intrinsically involved in ensuring the safety, reliability and efficiency of both structural and mechanical systems. A few of these include the following: (a) sound design, (b) proper material selection, (c) application of economically feasible and technically sound primary and secondary fabrication procedures, and (d) robust construction practices [5]. In almost every case, fracture represents the final stage in the useful life of an engineering component or structure, and can occur due to various factors. These factors essentially arise from the independent and conjoint influence of the following: (i) improved design, (ii) incorrect material selection, (iii) incorrect fabrication procedures, (iv) flawed construction processes, and (v) incorrect construction practice. All of these are often exacerbated by contributions from the environment. Development of newer products and finding appropriate applications for high strength steel necessitates that a careful consideration be given to all pertinent limit states, design procedures, fabrication practices and construction processes coupled with a careful evaluation of all potential end-uses so as to help ensure safe and reliable operation.

The mechanical properties to include fracture toughness of high strength steel are often governed by the independent or conjoint influences of (a) chemical composition, (b) processing history and development of intrinsic microstructural features, (c) geometry or part thickness, (d) temperature of operation, (e) loading-rate, and (f) presence of constraints at the crack (flaw) tip [6-12]. Conditions that tend to minimize constraints in a structure are almost always beneficial for enhancing the ability of a metal to plastically deform. This facilitates in improving the fracture toughness and overall damage tolerance capability of the high strength steel. Factors, such as, (i) an increase in thickness of the part, (ii) incorporation of engineering notches, (iii) increasing the loading rate; and (iv) lowering of the operating temperature are known to be detrimental to both ductility and fracture toughness of the chosen metal and related engineering structure [13-17].

The purpose of this paper is to present and discuss the influence of alloy chemistry, processing and test temperature on impact fracture behavior of the four high strength steels while concurrently comparing the results of the chosen steels under identical conditions. The deformed and failed test samples of each high strength steel were then examined in a scanning electron microscope for understanding impact fracture behavior, specifically the role of test temperature and microstructural features in governing the kinetics of fracture. The dynamic response characteristics of each steel are discussed in light of the mutually interactive influences of nature of material processing, material microstructure, test temperature, nature of loading and macroscopic aspects of fracture.

2. MATERIALS

The composition of the four high strength steels chosen for this experimental study is provided in Table 1. Presence of carbon provides solid solution strengthening as well as hardenability through the formation and presence of alloy carbides. The alloy carbides serve to enhance both the high temperature resistance and overall creep strength of a predominantly ferrite matrix. The presence of elements like chromium [Cr], molybdenum [Mo], Cobalt [Co] assists in the formation and presence of carbide particles in the microstructure, which contributes to enhancing the strength of the steel matrix. However, the presence and distribution of carbide particles in the microstructure is detrimental to fracture toughness or impact resistance arising as a result of an increase in the number of potential sites for the formation of fine microscopic cracks. Presence of nickel [Ni] facilitates in lowering the transition temperature while concurrently enhancing toughness and stabilizing the austenite that is present in the material. The presence of molybdenum in an alloy steel assists in refining the grain size, in addition to its role in forming molybdenum carbides and resultant influence in enhancing toughness [18].

The high strength steels designated by the manufacturer as AerMet100 (UNS K92580) and PremoMet™ 290 were produced through vacuum induction melting (VIM) and vacuum arc re-melting (VAR) route and subsequently cast as ingots. The high strength steels designated by the manufacturer as 300M (UNS K44220) and Tenax™ 310 were produced by Arc/VAR processing [Arc being the initial air-melt operation to produce electrodes from subsequent VAR processing; VAR: Vacuum Arc Re-melt] The four high strength steels used in this study were provided by the manufacturer [Carpenter Technology Corporation (Reading, PA, USA)].

AerMet®100 is a high strength steel possessing high hardness and high strength coupled with exceptional ductility and toughness. This steel is used for designing components requiring high strength, high fracture toughness, exceptional resistance to stress corrosion cracking, and good fatigue resistance [19]. The material has a nominal fracture toughness of 126 MPa $\sqrt{(m)}$ and tensile yield strength of 1724 MPa [19]. The steel designated as 300M has less strength and distinctly less fracture toughness than AerMet100 [20]. The PremoMet 290 steel and Tenax 310 steel are both free of cobalt. Further, these two steels have a combination of high strength and toughness in the quenched and tempered condition. These two steels attain an ultimate tensile strength of 2040 MPa coupled with a minimum fracture toughness of 77 MPa $\sqrt{(m)}$ and excellent fatigue life [20].

3. EXPERIMENTAL PROCEDURES

3.1 MICROSTRUCTURAL CHARACTERIZATION Samples of the four chosen high strength steels were prepared in accordance with standard procedures used for metallographic preparation of metal samples. This involved coarse polish using progressively finer grades of silicon carbide (SiC) impregnated emery paper (i.e., 320-, 400-, and 600-grit) followed by fine polishing using 5 micron and 1.0 micron alumina-based polishing compound suspended in distilled water as the lubricant. The as-polished samples were etched using nital; a solution mixture of nitric acid in methanol. Etching helped reveal the grain boundaries, morphology of the grains, and other intrinsic features, such as, location and morphology and distribution of the second-phase particles in the microstructure. The polished and etched samples were examined in an optical microscope, at low magnifications, and photographed using standard bright field illumination technique.

3.2 IMPACT TESTING Charpy V-Notch specimens were prepared in conformance with specifications outlined in ASTM E-23 [21]. Three replicate samples were tested at each of the six chosen test temperatures. In all, a total of 18 specimens were deformed under conditions of impact loading. Test samples were brought to the desired temperature by immersing in environments of:

(a) Liquid nitrogen (T = -180°C);

(b) Dry ice (T = -55°C);

(c) Ordinary ice (T = 0°C);

(d) Room temperature (T = 25°C),

(e) Boiling water (T = 98°C), and

(f) Furnace (T = 170°C).

The samples were immersed in a specific environment for full 30 minutes prior to the initiation of testing. Specimens evaluated at the higher test temperature (T = 170°C) were placed in a Blue-M Moldatherm box furnace and allowed to soak at the temperature for well over 30 minutes prior to testing. The Charpy V-Notch specimens were removed from the respective environments and quickly placed in the test fixture of the impact test machine (Model: Tinius-Olsen) with a capacity of 300 ft-lbs. This was followed by a quick release of the impact hammer, i.e., the pendulum. The total energy absorbed by the sample to failure was directly read from the graduated scale on the test machine.

3.3 FAILURE ANALYSIS Fracture surfaces of the dynamically deformed and failed test samples were examined in a scanning electron microscope (SEM) so as to determine the macroscopic fracture mode, and to concurrently characterize temperature influences on the fine-scale topography and microscopic mechanisms governing fracture. The macroscopic mode refers to the global nature of failure, while the microscopic mechanism refers to 'local' failure processes, such as: (1) microscopic void formation, microscopic void growth and their eventual coalescence; and (2) nature of cracking. Samples for SEM observation were obtained from the dynamically deformed and failed specimen by sectioning parallel to the fracture surface.

4. RESULTS AND DISCUSSION

4.1 INITIAL MICROSTRUCTURE The microstructure of the as-received or as-provided high strength steels is shown in **Figure 1** as optical micrographs. The observed microstructure is quite typical of the high strength steels revealing essentially a combination of martensite and ferrite. A higher carbon content in the steel resulted in a greater volume fraction of martensite. The presence and overall significance of martensite was

(a) Noticeable and present in large numbers in the lath morphology for AerMet 100 and PremoMet 290 that were produced through vacuum induction melting (VIM) and vacuum arc re-melting (VAR).

(b) For 300M and Tenax 310 produced by vacuum arc re-melting the martensite was much finer in size and intermingled with sizeable pockets of ferrite rich region. The presence of these features, namely, morphology, size and distribution of martensite and relative amount of ferrite has an influence on impact response and impact properties.

4.2 IMPACT TOUGHNESS PROPERTY The impact toughness properties of the four candidate high strength steels are summarized in **Table 2**. As expected and observed for the family of high strength steels, the amount of energy absorbed, during impact loading, increases with an increase in test temperature. Variation of impact fracture energy absorbed (N-m) as a function of test temperature is shown in **Figure 2** for AerMet 100 and PremoMet 290, and in **Figure 3** for 300M and Tenax™ 310. For all the four high strength steels a characteristic curve depicting an increase in absorbed energy with test temperature is evident.

The characteristic curve depicted by each of the candidate high strength steels essentially comprises of two distinct regions as seen in Figure 2 and Figure 3. During the early stages, stable crack propagation is promoted and occurs before culminating in failure. In this region the energy absorbed, or toughness of the material, increases linearly with an increase in test temperature. Such an increase is ascribed to be due to an increase in "localized" microplastic deformation ahead of the propagating crack and the resultant intrinsic microscopic mechanisms governing fracture. During the later stages the high energy absorbing capability of each of the high strength steels is ascribed to be due to fracture by ductile tearing. The observable difference between the sample in the early stage and sample in the later stage is the severity of tearing associated with ductile failure.

At a given test temperature there is noticeable difference in impact toughness of AerMet 100 and PremoMet 290 both produced by vacuum induction melting and vacuum arc re-melting. However, at a given test temperature minimal to no difference in impact toughness was evident for 300 M and Tenax 310 both produced by vacuum arc re-melting

The scanning electron micrographs shown in **Figures 4-9** support the observations made from measurement of the energy absorbed during an impact test as a function of test temperature.

Table 1: Nominal chemical composition of the chosen materials

Material	C	Mn	Si	P	V	Cr	Ni	Mo	Cu	Co
AerMet 100	0.238	<0.01	0.03	0.002	-	2.99	11.2	1.18	<0.01	13.41
300M	0.43	0.75	1.67	0.005	0.08	0.80	1.76	0.38	0.04	<0.01
PremoMet 290	0.404	0.79	1.50	0.003	0.30	1.29	3.82	0.50	0.58	0.01
Tenax™ 310	0.401	0.63	2.03	0.004	0.31	1.26	3.76	1.01	0.53	0.01

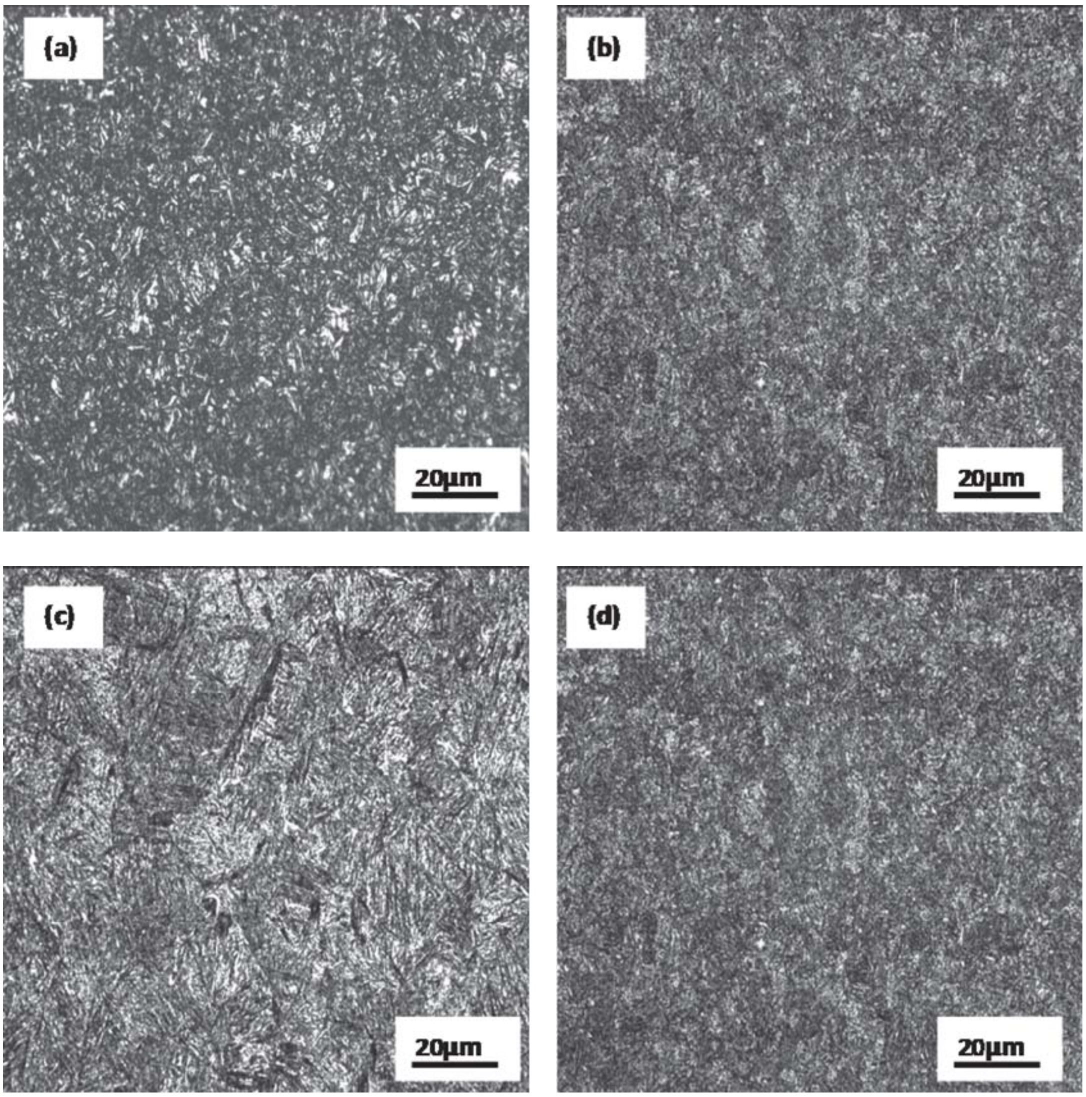

Figure 1: Optical Micrographs showing as-received microstructure of (a) AerMet100; (b) PremoMet™ 290; (c) 300M, and (d) Tenax™ 310

Table 2: The Charpy V-Notch Impact test values of the four steels at the different temperatures.

MATERIAL	Liquid Nitrogen (N-m) T=-180°C	Dry Ice (N-m) T= -55°C	Ordinary Ice (N-m) T= 0 °C	Room Temp (N-m) T= 25°C	Boiling water (N-m) T= 95°C	Furnace (N-m) T= 170°C
AerMet 100	19	30	53	56	58	58
300 M	15	23	31	32	37	41
PremoMet™ 290	15	33	34	36	37	40
Tenax™ 310	15	27	35	35	37	38

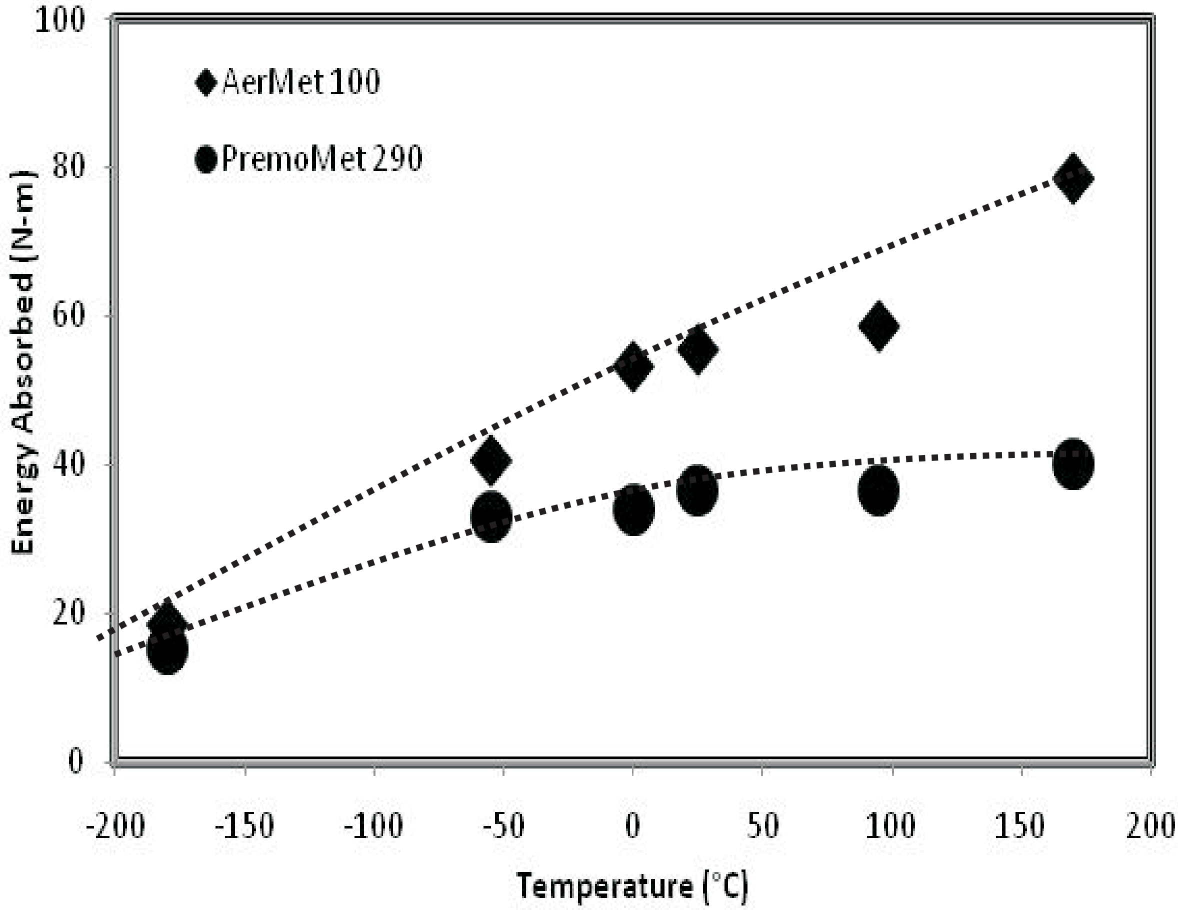

Figure. 2. Variation of energy absorbed (N-m) as a function of test temperature for the two steels AerMet100 and PremoMet290.

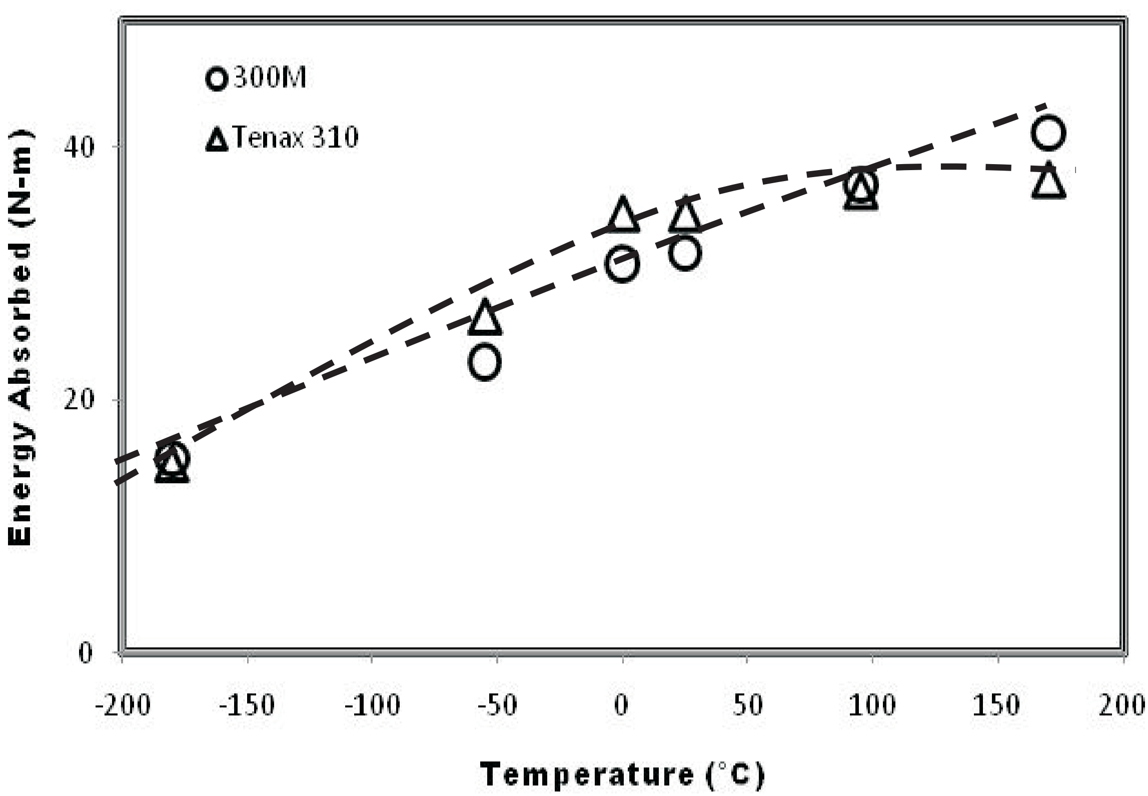

Figure. 3. Variation of energy absorbed (N-m) as a function of test temperature for the two steels 300M and Tenax™ 310.

4.3 IMPACT FRACTURE BEHAVIOR

4.3.1 IMPACT FRACTURE OF AERMET® 100 The fracture surface features of AerMet100 deformed at -180°C are shown in **Figure 4.** A vast majority of the fracture surface is covered with a population of fine microscopic voids and dimples. These features are reminiscent of globally ductile behavior even at this low a test temperature. The overall morphology of the test sample was essentially smooth with lack of observable macroscopic cracks and other features reminiscent of globally brittle behavior (**Figure 4-a**). High magnification observation of (a) revealed a population of voids of varying size along with dimples. At the next higher allowable magnification of the scanning electron microscope regions of the micrograph shown in (b) revealed clearly the morphology of the fine microscopic voids and their distribution on the impact fracture surface (**Figure 4-c**). The macroscopic and fine microscopic voids have little time to grow and eventually coalesce to form one or more macroscopic cracks (**Figure 4-d**). The presence of few yet isolated populations of fine microscopic cracks provides evidence of locally brittle failure mechanisms.

The fracture surfaces of the CVN sample dynamically deformed at room temperature (25° C) are shown in **Figure 5.** Fracture was visibly rough at the macroscopic level **(Figure 5-a**) with an absence of features reminiscent of globally brittle fracture. Careful examination of the fracture surface at higher magnifications in the region immediately adjacent to the notch revealed an absence of fine microscopic cracks but a shallow and well dispersed population of dimples; features reminiscent of ductile failure mechanisms operating at the 'local' level (**Figure 5-b**). At gradually higher magnifications was revealed the size, morphology and distribution of the fine microscopic crack surrounded by a healthy population of dimples **(Figure 5-c**). The overload fracture surface revealed a noticeable population of fine microscopic cracks and shallow pockets of fine microscopic voids and shallow dimples (**Figure 5-d**).

The fracture surfaces of the CVN sample dynamically deformed at the highest test temperature used in this study, i.e., 170°C, are shown in **Figure 6.** Fracture was visibly rough at the macroscopic level **(Figure 6-a**) with an absence of features reminiscent of globally brittle fracture. Careful examination of the fracture surface at higher magnifications in the region immediately adjacent to the notch revealed fine microscopic cracks intermingled with a rich population of dimples; features reminiscent of the brittle and ductile failure mechanisms operating at the 'local' level. At gradually higher magnifications was revealed the size, morphology and distribution of the fine microscopic cracks **(Figure 6-c**). The overload fracture surface revealed a noticeable population of fine microscopic voids intermingled with shallow elongated dimples (**Figure 6-d**). Elongation of the dimples results from the occurrence of ductile shear failure or due to the presence of localized Mode II deformation field at the microscopic level.

4.3.2 IMPACT FRACTURE OF 300M The scanning electron micrographs of the test samples deformed at the cryogenic temperature, i.e., -180°C, at room temperature (25° C) and at the highest test temperature (170°C) are shown in **Figure 7**, **Figure 8** and **Figure 9**. These micrographs partially support the observation of an increase in energy absorbed with an increase in test temperature.

The fracture surface features of the CVN test sample dynamically deformed at -180 C are shown in **Figure 7**. Overall morphology of failure (**Figure 7-a**) failed to reveal features reminiscent of globally brittle behavior, Careful high magnification observation in the region immediately adjacent to the notch revealed a population of voids of varying size and their random distribution through the fracture surface **(Figure 7-b**). At higher magnifications in the region away from the notch revealed an array of microscopic cracks intermingled with pockets of cleavage facets. The cleavage facets were essentially flat and near featureless (**Figure 7-c).** High magnification observation in the region of overload and final tearing revealed a population of shallow dimples of varying size, shape and distribution (**Figure 7-d**).

Fracture surfaces of this alloy steel sample that was deformed in impact at room temperature (25 C) are shown in **Figure 8**. Overall morphology of failure was essentially flat with clear indication of damage radiating away from the notch (**Figure 8-a**). Careful high magnification observation in the notch region revealed a random distribution of macroscopic and fine microscopic voids reminiscent of locally operative ductile failure mechanisms (**Figure 8-b**). High magnification observation in the region away from the notch revealed a healthy population of shallow dimples and fine microscopic voids (**Figure 8-c**), features reminiscent of locally operating ductile failure mechanisms. At gradually higher magnifications isolated microscopic cracks were evident, few and far between **(Figure 8-d**).

The fracture surface features of the CVN test sample dynamically deformed at the highest test temperature used in this study, i.e., 170°C are shown in **Figure 9.** Macroscopically failure radiated outward from the root of the notch similar to the observation of the sample deformed at the lowest test temperature, i.e., -170°C (**Figure 9-a)**. High magnification observation in the region immediately adjacent to the notch revealed a healthy population of shallow dimples intermingled with voids of varying size, features reminiscent of locally ductile failure mechanisms (**Figure 9-b**). The fine microscopic voids had limited time to grow and coalesce to form very fine microscopic cracks surrounded by a large population of essentially ductile dimples (**Figure 9-c**). Fine microscopic cracks intermingled with a random distribution of shallow dimples were evident in the region of 'tearing' or overload (**Figure 9-d**). These features are indicative of predominantly ductile with trace amounts of brittle failure mechanisms occurring at the 'local' level.

4.3.3 Impact Fracture of PremoMet™ 290 The scanning electron micrographs of this high strength steel are shown in **Figure 10, Figure 11** and **Figure 12** and support the observation made from measurement of impact energy absorbed as a function of test temperature. The fracture surface features associated with the Charpy V-notch test specimens that was dynamically deformed at the lowest test temperature (-180 C) is shown in **Figure 10.** Careful and cautious observation revealed failure to have initiated at the root of the notch and propagated outward radially (**Figure 10-a**) giving an overall appearance of ductile failure at the macroscopic level. Observation of the region surrounding the root of the notch at the higher allowable magnifications revealed a population of fine microscopic voids and an absence of features reminiscent of locally brittle failure (**Figure 10-b**). The morphology and shape of the microscopic voids revealed them to be of varying size and randomly distributed through the fracture surface. Even at this low a test temperature this high strength steel revealed features reminiscent of locally ductile mechanisms. The region of 'tearing' prior to catastrophic failure revealed isolated microscopic cracks resulting from the coalescence of the existing fine microscopic voids (**Figure 10-d).** The microscopic cracks were surrounded by a healthy population of dimples are reminiscent of the locally operating brittle and ductile failure mechanisms.

The fracture surfaces of this alloy steel sample that was deformed in impact loading at room temperature (25 C) are shown in Figure 11. Overall morphology of failure was essentially flat with the damage radiating outward from the notch (Figure 11-a). High magnification observation in the region immediately adjacent to the notch revealed a noticeable and healthy population of fine microscopic voids and isolated microscopic cracks (**Figure 11-b**). These intrinsic features are reminiscent of the locally ductile and brittle failure mechanisms. At gradually higher allowable magnifications of the scanning electron microscope this region revealed with clarity the morphology, size and distribution of the fine microscopic voids **(Figure 11-c**), features reminiscent of locally operating ductile failure mechanisms. High magnification observation at a region located at a noticeable distance from the notch revealed the shallow nature and distribution of the dimples intermingled with the fine microscopic voids, reminiscent of locally operating ductile failure mechanisms (**Figure 11-d**).

The fracture surface features observed for the CVN sample deformed at the higher test temperature, i.e., 170C, are shown in **Figure 12**. Overall morphology of fracture was no different than the test sample that was deformed at the lowest temperature (-180^{o}C) (**Figure 12-a**). The region immediately adjacent to the root of the notch showed voids of varying size, shallow and healthy distribution of dimples intermingled with isolated microscopic cracks (**Figure 12-b**). These features are reminiscent of the locally operating ductile and limited brittle failure mechanisms. At even higher observations careful examination of selected regions of the fracture surface revealed a fine array of microscopic cracks that were intermingled with microscopic voids (**Figure 12-c).** At region far away from the root of the notch and well into the 'tearing' domain the predominant feature covering the fracture surface was dimples and they were near identical in both size and shape but overall shallow in appearance **(Figure 12-d**). On an average the energy absorbed during impact at this test temperature (170^{o}C) is 2.7 times greater than the energy absorbed by the sample dynamically deformed at -170^{o}C.

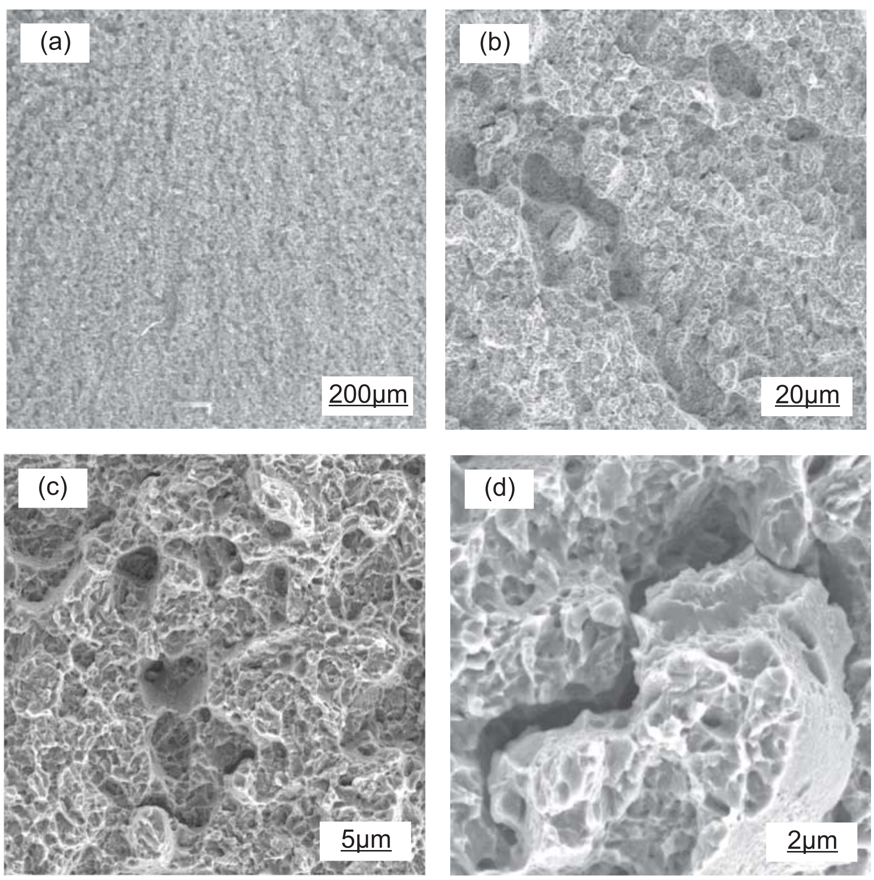

Figure 4: Scanning electron micrographs of Aermet100 deformed under impact following exposure in liquid nitrogen at – 180^{o}C, showing:

(a) Overall morphology of failure.
(b) High magnification of (a) showing a healthy population of microscopic voids and dimples
(c) Morphology of the fine microscopic voids and their distribution
(d) Isolated populations of fine microscopic cracks provides evidence of locally brittle failure mechanisms

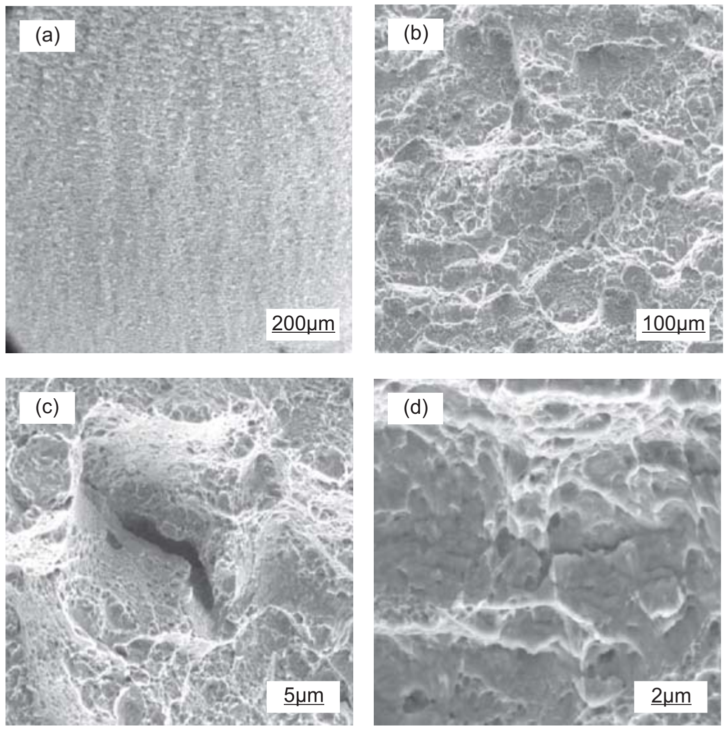

Figure 5. Scanning electron micrographs of Aermet100 deformed under impact in the room temperature environment at 25°C, showing:

(a) The as-ruptured morphology of failure

(b) High magnification observation of the region immediately adjacent to the notch.

(c) Macroscopic crack surrounded by a healthy population of shallow dimples.

(d) Fine microscopic cracks separating the region in the vicinity of notch and overload.

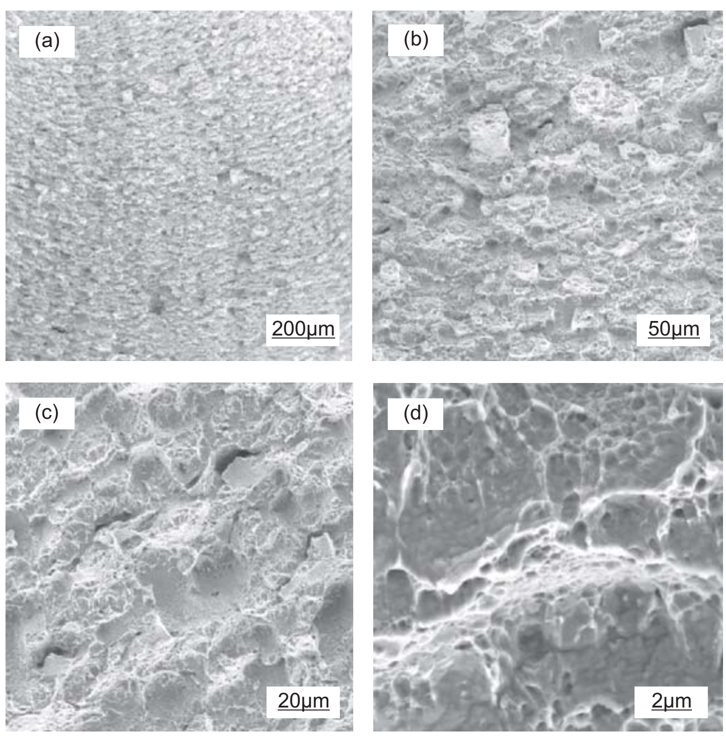

Figure 6: Scanning electron micrographs of Aermet100 deformed under impact following exposure in a furnace at 170°C, showing

(a) Overall morphology of failure.

(b) High magnification observation in the region immediately adjacent to the notch showing isolated fine microscopic cracks and a population of dimples.

(c) High magnification observation of (b) showing the size and Morphology of the microscopic cracks.

(d) Microscopic voids and pockets of shallow dimples.

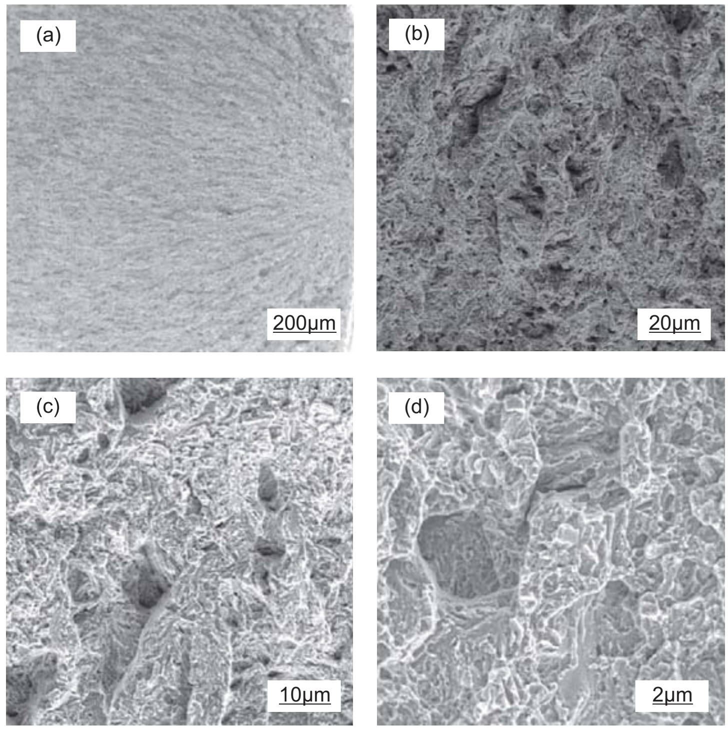

Figure 7: Scanning electron micrographs of 300M deformed under impact following exposure in liquid nitrogen at – 180°C, showing:
(a) Overall morphology of failure.
(b) High magnification observation in the region immediately adjacent to the notch showing voids of varying size and their random distribution.
(c) High magnification observation of the impact fracture surface away from the notch.
(d) A healthy population of shallow dimples of varying size and shape.

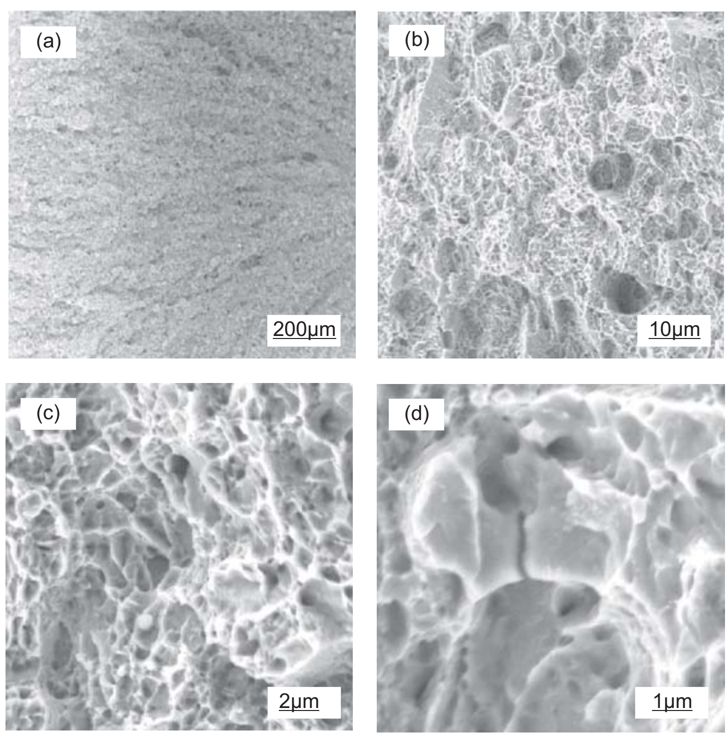

Figure 8: Scanning electron micrographs of 300M deformed under impact in the room temperature (25°C) laboratory air environment, showing:
(a) The overall morphology of failure as it radiates away from the notch.
(b) High magnification observation in the notch region showing a random distribution of macroscopic and fine microscopic voids.
(c) The distribution and shape of shallow dimples and fine microscopic voids.
(d) Isolated microscopic crack in a predominantly ductile region.

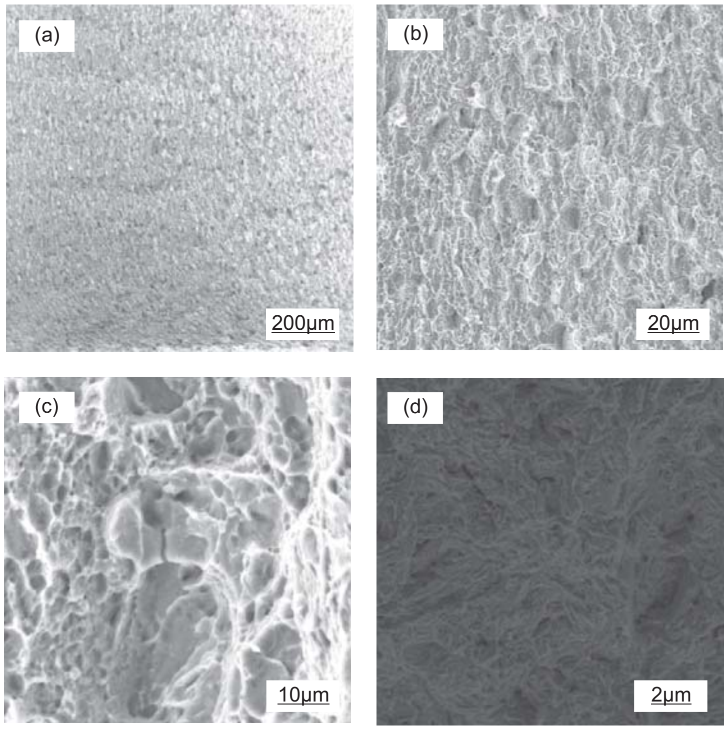

Figure 9: Scanning electron micrographs of 300M deformed under impact following exposure in a furnace at 170^{o}C, showing

(a) Overall morphology of failure as it radiates outward from the root of the notch.

(b) High magnification observation in the region adjacent to the notch reminiscent of locally ductile failure mechanisms.

(c) Microvoid coalescence to form fine microscopic crack surrounded by dimples

(d) Microcracks and random distribution of shallow dimples in the region of overload.

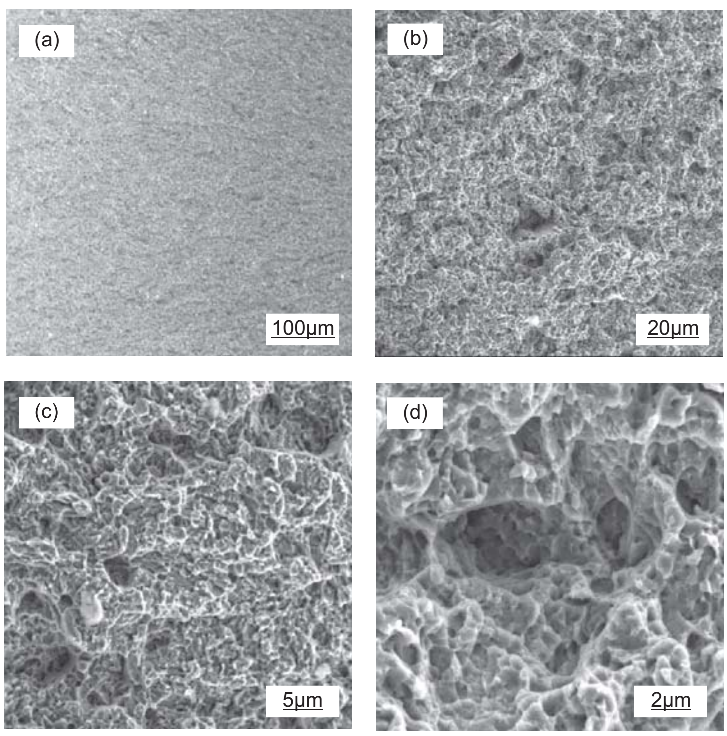

Figure 10. Scanning electron micrographs of PremoMet 290 deformed under impact following exposure in liquid nitrogen at – 180^{o}C, showing:

(a) Overall morphology of failure as damage radiates outward from the notch.

(b) The region adjacent to the notch showing a healthy population of fine microscopic voids.

(c) High magnification of (b) showing the morphology and shape of the microscopic voids.

(d) An array of fine microscopic cracks on the overload fracture surface.

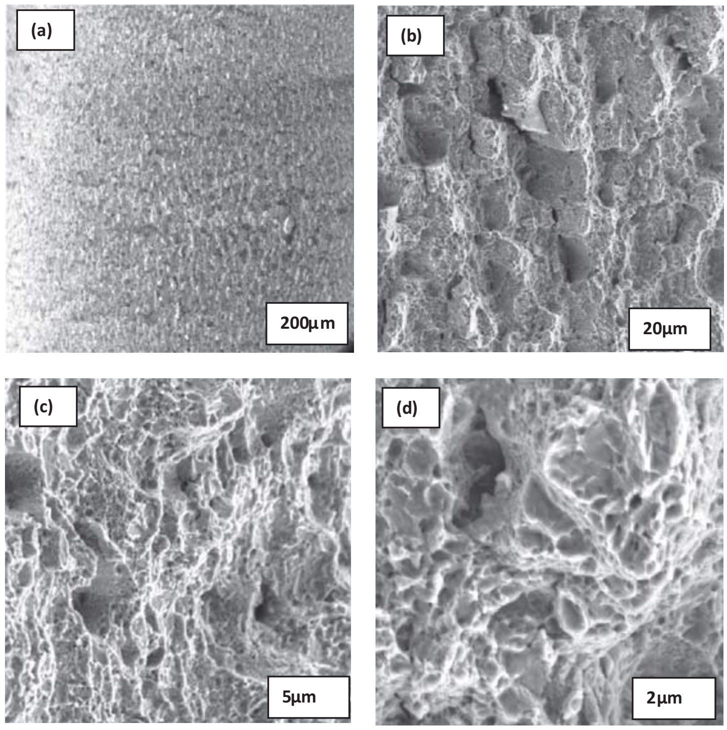

Figure 11: Scanning electron micrographs of PremoMet 290 deformed under impact in the room temperature (25°C) laboratory air environment, showing:

(a) Overall morphology of failure
(b) The region adjacent to the notch showing a healthy population of fine microscopic voids and isolated microscopic cracks.
(c) High magnification of (b) showing the morphology, size and Distribution of the microscopic voids.
(d) High magnification observation of (c) showing shallow nature and distribution of the dimples intermingled with fine microscopic voids.

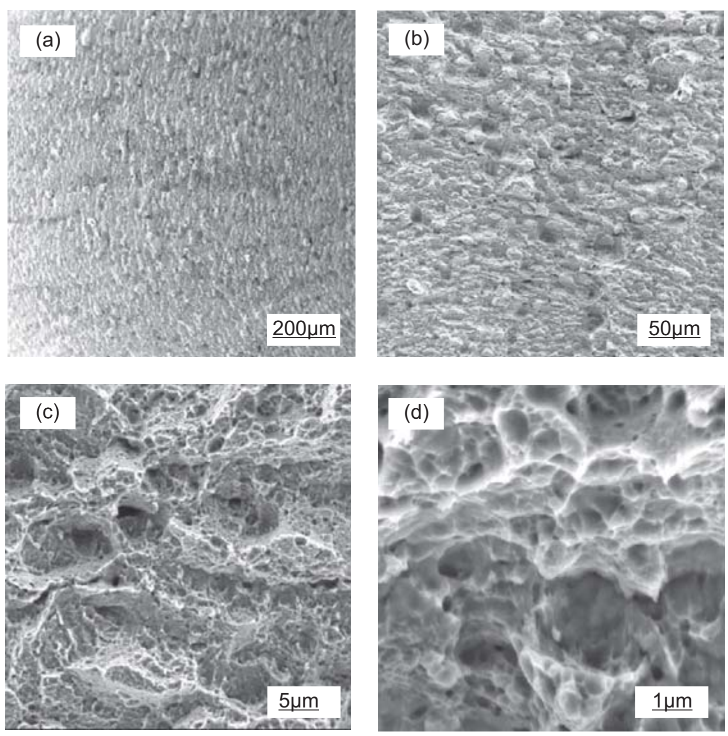

Figure 12: Scanning electron micrographs of PremoMet 290 deformed under impact following exposure in a furnace 170°C, showing:

(a) Overall morphology of the impact fracture surface.
(b) The region adjacent to the notch showing features reminiscent of ductile and brittle failure mechanisms.
(c) An array of fine microscopic cracks intermingled with microscopic voids.
(d) The size, shape and shallow nature of the dimples in the region away from the notch tip.

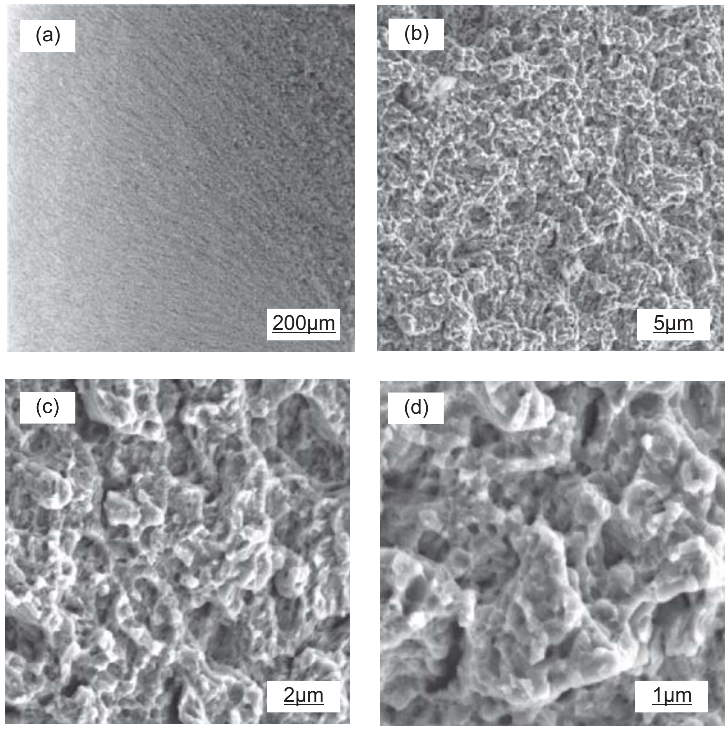

Figure 13: Scanning electron micrographs of Tenax™ 310 deformed under impact following exposure in liquid nitrogen at – 180°C, showing:

(a) Overall morphology of the fracture surface.
(b) High magnification in the region adjacent to the notch tip.
(c) High magnification of (b) showing a healthy population of microscopic voids, dimples and microscopic cracks.
(d) Shallow nature of the dimples and coalescence of microscopic voids to form microscopic cracks.

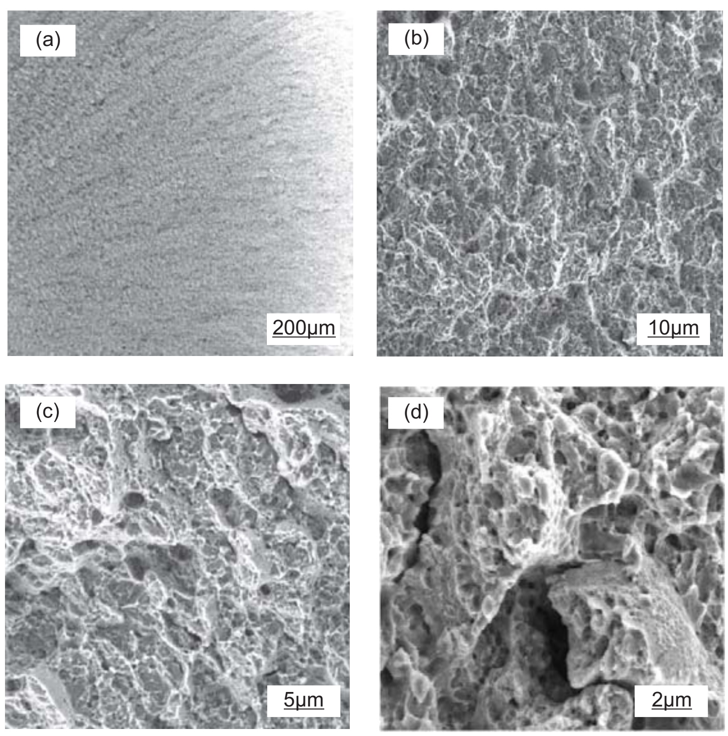

Figure 14: Scanning electron micrographs of Tenax™ 310 deformed under impact in the room temperature (25°C) laboratory air environment, showing:

(a) Overall morphology of the fracture as it radiates outward from the notch tip.
(b) High magnification showing the features adjacent to the notch.
(c) High magnification of (b) showing the size and distribution of the microscopic voids.
(d) Macroscopic cracks surrounded by population of fine microscopic voids and dimples.

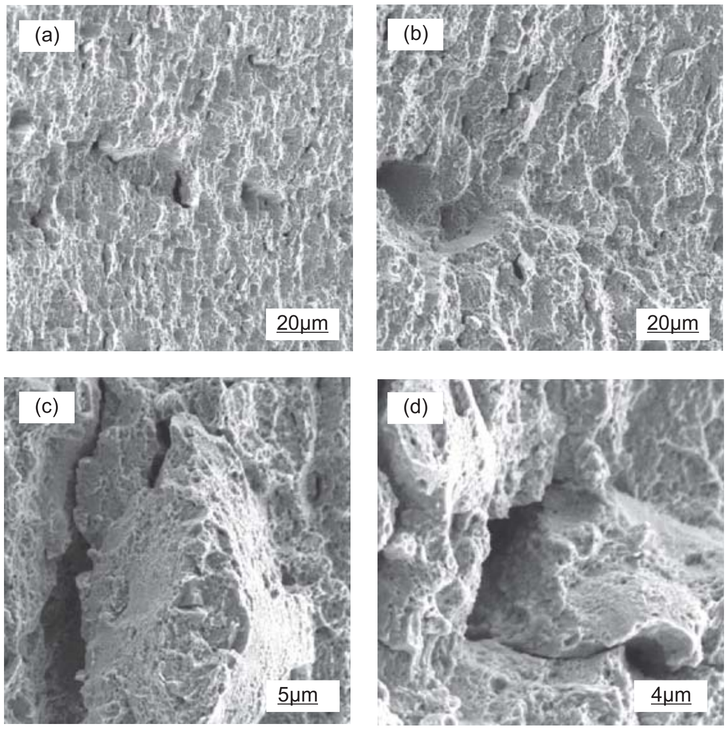

Figure 15: Scanning electron micrographs of Tenax™ 310 deformed under impact following exposure in a furnace at 170°C, showing:

(a) Overall Morphology of the fracture surface.
(b) The region immediately adjacent to the notch showing a population of microscopic cracks, microvoids and shallow dimples.
(c) High magnification of (b) showing profile of a typical microscopic cracks.
(d) Distinct macroscopic crack in the region away from the notch tip.

4.3.4 IMPACT FRACTURE OF TENAX™ 310 The fracture surface features of the CVN test sample that was dynamically deformed at the lowest test temperature of -180°C are shown in **Figure 13.** Overall morphology of fracture was essentially smooth and radiating outward from the root of the notch (**Figure 13-a**). High magnification observation in this region, immediately adjacent to the notch tip, revealed a large population of dimples intermingled with both macroscopic and fine microscopic voids, features indicative or suggestive of 'locally' operating ductile failure mechanisms (**Figure 13-b**). Continued high magnification observation of this region revealed a sizeable population of microscopic voids, dimples of varying size and shape, and an isolated distribution of microscopic cracks (**Figure 13-c).** The dimples were shallow in nature. The limited growth and eventual coalescence of the closely spaced microscopic voids resulted in the formation of isolated microscopic cracks; few and far in-between (**Figure 13-d**).

The fracture surface morphology and intrinsic microscopic features of this alloy steel sample deformed at room temperature (25°C) are shown in **Figure 14**,. At low magnification revealed the damage to radiate outward from the tip of the notch (**Figure 14-a**). Gradual high magnification observation in the region of the notch revealed a combination of voids, shallow dimples and randomly distributed fine microscopic cracks (**Figure 14-b**). At gradually increasing magnifications this region also revealed the size, distribution and morphology of the microscopic voids (**Figure 14-c),** features which are reminiscent of locally operating ductile failure mechanisms. In the region at a distance from the notch tip and approaching overload the fracture surface revealed macroscopic cracks surrounded by a noticeable population of fine microscopic voids and dimples (**Figure 14-d**); these features again indicative of locally operating brittle and ductile failure mechanisms.

The fracture surface features of the CVN test sample that was deformed under conditions of impact at the highest test temperature (180°C) are shown in **Figure 15.** Overall morphology of the fracture surface was essentially flat and quite similar to the surface of the test sample deformed at the lowest test temperature (-170°C) (**Figure 15-a**). The region immediately adjacent to the notch when viewed at gradually increasing magnifications of scanning microscope revealed a sizeable population of microscopic cracks, microscopic voids of varying shape intermingled with a sizeable population of shallow dimples (**Figure 15-b**). The presence of these features is indicative of the locally operating ductile and brittle failure mechanisms. The profile or shape of a typical microscopic crack observed in this region is shown in **Figure 15-c**. In the region of ductile 'tearing; microscopic cracking was observed to be the dominant fracture and covered a sizeable portion of the fracture surface in this region **(Figure 15-d).** The presence of these fine microscopic cracks is clearly indicative of locally brittle failure mechanisms. The transgranular region immediately adjacent to the macroscopic cracks was either flat or covered with pockets of shallow dimples. The impact energy absorbed by this test sample is 2.4 times greater than the energy absorbed by the CVN test sample deformed at the lowest test temperature (-180°C).

5. CONCLUSIONS

In this study the influence of test temperature on impact toughness property and fracture behavior of four high strength steels having varying chemical composition and processing history was investigated. The following are the key findings.

1. The initial microstructure of all four high strength steels revealed varying amounts of martensite and ferrite.

2. Charpy impact tests on each of the chosen high strength steel were conducted at temperatures ranging from -180°C to +170°C. Each of the chosen high strength steels revealed an increase in energy absorbed with test temperature. At a given test temperature the difference in energy absorbed between PremoMet 290 and AerMet 100 was noticeably different and dictated by chemical composition. Also, minimum to no difference in energy absorbed between 300M and Tenax™ 310 processed by vacuum arc re-melting.

3. For a given high strength steel the macroscopic fracture mode was flat at all of the test temperatures the surfaces were examined in the scanning electron microscope. At progressively higher magnification the fracture surface revealed a sizeable population of dimples intermingled with fine microscopic voids of varying size and shape and isolated microscopic cracks. These features are reminiscent of a predominantly locally ductile failure mechanisms with trace amounts of brittle failure mechanism.

4. Over the entire range of test temperatures examined the overall fracture surface morphology and intrinsic microscopic features observed on the fracture surface was found to be nearly identical for the four high strength steels.

ACKNOWLEDGEMENTS

This research was made possible through material, test samples and limited funding provided by **Carpenter Technology Corporation** (Reading, PA, USA). **Mr. Manigandan Kannan** (*Graduate student*: Department of Mechanical Engineering, The University of Akron) extends thanks and appreciation to the University for providing support through tuition scholarship.

REFERENCES

1. Speich, G.R, Dabkowski, D.S., and Porter, L.F., Metallurgical Transactions, Vol. 4, 1973, pp; 303-315.
2. Innovations in *Ultrahigh Strength Steel Technology*, Proceedings of the 34th Sagamore Army Materials Conference (editors: G.B. Olson, M. Azrin and E.S. Wright), US Army Materials Technology Laboratory, Watertown, MA 1990, pp. 3-65, B.G. Olson.
3. G.B. Olson, M. Azrin, E.S. Wright: *Innovations in Ultrahigh Strength Steel Technology* (Editors), US Army Materials Technology Laboratory, Watertown, MA, 1990, pp. 89-109.
4. Figueroa, D., Robinson, M.J., Corrosion Science 52 (2010) 1593–1602 .
5. Zia Ebrahimi, F., and Krauss, G.: Metallurgical Transactions 14A (1983) 1109–1119.
6. Wood, W.E: Metallurgical Transactions, Vol. 8A, 1977, pp. 1195-1199.
7. Ritchie, R.O., and Horn, R.M.: Metallurgical Transactions, Vol. 9A, 1978, pp. 331-341.
8. Narasimha Rao, B.V., and Thomas, G.: Metallurgical Transactions, Vol. 11A, 1980, pp. 441-457.
9. Zia Ebrahimi, F and Krauss, G.: Acta Metallurgica, Viol. 32, 1984, pp. 1756-1777.
10. Lai, G.Y.: Materials Science and Engineering, Vol. 19, 1975, pp. 153-156.
11. Garrison, W.M., Jr., and Moody, N.R.: Metallurgical Transactions, 1987, Vol. 18A, pp. 1257-1263.
12. Kim, B.C., Lee, S., Lee, D.Y., and Kim, N.J.: Metallurgical Transactions, Vol. 22A, 1991, pp. 1889-1892.
13. Garrison, W.M.: Scripta Metallurgica, Vol. 18, 1984, pp. 583-586.
14. Garrison, W.M.: Metallurgical Transactions, Vol. 17A, 1986, pp. 669-678.G.
15. Linanza, M.A., Romero, J.L., Rodriguez-Illabe, J.M., and Urcola, J.J.: Scripta Metallurgica Materialia, Vol. 32, 1995, pp. 395-400.
16. Linanza, M.A., Romero, J.L., Rodriguez-Illabe, J.M., and Urcola, J.J.: Scripta Metallurgica, Vol. 29, 1993, pp. 451-456.
17. Leap, M.J., and Wingert, J.C.: Metallurgical and Materials Transactions, Vol. 30A, January 1999.
18. *Deformation and Fracture Mechanics of Engineering Materials*, Second Edition, John Wiley and Sons, 1983, R. Hertzberg
19. Online material manual of AerMet steels. Carpenter Technology Corporation, Reading, PA, USA, 2004.
20. Online Material Manual of PremoMet Alloys: Carpenter Technology Corporation, Reading, PA, USA, 2005.

HIGH PERFORMANCE LOW POWER FLIP-FLOP BY USING CONDITIONAL DISCHARGE TECHNIQUE

Jyoti Kohar
E-mail: jyotikohar@gmail.com, Ph. No.- 09891547077
Gurgaon College of Engineering, Bilaspur Tauru Road, Gurgaon(HR), India

Ankit Malik
E-mail: ankitmalik.biet@gmail.com, Ph. No.- 09972720957
CISCO, Cessna Business Park Building 11, Level –G, Bangalore—560087, Karnataka

Vijeta
E-mail: vijetakohar15@gmail.com, Ph. No.- 09343965969
Banasthali University, P.O. Banasthali Vidyapith, Rajasthan – 304022

ABSTRACT

The principle goal of Conditional Discharge Technique for high performance flip-flops is reviewed in terms of power and delay. In this paper high performance flip-flops are categorized in two types namely Conditional Precharge and Conditional Capture flip-flops for reducing the internal switching activity. Application of the Conditional techniques results in improvement of Energy-Delay product and saving of power consumption for quiet input. Conditional Discharge flip flop results in generating less glitch at the output with small D-to-Q delay. Power consumption is reduced by avoiding unnecessary internal node transition. In this paper a comparison summary of recent results of flip-flop characteristics is also reviewed. Conditional Discharge technique is most suitable for VLSI system design.

Keywords: *Digital CMOS, flip-flop, low power, very large scale integration (VLSI).*

1. INTRODUCTION

Power consumption in high-performance integrated circuits has been one of the most serious limitations in high-performance designs recently. Power optimization techniques are applied in different levels of digital design. In order to optimize the power dissipation of digital systems low-power methodology should be applied throughout the design process. VLSI designers have used speed of the circuit as the performance metric. Two conflicting constraints in this field are high performance and small area. But now a day's power dissipation is becoming an important in a design. Low power design is a new era in VLSI technology. Low power design is used for portable applications such as wristwatches and pacemakers as well as to reduce the power of high performance systems. Systems with high clock frequency are emerging with improved operation speed and large integration density. Low power design basically deals with power estimation, its analysis and power minimization [1].

There are number of flip-flops techniques with internal activity gated upon the actual requirement to carry out signal transition. These conditional techniques based on clock pulse generation [2].The flip-flop's output is checked and the transition is allowed only if it is used to change the value of output. The choice of flip flop and its design has a profound effect in decreasing the power dissipation. A wide selection of different flip-flops is found in the literature[3-8].Pulse triggered flip-flops are better than master slave flip-flops in performance due to timing issues.

The components of sequential circuit in a CMOS circuit are considered as major factors to the power dissipation since one of the input in it of certain component is the clock which is the only signal that switches all the time. According to the recent studies, clock signal in digitals computers consume a large percentage (15%-45%) of the system power. So by reducing the power dissipation, we can reduce the power dissipation to a greater extent in digital VLSI circuits. This goal can be achieved by two means. Firstly by eliminating the waste power dissipation caused by switching the clock in non triggering direction. Secondly, to block the clock signal feeding into the flip-flops during their holding states so as to reduce the power dissipation. To reduce the power consumption in flip-flops Conditional capture, clock-on-demand ,data transition look-ahead techniques have been developed.

2. CONDITIONAL TECHNIQUES FOR LOW POWER AND HIGH PERFORMANCE DESIGN

One effective technique to obtain power saving in case of flip-flops is based on the utilization of dynamic structure. Lots of power is wasted in flip-flops which are using dynamic behavior due to the internal switching activity. By reducing the unnecessary switching activities, we can reduce the overall power dissipation. So to reduce the internal switching activities, we can use two techniques namely Conditional precharge technique and Conditional capture technique.

Conditional capture flip-flop has been developed to reduce the power consumption in internal nodes of a no. of high performance flip-flops. Major advantage of CCFF is that there is no speed penalty. Setup time of CCFF is increased in comparison to Hybrid Latch Flip-Flop (HLFF).There are two main reason behind it. First is the large recovery time on the node Q and second is increase in sampling time for capturing input 'Low'. Many additional transistors are needed in Condition capture technique for some flip-flops like Semi-Dynamic Flip-flop(SDFF).Conditional Precharge Flip-Flop(CPFF) was proposed by Nedovic. In this technique internal node precharging is determined by the output signal. CPFF has large setup time similar to CCFF. To solve this problem improved version of CPFF was introduced without consumption cost. A new technique Conditional discharge technique is also used for the same purpose. This technique will overcome the limitations of the techniques discussed above. This paper reviews all these three Conditional techniques. In literature many techniques are discussed [9-10].

3. CONDITIONAL PRECHARGE TECHNIQUE

In this technique the discharging path is controlled to avoid the precharging of the internal node when the input remains high as shown in fig 1 which depict the general scheme of Conditional precharge technique.

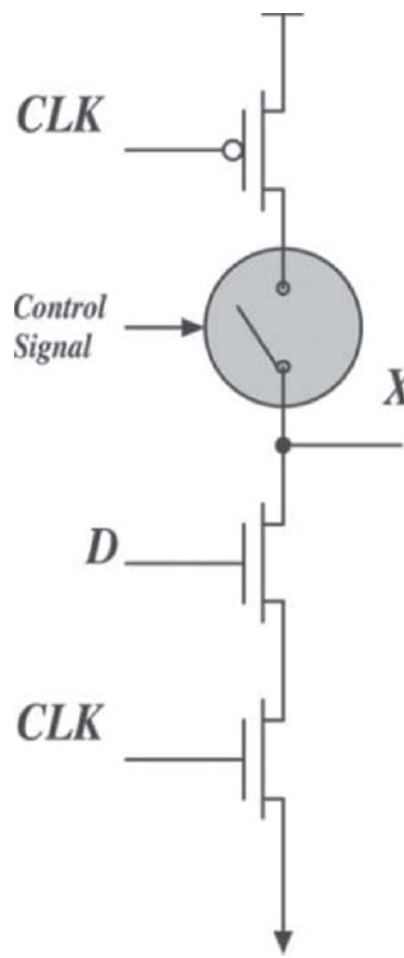

Fig. 1 Conditional precharge technique.

To sort out these charging and discharging activities a simple pmos transistor is used in the precharging path. This flip-flop cause higher setup time for high-to-low transition. A no. of flip-flops used this technique. For example CPFF [2],DE-CPFF[9] and CP-SAFF[11].The controlling signal is the output Q in case of CPFF and dual edge clocking conditional precharge flip-flop (DE-CPFF) and in CP-SAFF ,the control signal is the input D.

4. CONDITIONAL CAPTURE TECHNIQUE

This technique is very attractive in terms of high performance VLSI implementation. The purpose of Conditional Capture technique is that to derive the internal nodes significant portion of the power is consumed and the output remain the same. By disabling the redundant internal transtion, it is possible to achieve significant power reduction. Two types of Conditional Capture technique have been discussed in [5] namely single ended and differential implementation. The main disadvantages of this technique is related to increased in setup time for zero sampling time. So setup time is the limiting performance parameter. Conditional Capture technique is totally based on clock gating idea. This technique is shown in fig 2. Conditional Capture technique is mostly used for implicit pulse triggered flip-flop, for example CCFF. In this flip-flop, a transparency window is used for the sampling of the input. Transparency window is determined by the time when both transistor are on at the same time. The output depend on the input means output Q will be high when input is high.

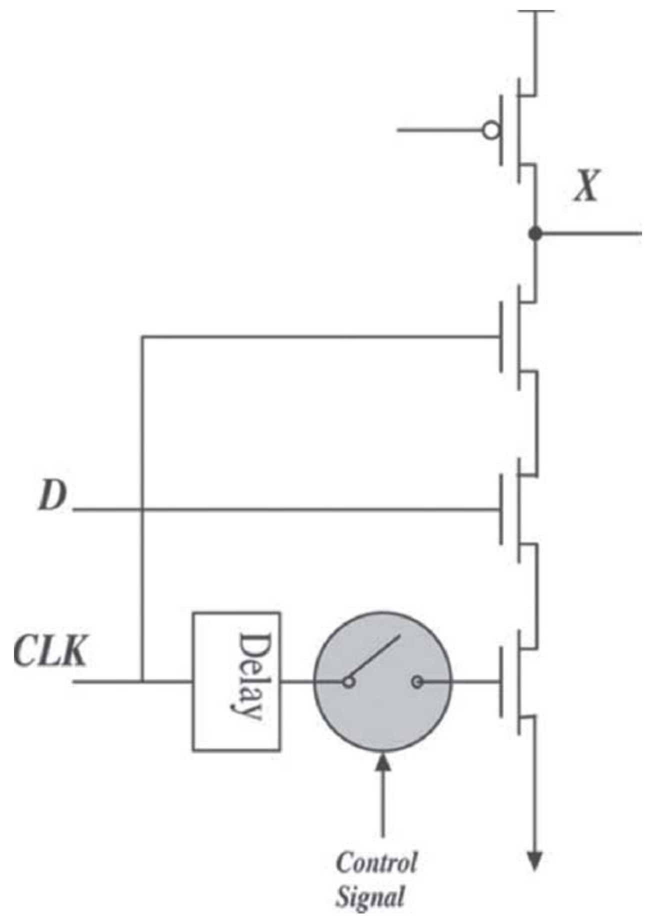

Fig. 2. Conditional capture technique.

Clock gating in the Conditional Capture technique results in redundant power consumption. Conditional Precharge technique is better than Conditional Capture technique in terms of Energy-Delay-Product(EDP) means it reduce the EDP. But Conditional Precharge technique can only be applied to ip-FF.

5. CONDITIONAL DISCHARGE TECHNIQUE

Power saving approach ,clock-gating used in Conditional Capture Technique results in redundant power consumed by the gate controlling the delivery of the delayed clock to the flip-flop and Conditional Precharge Technique can only be applied to implicit flip-flop. So to overcome these limitation of these technique, a new technique, Conditional Discharge Technique is used. This technique can be used for both implicit as well as explicit pulse triggered flip-flops.This technique is used to present a new flip-flop Conditional Discharge flip-flop. Conditional Discharge Technique controlled the discharge path,when input is stable(High) and eliminate the extra switching activity. CDFF use a pulse generator which is suitable for double edge sampling.CDFF has two stages.

First is responsible for capturing the Low-to-High transition and second stage captures the High-to-Low input transition. CDFF features less switching noise generation which is very important issue in mixed signal circuits.

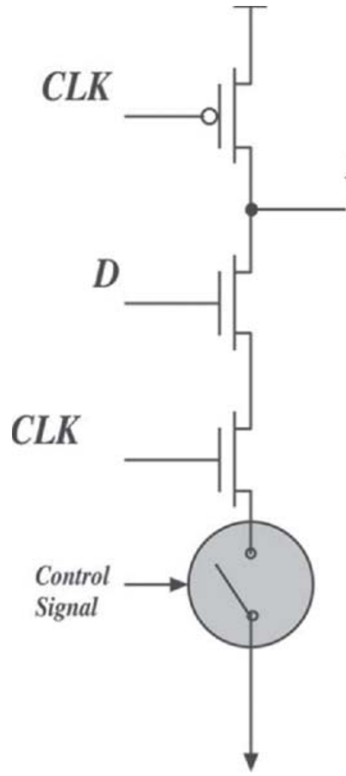

Fig. 3. Conditional Discharge technique.

6. COMPARISON OF POWER SAVING TECHNIQUES

There are no. of different approaches to reduce the power consumption for various clocking schemes. Flip-Flop design plays an important role in reducing cycle time and power consumption.

1) Statistical power reduction flip-flops reduce the power consumption by removing redundant internal node switching.
2) Small swing clock flip-flops reduce the power consumption by reducing the clock voltage swing.
3) Clock frequency of Double edge triggered flip-flop(DETFF) can be reduced to half and hence the clock network power can be reduced by half.
4) Clocking-Gating is very widely used technique. It can reduce power consumption in flip-flop, clock network and combinational block. Single phase clocking can save clock tree power consumption by 30% compared to two phase clocking [12].Logic embedding capability inside the flip-flop can reduce the power and overall delay.
5) Clock tree topology and no. of clock buffers inserted should be optimized to reduce skew and power consumption.

7. CONCLUSION

Power estimation and optimization are needed to formulate a low power design, which is required for current and future VLSI design. In this paper conditional internal activity flip-flop technique are reviewed. A new technique, Conditional discharge is also reviewed. It reduces the switching activity of some internal nodes in flip-flop. This technique is applied to new flip-flop named CDFF. The Conditional Discharge Technique could be applied to implicit pulsed flip-flops like ip-DCO and HLFF. Comparison of some power saving technique is also summed up. Conditional Technique is suitable for the application in the high performance VLSI circuits in future.

REFERENCES

1. Singh D., Rabaey J. M., Pedram M., Catthoor F., Rajgopal S., Seghal N. and Mozdzen T. J., Power conscious CAD tools and methodologies: A perspective Proc. of the IEEE,83(4):570-593,1995.

2. Nedovic N., Oklobdzija V.G.,"Hybrid latch flip-flop with improved power efficiency",Proceedings of SBCCI, p211-215,September 2000.

3. Kawaguchi H. and Sakurai T., “A reduced clock-swing flip-flop (RCSFF) for 63% power reduction,” *IEEE J. Solid-State Circuits*, vol. 33, pp. 807–811, May 1998.

4. Ko U. and Balsara P. , “High-performance energy-efficient D-flip-flop circuits,” *IEEE Trans. VLSI Syst.*, vol. 8, pp. 94–98, Feb. 2000.

5. Kong B., Kim S., and Jun Y. , “Conditional-capture flip-flop for statistical power reduction,” *IEEE J. Solid-State Circuits*, vol. 36, pp. 1263–1271, Aug. 2001.

6. Partovi H., Burd R., Salim U. , Weber F., DiGregorio L., and Draper D., “Flow-through latch and edge-triggered flip-flop hybrid elements,” in *Proc. Dig. ISSCC*, Feb. 1996, pp. 138–139.

7. Klass F., Amir C., Das A., Aingaran K., Wang C., Truong R. , Mehta A., Heald R., and Yee G., “Semi-dynamic and dynamic flip-flops with embedded logic,” in *Proc. Symp. VLSI Circuits, Dig. Tech. Papers*, June 1998, pp. 108–109.

8. Nedovic N., Aleksic M., and Oklobdzija V.G., “Conditional precharge techniques for power-efficient dual-edge clocking,” in *Proc. Int. Symp. Low-Power Electronics . Design*, Monterey, CA, Aug. 12–14, 2002, pp. 56–59.

9. Horowitz M., *“Low-Power Digital Design”*, Proceedings of the 1994 IEEE Symposium on Low-Power Electronics, 1994.

10. Zhang Y., Yang H., and Wang H.,”Low clock-swing conditional- precharge flip-flop for more than 30% power reduction,”Electron .Lett., vol.36 , no.9 , pp.785-786,Apr.2000.11Markovic D., Nikolic B. and Brodersen R.,”Analysis and design of low-energy flip-flops,” in IEEE Int. Symp. Low-Power Electronics and Design,Aug. 2001,pp. 52-55.

MATHEMATICAL MODELLING OF SOLAR-BASED-INVERTER WITH MAXIMUM POWER POINT TRACKING

Ch.Venketeswara Rao,
Assoc. Professor in EEE, SVECW, Bhimavaram, A.P ; chvr_4581@yahoo.co.in, 09848504581.

Dr. S.S. Tulasi Ram,
Professor in EEE, JNTUK, Kakinada, A.P.

Dr. B. Brahmaiah
Professor and Dean (R&D) in EEE, GEC, Gudlavalleru, A.P.

Prof. B.J.J. Raju
Administration officer in cricket stadium, Vishakhapatnam, A.P.

ABSTRACT

This paper proposes a mathematical model for solar based inverter with maximum power point tracking with approximately 300W of power generation and output voltage of 230V. The proposed structure consists of solar cells, battery, controller, inverter, and load. Additionally, the MPPT is realized by using improved P&O method with adoptive step algorithm. A DC-DC boost converter was chosen to step up the input DC voltage of the PV module while the DC-AC single-phase full-bridge square-wave inverter was chosen to convert the input DC comes from boost converter into AC element. Detailed description about the design and implementation of the proposed battery charger is also discussed. In this paper simple mathematical models are developed for each individual stages of solar inverter. The implementation is done using Matlab/Simulink, a simulation program that provides a graphical interface for building models as solar inverter block diagrams. The solar inverter model has established in this paper based on transfer function modeling which yields the similar performance as the theoretical predictions.

Keywords: *PV module, MPPT, battery charger, Boost converter, H-bridge inverter.*

1. INTRODUCTION

Energy is the most fundamental and essential of all resources. Current forms of energy in use emanate from the fission and fusion of atomic nuclei or from energy stored in the earth. The problem with both fission and fusion is that they have dangerous radioactivity and side effects. As a result, most of the production of energy in modem society is heavily dependent on very limited supplies of non-renewable resources, particularly fossil fuels. As the world's energy demands rise and resources become scarce the utilization of clean natural primary energies such as solar radiation and wind power will have to be deployed in the future. In an age of environmentally friendly energy use, this is a major imperative.

When electrical energy is generated from fossil resources, the conversion efficiency is important, as the resources are limited and costly, when the primary energy such as solar energy is used; the challenge is different [4]. The radiation energy converted into electrical energy has to be maximized while the conversion efficiency becomes less important.

As reported in [1] this topology can be used in high power ranges providing high system flexibility. A power conditioning system linking the solar array and the utility grid is needed to facilitate an efficient energy transfer between them; this implies that the power stage has to be able to extract the maximum amount of energy from the PV and to assure that the output current presents both low harmonic distortion and robustness in front of system's perturbations.

In order to extract the maximum amount of energy the PV system must be capable of tracking the solar arrays maximum power point (MPP) that varies with the solar radiation value and temperature. Several MPPT algorithms have been proposed, namely, Perturbation and Observation (P&O), incremental conductance, fuzzy based algorithms, etc. They differ from its complexity and tracking accuracy but they all required sensing the PV current and/or the PV voltage. In the present document a MPPT algorithm based in the one presented in [10] is proposed.

Then, regarding the proper DC-DC boost converter was chosen to step up the input DC voltage of the PV module while the DC-AC single-phase full-bridge square-wave inverter was chosen to convert the input DC comes from boost converter into AC element. DC-AC conversion, using sliding mode control described in [2] shows good performance in front of input voltage and load perturbations. This paper presents the control design of a solar inverter for PV-grid connected systems, gathering all the advantages of a string inverter topology. Finally, a comparison of transfer function modeling which yields the similar performance as the theoretical predictions.

This paper is organized as follows. The modular structure of the PV inverter is presented in section II. Section III shows the validation of the theoretical predictions by means of Matlab/Simulink simulations. Also conclusions of the work are reported in section III and results are discussed in section IV.

2. MATHEMATICAL MODEL

Figure 1 show the basic structure, which consists in the connection of three cascaded stages. The first stage is a step boost converter-based loss-free resistor with maximum power point tracking. The second stage uses to transforms a dc voltage into a fully rectified current of 100 Hz. The H-bridge performs the dc-ac conversion and subsequently a 50 Hz transformer with a 1:13 transformer ratio provides the connection to the mains. And also a battery backup connected to a Voltage step up boost converter.

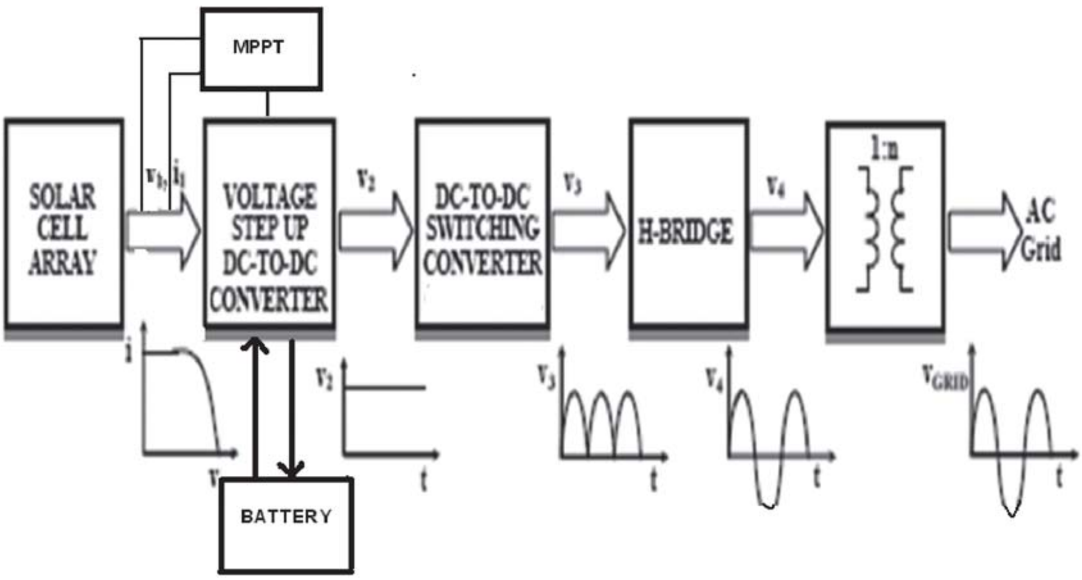

Fig. 1. Block diagram of a solar inverter

2.1 SOLAR CELL ARRAY MODEL According to physical structure and output characteristic of solar cell, we have easy access to mathematical model. Solar cell is actually a p-n junction, which characteristic is similar to diodes. The various parameters of the solar cell are modeled as follows (see Fig. 2) [6]. The current source generates the photocurrent Iph, which is proportional to the solar irradiation.

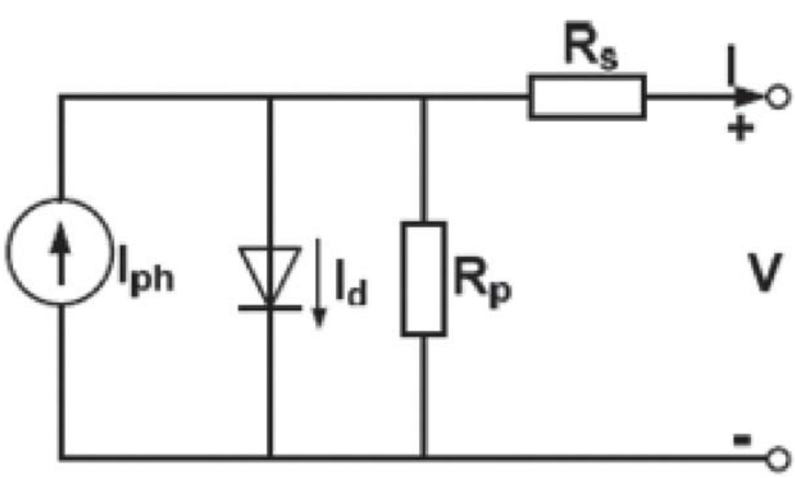

Fig. 2. Equivalent circuit of a solar cell

MODELING OF PHOTOVOLTAIC GENERATION:

Photovoltaic cell is a non-linear device and can be represented as a current source in parallel with diode as shown in the circuit in Fig. 1 (Villalva et al., 2009).

The practical PV cell model includes the connection of series and parallel internal resistance, namely R_s and R_p, which is expressed as the following equation:

$$I = I_{Pv,cell} - I_o[exp(V + R_a\, I|V_t a) - 1] \quad (1)$$

where: I = the photovoltaic output current
V = the photovoltaic output voltage
V_T = KT/q =26mV at room temperature

K=Boltzmann's constant ($1.38*10^{-23}$ joules/Kelvin's.)
q = electron charge ($1.6*10^{-19}$ coulombs)
T = absolute temperature in Kelvin's

The is the light generated current produced by a photovoltaic cell which has a linear relationship with the solar irradiance and temperature, as shown in the following equation:

$$I_{Pv,cell} = (I_{Pv,n} + K_i\,\Delta T)\,\frac{G}{G_n} \quad (2)$$

where, $I_{PV,n}$ is the light generated current at the nominal condition which are 25°C and 1000 W m ^{2}, $\Delta T = T\text{-}T_n$ where T and T_n is the actual and nominal temperature in unit Kelvin, K respectively. While G (W m ^{2}) is the solar irradiation by the PV surface and G_n is the nominal solar irradiation (Villalva et al., 2009).

Table 1: The electrical characteristic of BP340 PV module

Parameter	**Variable**	**Value**
Maximum power	Pmpp	85 W
Voltage at P_{max}	Vmpp	17.3 V
Current at P_{max}	Impp	5 A
Short-circuit current	ISC	2.54 A
Open-circuit voltage	VOC	20 V
Temperature coefficient of open-circuit voltage	K_v	-(80±10) mV/°C
Temperature coefficient of short-circuit current	Ki	(0.065±0.015)%/°C

The diode saturation current, I_0 and its dependence on the temperature may be expressed by:

$$I_o = \frac{I_{sc,n} + K_i\,\Delta T}{exp\left(\dfrac{V_{oc,n} + K_v \Delta T}{a V_t}\right) - 1} \quad (3)$$

where K_v and K_i is the open-circuit voltage/temperature coefficient and the short-circuit current/temperature coefficient. While I_{SC} and $V_{OC,n}$ are the short-circuit current and open-circuit voltage under the nominal condition respectively. The BP340 solar module is chosen for the PV module modeling. The electrical characteristics given by datasheet are shown in Table 1. This module consisting of 36 cells connected in 2 parallel strings. The model of PV module was implemented in MATLAB/Simulink using Eq.(3). The model yields the PV current I, using the electrical parameter of the module (I_{SC}, V_{OC}) and the variables Voltage, Irradiation (G) and Temperature (T) as the inputs to the model.

The simulated I-V and P-V characteristic curves are shown in the Fig. 3 and 4 respectively, where the model is simulated for a series of solar irradiances and different temperatures. The results show that the PV module is capable of reproducing the electrical characteristics as mentioned in Table 1.

2.2 VOLTAGE STEP-UP STAGE WITH MPTT FUNCTION This stage has two objectives, i.e., absorbing the maximum power from the solar panel and step-up the voltage in order to decrease the conduction losses. Note that the impedance matching in a solar is the electronic function that imposes the panel operation at the maximum power point. The impedance matching is performed by a loss-free resistor.

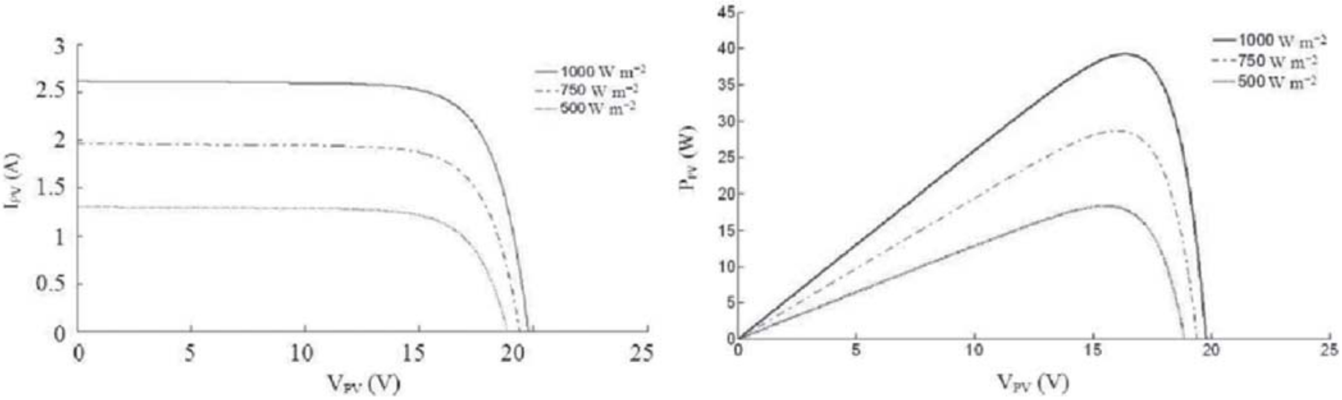

Fig. 3: PV module characteristic curves plotted under different irradiances, (a) I-V curve; (b) P-V curve

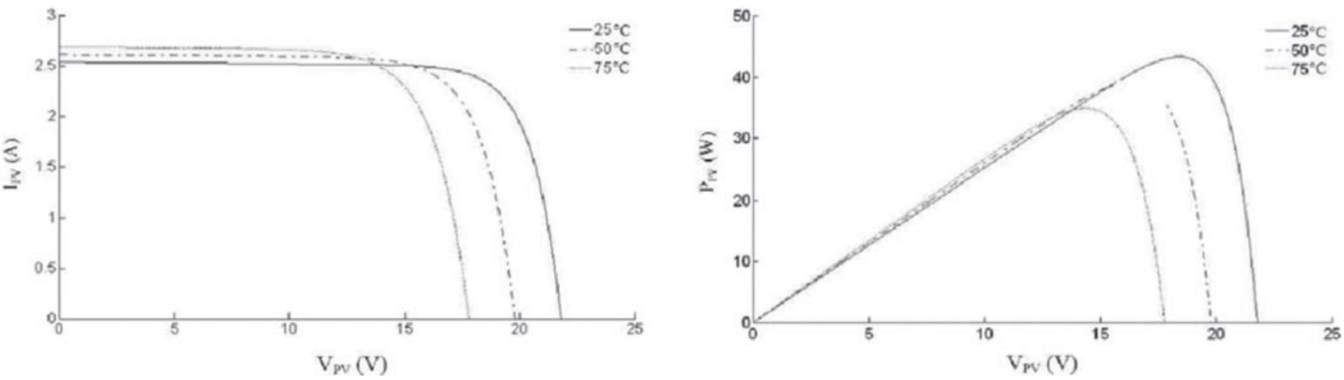

Fig. 4: PV module characteristic curves plotted for different temperatures, (a) I-V curve**;** (b) P-V curve

It was shown in 2 that the boost converter can behave as a loss-free resistor due to the action of a sliding-mode control loop. In this case, the goal is to design a converter structure whose steady–state equations at their input and output ports are the following

$$V_o = \frac{1}{1-D} V_{in} \tag{4}$$

Where D is the duty ratio of a converter, Vo and Vin are the input and output voltages of converter. Figure 5 shows the block diagram of a DC-to-DC switching converter with a sliding-mode regulation loop with sliding surface

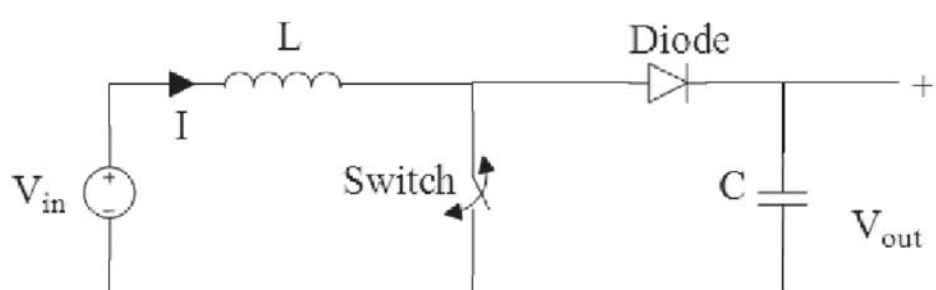

Fig.5: The schematic diagram of a Boost converter

2.3 MPPT CONTROL APPROACH The objective of maximum power point racking is to move the solar array operating voltage close to the maximum power point under changing atmospheric conditions in order to draw the maximum power from the array. This maximum power point is positioned at the operating solar array voltage that is necessary to extract maximum power from the array. Under varying conditions, there is only one point of operation that will extract maximum power. The variation of its position under changing settings emphasizes the need for a power-tracking algorithm for increased efficiency. Maximum power point tracking is also used to provide a constant voltage as required by the load. Figure.6. shows the maximum power point tracking algorithm by perturbation and observation method. This method is used for system accuracy.

2.4 DC-DC BUCK SWITCHING CONVERTER The aim of this stage is to transform the DC voltage at the output of the LFR into fully rectified sinusoidal waveform of 100 Hz. A buck converter acting as a G-semi-gyrator with controlled output current is used to perform the transformation.

A power gyrator is a two-port element characterized by the following equations

$$I_1 = g\,V_2 \tag{5}$$

$$I_2 = g\,V_1 \tag{6}$$

where V_1, V2, I1, and I2 are respectively the steady-state average values of input voltage, output voltage, input current and output current.

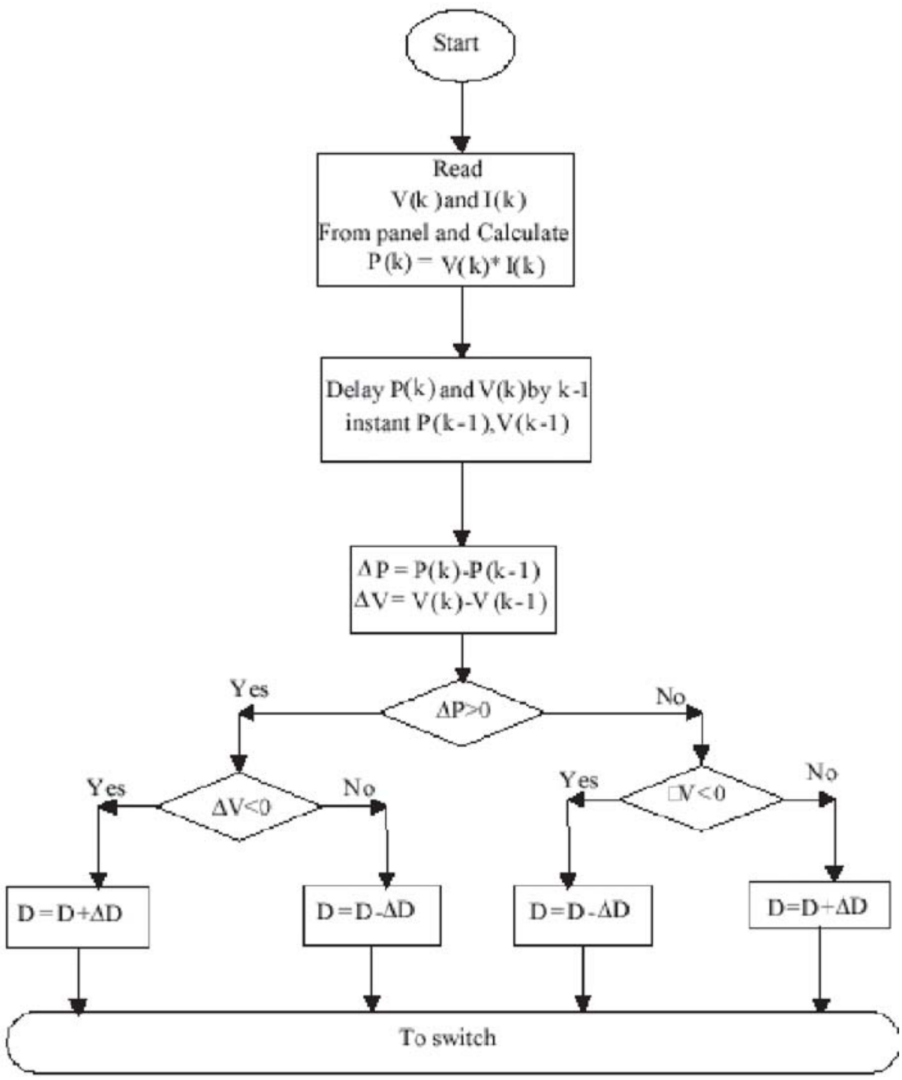

Fig.6: The flowchart of P and O MPPT algorithm

A classification and synthesis of power gyrators was presented in [9] where the notion of semi-gyrator was also defined. Note that a semi-gyrator satisfies the same Eq. (3) and Eq.(4) than the gyrator but the current can be discontinuous in either the input or output port. Thus, a semi-gyrator of type G with controlled output current has a pulsating input current whose steady-state average value is proportional to the steady-state average output voltage and whose output current is a continuous function with a steady–state value proportional to the DC input voltage. Figure.7 illustrates the block diagram of a semi-gyrator of type G with controlled output current where the gyrator conductance g is a fully rectified sinusoidal waveform of 100 Hz. Therefore, the output current will be proportional to the input voltage, the proportionality constant being a time-varying function g (t) .Since g (t) is a fully rectified waveform, the output current will have the same shape and its amplitude will depend on both g (t) and input voltage whose value will in turn depend on the power supplied by the PV panel.

The semi-gyrator is implemented by means of a buck converter as the one shown in Figure5 due to efficiency reasons. The buck converter can be described by the following set of differential equations:

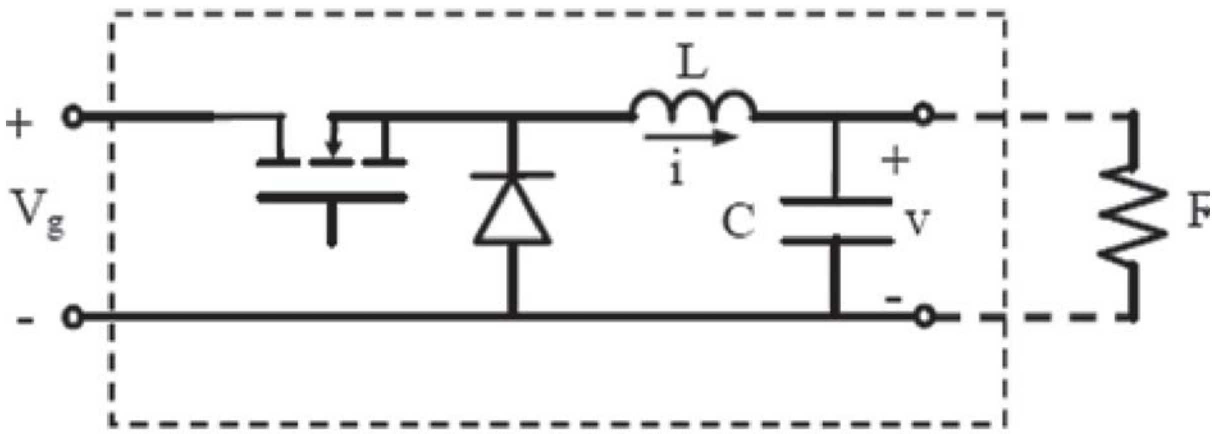

Fig. 7: Schematic diagram of a DC-DC buck converter

$$\frac{di}{dt} = \frac{V_g}{L} u - \frac{v}{L} \tag{7}$$

$$\frac{dv}{dt} = \frac{i}{C} - \frac{v}{RC} \tag{8}$$

where u is a control variable characterized by u = 1 during Ton and u = 0 during T off.

2.5 H-BRIDGE AND GRID CONNECTION Figure 8 shows the configuration of an H-bridge, which is used to perform the conversion of the DC fully Rectified sinusoidal current of 100 Hz at the gyrator output port into a sinusoidal voltage of 50 Hz which eventually is delivered to the grid by means of a low frequency transformer.

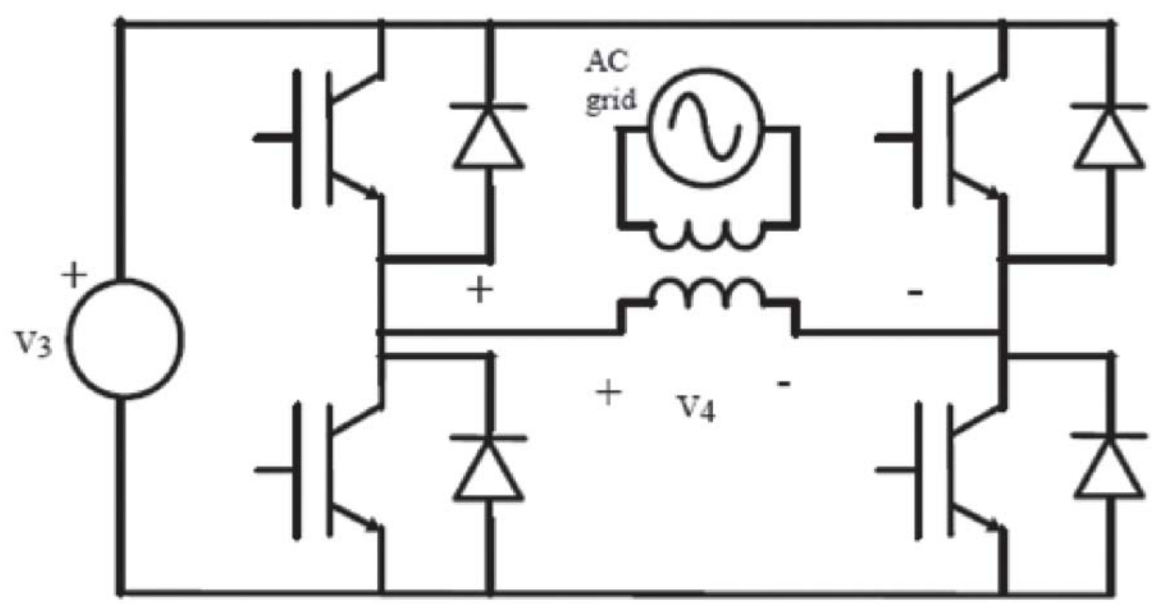

Fig.8: H-bridge and grid connection

3. SIMULATION RESULTS

In this section, Matlab/Simulink simulations of each stage of the PV sinusoidal inverter depicted in figure 1 are presented. Figure 9 illustrates the simulation scheme used for the proposed solar inverter structure. The simulation parameters for boost-based LFR are L_{BOOST}=170µH, C_{BOOST} = 20mF. The output capacitance of the LFR has to ensure the energy supply during a specified time elapse in case that a sudden break of the solar energy supply is produced. One of the objectives of the design is that the grid connection will result in minimum perturbations to the mains. The buck converter based semi-gyrator has an inductance L_{BUCK} =150µH. In both converters the variable switching frequency has been limited to 200 kHz by means of a hysteretic comparator .The solar panel model employed in the simulation has open -circuit voltage of 20V , a short-circuit current of 5A and a maximum power of 85 W .

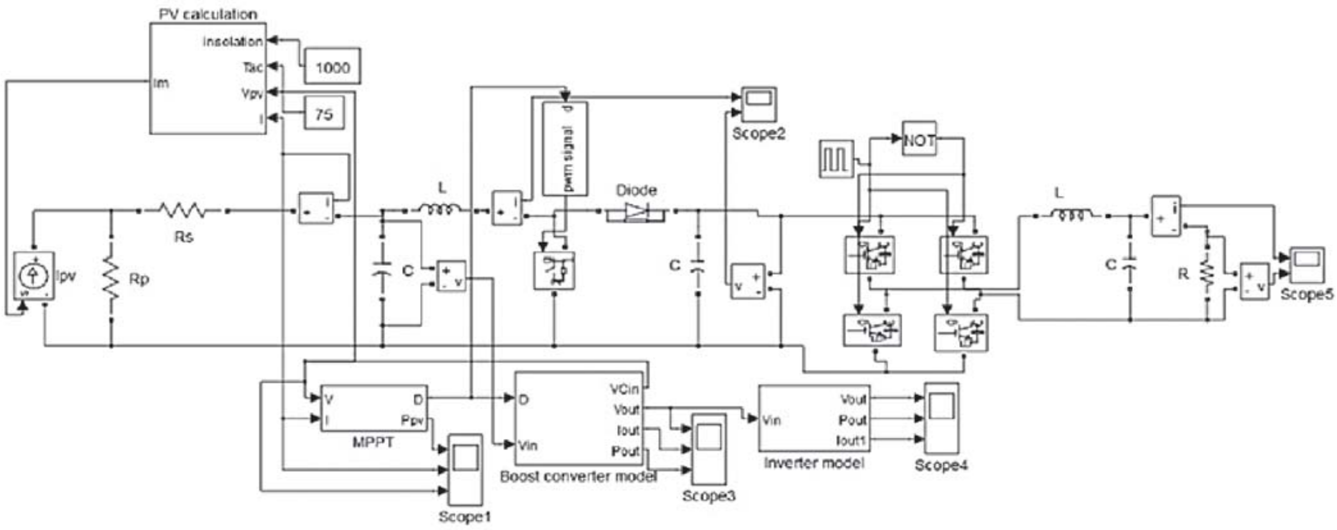

Fig.9: The circuitry photovoltaic system developed in MATLAB/Simulink

Figure.10 illustrates the power delivered by the solar panel, the LFR output voltage, the semi-gyrator output current, the grid voltage and the current supplied to the mains assuming a constant irradiance and a maximum power of 62 W.

Figure.11 depicts the start–up of both LFR and semi-gyrator. It can be observed that the current delivered to the grid increases proportionally to the LFR output voltage, this corroborating the expected behavior of controlled current-source at the output of the semi-gyrator.

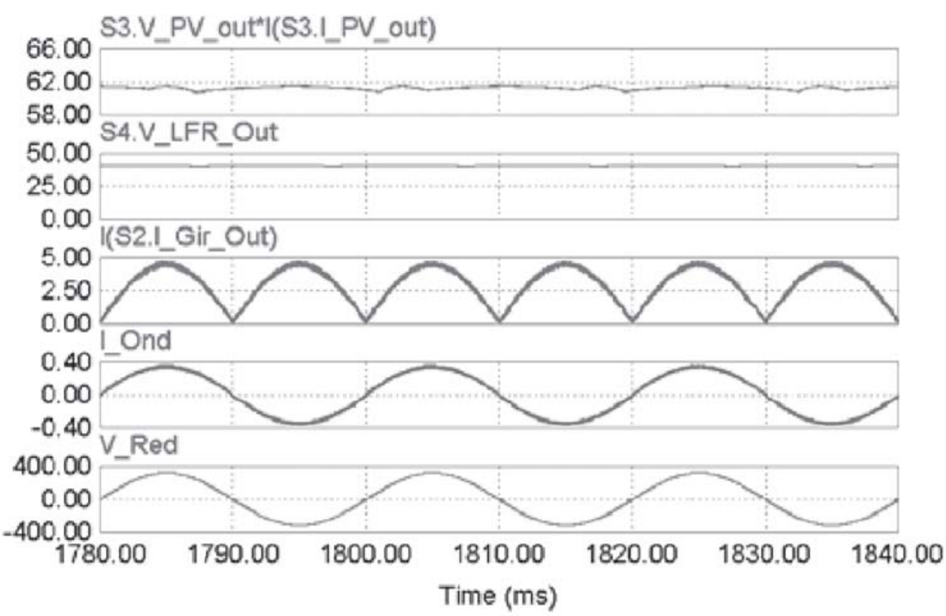

Fig. 10: steady state response of the PV inverter

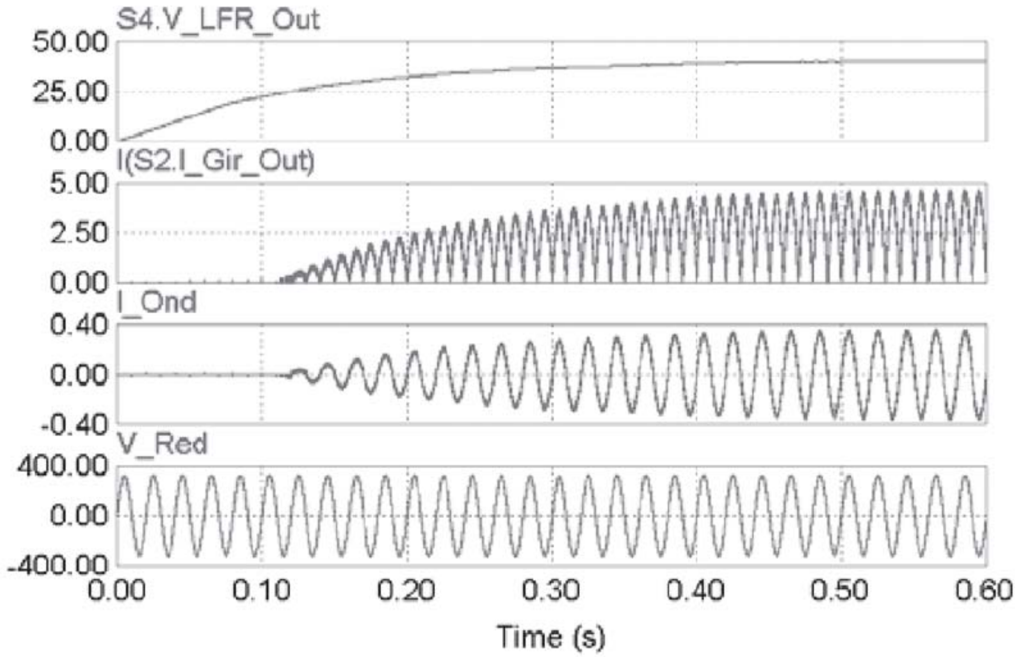

Fig.11 PV inverter start up

4. CONCLUSIONS

The problem of dc-ac conversion in PV systems with grid connection has been studied in this work. A solar inverter structure based on canonical elements for energy processing has been presented. The proposed structure has been validated by means of MATLAB/SIMULINK simulation. The implementation of a prototype with two modules is in progress.

ACKNOWLEDGEMENT

This research was supported by my beloved guides and my collègues.

REFERENCES

1. *A. Cid -Pastor, L. Martínez- Salamero, A. El Aroud and D. Hernando "Analysis of a Modular one – phase pv inverter"*, Escola Technica Superior d'Enginyeria, Universitat Rovirai Virgili, Tarragona, 43007, Spain.

2. Mohd Saifuzam Jamri and Tan Chee Wei: *Modeling and Control of a Photovoltaic Energy System Using theState-Space Averaging Technique"* ISSN 1546-9239 @2010 science publications.

3. *S.* ARMSTRONG, W.G. HURLEY,"*Self regulating Maximum power point tracking for solar energy systems"* Stanley R. Bull "Renewable Energy Today and Tomorrow" Proceedings of the IEEE, Vol. 89, No. 8,August 2001, pp 1216-1226.

4. A. Cid-Pastor, L. Martinez-Salamero, U. Ribes y A. El Aroudi, "Análisis y diseño de un resistor libre de pérdidas basado en un convertidor elevador controlado enmodo deslizante," SAAEI'07, Puebla, Mexico, Septiembre 2007.

5. A. Cid-Pastor, L. Martínez-Salamero, C. Alonso, B. Estibals, J. Alzieu, G. Schweitz, and D. Shmilovitz , "Analysis and design of power gyrators in sliding-mode operation" *IEE Proceedings Electric Power Applications,* Vol. 152, No. 4, July 2005, pp. 821-826.

6. Salhi, R.E.B.M., 2009. Maximum power point tracking controller for PV systems using a PI regulator with boost DC/DC converter.ICGSTACSE.J. 8:2127.http://www.icgst.com/acse/Volume8/Issue3/P11107 10002.pdf.

7. Theocharis, A.D., A. Menti, J. Milias-Argitis and T. Zacharias, 2005. Modeling and simulation of a single-phase residential photovoltaic system. Proceeding of the IEEE Russia Power Tech, June 27-30, IEEE Computer Society, St. Petersburg, and pp: 1-7. DOI: 10.1109/PTC.2005.4524407.

DESIGN AND FPGA IMPLEMENTATION OF FEED FORWARD NEURAL NETWORK FOR FIR FILTER

Mohammed Waseem
M.Tech [VLSI and Embedded Systems], RVCE, Bangalore, Karnataka
E-mail: mohd.was@gmail.com

M.S. Suma
Asst. Prof, Dept of ECE, RVCE, Bangalore, Karnataka
E-mail: sumams@rvce.in

Cyril Prasanna Raj P
Prof. and HOD, Dept of EEE, MSRSAS, Bangalore, Karnataka
E-mail: cyril@msrsas.org

ABSTRACT

Several nonlinear techniques based on neural networks have been developed for designing different kinds of Finite Impulse Response (FIR) filters. The representative technique constructs the energy function of the network, which coincides with the error function of the filter design. When the network converges, it achieves the optimal solution. A circuit for FIR filter is devised by using feedforward neural network. In this approach we formulate the error function in the optimization of the FIR filter as a Lyapunov energy function using which the related parameters are found. By using these parameters and input to the network, the optimal filter coefficients of the FIR filter can be derived when the network achieves its convergence. The proposed approach can achieve a notable reduction both in the amount of computation required and hardware complexity. Simulation results indicate the effectiveness of the proposed approach. In this work, a Simulink model for FIR filter is developed and validated, based on filter input and output feed forward network is trained to minimize error. Optimum weights and biases are obtained; using which Hardware Description Language (HDL) model for Neural Network based filter is developed and validated. The RTL model is implemented using Xilinx Field-programmable Gate Array (FPGA). The design is optimized for power of 1.01485 W and memory 540916 kilobytes. The model developed can also be implemented on ASIC technology.

Keywords: *Finite Impulse Response (FIR), Neural Networks (NN), Lyapunov function, Feedforward networks, Simulink, Field-programmable Gate Array (FPGA)*

1. INTRODUCTION

Finite Impulse Response (FIR) filters can be generally designed by using the windowing methods or the optimization methods. The windowing method is the simplest approach for obtaining the coefficients of FIR filters. However, the designed filters are not optimal in any sense. The optimization methods approximate a desired behaviour by minimizing an error function that is formulated by using the L_2 or $L\infty$ norm. The least-squares methods [1], [2] have received considerable attention and investigation, since analytical solution can be obtained in the L_2 sense. To obtain the optimal filter coefficients, a time consuming iterative procedure or matrix inversion operation is often needed. Furthermore, numerical errors may commonly arise when the length of filter is long [2]. This is due to ill conditioning of a set of linear equations associated matrix. The approaches mentioned above are generally based on linear algebra methods that cannot meet real-time requirement.

Several nonlinear techniques based on neural networks [3]-[5] have been developed for designing different kinds of FIR filters. The representative technique in [3] constructs the energy function of the network coincides with the error function of the filter design. When the network converges, it achieves the optimal solution. Nevertheless, the required neurons are proportional to the sampling grid in frequency domain. Furthermore, the amount of neurons required strongly relates to the hardware cost and IC area when implemented in hardware. Hence, the sampling grid of frequency heavily affects the hardware cost and computational requirement of the neural-based approach.

2. NEURAL NETWORKS

Neural networks are composed of simple elements operating in parallel. These elements are inspired by biological nervous systems. As in nature, the connections between elements largely determine the network function. You can train a neural network to perform a particular function by adjusting the values of the connections (weights) between elements. Typically, neural networks are adjusted, or trained, so that a particular input leads to a specific target output. The next figure illustrates such a situation. There, the network is adjusted, based on a comparison of the output and the target, until the network output matches the target. Many such input/target pairs are needed to train a network.

2.1. FEEDFORWARD NETWORK Feedforward networks often have one or more hidden layers of sigmoid neurons followed by an output layer of linear neurons. Multiple layers of neurons with nonlinear transfer functions allow the network to learn nonlinear and linear relationships between input and output vectors. The linear output layer lets the network produce values outside the range -1 to +1. On the other hand, if you want to constrain the outputs of a network (such as between 0 and 1), then the output layer should use a sigmoid transfer function (such as logsig). For multiple-layer networks the number of layers determines the superscript on the weight matrices. The appropriate notation is used in the two-layer tansig/purelin network as shown in Fig. 1. This network can be used as a general function approximator. It can approximate any function with a finite number of discontinuities arbitrarily well, given sufficient neurons in the hidden layer.

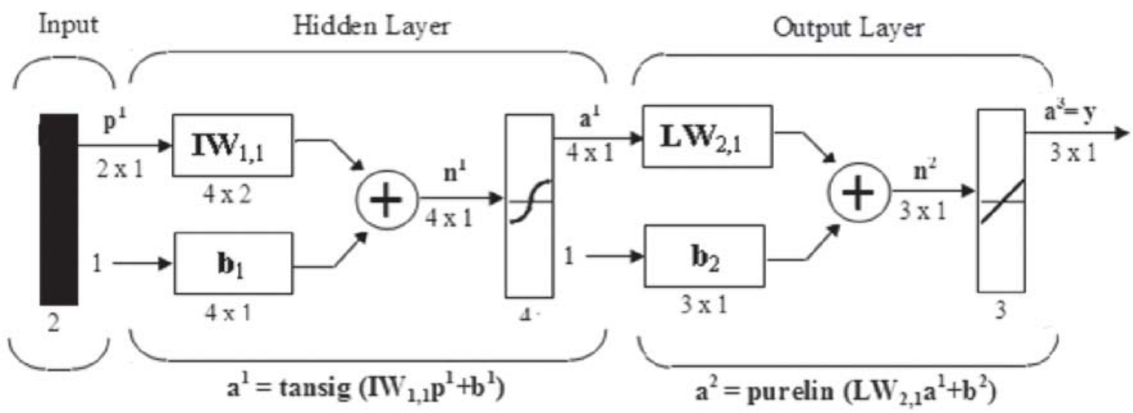

Fig. 1: Feedforward network

The first step in training a feedforward network is to create the network object. The function newff creates a feedforward network. It requires three arguments and returns the network object. The first argument is a matrix of sample R-element input vectors. The second argument is a matrix of sample S-element target vectors. The sample inputs and outputs are used to set up network input and output dimensions and parameters. The third argument is an array containing the sizes of each hidden layer.

3. FILTER DESIGN

MATLAB programs are used to design FIR filter for evaluating the performance of the proposed neural-based approach.

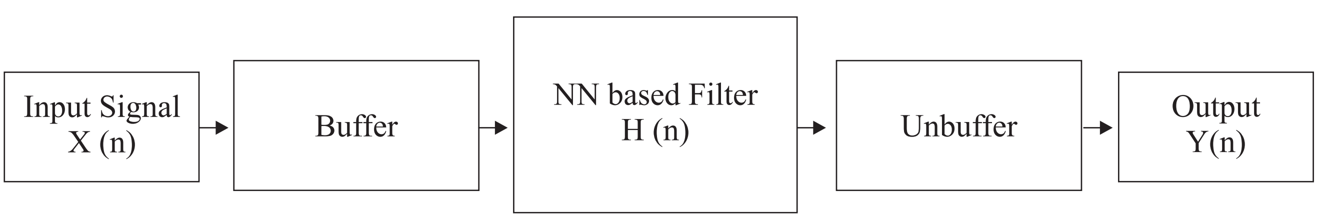

Fig. 2: Block diagram

The block diagram is as shown in Fig. 2. The input signal is the binary data. The Buffer block redistributes the input samples to a new frame size. Buffering to a larger frame size yields an output with a slower frame rate than the input. Buffering to a smaller frame size yields an output with a faster frame rate than the input. The block coordinates the output frame size and frame rate of nonoverlapping buffers such that the sample period of the signal is the same at both the input and output: $T_{so} = T_{si}$. The Unbuffer block adjusts the output rate so that the sample period is the same at both the input and output, $T_{so}=T_{si}$. Therefore, the output sample period for an input of frame size M_i and frame period T_{fi} is T_{fi}/M_i, which represents a rate M_i times higher than the input frame rate.

The neural network filter design [6] is as follows: The weighted square error function can be expressed as

$$\varepsilon_2 = \sum_{i=0}^{Nu-1} \sum_{j=0}^{Nu-1} [\sum_{l=1}^{L} W(\omega_l)\varphi_i(\omega_l)\varphi_j(\omega_l)] a_i a_j - 2\sum_{i=o}^{Nu-1} [\sum_{l=1}^{L} W(\omega_l) A_N \varphi_i(\omega_l)] a_i + \sum_{l=1}^{L} W(\omega_l) A^2_N(\omega l) \quad (1)$$

The state dynamics of NN can be characterized by the following set of coupled nonlinear differential equations

$$du_i / dt = - u_i / \tau_i + \sum_{j=1}^{p} T_{ij} v_j + I_i \quad (2)$$

$$v_i = g(u_i) = \frac{1}{1+e^{-ui/\lambda}} \quad (3)$$

where $\tau_i = C_i \rho_i$ is a time constant, ρ_i is the parallel combination of R_i and R_{ij} . R_{ij} is the resistive feedback between neurons j and i which must be positive, in general, $R_{ij} = 1/|T_{ij}|$. u_i and v_i are the internal and output state of the i-th neuron, C_i and R_i are the input capacitance and resistance, p is the number of neurons required for the network, Ii is an external input to the neuron and T_{ij} is the interconnection strengths. The neuron activation function $g(u_i)$ is generally determined by a sigmoid function with λ determining the slope of the function. The NN would generate a good solution if the objective function of any optimization problem can be related with a Lyapunov energy function given as

$$E_L = -\frac{1}{2}\sum_{i=1}^{p} \sum_{j=1}^{p} T_{ij} v_i v_j - \sum_{i=1}^{p} I_i v_i \quad (4)$$

Using this observation, the corresponding NN parameters of T_{ij} , I_i and p for the design of FIR Nyquist filter can be identified as indicated from a comparison of Eq. (4) with Eq. (1) by neglecting the constant term. That is,

$$T_{ij} = -\sum_{l=1}^{L} W(\omega_l)\varphi_{i\text{-}1}(\omega_l)\varphi_{j\text{-}1}(\omega_l) \quad (5)$$

$$I_i = \sum_{l=1}^{L} W(\omega_l) A_N \varphi_{i\text{-}1}(\omega_l) \quad (6)$$

$$p = N_u \quad (7)$$

where $v_i = a_{i-1}$, $1 \leqslant i, j \leqslant N_u$. Once the interconnection strength T_{ij} and bias current I_i have been obtained, the dynamic equation of the NN in Eq. (2) can be used directly. When the system reaches a stable configuration in which $dE_L/dt = du_i/dt = \partial E_L / \partial v_i = 0$, it has the form

$$\sum_{j=1}^{p} T_{ij} v_j = - I_i$$

Substituting Eq. (5) and Eq. (6) into this equation, it is equivalent to the normal equation of the general least-squares (LS) solution obtained from Eq. (1). Since Eq. (1) is a convex quadratic function, it has a unique solution a_{LS}. To check the status of equilibrium points, the second derivative of the objective function in the filter design is given $\nabla^2\varepsilon_2 = \sum_{l=1}^{L} W(\omega l)\varphi_{i-1}(\omega l)\varphi_{j-1}(\omega l)$ which is a positive definite matrix. Hence, there exists only one local minimum, and this particular one is also the global minimum in the error-performance surface.

When the dynamic equation achieves its stable configuration, the output state of the NN yields the optimal filter coefficients an. The proposed structure uses notably the same number of g neurons to implement the WLS design of FIR Nyquist filters. Comparing this to the methods presented by the f neurons are replaced by the general blocks of multiplication and subtraction for the error function calculation. Therefore, the architecture of the proposed technique is much simpler and regular, and so it can reduce the computational complexity and hardware cost when implemented in real-time.

With a digital simulation of this NN system implementing the filter design task, it has been shown by that Eq. (2) can be approximated to

$$\Delta u_i = -\frac{ui(t+\Delta t)-ui(t)}{\tau i} + (\sum_{j=1}^{p} T_{ij} v_j + I_i)\,\Delta \approx (\sum_{j=1}^{p} T_{ij} v_j + I_i)\,\Delta t)$$

Where Δt is a sufficiently small value,$[u_i(t + \Delta t) - u_i(t)] \ll \tau_i$. In addition, the term u_i/τ_i was ignored for improving the convergence speed. Thus, the input state u_i can be iteratively updated at the (t+1) thiteration by

$$u_i(t+1) = u_i(t) + \Delta u_i \text{ , for } 1 \le i \le p$$

Since the non-decreasing and nonlinear activation functions can guarantee the network to be gradient descent, any neuron with a non-negative slope can be selected such that the convergence to a local minimum is guaranteed only if $dv_i/du_i \geqslant 0$ for all i's. In the proposed approach, the output values are calculated using a soft limiter type neuron selected as

$$v_i = g(u_i) = \left\{\begin{matrix} b & \text{if } ui \ge b\lambda, \\ \frac{ui}{\lambda} & \text{if } |ui| < b\lambda, \\ -b & \text{if } \le b\lambda. \end{matrix}\right\}$$

where b and $1/\lambda$ are the dynamic range and slope of the soft limiter, respectively. The value of λ obviously affects the convergence speed, and the value of b should be chosen larger than the maximum possible value of a_n; otherwise, the NN would be sometimes saturated.

4. SOFTWARE REFERENCE MODEL

The Simulink block of reconfigurable FIR filter is as shown in Fig. 3. Simulink block of FIR filter is designed using the FDA (Filter Design and Analysis) tool in matlab. The cut-off frequency is given to the FDA tool as required. Multiple signals are given to check the performance of filter. Frequency domain and Time domain responses are checked in Spectrum scope and scope respectively. Simout values of individual signals are determined. These values are then given as input to Neural Network Algorithm, developed in matlab, for training.

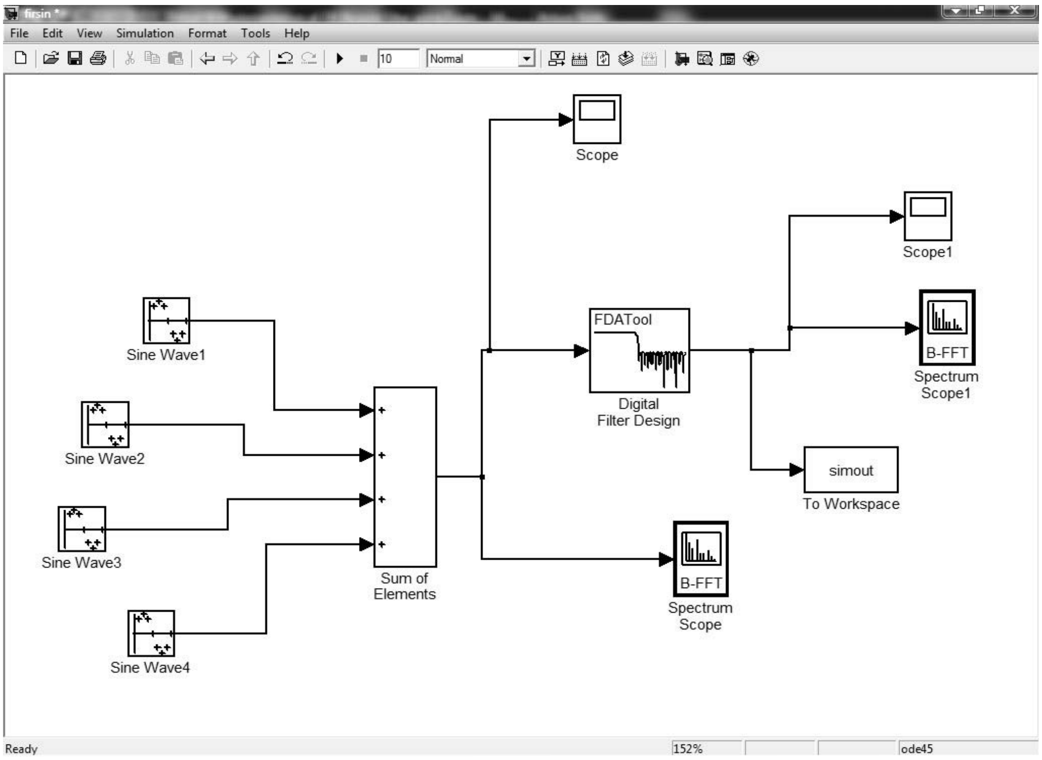

Fig. 3: Simulink Model of FIR filter

Filter Design and Analysis Tool in the Signal Processing Toolbox™ product is a powerful user interface for designing and analyzing filters. This is as shown in Fig. 4. FDA Tool enables you to design digital FIR or IIR filters by setting filter performance specifications, by importing filters from your MATLAB workspace, or by directly specifying filter coefficients. FDA Tool also provides tools for analyzing filters, such as magnitude and phase response plots and pole-zero plots. By entering the fdatool command in the MATLAB Command Window, the Filter Design & Analysis Tool dialog box appears.

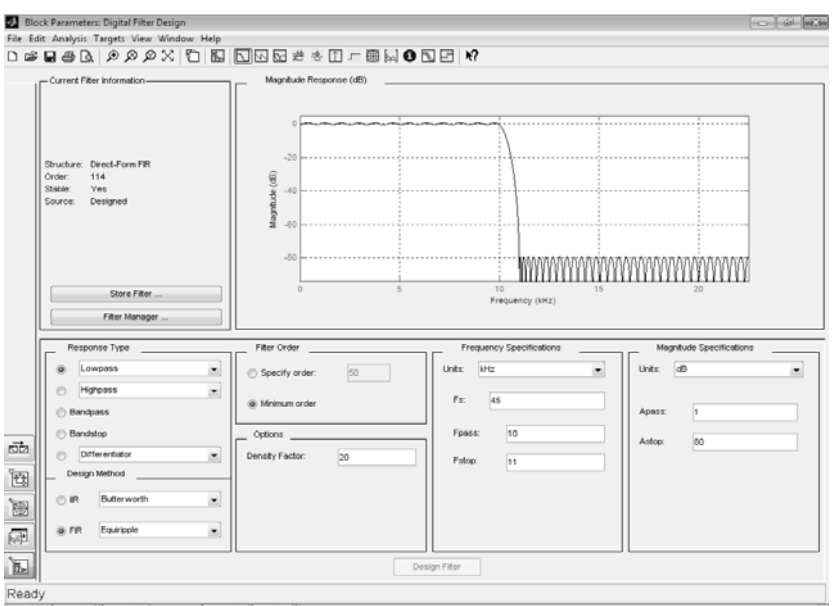

Fig. 4: FDA Tool window

The To Workspace block writes its input to the workspace. The block writes its output to an array or structure that has the name specified by the block's Variable name parameter. The Save format parameter determines the output format. Selecting this option causes the To Workspace block to save the input as an N-dimensional array where N is one more than the number of dimensions of the input signal. For example, if the input signal is a 1-D array (i.e., a vector), the resulting workspace array is two-dimensional. If the input signal is a 2-D array (i.e., a matrix), the array is three-dimensional. The way samples are stored in the array depends on whether the input signal is a scalar or vector or a matrix. If the input is a scalar or a vector, each input sample is output as a row of the array.

5. SIMULATIONS

Simulink block of FIR filter is designed using the FDA tool in matlab. The cut-off frequency is given to the FDA tool as required. The cut-off frequency is given as 10KHz to the FDA tool. Multiple signals of 2KHz, 8KHz, 15KHz, 20KHz are given to check the performance of filter. Each signal given, has an amplitude of 5. Number of samples per period for each signal is specified as 3. Frequency domain responses are checked in Spectrum scope. When the Simulink model is simulated, the filter performs as per the cut-off and passes only the low frequency signals i.e. 2KHz & 8KHz. It filters out the high frequency signals i.e. 15KHz & 20KHz since it's a low pass filter. Frequency domain response is checked in Spectrum scope. The responses as shown in Fig. 5 (a) & Fig. 5 (b)

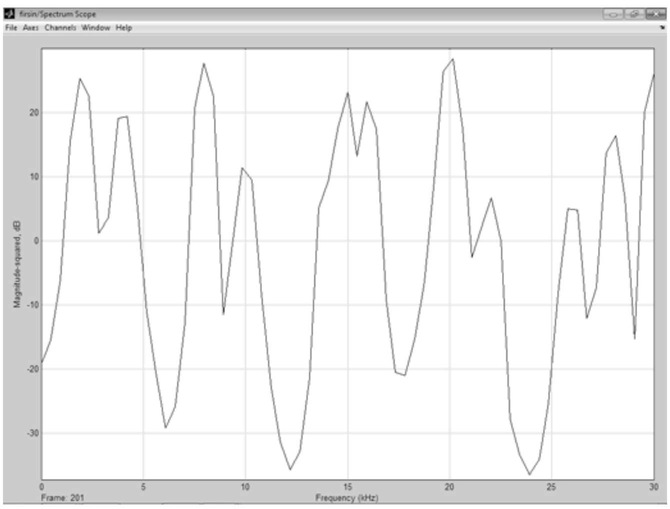

Fig. 5 (a): Multiple signals given as inputs

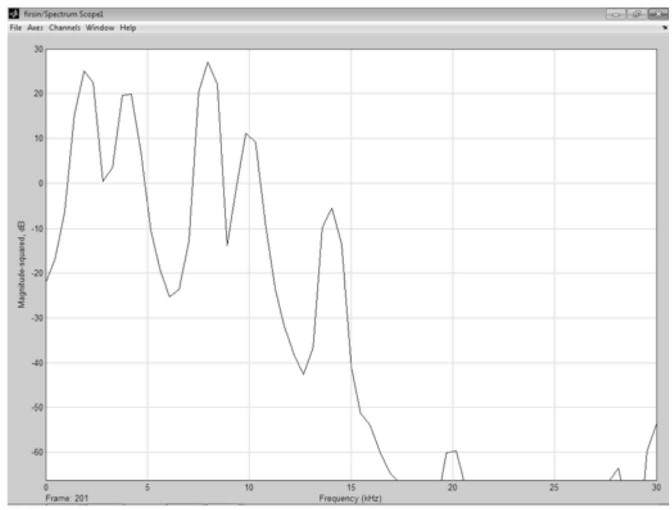

Fig. 5 (b): Filtered output

The generated simout values are then given as input to Neural Network Algorithm developed in matlab, for training. Neural Network is tested with filter. The generated Feed Forward Neural Network is as shown in Fig. 6. The coefficients of this network are obtained from matlab command window. The coefficients obtained are Input weights (IW), Layer weights (LW) and biases b(1) & b(2). A verilog code is developed for the network and is implemented on FPGA. The Input weights (IW), Layer weights (LW) and biases b(1) & b(2) are given as inputs in the verilog code. The simulation results of this code are checked and compared with that of Chip Scope results obtained as a result of FPGA implementation.

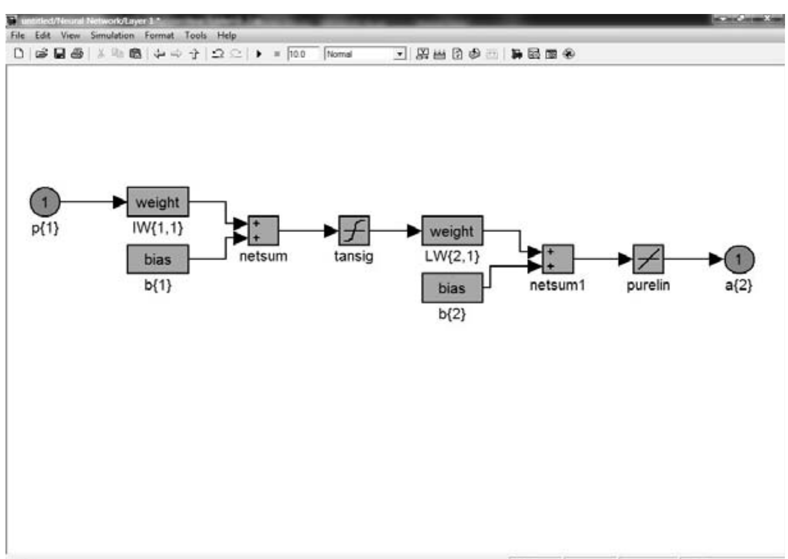

Fig. 6: Generated Feedforward neural network

6. COMPARISON OF SIMULATIONS

Top Module is the combination of both hidden layer and output layer which forms the complete Feedforward neural network. The output of this Top module is the final output. The verilog coding is done for this network and inputs are specified as parameters. The Feed Forward Network is designed for 50 inputs. The verilog code developed for this network experiences IO bound issues when implemented on FPGA. Hence the inputs and outputs are considerably reduced to implement the design. The simulation result using Verilog Compiler Simulator (VCS) is as shown in Fig. 7.

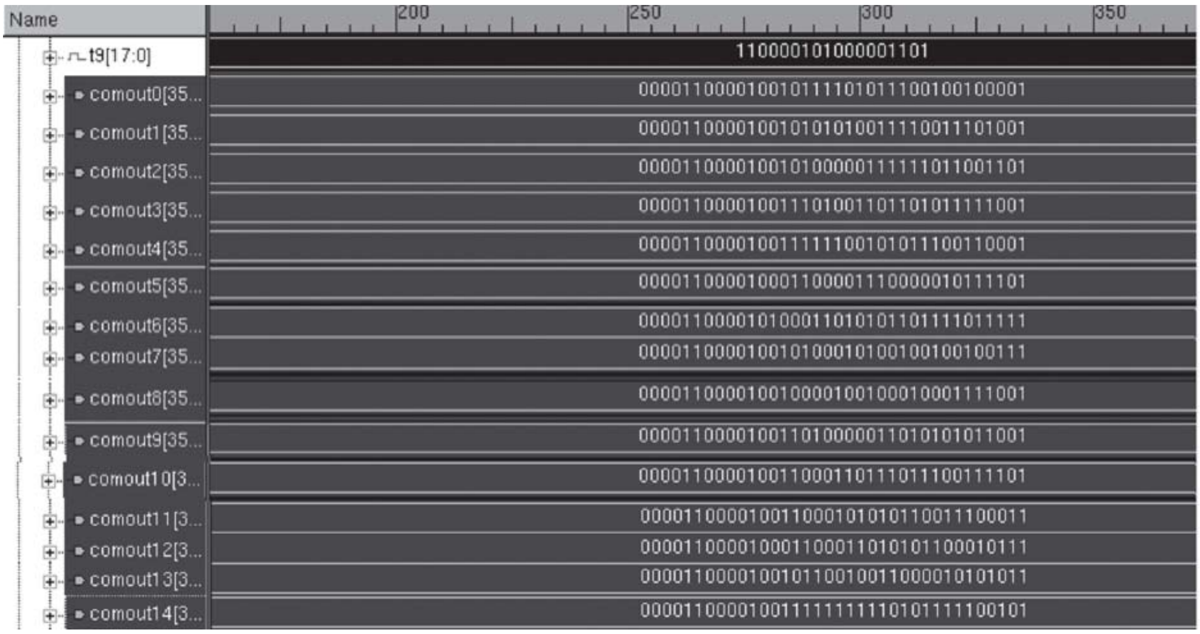

Fig. 7 Top Module simulation in VCS

The Xilinx ChipScope tools are added to our Verilog design to capture input and output directly from the FPGA hardware. The design is again synthesized using Xilinx ISE and implemented on Virtex-5 FPGA board. The ChipScope simulation is as shown in Fig. 8.

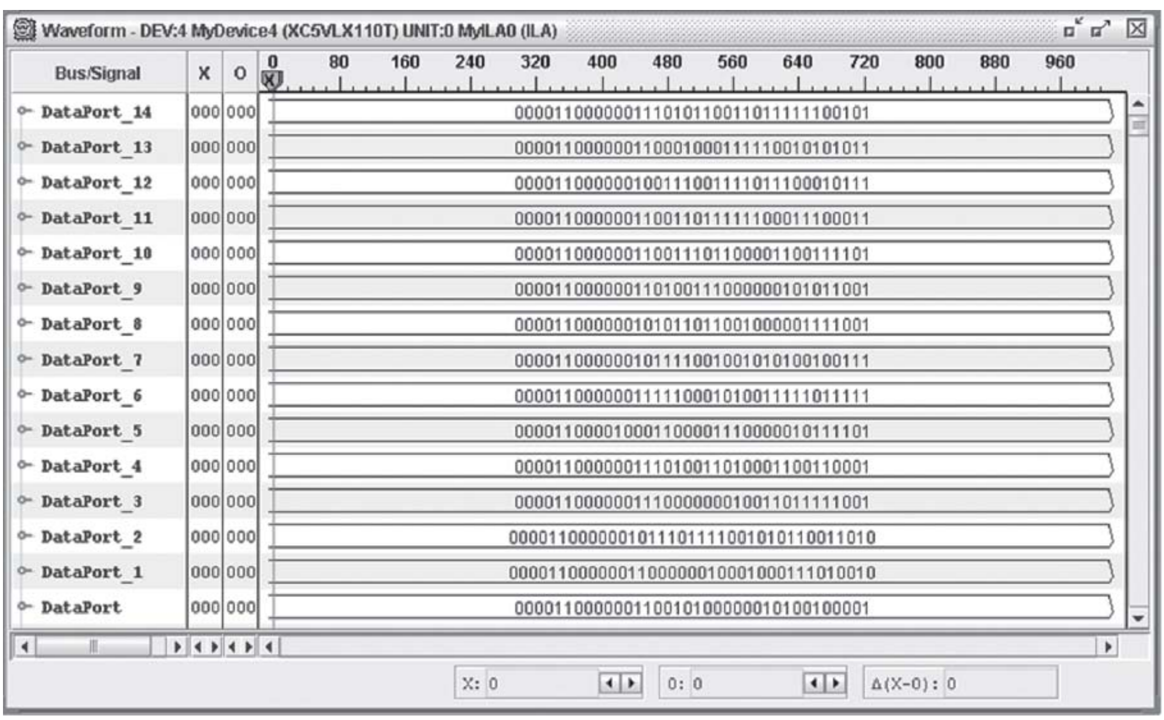

Fig. 8: Top Module simulation in ChipScope pro

7. HARDWARE DESCRIPTION OF FPGA

In our experimentation, Xilinx Virtex5 (device xc5vlx110t) with 1000K gate count FPGA is used [7]. It has total 10K numbers of configurable logic blocks (CLBs) arranged in 32 X 28 matrix fashion. Each CLB has four slices and two of them are named as SLICEM and rest two as SLICEL. Each SLICEM can be used as 16 bit (embedded) shift register (SRL16). Number of LUT Flip Flop pairs used is 4666 out of 69120. Number of bonded IOBs used are 558 out of 640. IOB Flip Flops/Latches used are 15. Number of BUFG/BUFGCTRLs is 1 out of 32. Because of our efficient FPGA implementation technique, sufficient FPGA resources are made available for implementing other circuitry of the FIR filter.

8. SYNTHESIS RESULTS

Selected Device: 5vlx110tff1136-1
Slice Logic Utilization:

Number of Slice LUTs:	4666	out of	69120	6%
Number used as Logic:	4666	out of	69120	6%

IO Utilization:

Number of IOs:	558			
Number of bonded IOBs:	558	out of	640	87%
IOB Flip Flops/Latches:	15			
Number of BUFG/BUFGCTRLs:	1	out of	32	3%

Total memory usage is 540916 kilobytes
Total Power: 1.01485 W

9. CONCLUSION AND FUTURE WORK

This paper presents design of FIR filter using Neural Networks and its implementation. Simulink block of FIR filter is designed using the FDA tool in matlab. The cut-off frequency is given to the FDA tool as required. Multiple signals are given to check the performance of filter. Frequency domain and Time domain responses are checked in Spectrum scope and scope respectively. Simout values of individual signals are determined. These values are then given as input to Neural Network Algorithm, developed in matlab, for training. Verilog code of the model is developed for simulation on VCS (Verilog Compiler Simulator). The FPGA implementation is done using Xilinx ISE 10.1. The implementation is performed on Virtex-5 FPGA board. Once the interfacing is done, the corresponding programming file for the top module is generated. The target device is then configured so that the generated programming file can be successfully dumped on Virtex-5. The design is then analyzed using Chip Scope Pro. The Chip Scope output is observed. The Chip Scope output is successfully compared with VCS simulation output. The design is optimized for power of 1.01485 W and memory 540916 Kb. The RTL model can successfully implemented on ASIC.

ACKNOWLEDGEMENT

This work is carried out at MSRSAS, Bangalore as part of final year M.Tech. project work. The authors would like to thank the management of RVCE, Bangalore for providing support in carrying out their work.

REFERENCES

1. P. P. Vaidyanathan and T. Q. Nguyen, "*Eigenfilters: A new approach to least squares FIR filter design and applications*," *IEEE Trans. Circuits Syst.*, vol. CAS-34, no. 1, pp. 11–23, Jan. 1987.
2. M. Okuda, M. Ikehara, and S. Takahashi, "*Fast and stable least-squares approach for the design of linear phase FIR filters*," *IEEE Trans. Signal Process.*, vol. 46, no. 6, pp. 1485–1493, Jun. 1998.
3. D. Bhattacharya and A. Antoniou, "*Real-time design of FIR filters by feedback neural networks*," *IEEE Signal Process. Lett.*, vol. 3, no. 5, pp. 158–161, May 1996.
4. D. Bhattacharya and A. Antoniou, "*Design of equiripple FIR filters using a feedback neural network*," *IEEE Trans. Circuits Syst. II, Analog Digit. Signal Process.*, vol. 45, no. 4, pp. 527–531, Apr. 1998.
5. Y. D. Jou, "*Neural least-squares design of higher order digital differentiators,*" *IEEE Signal Process. Lett.*, vol. 12, no. 1, pp. 9–12, Jan. 2005.
6. Yue-Dar Jou, Fu-Kun Chen "*WLS design of FIR Nyquist filter based on neural networks*," Digital Signal Process (2010) doi:10.1016/j.dsp.2010.07.001
7. http://www.xilinx.com/products/virtex5/index.htm
8. www.elsevier.com/locate/vlsi.

USE OF 3-D HSV HISTOGRAM EQUALIZATION AND ADAPTIVE HSV SEGEMENTATION FOR CONTENT BASED IMAGE RETRIEVAL

Ms. Venu Shah
Lecturer, Electronics and telecommunication department
Atharva College of Engineering, Mumbai, India
shah_venu@yahoo.com
0919987772958

Ms. Archana Choudhary
Lecturer, Electronics and telecommunication department
Atharva College of Engineering, Mumbai, India,
arch2309@rediffmail.com

Prof. Kavita Tewari
Head, Electronics department,VESIT,Chembur,
Mumbai, India
ktewari_vesit@yahoo.co.in

ABSTRACT

Content-based image retrieval system based on color shades in the image is accomplished in this image. HSV color space quantifies the color space into different regions and thereby calculating its mean and Euclidian distance the color vector can be derived.

Keywords: *CBIR, Histogram equalization*, *adaptive HSV segmentation.*

1. INTRODUCTION

All The recent development of multimedia databases has led to extensive application of digital library and image search engines. This has resulted in an increased need for more efficient Content Based Image Retrieval [1], [2], [3]. The term 'content' in this context might refer to colors [4], [5], shapes [6], textures [7], features [8] or any other information that can be derived from the image itself. The term 'content' in this context might refer to colors, shapes, textures, or any other information that can be derived from the image itself. Here we are combining the two approaches viz. feature extraction and color extraction to obtain more efficient image retrieval.

Common CBIR systems perform two main operations in their approach [1], [9].The first one is feature extraction (FE) [8], where a set of features, called image signature or feature vector. Features of an image should have a strong relationship with semantic meaning of the image. In second step, CBIR system retrieves the relevant images from the image data base for the given query image, by comparing the feature of the query image and images in the database.

2. HSV HISTOGRAM EQUALIZATION

In image retrieval systems colour histogram is the most commonly used feature. The main reason is that it is independent of image size and orientation. Also it is one of the most straight-forward features utilized by humans for visual recognition and discrimination. Statistically, it denotes the joint probability of the intensities of the three colour channels. Once the image is segmented, from each region the colour histogram is extracted. The major statistical data that are extracted are histogram mean, standard deviation, and median for each colour channel i.e. Red, Green, and Blue. So totally 3× 3 = 9 features per segment are obtained. All the segments need not be considered, but only segments that are dominant may be considered, because this would speed up the calculation and may not significantly affect the end result.

Content-based image retrieval is the task of searching images in databases by analyzing the image contents. In this demo, a simple image retrieval method is presented, based on the color distribution of the images. The user simply provides an "example" image and the search is based upon that example (query by image example). For this first version of the demo no relevance feedback is used.

Almost 1000 images have been used for populating the database. For each image a 3-D histogram of it's HSV values is computed. At the end of the training stage, all 3D HSV histograms are stored in the same .mat file. In order to retrieve M (user-defined) query results, the following steps are executed:

The 3D (HSV) histogram of the query image is computed. Then, the number of bins in each direction (i.e., HSV space) is duplicated by means of interpolation.

For each image i in the database:

1. Load its histogram Hist(I).
2. Use interpolation for duplicating the number of bins in each direction.
3. For each 3-D hist bin, compute the distance (D) between the hist of the query image and the i-th database image.
4. Keep only distances (D2) for which, the respective hist bins of the query image are larger than a predefined threshold T (let L2 the number of these distances).
5. Use a 2nd threshold: find the distance (D3) values which are smaller than T2, and let L3 be the number of such values.
6. Calculate the similarity measure is defined as: S(i) = L2 * average(D3) / (L3^2).
7. Sort the similarity vector and prompt the user with the images that have the M smaller S values.

3. ADAPTIVE SEGMENTATION FOR HSV COLOR SPACE

The image retrieval process using adaptive segmentation of HSV is carried out by converting its RGB colour space to HSV colour space using the formulae given in figure as follows:

$$H = \cos^{-1}\left\{\frac{\frac{1}{2}[(R-G)+(R-B)]}{\sqrt{(R-G)^2+(R-B)(G-B)}}\right. \tag{6}$$

$$S = 1 - \frac{3}{R-G+B}[\min\ (R,G,B)] \tag{7}$$

$$V = \frac{1}{3}(R+G+B) \tag{8}$$

Since the RGB values generally lie in the range of 0 to 255 we need to use the formulae given below, which will convert the Hue values between 0° and 360°, Saturation values between 0 and 1 and values between 0 and 1.

$$H = \left[\left(\frac{H}{255}\right) * 360\right] |360| \tag{9}$$

$$S = \frac{S}{255} \tag{10}$$

$$V = \frac{V}{255} \tag{11}$$

After the conversion from RGB colour space to HSV colour space of the entire image, the image is divided into m different regions depending on the values of hue and saturation.

The TABLE I illustrates the fact that the hue is divided into partitions of 20° is done in order to separate the 3 primary colours and yellow magenta and cyan into 3 sub-divisions each. And the saturation for each hue is further sub-divided by 0.2.

Thus, 18*5=90 different regions of colour distribution in the image.

Table I. Different Ranges of Hue and Saturation used in image retrieval Process

S#	Hue	Saturation
1	0<H<20	S<0.2
2		0.2<=S<0.4
3		0.4<S<=0.6
4		0.6<S<=0.8
5		S>=0.8
...	...	...
7	340<H<360	S<0.2
8		0.2<=S<0.4
9		0.4<S<=0.6
10		0.6<S<=0.8
90		S>=0.8

After dividing the image into various regions using table given above the pixels present in each region of the image are selected. Then the corresponding hue values are extracted and grouped together to form a hue vector.

This vector for every region is divided into n segments depending on the number of pixels in the hue vector of the region. If the number of pixels in the region are more the hue vector will be divided into more number of segments and if the number of pixels in the region are less the hue vector will be divided into less number of segments.

In order to partition the regions into various segments we need to use the following equation.

$$n_i=(X_i/T)*T_s \quad ,0<i\leq m \tag{12}$$

where, n_i represents the number of segments in region I, X_i represents the number of pixels in region i (where i ranges from 1 to m), T represents total number of pixels of the image, and TS represents total number of required segments of the entire HSV image.

After this process of breaking the various regions into segments the necessary colour distribution information is calculated by finding the maximum occurrence in each segment by using the hue histogram. Using this information we can generate the feature vector of the image.

In order to perform an image retrieval operation we need to generate a feature vector for the database image from individual regions. This feature vector is used in comparing both the images by using the Euclidean distance equation. Segments in each region of the query image are compared with the corresponding region of the database image using the Euclidean distance equation as given in eqn (5). Once the Euclidean distance of the individual regions is computed the mean of all the regions is computed to get the final distance that can be used to compare various images. Database images having a lower distance will be similar to the original image.

4. ADAPTIVE HSV SEGMENTATION

Steps for proposed algorithm for Colour Extraction:

1. Take a query input image.
2. Convert the image from RGB colour space to HSV colour space.
3. Divide the image into different areas based on the ranges mentioned in TABLE I.
4. Further divide the areas obtained into segments depending on the number of pixels in each area.
5. Find the maximum colour occurrence from each segment by calculating the mode of Hue values in it.
6. Find Euclidian distances of corresponding areas in query image and the database image considering the included segments individually.
7. Find the mean (M1) of all the Euclidian distances obtained in the previous step.

5. RESULTS

Adaptive HSV segementation and 3-D HSV Histogram equalization both give good results.

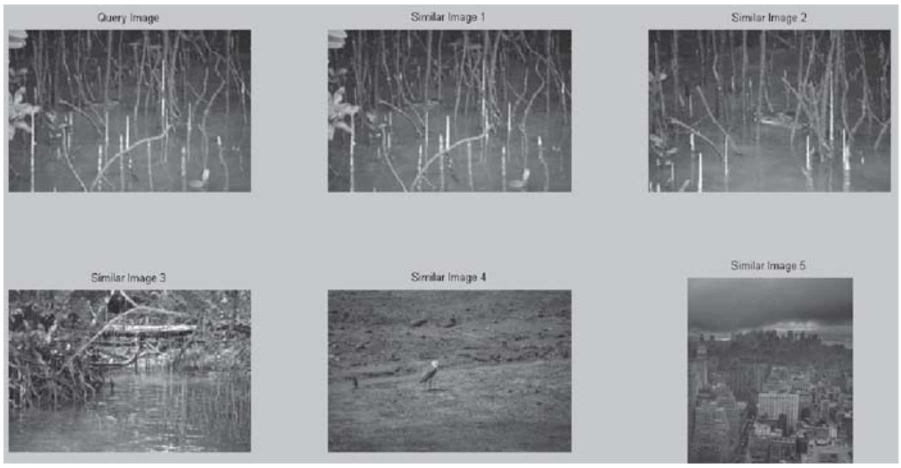

3a

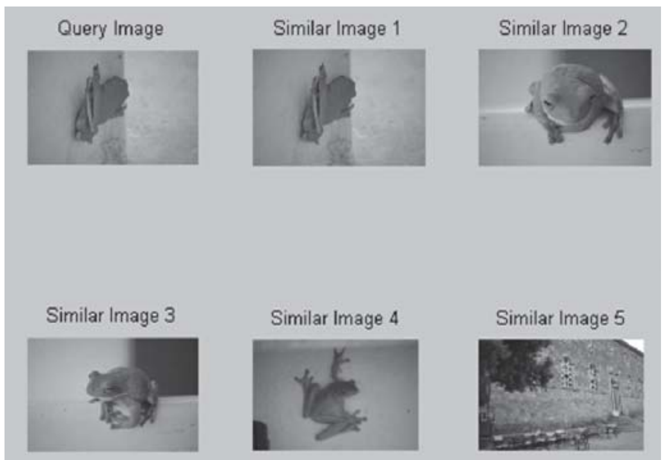

3b

FIG.3 a and b: EXPERIMENT RESULT USING 3-D HSV HISTOGRAM EQUALISATION

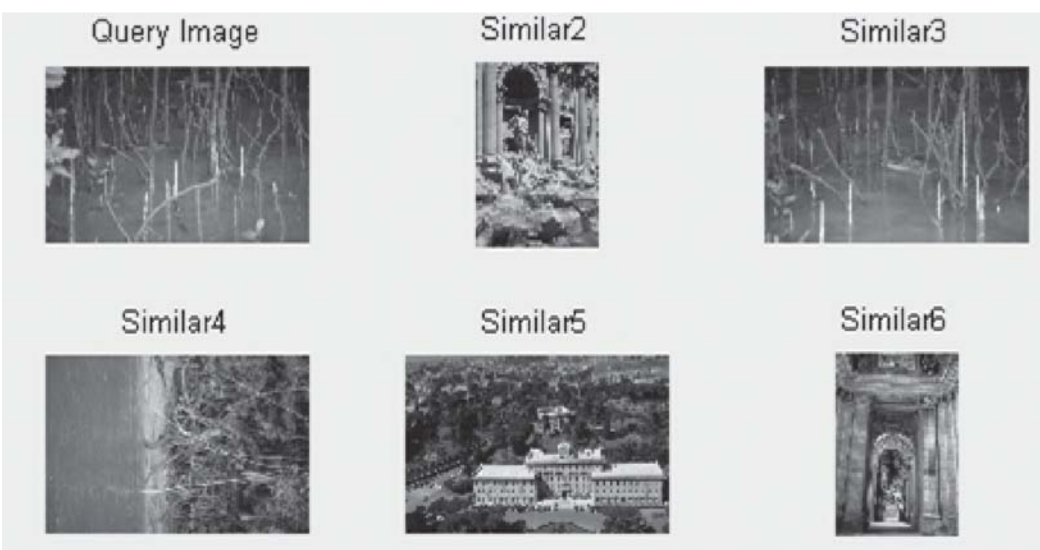

4a

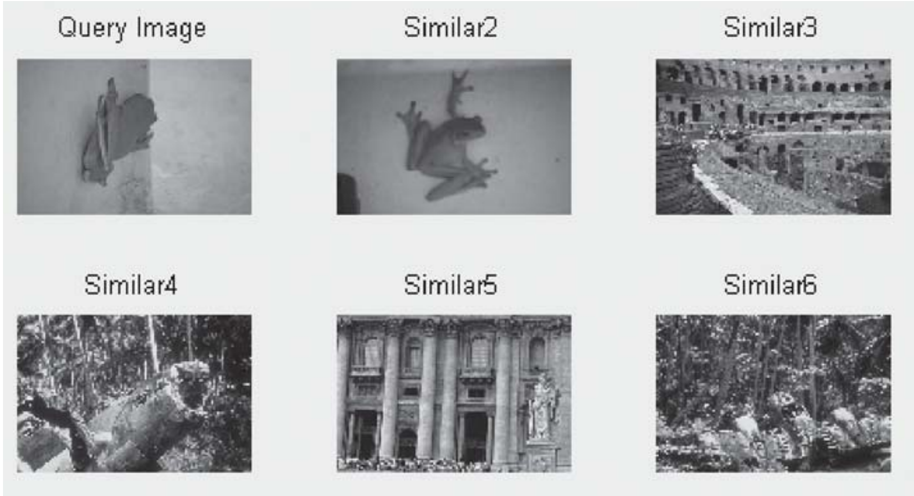

4b

FIG. 4 a and b EXPERIMENT RESULTS ADAPTIVE HSV SEGMENTATION

6. CONCLUSION

The image retrieval process involves use of either Adaptive segmentation of HSV color space for image retrieval or 3D-HSV histogram.

Adaptive Segmentation of HSV colour space takes place by calculating the mean of the resulting Euclidean distances obtained and arranging the values in ascending order and thereby the best image being arranged at the top.
While in 3D-color histogram, closet histogram values are used to obtain closer resembling images.

ACKNOWLEDGMENT

We are very thankful to the Electronics and telecommunications department of Vivekanand Education Society's College of Information and Technology and AET's Atharva College of engineering for providing us with the necessary facilities to complete our research in the field CBIR. We also thank our family, friends for supporting us throughout our research.

REFERENCES

1. J. Han and K. Ma, "Fuzzy Color Histogram and Its Use in Color Image Retrieval", IEEE Trans. On Image Processing, vol. 11, pp. 944 – 952, Aug. 2002.
2. H.B.Kekre, Sudeep D. Thepade, "Rendering Futuristic Image Retrieval System", In Proc. of National Conference EC2IT-2009, KJSCOE, Mumbai, 20-21 Mar 2009.
3. N.Krishnan, M.Sheerin Banu, C.Callins Christiyana, **"**Content Based Image Retrieval using Dominant Color Identification Based on Foreground Objects**",** In International Conference on Computational Intelligence and Multimedia Applications, 2007.
4. Youngeun An, Muhammad Riaz and Jongan Park, "CBIR based on adaptive segmentation of HSV color space," 2010, 12th International Conference on Computer Modelling and Simulation.
5. C. Y. Wu, X.Y. Tai and J.Y. Zhao, "Image Retrieval Based on Color Feature," Computer applications, 2004, Vol. 24, No. 6, pp. 135-137.
6. X.J. Zhang, Research on color feature based image retrieval. Master degree thesis, Liaoning technical university, 2005.
7. Gonzalez, Rafael C. & Woods, Richard E. (2002). Thresholding. In Digital Image Processing, pp. 595–611. Pearson Education. ISBN 81-7808-629-8.
8. Shapiro, Linda G. & Stockman, George C. (2002). "Computer Vision". Prentice Hall. ISBN 0-13-030796-3.

A SMART TEMPERATURE MEASURING TECHNIQUE USING THERMISTOR

Santhosh K V
Research Scholar, Dept of Electrical Engineering,
NIT Silchar, Assam
E-mail: kv.santhu@gmail.com

Dr. B K Roy
Associate Professor, Dept of Electrical Engineering,
NIT Silchar, Assam
E-mail: bkr_nits@yahoo.co.in

ABSTRACT

This paper aims to design of a smart temperature measuring instrument. The objectives of this work are to eliminate the effect of (i) the nonlinearity in the Thermistor, (ii) the interference of temperature coefficient (β), (iii) the resistance at reference temperature (R_o). Since the output of thermistor is resistance we make use of a voltage divider circuit followed by buffer circuit to convert the signal corresponding to change in temperature into voltage. An ANN block is added in cascade to this circuit. This arrangement helps to linearise the overall system and make it independent of temperature coefficient and resistance due to reference temperature of the thermistor. Since the proposed temperature measuring instrument (i) produces a linear relation between input temperature and (ii) output voltage and output independent of physical properties of thermistor, thus the present work is smart and avoids the requirement of repeated calibration every time the thermistor is replaced.

Similar work was reported in the paper "A Technique to extend the linearity range of Thermistor using ANN" [2], where scheme was proposed to linearise the temperature measuring system. An improvement of the reported work [2] is proposed in the present paper by designing the temperature measuring technique independent of temperature coefficient and reference resistance.

Index Terms: *Artificial Neural Networks, Thermistor, Sensor Modelling*

1. INTRODUCTION

Temperature is one of the most frequently used process measurements. Almost all chemical processes and reactions are temperature dependent. In chemical plants, temperature is frequently the only indication of the progress of a process. Where the temperature is critical to the reaction, a considerable loss of product may results from incorrect measurement of temperatures. In some cases, loss of control of temperature can results in catastrophic plant failure with consequent damages and possible loss of life. There are many other areas of industry in which temperature measurement is essential. Such applications include steam raising and electricity generation, plastics manufacture and molding, milk and dairy products, and many other areas of the food industries. Thus, an accurate and precise measurement of temperature is very important. There is various contact type electrical temperature sensors used for the measurement of temperature. Thermistor is one such commonly used sensor. High sensitivity and low power dissipation are the main two characteristics of thermistor which promotes its use over the other temperature sensors. However in a thermistor, the problem of high non linear response characteristics restricted the use this sensor. In practice this problem of nonlinearity is overcome by using some calibration techniques. Even after calibration there may be some error, and the process of calibration is to be repeated every time a thermistor is replaced, which is time consuming and may demand for a change in hardware also. This increases the time and effective cost of the instrument.

To overcome the above problems, a method has been proposed in this paper using the concept of ANN. The ANN model is added in cascade to the buffer circuit and is trained to achieve the output of the instrument liner and independent of physical parameters like temperature coefficient (β) and resistance at reference temperature (R_o).

The paper is organised as follows: After introduction in Section 1, a brief description on Thermistor is given in Section 2. The output of the Thermistor is resistance; A brief discussion on data conversion i.e. voltage divider circuit and buffer circuit is discussed in Section 3. Section 4 deals with the problem statement followed by proposed solution in Section 5. Finally, results and conclusion is given in Section 6.

2. THERMISTOR

A thermistor is a temperature-sensing element composed of sintered semiconductor material which exhibits a large change in resistance proportional to a small change in temperature. Thermistors usually have negative temperature coefficients which mean the resistance of the thermistor decreases as the temperature increases. The negative exponential function that best describes the resistance-temperature (R-T) characteristic of an NTC can be interpolated using different equations. The Steinhart-Hart equation is the most accepted equation [3, 4] and is described as:

$$R_T = R_0 \left(e^{\beta(T_0 - T)/T_0 T}\right) \tag{1}$$

where
R_T: Thermistor resistance at temperature T
R_0: Resistance at a specified reference temperature T_0
β: Temperature coefficient

3. DATA CONVERSION CIRCUIT

The block diagram representation of the proposed instrument is given in Fig 1

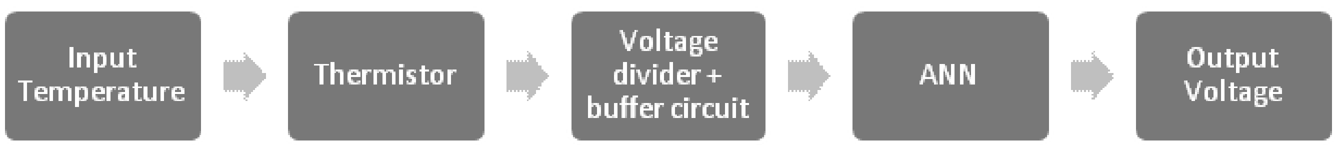

Fig 1. Block diagram of the proposed instrument

A voltage divider (also known as a potential divider) is a simple linear circuit that produces an output voltage (V_1) that is a fraction of its reference voltage (V). Voltage division refers to the partitioning of a voltage among the components of the divider. The formula governing a voltage divider is given as:

$$V_1 = V\left(\frac{R_T}{R_T + R_1}\right) \tag{2}$$

The output of voltage divider circuit is fed to a buffer amplifier as shown in Fig 2. The buffer amplifier is a unity gain amplifier.

A buffer amplifier is used to transfer a voltage from a first circuit, having a high output impedance level, to a second circuit with a low input impedance level. The interposed buffer amplifier prevents the second circuit from loading the first circuit unacceptably and interfering with its desired operation [5].

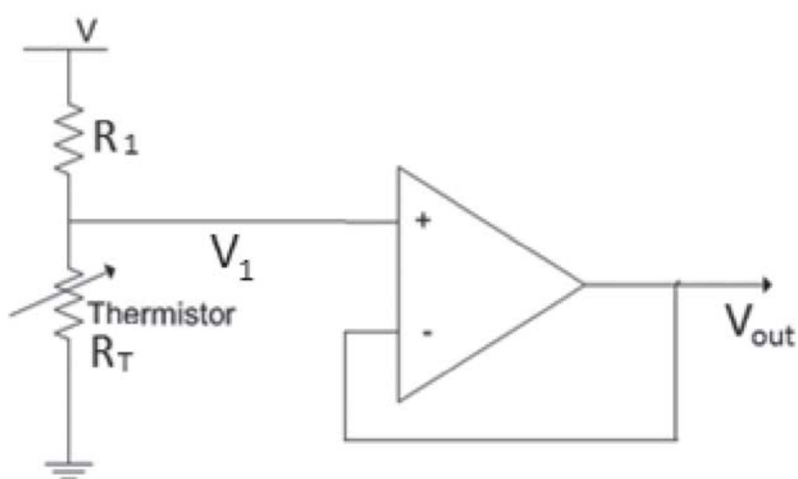

Fig.2: Data conversion circuit for Thermistor

4. PROBLEM STATEMENT

In these section characteristics of thermistor are simulated to understand the difficulties associated with the available measuring scheme. For this purpose, simulation is carried out with three different β. These are $\beta_1 = 3000$, $\beta_2 = 6000$ and $\beta_3 = 9000$. Further three different R_o are considered. These are $R_1 = 2$ KΩ, $R_2 = 4$ KΩ and $R_3 = 6$ KΩ. These values are used to find the output resistance of thermistor with respect to various values of input temperatures considering a particular β and R_o. These output resistances are used as input of voltage divider circuit and by using eqn (2) its converted to voltage.

The MATLAB environment is used of and the following characteristics are found

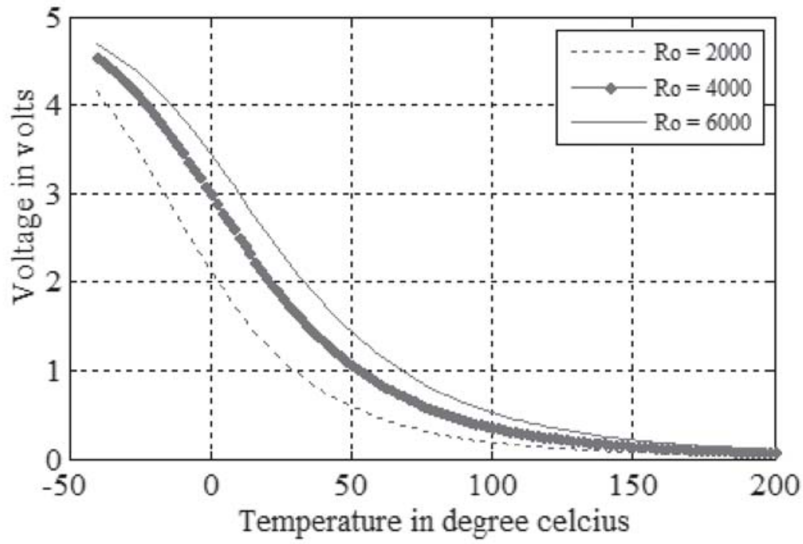

Fig 3. Buffer outputs for change in temperature with various values of R_o and at $\beta = 3000$

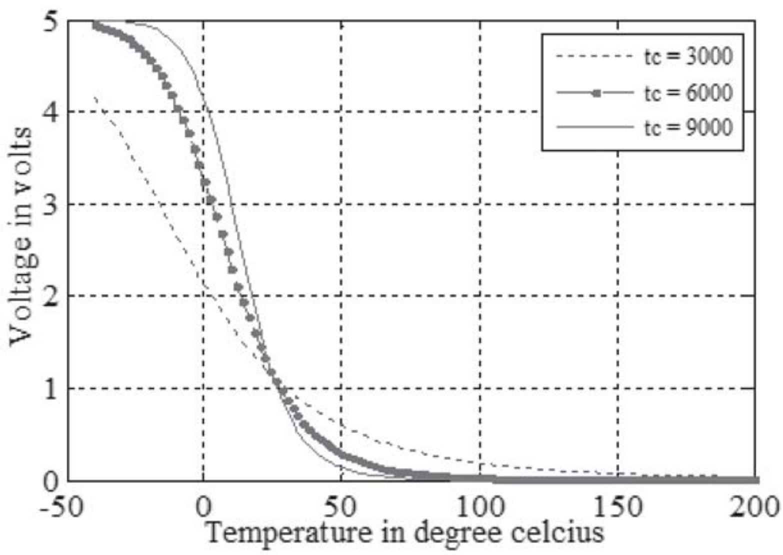

Fig 4. Buffer outputs for change in temperature with various values of β and at $R_o = 2000$

Fig 3 and Fig 4 shows the variation of voltage with the change in temperature considering different β and R_o. It has been observed from the above graphs (Fig 3 and Fig 4) that the output from the buffer circuit has a non linear relation. Datasheet of thermistor suggests that the input range of 20% to 50% of full scale is used in practice. The output voltage also varies with the change in β and R_o. These are the reasons which have made the user to go for calibration techniques using some circuits. These conventional techniques have a drawback that its time consuming and need to be calibrated every time a thermistor is changed in the system and the use is restricted only to a portion of full scale.

To overcome these drawbacks, this paper makes an attempt to design a model incorporating intelligence to produce linear output and to make the system independent of reference resistance and temperature coefficient using the concept of artificial neural network.

Problem statement: given an arrangement consisting of thermistor in cascade with voltage divider circuit and buffer circuit, design an intelligent temperature measuring instrument having the following properties:

i. Independent of R_o.

ii. Independent of β.

iii. Output bears a linear relation with the input temperature.

iv. Full scale input range can be measured.

5. PROBLEM SOLUTION

To overcome the drawbacks discussed in the earlier section, an Artificial Neural Network (ANN) model is cascaded after buffer circuit. This model is designed using the neural network toolbox of MATLAB [1].

The first step in developing a neural network is to create a database. The output voltage of the system for the change in temperature, β and R_o is stored in one matrix; which forms the input matrix for the ANN model. The output matrix would be the target matrix consisting of data having a linear relation with the temperature.

A: STRUCTURE OF NEURAL NETWORK MODEL:

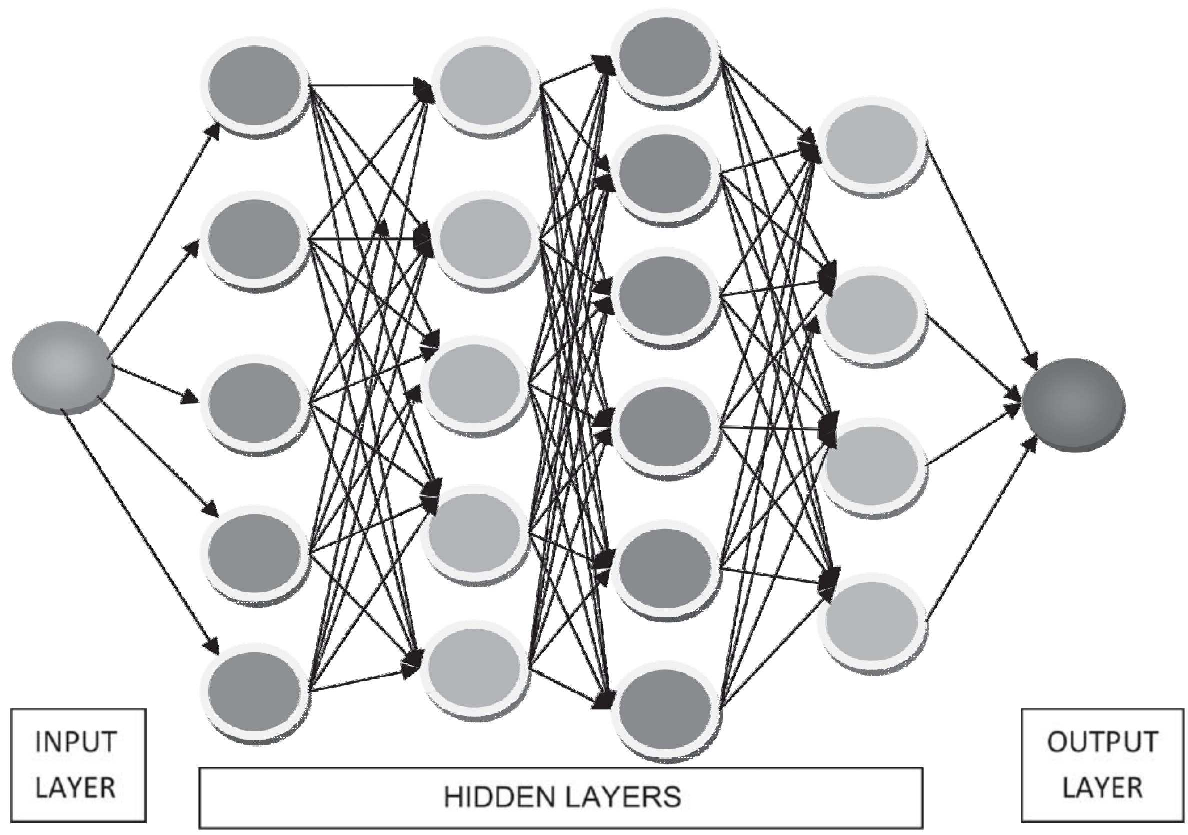

Fig 5. ANN architecture

The Fig. 5 shows the architecture of ANN model so found for the optimal system condition. The ANN model considered here is Multilayer Perceptron (MLP), having an input layer, output layer and 4 hidden layers, with each of the hidden layer consisting of 5, 5, 6 and 4 neurons respectively.

B: TRAINNG

With the help of the simulated data the neural network is trained having architecture as shown in Fig 6. The process of varying the weights to achieve the output is called training. The neural network algorithm uses back propagation neural network trained by ant colony optimization [5, 6 and 7].

To satisfy the linearity property between input temperature and output voltage signal, the target graph is considered as shown in Fig 6.

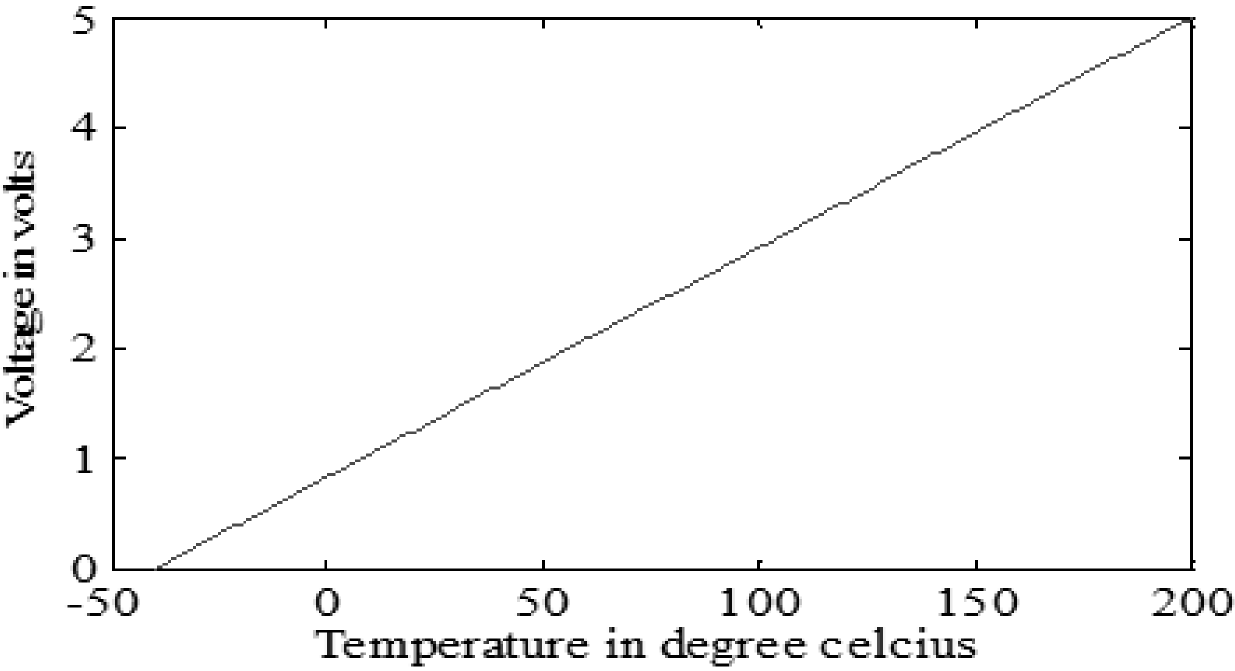

Fig 6. Target graph

TABLE 1: Summarizes the require data for training.

<table>
<tr><td colspan="6">OPTIMIZED PARAMETERS OF THE NEURAL NETWORKS MODEL</td></tr>
<tr><td colspan="2" rowspan="3">Database</td><td colspan="2">Training base</td><td colspan="2">84</td></tr>
<tr><td colspan="2">Validation base</td><td colspan="2">28</td></tr>
<tr><td colspan="2">Test base</td><td colspan="2">28</td></tr>
<tr><td colspan="2" rowspan="4">No of neurons in</td><td colspan="2">1st layer</td><td colspan="2">5</td></tr>
<tr><td colspan="2">2nd layer</td><td colspan="2">5</td></tr>
<tr><td colspan="2">3rd layer</td><td colspan="2">6</td></tr>
<tr><td colspan="2">4th layer</td><td colspan="2">4</td></tr>
<tr><td colspan="2" rowspan="5">Transfer function of</td><td colspan="2">1st layer</td><td colspan="2">logsig</td></tr>
<tr><td colspan="2">2nd layer</td><td colspan="2">logsig</td></tr>
<tr><td colspan="2">3rd layer</td><td colspan="2">logsig</td></tr>
<tr><td colspan="2">4th layer</td><td colspan="2">logsig</td></tr>
<tr><td colspan="2">Output layer</td><td colspan="2">linear</td></tr>
<tr><td rowspan="3">Input</td><td></td><td>Temperature</td><td colspan="2">Temperature coefficient (β)</td><td>Reference resistance(R_o)</td></tr>
<tr><td>min</td><td>-40°C</td><td colspan="2">3000</td><td>2 KΩ</td></tr>
<tr><td>max</td><td>200°C</td><td colspan="2">9000</td><td>6 KΩ</td></tr>
<tr><td colspan="2" rowspan="3">MSE</td><td colspan="2">Training</td><td colspan="2">0.428E-09</td></tr>
<tr><td colspan="2">Validation</td><td colspan="2">4.265E-09</td></tr>
<tr><td colspan="2">Test</td><td colspan="2">5.937E-08</td></tr>
<tr><td colspan="2" rowspan="3">R</td><td colspan="2">Training</td><td colspan="2">0.9999990</td></tr>
<tr><td colspan="2">Validation</td><td colspan="2">0.9999996</td></tr>
<tr><td colspan="2">Test</td><td colspan="2">0.9999990</td></tr>
</table>

C: FLOW CHART

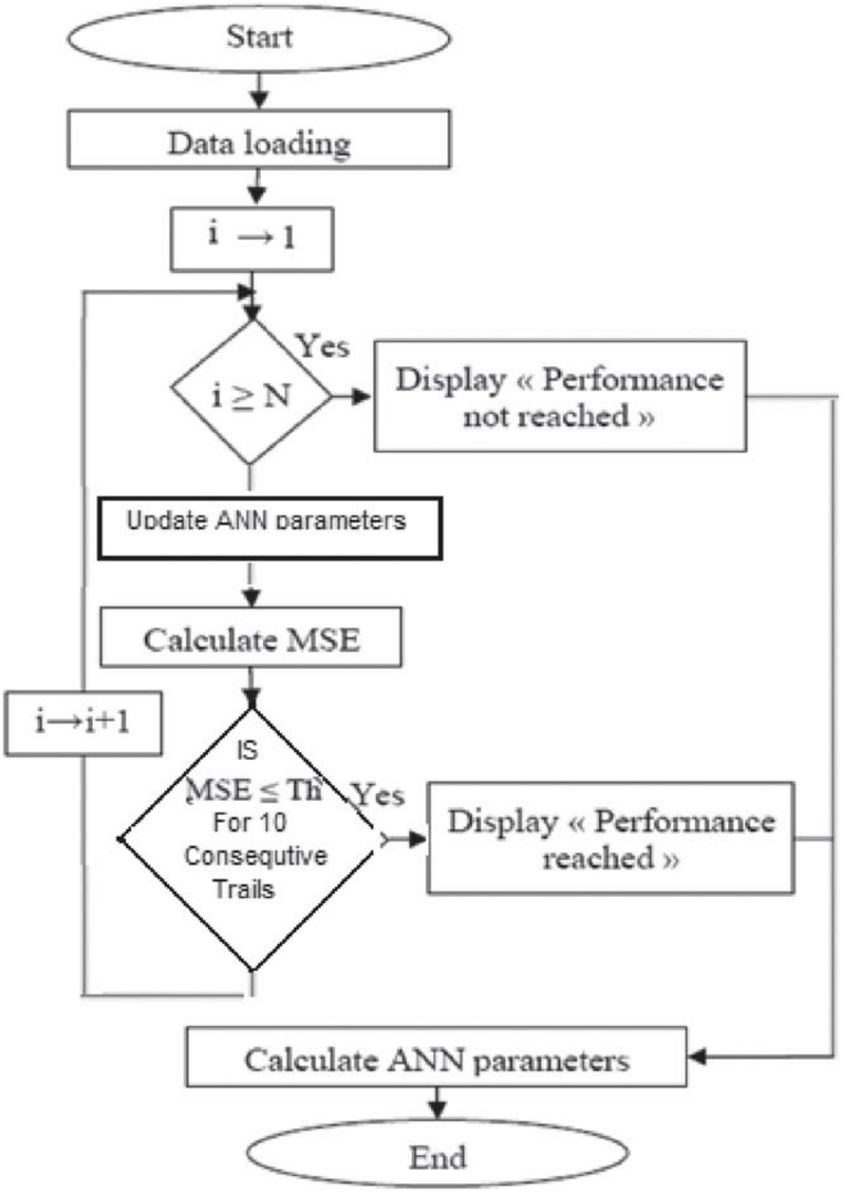

Fig. 7: Flow chart of neural network

The functionality of ANN can be explained as given below. First the data is initialized: like training base (60%), test base (20%), validation base (20%), number of layers and neurons, type of the transfer functions, number of iteration and estimate threshold. The network is trained to compute the weights. Once the weights are computed, it is verified to have mean square error (MSE) is less than estimate error threshold (Th) for at least 10 consecutive readings. If the above condition is satisfied the whole model is saved, else the iteration for updates of ANN parameters continue till it reaches the maximum value and then the model is saved with cautioned that performance not reached. Else the system will accept a new set of data to satisfy the conditions. After the network is trained the following should be kept in mind, MSE is the average squared difference between outputs and targets. Lower value of MSE is better. Zero MSE means no error. Regression R measures the correlation between outputs and targets. An R value of 1 means a close relationship, 0 a random relationship [9].

6. RESULT AND CONCLUSION

The proposed ANN is trained, validated and tested with the simulated data. Once the training is over, the system with thermistor along with other modules in cascade as shown in Fig 2 is subjected to various test inputs corresponding to different temperature at a particular temperature coefficient, reference resistance, all within the specified range. For testing purposes the range of temperature is considered from -40 to 200 °C, the range of β is 3000 to 9000; range of R_o is 2 KΩ to 6 KΩ. The outputs of system with ANN are noted corresponding to various input temperature at different values of β and R_o within the range the input output result is plotted and is shown in Fig 8. The output graph is matching the target graph as shown in Fig 6.

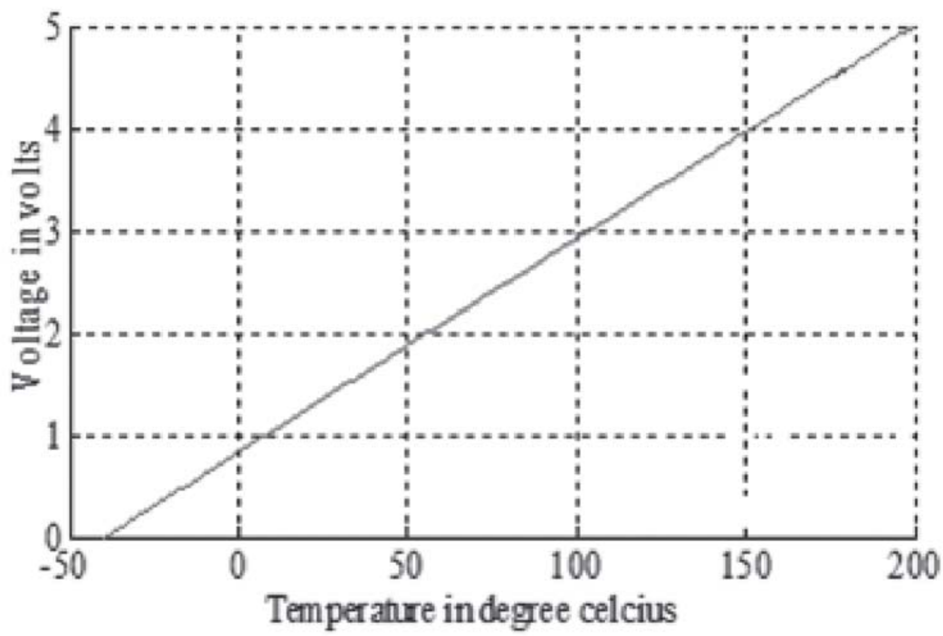

Fig 8. Response of the system with variable R_o and β

It is evident from the Fig 8, that the proposed measuring technique discussed has incorporated intelligence to the thermistor; it has increased the linearity range of the thermistor. Also the output is independent of the β and R_o. Thus if the thermistor is replaced by another thermistor having different β and R_o, the system does not require any calibration to produce accurate results. An improvement of the reported work [2] is proposed in the present paper by designing the temperature measuring technique independent of temperature coefficient and reference resistance.

REFERENCES

1. Jagdish Chandra Patra, Alex C. Kot, Ganapati Panda, "An Intelligent Pressure Sensor Using Neural Networks". IEEE transactions on instrumentation and measurement, vol.49, pp 829-834, August 2000.

2. Santhosh K V, B K Roy, "A Technique to extend the linearity range of Thermistor using ANN", National conference on Computational Control Systems and Optimization, Bangalore, pp 021, May 2011.

3. Steinhart, J.S. and Hart, S.R., "Calibration Curves for Thermistors," *Deep Sea Research*, 15:497, 1968.

4. Neubert, H. K. P. "*Instrument Transducers: an Introduction to their Performance and Design",* Clarendon Press, Oxford (1975).

5. E. O Deoblin, "Measurement Systems Application and Design" Mc Graw Hill

6. Jeng-Bin Li, Yun-Kung Chung, "A Novel Back propagation Neural Network Training Algorithm Designed by an Ant Colony Optimization" IEEE/PES Transmission and Distribution Conference & Exhibition: Asia and Pacific Dalian, China 2005.

7. L. Bianchi, L.M. Gambardella, M.Dorigo "An ant colony optimization approach to the probabilistic traveling salesman problem" . *In Proceedings of PPSN-VII, Seventh Inter*17 *national Conference on Parallel Problem Solving from Nature*, Lecture Notes in Computer Science. Springer Verlag, Berlin, Germany, 2002.

8. Stuart Russell and Peter Norvig. "*Artificial Intelligence A Modern Approach"*

9. K. Madsen, H.B. Nielsen, O. Tingleff "Methods for Non-Linear Least Squares Problems "

 ISSN No. 2231-3273

TRANSMISSION RATE OF NON-COOPERATIVE ROUTING IN AD HOC NETWORK

K.Vanisree
Asst.Professor, Department of ECE
Krishnamurthy Institute of Technology, Hyderabad, Andhra Pradesh
E-mail : vaishnav_56@yahoo.co.in, Mobile : 09959449708

V.S.K.Reddy
Principal, Malla Reddy College of Engineering &Technology, Hyderabad, Andhra Pradesh
E-mail: vskreddy2003@gmail.com

MJC Prasad
Professor, Department of ECE
Malla Reddy Engineering. College, Hyderabad, Andhra Pradesh
E-mail: jagadishnatta@gmail.com

ABSTRACT

This paper analyzes routing in lossy networks under the assumption of non-cooperative aspect of existing routing protocols. We study the three existing non-cooperative routing protocols namely AODV, DSDV, and DSR under different topologies and under different communication traffic pattern to analyze its performance under each of the scenario and traffic. We also analyze them based on various number communications i.e. number of flows. We try to find among the non-cooperative protocols which one performs better under given scenario and traffic.

Keywords: *Non-cooperative transmission, energy efficiency, routing protocol, Packet delivery ratio, end-to-end delay Packet drop, energy consumption, flow., tranismission rate.*

1. INTRODUCTION

A mobile ad hoc network (MANET), sometimes called a mobile mesh network, is a self-configuring network of mobile devices connected by wireless links. Each device in a MANET is free to move independently in any direction, and will therefore change its links to other devices frequently. Each must forward traffic unrelated to its own use, and therefore be a router. Such networks may operate by themselves or may be connected to the larger Internet. The primary challenge in building a MANET is equipping each device to continuously maintain the information required to properly route traffic and have enough energy to keep it alive.

From the energy point of view, nodes spend most of their energy in transmitting data, but in many applications these nodes are small and have limited energy supply such as in wireless sensor networks. Much work has been done in this area to reduce the total required transmit power going from a source node to a destination node by choosing a transmission scheme that requires the minimum amount of transmit power.

In large scale networks, the control decision are often has to be taken at the each end user or node in accordance with the requirement and performance metrics. Such networks are called as non-cooperative networks. Non-cooperative routing has been under study for a long time under the concept of traffic and telecommunications networks.
In this paper, the performance of three existing non-cooperative protocols are studied, namely AODV, DSDV and DSR under different topologies and traffic scenarios to see which of them performs better in a given scenario. The paper gives detailed about the scenarios and traffic pattern taken for the comparison study and also gives the results in detail for better understanding of these three protocols.

The paper is organized as follows. Section-II discusses the related work done in this field and gives a brief but yet an elaborate description of three non-cooperative protocols under study. In section-III, the system model is given and in the next section (IV), we give the performance metrics taken up for this study. In section V the simulation results and discussions are given. In section-VI the conclusion is presented followed by the future work in section VII.

2. RELATED WORK

There has been quite a few no. of studies done based on these three protocols. In paper [1] a study on AODV protocol of two flavours namely AODV-UU and AODV-UCSB under different load and packet sizes. In paper [6] the on-demand routing protocols namely AODV and DSR have been compared under varying load, mobility, network size and connectivity. In that paper, it is shown that under high pause time DSR performs better and under high mobility AODV performs better. It is also shown that the overhead routing is higher in case of AODV compared to DSR. In paper [7], the authors have studied the three protocols under grid environment and concluded that AODV is the better one in the given scenario of mobility pattern model with varying degree of pause time. In the following chapters a brief yet elaborate description about the non-cooperative protocols taken up for the study purpose is given.

2.1 AD HOC ON-DEMAND DISTANCE VECTOR (AODV): The routing protocol is an on-demand routing protocol designed for mobile ad hoc networks. AODV is capable of both unicast and multicast routing. It is an on demand algorithm, means that it builds routes between nodes only as desired by source nodes. It maintains these routes as long as they are needed by the sources. Additionally, AODV forms trees which connect multicast group members. The trees are composed of the group members and the nodes needed to connect the members. AODV uses sequence numbers to ensure the freshness of routes. It is loop-free, self-starting, and scales to large numbers of mobile nodes. It is used to pass messages from one computer or node to another one to which it cannot directly communicate. It does this by passing the message along its neighbors to reach the receiver. This route is formed by discovering the routes through which data can be passed. It also makes sure there is no loop in the identified route and it also tries to find the shortest path route between the source and the receiver. It can also handle changes in nodes link, route links and can create new routes if it finds an error in the existing route.

AODV builds routes using a route request / route reply query cycle. When a source node desires a route to a destination for which it does not already have a route, it broadcasts a route request (RREQ) packet across the network. Nodes receiving this packet update their information for the source node and set up backwards pointers to the source node in the route tables. In addition to the source node's IP address, current sequence number, and broadcast ID, the RREQ also contains the most recent sequence number for the destination of which the source node is aware. A node receiving the RREQ may send a route reply (RREP) if it is either the destination or if it has a route to the destination with corresponding sequence number greater than or equal to that contained in the RREQ. If this is the case, it unicasts a RREP back to the source. Otherwise, it rebroadcasts the RREQ. Nodes keep track of the RREQ's source IP address and broadcast ID. If they receive a RREQ which they have already processed, they discard the RREQ and do not forward it.

As the RREP propagates back to the source, nodes set up forward pointers to the destination. Once the source node receives the RREP, it may begin to forward data packets to the destination. If the source later receives a RREP containing a greater sequence number or contains the same sequence number with a smaller hop count, it may update its routing information for that destination and begin using the better route.

As long as the route remains active, it will continue to be maintained. A route is considered active as long as there are data packets periodically traveling from the source to the destination along that path. Once the source stops sending data packets, the links will time out and eventually be deleted from the intermediate node routing tables. If a link break occurs while the route is active, the node upstream of the break propagates a route error (RERR) message to the source node to inform it of the now unreachable destination(s). After receiving the RERR, if the source node still desires the route, it can reinitiate route discovery.

The following figure illustrates the reverse path and forward path formation that takes place during RREQ and RREP phases.

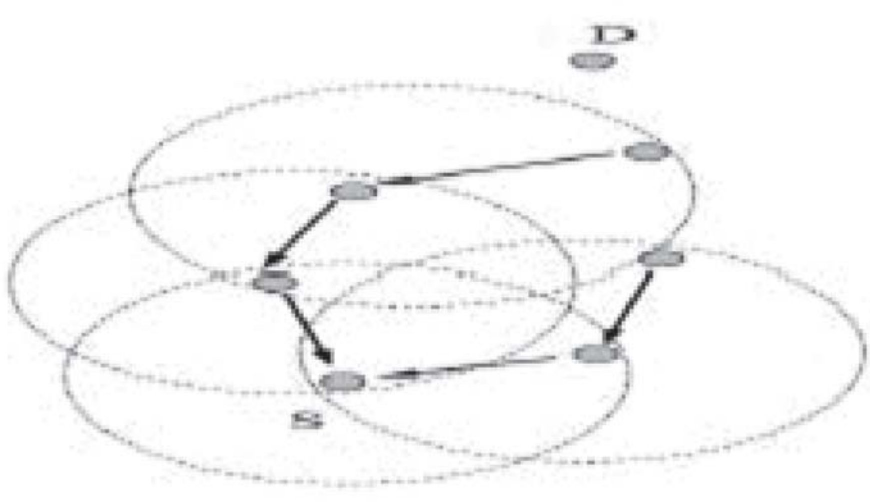

FIG. 1: Reverse path information using RREQ

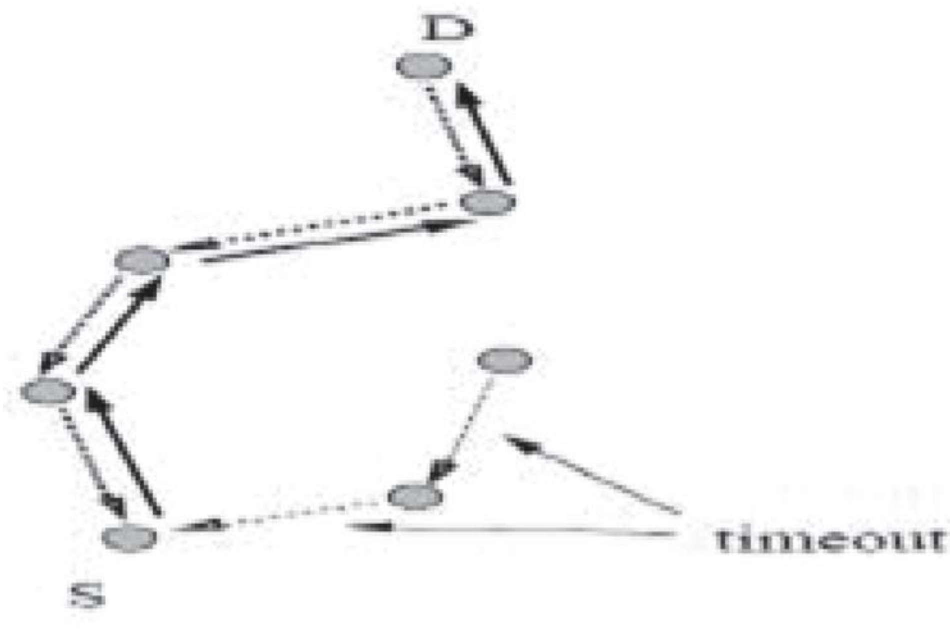

FIG 2: Forward path information during RREP.

2.2 DYNAMIC SOURCE ROUTING PROTOCOL (DSR) Dynamic Source Routing (DSR) is a routing protocol for wireless mesh networks. It is similar to AODV in that it forms a route on-demand when a transmitting computer requests one. However, it uses source routing instead of relying on the routing table at each intermediate device. It is a simple on demand routing protocol designed for use in multi-hop wireless ad hoc networks. DSR allows the network to be completely self-organizing and self-configuring, without the need for any existing network infrastructure or administration. The main difference between AODV and DSR is that while in the former, the route to the destination is maintained at each node; in the latter it is the source which maintains the route to the destination. It is a reactive protocol.

Determining source routes requires accumulating the address of each device between the source and destination during route discovery. The accumulated path information is cached by nodes processing the route discovery packets. The learned paths are used to route packets. To accomplish source routing, the routed packets contain the address of each device the packet will traverse. This may result in high overhead for long paths or large addresses, like IPv6. To avoid using source routing, DSR optionally defines a flow id option that allows packets to be forwarded on a hop-by-hop basis.
This protocol is truly based on source routing whereby all the routing information is maintained (continually updated) at mobile nodes. It has only two major phases, which are Route Discovery and Route Maintenance. Route Reply would only be generated if the message has reached the intended destination node (route record which is initially contained in Route Request would be inserted into the Route Reply).

To return the Route Reply, the destination node must have a route to the source node. If the route is in the Destination Node's route cache, the route would be used. Otherwise, the node will reverse the route based on the route record in the Route Reply message header (this requires that all links are symmetric). In the event of fatal transmission, the Route Maintenance Phase is initiated whereby the Route Error packets are generated at a node. The erroneous hop will be removed from the node's route cache; all routes containing the hop are truncated at that point. Again, the Route Discovery Phase is initiated to determine the most viable route.

DSR protocol consists of two mechanism that allow it discover and maintain a route at the source.

1. Route Discovery: The mechanism by which a node **S** wishing to send a packet to a destination node **D** obtains a source route to **D.** Route Discovery is used only when **S** attempts to send a packet to **D** and does not already know a route to **D**.

When a source node wants to send a packet to a destination node, it first checks its route cache to see whether it has a route to the destination. If not, it will start building one by sending out the route request packet which is broadcast. All the forwarding nodes, will add their id in the source route tree and broadcast the packet. When the receiver gets the route request packet either using existing route the source or the one read from the route request packet will be used to forward the route reply message back to the sender.

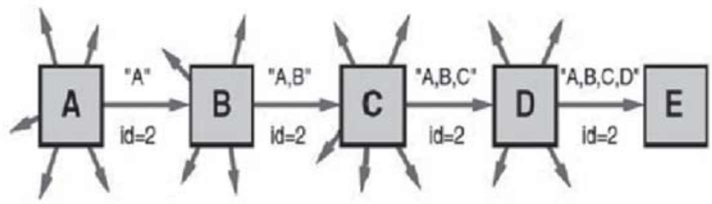

FIG 3. Route discovery phase

2. Route Maintenance: The mechanism by which node **S** is able to detect, while using a source route to **D**, if the network topology has changed such that it can no longer use its route to **D** because a link along the route no longer works. When Route Maintenance indicates a source route is broken, **S** can attempt to use any other route it happens to know to **D**, or can invoke Route Discovery again to find a new route. Route Maintenance is used only when **S** is actually sending packets to **D**.

When originating or forwarding a packet using a source route, each node transmitting the packet is responsible for confirming that the packet has been received by the next hop along the source route; the packet is retransmitted (up to a maximum number of attempts) until this confirmation of receipt is received. This is achieved by overhearing the packet being transmitted by the forwarded node. If it fails to overhear the packet, then it sends a route error message to the original sender telling where it failed to forward the packet.

2.3 DESTINATION SEQUENCED DISTANCE VECTOR (DSDV) Destination Sequenced Distance Vector (DSDV), also known as Distributed Bellman-Ford or RIP (Routing Information Protocol) is a proactive protocol, where each node maintains a table in which route every other nodes are maintained. It is a table driven protocol.

In this protocol each node maintains a view of the network topology with a cost for each link. Each node periodically broadcasts link costs to its outgoing links to all other nodes such as flooding. The table is periodically sent to all its neighbors to maintain topology.

The routing table consists of following entries.

- all available destinations
- the next node to reach to destination
- the number of hops to reach the destination.

Some of the problems that may arise in this protocol are

- All routing decisions are taken in a completely distributed fashion.
- Each node uses its local information for routing messages. However, the local information may be old and invalid.
- Local information may not be updated promptly.

This gives rise to loops. A message may loop around a cycle for a long time.

3. SYSTEM MODEL

3.1 METHODOLOGY The framework and skeleton overview for the performance evaluation of the chosen protocols is given. The techniques used are modeling the network, simulating the network and measuring the performance of the protocols.

Performance is the key criteria in all aspect of activity to measure the effectiveness of the system. We need to know the techniques to evaluate the performance of the given system and to know the best performer for the given price. The three techniques used are modeling, simulation and measurement.

Simulation is the simplest and best form compared to analytical modeling as it requires fewer assumptions and can have more details. Computer based simulation tool is best suitable as it is cost effective and consumes less time, also at the same time can deliver at a better speed and accuracy.

There are number of network simulator tool available for the project like OPNET, Glomosim, Qualnet and network simulator (NS-2) etc. Here we have chosen NS-2 as the computer network simulator.

3.2 ADVANTAGES OF NS-2 NS2 is an open-source simulation tool that runs on Linux. It is a discreet event simulator targeted at networking research and provides substantial support for simulation of routing, multicast protocols and IP protocols, such as UDP, TCP, RTP and SRM over wired and wireless (local and satellite) networks. It has many advantages that make it a useful tool, such as support for multiple protocols and the capability of graphically detailing network traffic. Additionally, NS2 supports several algorithms in routing and queuing. LAN routing and broadcasts are part of routing algorithms. Queuing algorithms include fair queuing, deficit round-robin and FIFO.

3.3 SIMULATION MODEL The nodes initial placement and movement pattern are given in a scenario file which the NS-2 accepts as one of the input parameters. The communication between randomly chosen source and destination nodes is also given as in a traffic file, which the NS-2 accepts as its second input parameters.

TABLE 1. THE BASIC ARCHITECTURE OF NS-2 SIMULATION MODEL

Channel	Channel/WirelessChannel
Propagation	Propagation/TwoRayGround
Network interface	Phy/WirelessPhy
MAC	Mac/802_11
Interface queue	Queue/DropTail/PriQueue
Link layer	LL
Antenna	Antenna/OmniAntenna
Interface queue length	500
No. of nodes	25,50,75,100
Protocols	AODV, DSDV, DSR
Simulation area size	1000 x 100 M
Simulation duration	100 secs
Type of communication	UDP/CBR
Packet size	200 bytes
Packet interval	4 pkts per second
# of communication	5

The output generated by the NS-2 simulator consists of a trace file, named *.tr, where each layer agent like UDP, AODV record their activities like sending a packet, receiving a packet etc.

The second output generated by NS-2 is a animation file, named *.nam, which when animated using NAM animator tool, will show what happens during the entire simulation period.

4. PERFORMANCE ANALYSIS

The performance metrics taken into account are

0 1. Packet delivery ratio %
1 2. end-to-end delay
2 3. Packet drop %
3 4. energy consumption
4 5. Throughput

4.1 PACKET DELIVERY RATIO % The packet delivery ratio (PDR) is defined as the ratio between no. of packets received by the receiver to the no. of packets sent by the corresponding sender.

4.2 END-TO-END DELAY – AVERAGE The average end-to-end delay is defined as the time taken by the packet to reach the receiver from the sender. The packet sent by the source will get delayed due to no. of reasons like being buffered at intermediate nodes, delays caused at MAC layer due to channel availability etc. The average delay is calculated by summing all the individual packet delays and dividing them by the total no. of packets received.

4.3 PACKET DROP % The Packet drop ratio is defined as the ratio between no. of packets dropped by the nodes to the total no. of packets generated by the respective senders.

4.4 ENERGY CONSUMPTION Every mobile node will consume energy for sending a packet, receiving a packet. This study concentrates on the total energy consumed by the mobile node during the simulation period.

5. RESULTS

Fig 4 shows the energy expended overall by each protocol. As AODV and DSR go for constructing routes on-demand they will experience more energy loss compared to DSDV where table is constructed once and updated as and when there is change in the neighborhood topology. As the no. of nodes are increased, all three protocols spend more or less same amount of energy as shown for 100 nodes in the graph.

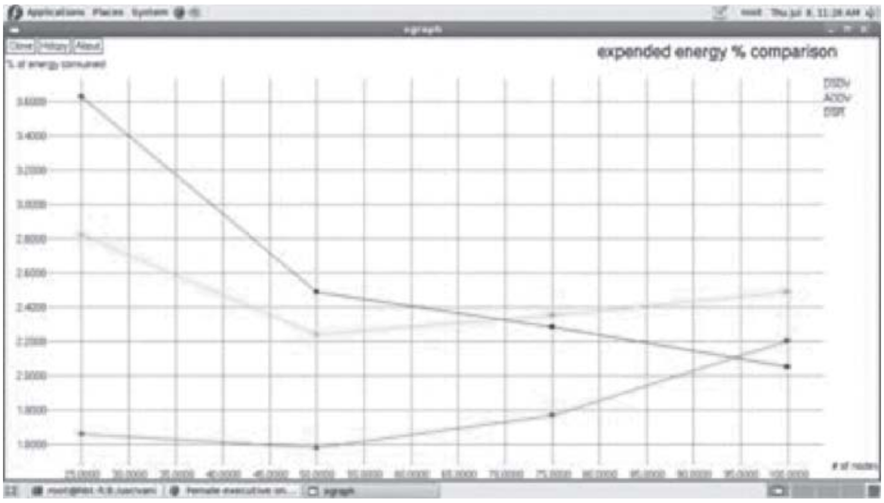

FIG 4. Energy comparison (Nodes Vs. Energy)

Fig 5 shows end-to-end delay for various no. of mobile nodes. As can be seen from the graph, when the no. of nodes is less it takes more time to reach the destination, whereas if the network has enough no. of nodes, the average end-to-end delay has come down.

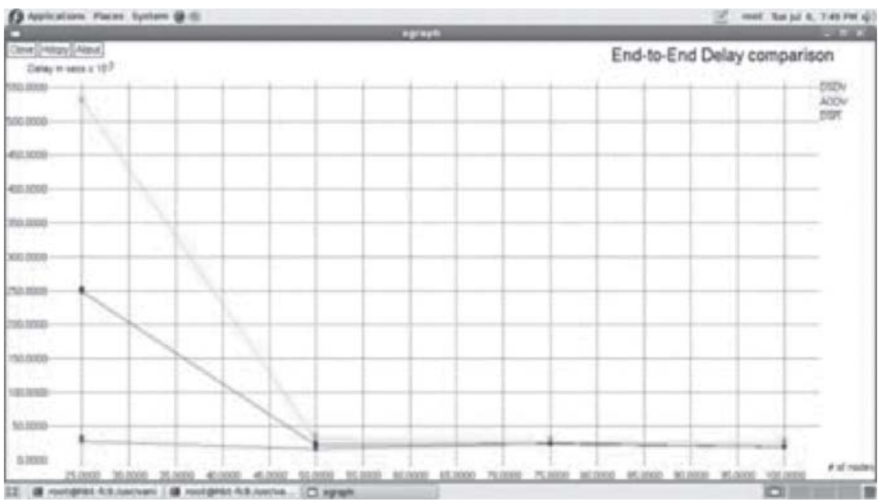

FIG 5. END –TO-END DELAY COMPARISON (Nodes Vs. Delay)

Fig 6 shows the drop % of three protocols. As AODV and DSR are of on-demand routing protocols, they tend to maintain the routes in a valid state always compared to DSDV which is table driven protocol (i.e proactive protocol). So it drops more packets compared to other two, as some of its table entries may not be correct.

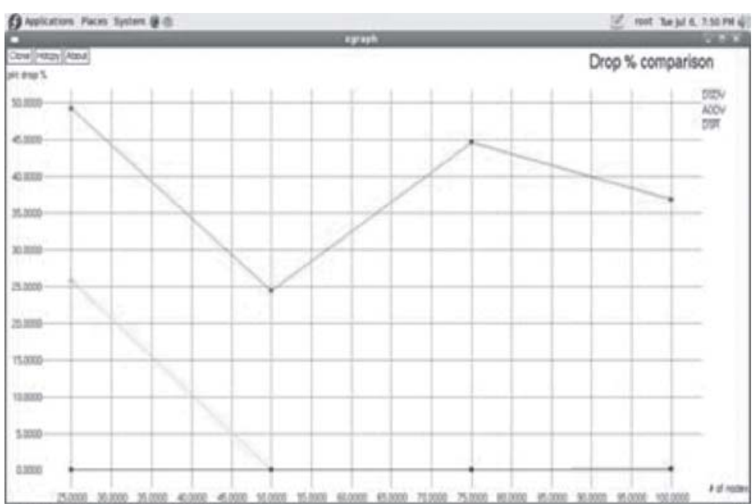

FIG 6. Drop % Comparison (Nodes Vs. Drop)

Fig 7 shows the packet delivery ratio % of the protocols under study. As expected the DSDV performs poor because of table driven routing architecture compared to other two protocols.

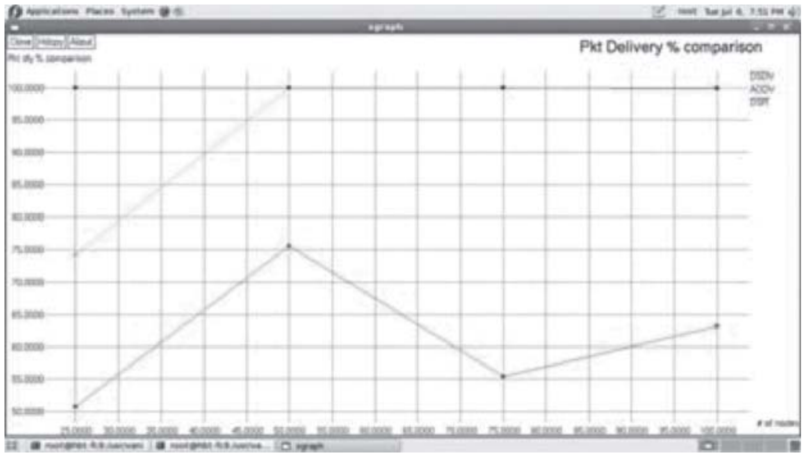

FIG 7. Packet Delivery % Comparison (Nodes Vs. pkt. Delivery)

Fig 8 shows The Throughput ie information received when the no of flows is high the information received is maximum in both AODV and DSR because DSDV is table driven routing architecture.

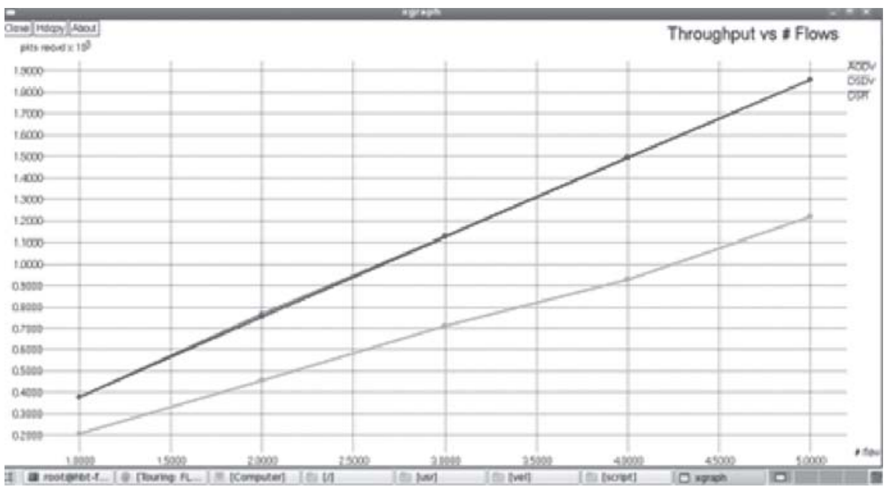

Fig 8. Throughtput Flows (hroughtput Vs Flows)

Fig 9 shows end-to-end delay for various no. of flows. As can be seen from the graph, when the no. of flows is more AODV performance better then other protocols.

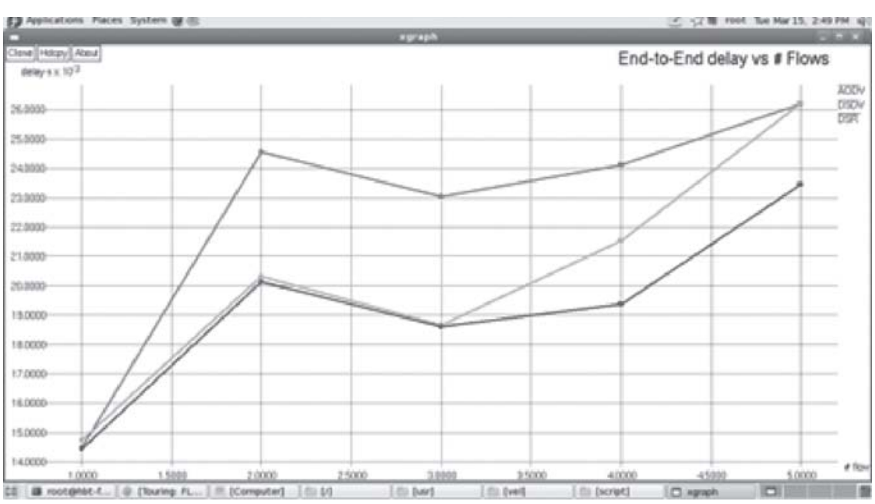

Fig 9 . End-to-End delay, Flows (End-to-End delay Vs Flows)

Fig 10 shows delivery ration % vs flows . When the number of communications is more the DSDV performs poor because of table driven routing architecture compared to other two protocols.

Fig 10. Delivery Ratio flows (Delivery Ratio Vs flows)

6. CONCLUSION

In this paper, the three non-cooperative protocols namely DSR, DSDV and AODV have been investigated. While DSDV falls in the category of proactive protocol, the other two falls under the category of reactive protocols. As proved by theoretical calculations, AODV and DSR performance are more or less on equal levels compared to DSDV. Both AODV and DSR almost deliver all the packets while the DSDV failed sometimes. The Throughput is maximum and almost same in ADOV and DSR.

7. FUTURE WORK

For the future work, it is proposed to convert any one of the non-cooperative routing protocols into a co-operative routing agent either based on nodes link cost or on the transmission power of individual nodes. Further scope is to introduce cooperativeness among the participating nodes in order to lessen the burden on one particular forwarding node. This may lead to better throughput, end-to-end delay and in-directly lead to lengthen the lifetime of the network. In order to achieve the last stated criteria, we plan to introduce a weigh factor for each node that will include both the link cost in terms of distance to be covered and success rate of transmission and the residual energy of the participating node. We also propose to go in for reliability aspect as well as diversity in the network for better lifetime of the network.

REFERNCES

1. Z.Alexander, Performance Evaluation of AODV Routing Protocol: Real-Life Measurements, SCC,June 2003.
2. Altman E, and Jimenez T., (2003). NS Simulator for Beginners. Lecture notes. Univ.de Los Andes, Merida, Venezuela and ESSI.Sophia-Antipolis, France.
3. D. Johnson, Dynamic Source Routing for Mobile Ad Hoc Networks, IEFT MANET Draft, April 2003.
4. S. Nesargi, R. Prakash, “MANETconf: Configuration of Hosts in a Mobile Ad Hoc Networks”, 21st Annual Joint Conf. of the IEEE Computer and Communications Societies (INFOCOM), Jun. 2002.
5. Wen,Y., Mobile Grid. (2002). Department of Computer Science, University of California, Santa Barbara, pp.1-7.
6. S. Das, C. Perkins, and E. Royer. Performance comparison of two on-demand routing protocols for ad hoc networks. In INFOCOM'2000 (1), pages 3–12, 2000.
7. K. Fall. ns notes and documentation. The VINT Project, 2000.
8. D.Johnson. Validation of wireless and mobile network models and simulation. In DARPA/NIST Network Simulation Validation Workshop, Fairfax, Virginia, USA, May 1999.

9. D. Johnson, D. Maltz, and J. Broch. DSR: The Dynamic Source Routing Protocol for Multihop Wireless Ad Hoc Networks. In Ad Hoc Networking, C. Perkins (ed), Chapter 5, pages 139–172, 2001.

10. Charles E. Perkins and Elizabeth M. Royer, “Ad Hoc On-Demand Distance Vector Routing,” in Proceedings of the 2nd IEEE Workshop on Mobile Computing Syslems and Applications, Feb. 1999, pp. 90-100.

11. David B. Johnson and David A. Maltz, "Dynamic source routing in adhoc wireless networks,” in Mobile computing, T. lmielinski and H. Kmh, Eds, Kluwer Academic, 1996, ch.5 .

12. David B. Johnson and David A. Maltz. Dynamic Source Routing in Ad Hoc Wireless Networks. In Mobile Computing, edited by Tomasz Imielinski and Hank Korth, chapter 5, pages 153–181. Kluwer Academic Publishers, 1996.

13. Perkins,C.E., and Bhagwat.P. (1994). Highly Dynamic Destination-Sequenced Distance-Vector Routing (DSDV) for Mobile Computers. ACM, pp.234 – 244.

The Network Simulator NS-2 homepage, http://www.isi.edu/nsnam/ns/

COMPUTATION OF RCS WITH TLM METHOD USING SECOND ORDER HIGDONS BOUNDARY OPERATORS

R. Srinivasa Rao
Professor, Dept of ECE,
Sree Vidyanikethan Engineering College,
Sree Sainatha Nagar, Tirupathi, Andhra Pradesh.
E-mail: rsrao55@hotmail.com

Dr. PV Subbaiah
Principal,
Amrita Sai Institute of Science and Technology
Paritala, Krishna Dist, Andhra Pradesh,
E-mail: pvs_ece2000@yahoo.co.in

ABSTRACT

Presented in this paper, is the computation of RCS of dielectric cubes of high relative permittivity by using time domain Transmission Line Matrix (TLM) method comparison of the results published measurements [1]. Since the high permittivity cubes reradiate a very long time, high quality absorbing boundary conditions having long term stability are required. To achieve these, second order boundary conditions derived from first order Higdon's boundary operators are used. Long term stability has been obtained by using proper discretization of the boundary operators (derivatives), and very low reflections have been obtained by concatenating two first order boundary operators. The RCS data computed with the TLM method agree very well with the measurements published in [1]. The frequency shift between the TLM results and the measurements is negligible, while a considerable frequency shift has been reported between results obtained with FDTD and measurement

Keywords: Transmission line matrix(TLM) method, Finite-difference time domain method(FDTD), Radar cross section (RCS).

1. INTRODUCTION

The TLM method is a time domain numerical technique in which both space and time are discretized [2]. The simulation of propagation of electromagnetic waves is done through scattering of impulses in a 3-D meshed network of transmission lines. This method can be used for computation of radar cross-section (RCS) of complex bodies. The RCS over a wide frequency bandwidth can be obtained from a single TLM simulation. Earlier studies on computation of RCS using the TLM method have concentrated mainly on perfectly conducting targets [3-6].

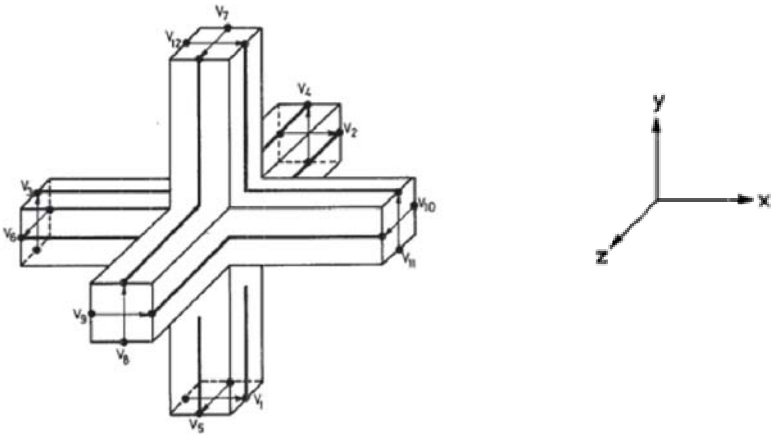

Fig. 1: The Symmetrical Condensed Node (SCN)

This paper studies the scattering properties of high permittivity dielectric cubes. As these cubes ring for a very long time, highly stable absorbing boundary conditions are required for a TLM analysis as compared to the perfectly conducting targets. Even though a number of absorbing boundary conditions have been reported in the literature, Higdon's absorbing boundary conditions [7] have been found to perform better than others [8]. The absorption properties in the required frequency range can be optimized by taking advantage of the prior information about the incident angles and by combining several first-order boundary operators [9-10]. Also, the long term stability can be obtained by choosing the proper finite differences for the boundary operators. We have used the symmetrical condensed node (SCN) TLM [11] shown in Fig.1 for obtaining the scattered tangential electric and magnetic fields on the fictitious current surfaces. The advantages of this node when compared to the expanded TLM node and Yee's FDTD node are the following: boundary description is easier, and all six field components can be defined at single points in space. It has six branches, each branch consisting of two uncoupled two-wire transmission lines. The 12 transmission lines linking the Cartesian mesh of nodes together have the characteristic impedance of free space. Each line is associated with two fields. For example, a voltage impulse incident upon the port 3 is associated with the field quantities E_y and H_z.

2. ABSORBING BOUNDARY CONDITIONS

To obtain good absorption over a wide range of incident angles, we have concatenated two first order Higdon's boundary operators to obtain a second-order absorbing boundary condition [9]. A voltage impulse reflected from the absorbing boundary can be computed from the knowledge of impulses in the cells in front of the boundary using the following equation:

$$\begin{aligned} V^n(m,j,k) &= (\alpha_1+\alpha_2)V^{n-1}(m,j,k) - \alpha_1\alpha_2 V^{n-2}(m,j,k) + (\beta_1+\beta_2)V^n(m-1,j,k) \\ &+ (\gamma_1+\gamma_2-\alpha_1\beta_2-\beta_1\alpha_2)V^{n-1}(m-1,j,k) - (\alpha_1\gamma_2+\gamma_1\alpha_2)V^{n-2}(m-1,j,k) \\ &- \beta_1\beta_2 V^n(m-2,j,k) - (\beta_1\gamma_2+\gamma_1\beta_2)V^{n-1}(m-2,j,k) - \gamma_1\gamma_2 V^{n-2}(m-2,j,k) \end{aligned} \tag{1}$$

The interpolation coefficients are

$$\alpha_i = \frac{[a-g_i(1-b)]}{[a-1-g_i(1-b)-\varepsilon_i\Delta l]}$$

$$\beta_i = \frac{(a-1+g_i b)}{[a-1-g_i(1-b)-\varepsilon_i\Delta l]}$$

$$\gamma_i = \frac{-(a+g_i b)}{[a-1-g_i(1-b)-\varepsilon_i\Delta l]} \tag{2}$$

where coefficients a and b are weighted time and space averages of the space and time differences, respectively. The parameters, ε_1 and ε_2 are damping factors. The parameter g_i is

$$g_i = \frac{\cos\theta_i}{c}\frac{\Delta l}{\Delta t} \tag{3}$$

where Δl and Δt are the space resolution and time step respectively . The angles θi are the incidence angles.

For the symmetrical condensed node $g_i = \cos\theta_i$. The values of a and b can be chosen to control the stability of the absorbing boundaries. According to Higdon [7], a must be less than or equal to 0.5 (for $a = b$) to get stable absorbing boundary conditions.

3. NEAR-FIELD TO FAR-FIELD TRANSFORMATION

To calculate the far field, we used the well known near to far field technique based on the equivalence principle. In this technique the far fields can be computed if the tangential electric and magnetic fields on a closed fictitious surface enclosing the scatterer are available. For computational convenience, a virtual cube is selected as the enclosing surface and the equivalent electric and the magnetic surface currents are calculated from TLM method computed fields. The electric and magnetic currents are calculated using respectively.

$$\mathbf{J} = \hat{\mathbf{n}} \times \mathbf{H}^s \tag{4}$$

and

$$\mathbf{M} = -\hat{\mathbf{n}} \times \mathbf{E}^s \tag{5}$$

Here, $\mathbf{E}^s$ and $\mathbf{H}^s$ are the scattered electric and magnetic fields, respectively, and, $\hat{\mathbf{n}}$ is the unit outward normal of the cube. Along each side of the cube the equivalent phasor currents are calculated using DFTs applied to the TLM computed tangential fields. From the available current densities, the electric and magnetic vector potentials can be calculated from the following equations:

$$\mathbf{A} = \frac{\mu_o}{4\pi}\int_s \mathbf{J}_s \frac{e^{-jkR}}{R} ds' \tag{6}$$

$$\mathbf{F} = \frac{\varepsilon_o}{4\pi}\int_s \mathbf{M}_s \frac{e^{-jkR}}{R} ds' \tag{7}$$

The phasor $E-$ and $H-$ fields due to the vector potentials are given by

$$\mathbf{E} = -j\omega\left[\mathbf{A} + \frac{1}{k^2}\nabla\left(\nabla\cdot\mathbf{A}\right)\right] - \frac{1}{\varepsilon_o}\nabla\times\mathbf{F} \tag{8}$$

$$\mathbf{H} = -j\omega\left[\mathbf{F} + \frac{1}{k^2}\nabla\left(\nabla\cdot\mathbf{F}\right)\right] + \frac{1}{\varepsilon_o}\nabla\times\mathbf{A} \tag{9}$$

Neglecting terms that diminish as order $1/r^2$ or faster and radial field components of negligible amplitude compared to θ and ϕ components, we obtain far electric field components as.

$$\mathbf{E}_\theta \equiv j\omega\left(\mathbf{A}_\theta + \eta_o\mathbf{F}_\phi\right) \tag{10}$$

$$\mathbf{E}_\phi \equiv -j\omega\left(\mathbf{A}_\phi - \eta_o\mathbf{F}_\theta\right) \tag{11}$$

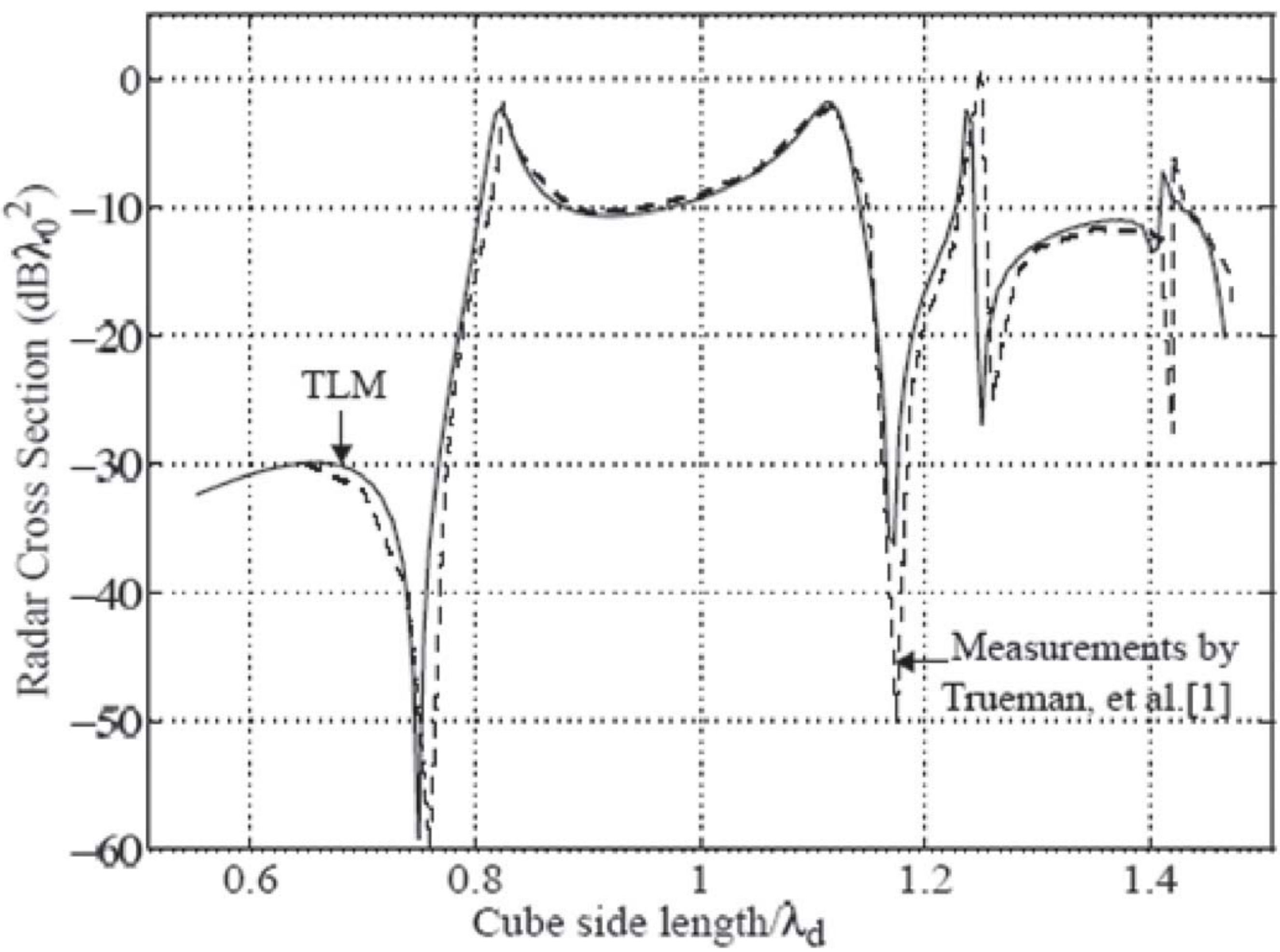

Fig. 2: RCS computed with 60,000 TLM time steps (cube side=8.97mm and ε_r = 37.84).

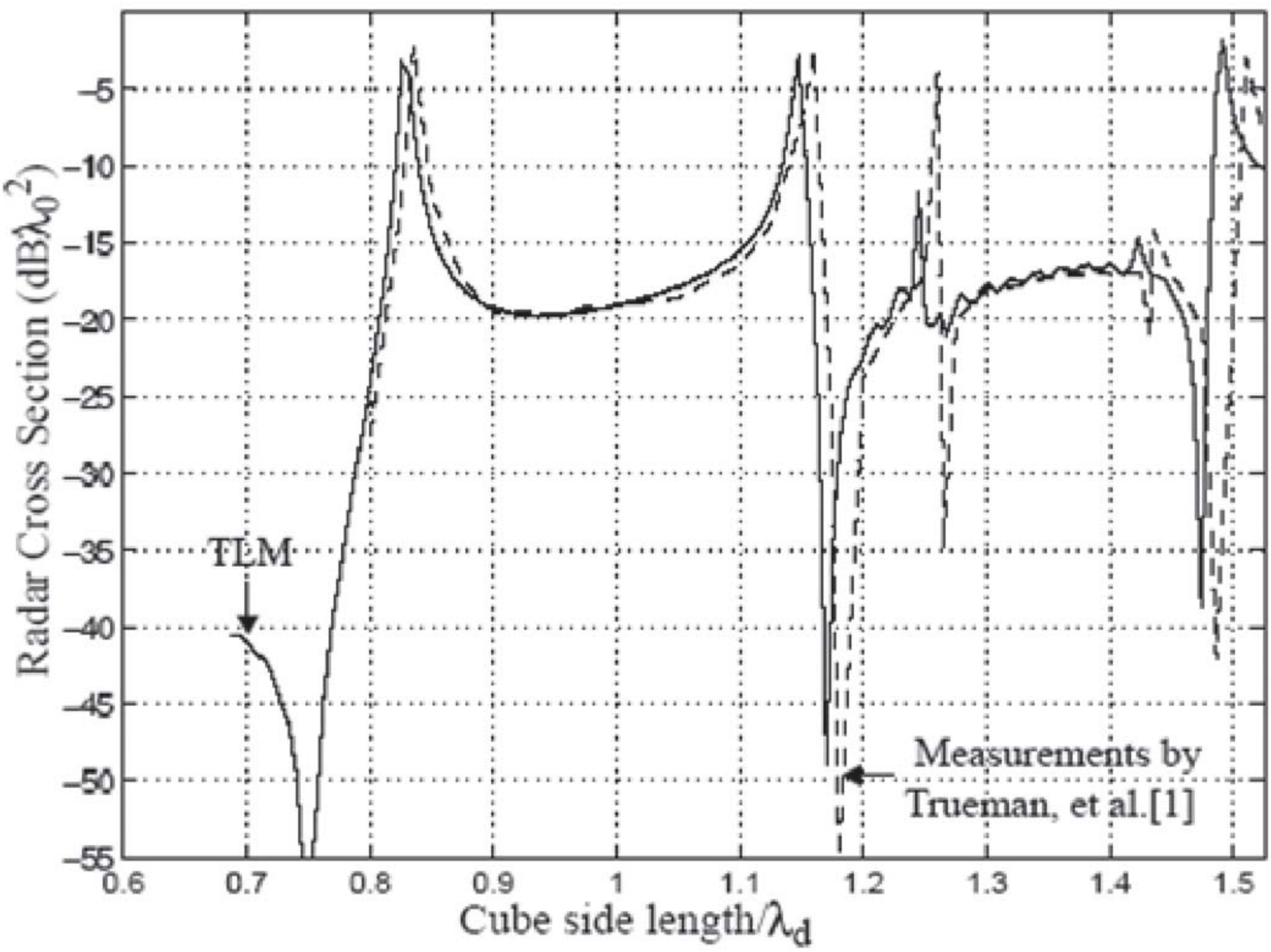

Fig. 3: RCS computed with 60,000 TLM time steps (cube side=7.72mm and ε_r = 79.64).

4. NUMERICAL RESULTS

The dielectric cube of size 8.97 mm and permittivity 37.84 was discretized into 15 SCN-TLM cells on each side. The space resolution and time step were 0.598 mm and 0.9966 *ps*, respectively. A plane wave with a electric field component E_y and magnetic field component H_z was incident on one face of the cube normally. This was achieved in the symmetrical condensed node by launching the impulses on branch 3. We have used a cosine modulated Gaussian pulse as the excitation to make sure that only the frequencies of interest were excited. The excitation Gaussian pulse width (corresponding to -34 dB) was 127Δt. The values of the incidence angles used in the design of the absorbing boundaries were 45^0 and 85^0 . The absorbing boundaries were placed 20 cells away from the cube surfaces.

Fig. 2 shows the RCS data computed with 60,000 time steps. They compare well with the measurements. Next, we have computed the RCS of a cube of size 7.72 mm and ε_r = 79.46 [1]. Again, the same TLM discretization as above (i.e., 15 cells along the length of the cube and 20 cells between the cube edge and the absorbing boundaries) was used. The space resolution and time step were 0.5147 mm and 0.8578 *ps*, respectively. The width of the cosine modulated Gaussian pulse was 148 Δt. Fig. 3 compares the computed RCS (using 60,000 TLM time steps) and measurement. They compare well except for a slight shift in the TLM results towards lower frequencies because of the coarseness error.

5. CONCLUSIONS

The RCS of high permittivity dielectric cubes has been obtained using the TLM method. The results agree very well with the measurements published in [1]. While the frequency shift between the TLM results and the measurements is negligible for ε_r=37.84, it is very small in the case of ε_r=79.46. A much larger shift has been reported in the FDTD analysis.

The present study shows that Higdon's absorbing boundaries have superior absorption and long term stability. Also, they are very efficient since they need to be placed only 20 cells away from the cube surfaces. The frequency domain near-field to far-field transformation technique requires huge disk space to store the tangential electric and magnetic fields on the fictitious current surfaces (of the order of 100 Mbytes for 100 frequency points). One way of avoiding this is to compute the far –fields directly in the time domain as done in [12]. In that case, Prony' s method can be applied to estimate the future time response from a short initial time response, leading to a very fast TLM analysis. Our future work will concentrate on these techniques.

REFERENCES

1. C.W. Trueman, S.J. Kubina, R.J. Luebbers, S.R. Mishra, and C. Larose, "RCS of High Permittivity Cubes by FDTD and by Measurement", *9th Annual Review of Progress in Applied Computational Electromagnetics* Digest, pp. 2-10, March 22-26, 1993, Monterey, CA.

2. W. J. R. Hoefer, "The Transmission Line Matrix (TLM) Method", in T. Itoh: *Numerical Techniques for Microwave and Millimeter Wave Passive Structures*, John Wiley & Sons, New York (1989).

3. F.J. German, G.K. Ghothard, L.S. Riggs, and P.M. Goggan, "The Calculation of Radar Crosssection (RCS) Using the TLM Method", Int. J. Numer. Modelling, vol. 2, no. 4, pp. 267-278, Dec. 1989.

4. N.R.S. Simons and E. Bridges, "Application of the TLM Method to Two-Dimensional Scattering Problems", Int. J. Numer. Modelling, vol. 5, pp. 93-110, 1992.

5. M. Khalladi, J.A. Morente, and J.A. Porti, "RCS of Arbitrarily-Shaped Targets with the TLM Method", *IEEE Trans. on Antennas and Propagation*, vol. 42, no. 6, pp.891-893, June 1994.

6. F.J. German, "General Electromagnetic Scattering Analysis by TLM Method", Electronics Letters, vol. 30, no. 9, pp. 689-690, 28th April 1994.

7. R. L. Higdon, "Numerical absorbing boundary condition for the wave equation," *Mathematics of Computation*, vol. 49, no. 179, pp. 65-91, July 1987.

8. D. Steich and R. Luebbers, "Comparison and Generation of Higher Order FDTD Absorbing Boundaries", *10th Annual Review of Progress in Applied Computational Electromagnetics* Digest, pp. 212-233, March 21-26, 1994, Monterey, CA.

9. C. Eswarappa and W.J.R. Hoefer, "One-Way Equation Absorbing Boundary Conditions for 3- D TLM Analysis of Planar and Quasi-planar Structures", *IEEE Trans. Microwave Theory Techniques*, vol. 42, no. 9, pp. 1669-1677, Sep. 1994.

10. Z. Chen, M.M. Ney , and W.J.R. Hoefer, "Absorbing and Connecting Boundary Conditions for the TLM Method", *EEE Trans. Microwave Theory Tech*., vol. MTT-41, no. 11, pp. 2016-2024, 1993.

11. P. B. Johns, "Symmetrical Condensed Node for the TLM method", *IEEE Trans. Microwave Theory Tech*., vol. MTT-35, no. 4, pp. 370-377, April 1987.

12. R.J. Luebbers, K.S. Kunz, M. Schneider and F . Hunsberger, "A Finite-Difference Time-Domain Near Zone to Far Zone Transformation", *IEEE Trans. on Antennas and Propagation*, vol. AP-39, No. 4, pp. 429-433, April 1991.

13. F. Akleman and L. Sevgi, "Radar cross section and antenna modeling with TLM method," *JINA'98 10th Int Symposium on Antennas*, Nice-France, November 14-16 1998.

14. L. Sevgi and S. Paker, "TLM based RCS calculations and antenna simulations," *AEU International J. of Electronics and Communication*, vol.52, pp.65-75, March 2005.

CODE OPTIMIZATION DURING PROCESSING OF HAMMING CODES IN A DATA COMMUNICATION SYSTEM

Rina Choudhary
Research scholar, Student member, IEEE
School of Electronics Devi Ahilya Vishwavidyalaya University, Indore-452001
E-mail: Rina.choudhary26@gmail.com

ABSTRACT

The data may get corrupted during communication. It is because of physical phenomenon (form of any interference). Hamming method enables correction of the block codes. An example, is Hamming code class of single and double error detecting and single error correcting block codes (Algebraic codes). Processing of Hamming codes at the encoder and decoder require the lengthier codes. This needs more fetches of instructions by the processing circuit. That consumes more energy. Present paper describes a method of use of common processing elements and objects. This optimizes the code and reduces the number of instructions fetched during processing.

Keywords: *Hamming code, Hamming distance, Error correction, Error detection, Code optimization, Parity check matrix, Generator matrix.*

1. INTRODUCTION

Richard E. Blahut described that each code word is a sequence of n binary symbol, and there are 2^k such code words in an (n,k) binary code. Therefore a code is described by $n.2^k$ binary symbol.

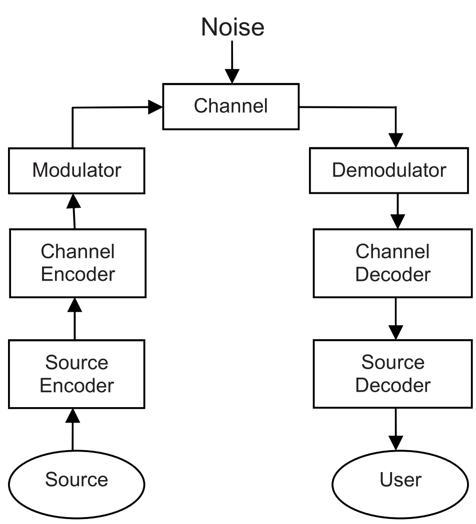

Fig. 1 Block diagram of Digital communication system

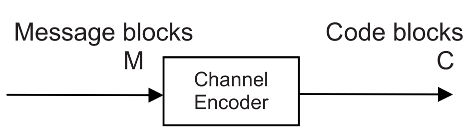

Fig. 2

A typical block diagram of digital communication system is shown in Fig.1

Consider (7, 4) Hamming code. Each block of data contains 7 bits and only 4 bits in a block are used to represent data, so only $2^4 = 16$ symbols may be represented in a block. Therefore transmitter send 4 bit data added extra 7 bits during transmission the same amount of information corrupted with noise so through added extra bits the receiver end can be predicted one bit error position and corrected it using some parameters.

1. Hamming distance
2. Generator matrix
3. Parity check matrix
4. Syndrome calculation

1.1 HAMMING DISTANCE Implementation of the encoding and decoding operations can be complicated because of very long block length. Hamming gives hamming distance, if there are two sequence of the same length of symbols from some fixed symbol alphabet, perhaps the binary alphabet [0 1], we shall want to measure how different those two sequences are from each other. This overcomes the problem. A good way is the measurements of the difference between the two sequence and count the number of places in which they differ.

Definition of Hamming distance: The Hamming distance d (x, y) between two q-ary sequence x and y of length n is the number of places in which x and y differ. For example

d (1001, 0100) =3

d (0011, 1100) =4

1.2 GENERATOR MATRIX Consider a Generator matrix (m×n), where **m** = Message bits, **n** = length of the code word and p= (n-m) digits are the parity check bits. It follows the characteristics that

(I) None of them can be all 0's.

(II) None of them can be any row of single one.

(III) Also any one row and column should not be repeated.

(IV) Parity check bits P should be chosen that all the rows are distinct and consist at least two 1's in them.

1.3 PARITY CHECK MATRIX If a message M with m bits (in binary 1 or 0) is to be transmitted, then, a code **C** with c bits must be generated (Fig 2).The length of **M** is related to that of **C** with the following equation:

$$c = m + p \leq 2p - 1 \qquad (1)$$

where

p = number of redundant bits

p is also called Parity bits.

Hamming's single error correcting and detecting code:

Once Parity check matrix chosen the Generator matrix G can be obtained by using below equation

$$2^{C-M} - 1 \geq C \qquad (2)$$

Or $$(C-M) \geq \log_2(C+1)$$

Or $$C \geq M + \log_2(C+1)$$

Thus the minimum size of the code words C can be determined easily.

The Parity check matrix (**H**) is

$$H = [P^T \vdots I_{n-m}]_{(n-m) \times n} \qquad (3)$$

Parity check matrix for (7, 4) Hamming code

$$H = \begin{bmatrix} 1 & 0 & 1 & 1 & 1 & 0 & 0 \\ 1 & 1 & 0 & 1 & 0 & 1 & 0 \\ 0 & 1 & 1 & 1 & 0 & 0 & 1 \end{bmatrix}_{3\times7}$$

So the Generator Matrix (G) is

$$\mathbf{G} = \begin{bmatrix} 1 & 0 & 0 & 0 & 1 & 1 & 0 \\ 0 & 1 & 0 & 0 & 0 & 1 & 1 \\ 0 & 0 & 1 & 0 & 1 & 0 & 1 \\ 0 & 0 & 0 & 1 & 1 & 1 & 1 \end{bmatrix}_{4\times7}$$

$$\underbrace{\quad\quad\quad\quad}_{Im} \quad \underbrace{\quad\quad\quad}_{P}$$

For a message block **M** = [1 0 0 1] the code word C is given as

C = M×G = [1 0 0 1 0 0 1]

where x-or operation work as:

0+0=0
0+1=1
1+0=1
1+1=1

Examples of some other code words are

Messages	Code words
0000	0000 000
0001	0001 111
0010	0010 101
0011	0011 010
0100	0100 011
0101	0101 100
0110	0110 110
0111	0111 001
1000	1000 110
1001	1001 001
1010	1010 011
1011	1011 100
1100	1100 101
1101	1101 010
1110	1110 000
1111	1111 111

1.4 SYNDROME CALCULATIONS

The Syndrome for the code word is given by

$S = CH^T = [0\,0\,0]$

If the error produces in 2nd bit from the left position during transmission, the received vector R will be

R = [1 1 0 1 0 0 1]
 = [1 1 0 1 0 0 1] [0 1 0 0 0 0 0] = C ⊕ E

And the syndrome of received vector R is

$$S = [R\,H^T]$$

$$S = [1\ 1\ 0\ 1\ 0\ 0\ 1] \begin{bmatrix} 1 & 1 & 0 \\ 0 & 1 & 1 \\ 1 & 0 & 1 \\ 1 & 1 & 1 \\ 1 & 0 & 0 \end{bmatrix}$$

$$S = [1\ 0\ 1] = EH^T$$

Here can be seen that the syndrome vector S as error in the second bit is equal to the second row of the transpose of parity check matrix (H^T).Also it shows that for this code a single error in the i^{th} bit of C leads to a syndrome vector that is equal to the i^{th} row of H^T.

$$G=\begin{pmatrix}
1\,0\,0\,0\,0\,0\,0\,0\,0\,0\,0\,0\,0\,0\,0\,0\,1\,1\,0\,0\,0 \\
0\,1\,0\,0\,0\,0\,0\,0\,0\,0\,0\,0\,0\,0\,0\,0\,0\,1\,1\,0\,0 \\
0\,0\,1\,0\,0\,0\,0\,0\,0\,0\,0\,0\,0\,0\,0\,0\,1\,0\,1\,0\,0 \\
0\,0\,0\,1\,0\,0\,0\,0\,0\,0\,0\,0\,0\,0\,0\,0\,1\,1\,1\,0\,0 \\
0\,0\,0\,0\,1\,0\,0\,0\,0\,0\,0\,0\,0\,0\,0\,0\,1\,1\,0\,1\,0 \\
0\,0\,0\,0\,0\,1\,0\,0\,0\,0\,0\,0\,0\,0\,0\,0\,0\,1\,1\,1\,0 \\
0\,0\,0\,0\,0\,0\,1\,0\,0\,0\,0\,0\,0\,0\,0\,0\,1\,0\,1\,1\,0 \\
0\,0\,0\,0\,0\,0\,0\,1\,0\,0\,0\,0\,0\,0\,0\,0\,1\,1\,1\,1\,0 \\
0\,0\,0\,0\,0\,0\,0\,0\,1\,0\,0\,0\,0\,0\,0\,0\,0\,1\,1\,0\,0\,1 \\
0\,0\,0\,0\,0\,0\,0\,0\,0\,1\,0\,0\,0\,0\,0\,0\,0\,0\,1\,1\,0\,1 \\
0\,0\,0\,0\,0\,0\,0\,0\,0\,0\,1\,0\,0\,0\,0\,0\,0\,1\,0\,1\,0\,1 \\
0\,0\,0\,0\,0\,0\,0\,0\,0\,0\,0\,1\,0\,0\,0\,0\,0\,1\,1\,1\,0\,1 \\
0\,0\,0\,0\,0\,0\,0\,0\,0\,0\,0\,0\,1\,0\,0\,0\,1\,1\,0\,1\,1 \\
0\,0\,0\,0\,0\,0\,0\,0\,0\,0\,0\,0\,0\,1\,0\,0\,0\,1\,1\,1\,1 \\
0\,0\,0\,0\,0\,0\,0\,0\,0\,0\,0\,0\,0\,0\,1\,0\,1\,0\,1\,1\,1 \\
\underbrace{0\,0\,0\,0\,0\,0\,0\,0\,0\,0\,0\,0\,0\,0\,0}_{I_k}\,\underbrace{1\,1\,1\,1\,1}_{P}\,1
\end{pmatrix} \quad 21\text{x}16$$

(21, 16) Generator matrix for 16 message bits shows

where

M=16 (Message bits length), C=21(Code word length).

P= (C-M) = 5(Parity check matrix).

The identity matrix $I_{m=}$M (Message bits).

Author finds that the most common part which works for number of block codes in this paper. If hard coded the generator matrix(G) for 16 message bits so we can find the common part for 8 bit data here the generator matrix is shown on below on 16 bit generator matrix (shaded part), and for 4 bit data the common part is shown on 16 bit generator matrix(shaded part).

Here the author is using only parity check matrix (P) where the 8 bit data is equal to the first 8 column of identity matrix. Therefore, there is no need for the additional computations for generating the data bits using identity matrix. For example, if one is having M = 8 (message bits length), then the code length will be C=12.

C=M×G.

Suppose data M=10010011, G (shaded part) so that C=100100110110

We are having 8 bits of data to be transmitted. So the code length will be 12 bits. We can find easily that the first 8 bits of code are same as the data bits and remaining 4 bits 0100 are obtained from the operation

Parity Bits code word= M×P

So it is not necessary to calculate the first 8 bits of code word, we can calculate only last four bits, minimizing the no. of operations calculations.

We minimize the number of calculations as follows:
We can skip multiplication of zeros in generator matrix. Since the Generator matrix G is known, we can identify the elements which are zero and skip that particular multiplication. This is further reduction in no. of calculations. If once we hard code the Generator matrix and parity check matrix for 16 bits the same matrix can be used for generation of 4 bit, 8 bit and with little modification 32 bit also, the same is applicable for hardware implementation. Although we are not generating generator matrix and parity check matrix on the fly the number of instructions generations are less thus reducing the energy consumption.

2. CONCLUSION

An approach is suggested whereby one finds the block of most common part and then the common blocks are reused for all other large number of data from encoder to decoder. An implementation of Hamming code based on this approach is also flexible for both hardware and software implementation. This is found that there is 50% optimization in the code-length, thus less number of instruction fetches in implementing Hamming code and thus 50% lesser energy consumption than without optimization.

REFERENCES

1. Richard E. Blahut, “Algebraic Codes for data Transmission”, Cambridge University Press, 2003.
2. R. Leupers, “Code Optimization Techniques for Embedded Processors” Kluwer Academic Publishers, Boston, 2000.
3. John G. Proakis, “Digital communications, Third Edition” McGraw-Hill International Editions, 1995.
4. “Optimization of the Hamming Code for Error Prone Media”, **Eltayeb S. Abuelyaman and Abdul-Aziz S.A1-SehibaniS.** *College of Computer and Information Sciences Prince Sultan University.* IJCSNS International Journal of Computer Science and Network Security, VOL.8 No.3, March 2008.
5. Encoding and decoding with the Hamming code, Foundations of Geometry University of Wyoming, Department of Mathematics, and math 4600-Fall 2006.

A SIMPLE ALGORITHM FOR FAST DETECTION AND QUANTIFICATION OF VOLTAGE DEVIATIONS USING SPACE VECTORS

P. Meena
Dept of Electrical & Electronics Engg.,
BMS College of Engineering, Bangalore.
E-mail: meenabms@gmail.com
Contact:9008658263

Dr. K. Uma Rao
Dept. of Electronics & Comm.Engg.,
RNS Institute of Technology, Bangalore.
E-mail: drumarao@yahoo.co.in
Contact:9980909893

Dr. Ravishankar Deekshit
Dept of Electrical & Electronics
BMS College of Engineering, Bangalore.
E-mail: ravi_yedatore@rediffmail.com
Contact:9844038911

ABSTRACT

This paper presents the use of the concept of space vector representation of three phase quantities, effectively in the detection and quantification of short duration voltage disturbances such as sags, swells, and interruptions in three phase balanced and unbalanced supply systems. Three phase balanced quantities can be represented by a synchronously rotating space vector of constant magnitude .The two phase equivalent of which on a stationary reference frame are orthogonal to each other. In the case of disturbances occurring on one or two phases of the supply, the positive sequence components of the unbalanced three phase waves are obtained and the resultant of their two phase equivalent is found out. This resultant , is sensed at every sampling instant .The magnitude of this space vector has a fixed value under normal conditions. Deviations from this value during short duration disturbances are measured. The deviation is used to generate a trigger after processing.This can facilitate classification of the type of disturbance, quantification of its magnitude, instant of occurrence, as well as duration of the disturbance needed for a disturbance parameters recorder. This can also be used to initiate the control system of a DVR (Dynamic voltage restorer), or a power line conditioner used for mitigation of the disturbance.The test of the algorithm was successfully done in simulation using Matlab / Simulink as well as Lab VIEW and deployed on the embedded controller compact-RIO(c- RIO) hardware unit which runs LAB VIEW code real time. The results obtained substantiates the effectiveness of the algorithm with respect to accuracy quantification as well as quickness of detection of the disturbances.

Keywords: *Space vectors, positive sequence component, resultant space vector , deviation, trigger , disturbance detection.*

1. INTRODUCTION

Any power problem that results in voltage, current or frequency deviations is a power quality (PQ) problem[1]. Disturbances in the supply system prevent end-user equipment from operating properly. Most common occurrences of voltage and current variations that can result in PQ problems include voltage interruptions, long and short duration voltage variations and transient electromagnetic disturbances apart from others. The need to supply distortion and disturbance free voltages to the end user loads has been the motivation for the study on PQ.

Ensuring a “high quality” of the supply voltage is the main requirement for ensuring a high “power quality.” The detection of the disturbances is one of the most qualifying points in the estimation of the “voltage quality” or “supply quality.” The correct assessment of the quality of the supplied voltage has become one of the key issues in the deregulated electricity market. Great attention is therefore paid to the definition of suitable indexes of voltage quality and the definition of suitable measurement procedures to evaluate these indexes.

As far as the definition of voltage quality is concerned, several recommendations have been issued by the standards organizations to define the acceptable voltage characteristics [3],[5][6],[7]. also in terms of the acceptable number and level of the disturbances superimposed to the voltage waveform and their characteristics. The Information Technology Industry Council (ITIC) has published a curve showing a voltage envelope that can be tolerated by most information technology equipment [2].This curve gives an idea of the voltage tolerance levels of the equipment and when compensation is required for supply voltages. The information provided by the above curve has been used in this work, for choosing a suitable value for the duration of the disturbance in the simulations.

Voltage sags are the most common which impact sensitive equipment that lack sufficient internal energy storage to ride through the sag. Computers and most other consumer electronics equipment, which consist of low-power electronic devices, are highly sensitive to voltage disturbances. Even if the equipment does tolerate the sag at some instances, repeated operation of under voltage relays unbalanced relays or quick-acting relays in emergency off (EMO) circuits can cause unnecessary shutdown of the entire system. It is also seen that the recovery of sag is at times misinterpreted as a “power up” causing reset circuits to trip incorrectly. The effect of disturbances on general equipment such as transformers, motors etc.,has been a reduction in the capacity, increased losses and reduction in life . The main source of sags are large increase in current due to faults, large starting currents drawn by motor loads, and operation of different types of load connected to the supply system.

By IEC standard [9] ,sag is defined as a short duration (half a cycle to one minute) decrease in the supply voltage between 0.1p.u. and 0.9 p.u. at rated power frequency. In most cases, the duration of the sag is between 10ms and 1 minute. The duration of voltage dips corresponds to the total time interval between sag initiation and recovery. The main characteristics of voltage sags are its magnitude and duration.

Voltage swells are caused by abrupt reduction in load on a circuit with poor voltage regulation or due to loose neutral connection. The miniaturization of electronic circuits and increase in operating speeds has made sensitive equipment more susceptible to interference and over voltage. Smaller size and densely packed chips decrease the heat dissipation. Lowering of operational voltages has made the equipment sensitive to even small over voltages. By IEC standard swell is defined as a short duration (few cycles to 1 minute) increase in the supply voltage between 1.1p.u. and 1.8 p.u at rated power frequency.

Interruptions can occur due to power system faults, equipment failures, and control malfunctions during which the magnitude of the phase voltages dip to a value less than 0.1 p.u.

There are many approaches reported on real-time disturbance detection in three phase supply systems. Some of them are based on the conversion of ac voltages to a dc voltage that is obtained from a rectifier-filter arrangement. Any disturbance in the ac supply is reflected as a change in the dc level. When the disturbance is unbalanced, some ripple accompanies the change in the dc level which requires additional stages to convert the change to a trigger signal. The drawback of the above method is in the delay brought about by the filter.

There are numerous methods reported based on wavelet analysis of voltage signals such as in [10],. The wavelet transform is a complex, time-consuming algorithm very useful when the disturbances have to be classified into families, according to their characteristics .This can be done off line with algorithms for analysis of the disturbed signal after detection.

In [4], a method has been proposed for real-time detection by obtaining the d-q components of a three phase voltage signal on a synchronously rotating reference frame. However, this method indicates delay in the detection of the disturbances in the case of three phase as well as two phase sags .A significant increase in the delay is observed in the case of single phase disturbances. During unbalanced conditions using the above method, the resultant of the d-q components which is used to track the disturbance is superposed with oscillations which need an additional processing stage causing a delay in the detection.

In [11], an algorithm based on phase space is proposed for fault detection in comparison with the cumulative sum method of fault detection and the response time of detection is observed to be about one fourth of a cycle time period. However, this paper presents a simple detection algorithm based on the method of Space Vectors that facilitates a real-time detection, quantification of the magnitude of the disturbance, time of occurrence, quickly and accurately in both balanced and unbalanced cases of occurrence of short duration voltage disturbances such as sags , swells. and interruptions. Since this method of detection involves quantization of the deviation of the value of the resultant from the standard reference value, it is more robust in the presence of noise . Real time testing of this algorithm has been conducted and is found to be accurate and quick.

2. PROPOSED METHOD

The three phasors namely V_a, V_b and V_c can be transformed mathematically into three vectors, V_{sa}, V_{sb}, V_{sc}, along the three spatial axes displaced by 120°.The resultant of these spatial components can be represented by a single equivalent rotating space vector [11], rotating at an uniform angular velocity of ω radians per second, called the resultant space vector $\vec{V}_{res}$, which can be resolved into components along the two orthogonal axes on a stationary reference frame namely, α and β . These orthogonal components of the space vector V_α and V_β, can be obtained from the knowledge of the original phasor values by means of a simple transformation given by,

$$\begin{bmatrix} V_\alpha \\ V_\beta \end{bmatrix} = \begin{bmatrix} 1 & -1/2 & -1/2 \\ 0 & \sqrt{3}/2 & -\sqrt{3}/2 \end{bmatrix} \begin{bmatrix} V_a \\ V_b \\ V_c \end{bmatrix} \tag{1}$$

The magnitude of the resultant space vector can hence be found as,

$$|\vec{V}_{res}| = \sqrt{V_\alpha^{\ 2} + V_\beta^{\ 2}} \tag{2}$$

Under balanced conditions, the phase voltages have a fixed magnitude of V and hence the resultant space vector has a fixed value given by,

$$|\vec{V}_{res}| = 3\frac{V}{2} \tag{3}$$

where, V is the phase voltage per unit. Under normal conditions with V as 1p.u.,

$$V_{ref} = 1.5\text{p.u} \tag{4}$$

$$V_{diff} = V_{ref} - |\vec{V}_{res}| \tag{5}$$

The magnitude of the resultant space vector $|\vec{V}_{res}|$, is a value which can be determined at every instant by sensing the three phase voltages of the utility using equations (1)and (2) .This value varies with changes in the level of the phase voltages(which happens during a disturbance). This value is compared with V_{ref} at every instant. The deviation V_{diff} is utilized in further processing to generate the trigger signal which quantifies the instants of start and end of the disturbance as well as the magnitude and type of the disturbance. The positive polarity of the deviation thus obtained, is indicative of sag which is a reduction in rms voltage between 0.1p.u.and 0.9p.u.The negative polarity of the deviation thus obtained is indicative of a swell, which is an increase in rms voltage between 1.1p.u and 1.8p.u. The deviation also detects an interruption which is a complete loss in the supply voltage to a level less than 0.1p.u for a period not exceeding one minute in one, or all the phases.

For disturbances of unequal magnitudes, the two phase equivalent of the positive sequence components on a stationary reference frame is found out. The process of evaluating the resultant and measuring the deviation from the nominal value under normal conditions is obtained as in the balanced case and passed on to the processing block.

3. DETECTION ALGORITHM

The disturbance detection algorithm must accomplish the following [4].

1. Detect all the disturbances whether occurring on one of the phases or on all the three phases immediately. Quick detection facilitates initiation of quick responses.
2. Clearly distinguish a disturbance from other variations by delivering a trip signal only if the disturbance is beyond specified ranges for that disturbance.

The stages involved in the detection process are as indicated in the block diagram shown in Fig1.below.

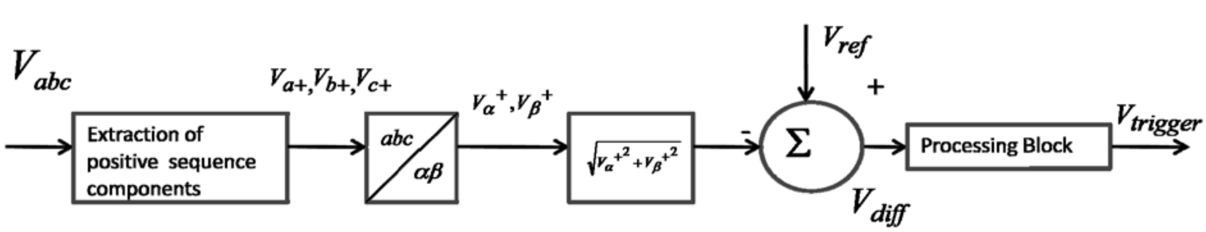

Fig.1.Block Diagram representation of the detection for balanced as well as unbalanced three phase disturbances

4. EXTRACTION OF POSITIVE SEQUENCE COMPONENTS AND PROCESSING OF THE INPUT SIGNAL

Consider a periodic three phase voltage signal Va , Vb and Vc with or without neutral conductor, this signal can be decomposed in the following way: into sequence components which are well known. The positive sequence components are extracted as follows,

$$\begin{bmatrix} V_a^+(t) \\ V_b^+(t) \\ V_c^+(t) \end{bmatrix} = \frac{-1}{3} \begin{bmatrix} -1 & 1\angle -60^\circ & 1\angle 60^\circ \\ 1\angle 60^\circ & -1 & 1\angle -60^\circ \\ 1\angle -60^\circ & 1\angle 60^\circ & -1 \end{bmatrix} \begin{bmatrix} V_a(t) \\ V_b(t) \\ V_c(t) \end{bmatrix} \tag{6}$$

The negative sequence components are extracted as follows,

$$\begin{bmatrix} V_a^-(t) \\ V_b^-(t) \\ V_c^-(t) \end{bmatrix} = \frac{-1}{3} \begin{bmatrix} -1 & 1\angle 60^\circ & 1\angle -60^\circ \\ 1\angle -60^\circ & -1 & 1\angle 60^\circ \\ 1\angle 60^\circ & 1\angle -60^\circ & -1 \end{bmatrix} \begin{bmatrix} V_a(t) \\ V_b(t) \\ V_c(t) \end{bmatrix} \tag{7}$$

These sequence components form a balanced set of three phasors.In this work the positive sequence components extracted are utilized therefore, a two phase transformation with reference to the stationary frame of reference is applied to the above components $|\overrightarrow{V}_{res}|$, to obtain according to (2). This value is now compared with the nominal value given in (5) to further obtain V_{diff}. This is further passed through a processing block. In this block the signal is passed through a hysteresis comparator .This has appropriate threshold levels set for switching at the output based on the specifications necessary for the identification of the disturbance. For example, for a sag ,the levels of threshold values are 0.10 and 0.90. The comparator block therefore helps distinguish the type of disturbance , by giving appropriate signals of the right polarity at its output. It also detects the starting point of occurrence and ending point of occurrence of the disturbance. The magnitude of the trigger signal quantifies the magnitude of the disturbance detected.

5. EVALUATION OF THE ALGORITHM FOR DIFFERENT CASES

5.1 INTERRUPTION IN ALL THREE PHASES Voltage interruption is the complete loss of voltage. Interruptions can be of short duration (lasting less than 2 minutes) or long duration. A disconnection of electricity causes an interruption - usually by the opening of a circuit breaker, line recloser, or fuse. This can occur due to power system faults, equipment failures, and control malfunctions.Fig.3(a),shows interruption in all the three phases during which the magnitude of the phase voltages are less than 0.1 p.u. and the magnitude of the resultant vector obtained $|\overrightarrow{V}_{res}|$, is as shown in Fig.3(b). The magnitude of the trigger signal generated from the processing block directly reflects the deviation in the magnitude of the resultant space vector $|\overrightarrow{V}_{res}|$, from the reference value V_{ref}

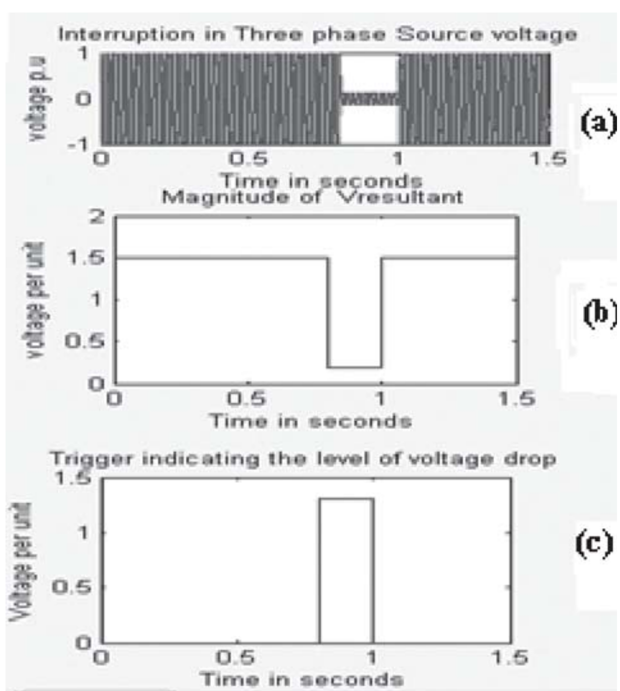

Fig.2. Detection of three phase interruption

Thus the trigger signal generated quantifies the time of occurrence, duration, as well as the level of deviation of the resultant space vector from the reference value during the disturbance which is nothing but the reflection of magnitude of the disturbance in all three phases. For estimating the error in the quantification of the magnitude of the disturbance using the above algorithm, the following are the steps followed . For example, the value $|\overrightarrow{V_{res}}|$, duing a disturbance level of 10% with phase voltages having a magnitude of 0.9 p.u is 1.35p.u as per equation (3).

The error in magnitude deviation detected by the algorithm $|\overrightarrow{V}_{trig,}|$ from the reference values $|\vec{V}_{diff}|$ for different sag levels can be estimated as shown.

$$\overrightarrow{V}_{err,} = |\vec{V}_{diff}| - |\overrightarrow{V}_{trig,}| \tag{6}$$

In this case the error in detection of deviation in magnitude during the disturbance is obtained as 0.67%.TABLE I shown indicates the magnitude of the trigger signal generated in response to the deviation of the resultant from its nominal value under normal conditions. From the table it is clear that there is no error . There was no delay observed in the instant of detection of the disturbance

5.2. INTERRUPTION IN TWO PHASES Fig.3 shown below shows the detection when the interruption is in two phases which is the unbalanced case. It is observed that the magnitude of the balanced positive sequence component is quantified. The resultant of the two phase components deviation of the resultant from the nominal value directly gives the level of sag which is (90%)in this case. It is observed that the magnitude of deviation is not the same as in the balanced case.

5.3. INTERRUPTION IN ONE PHASE This occurs during single line to ground fault in power systems. This is another case of unbalanced voltage sag. The figure shown below indicates the waveforms for the positive sequence component as well as the deviation in the resultant from the nominal value. The trigger signal quantifies the deviation. It is observed that the deviation value is different from that for a two phase unbalanced sag. The following tables indicate the magnitude of the resultant and deviation from its nominal value and trigger quantifying the deviation for the three cases such as balanced sag in all phases, unbalanced equal sags in two phases , and sag in one phase.

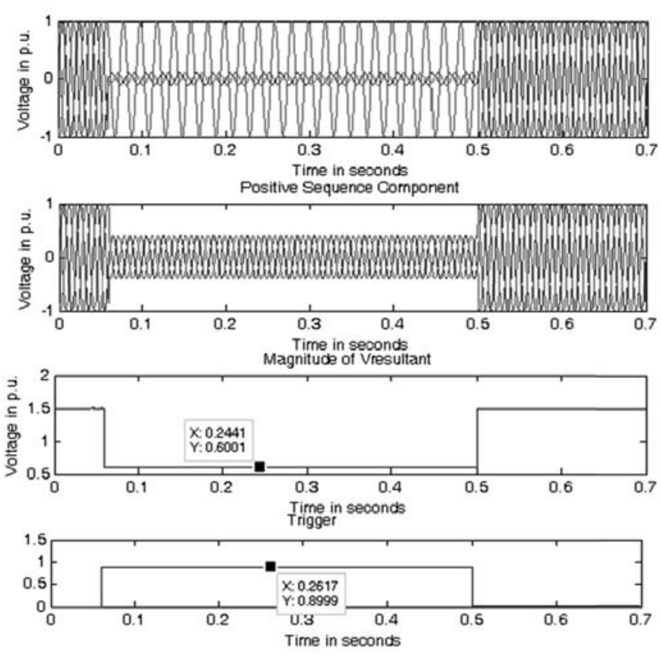

Fig.3. Detection of interruption in two phases

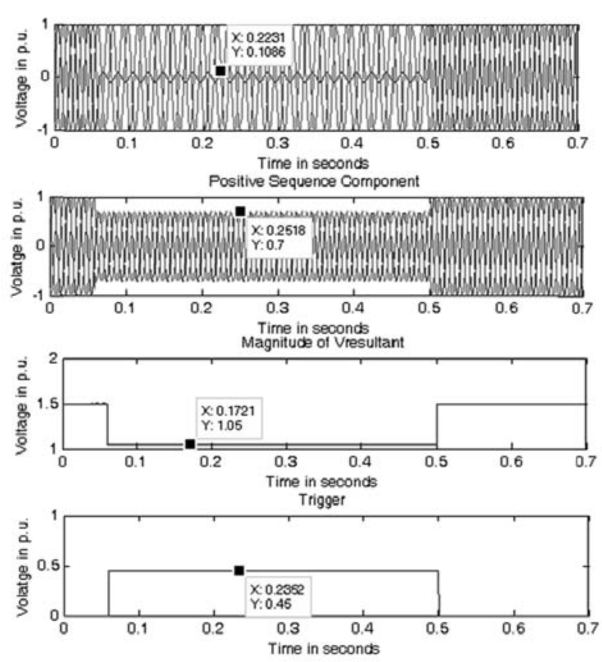

Fig.4. Detection of interruption in one phase

Figs 3 and 4 clearly indicate the effective detection and quantification of the deviation of Vresultant from its nominal values as per the tables

5.4. SWELL AND TRANSIENT IN ONE PHASE The cause for this disturbance includes start/stop of heavy loads, dynamic switching of loads at the terminals of a diesel-generator, unsymmetrical faults, and poorly regulated transformers. This may lead to damage of sensitive equipment.

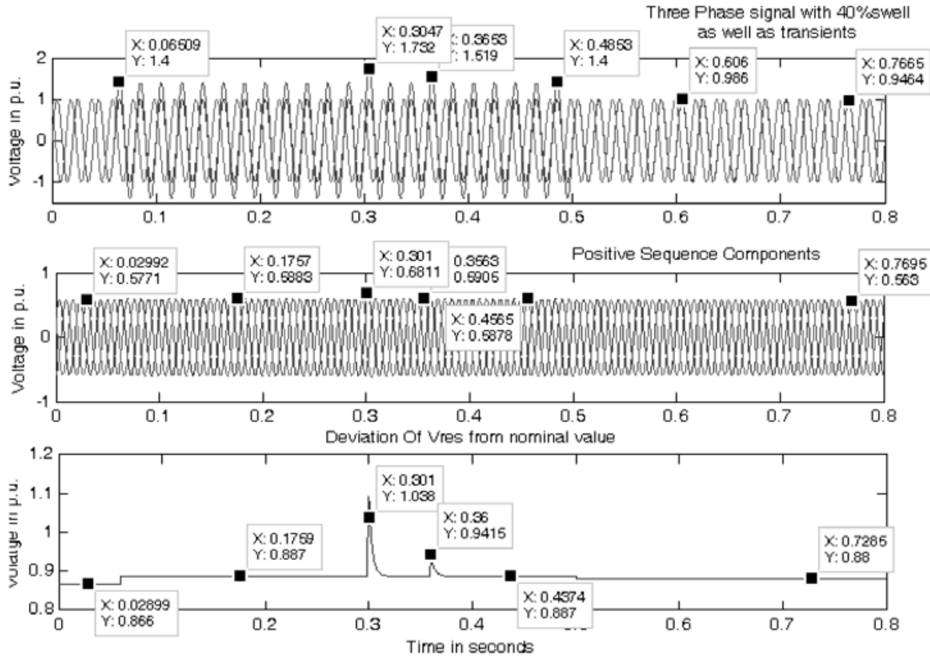

Fig.5: Detection during 40% swell and occurrence of transient in one of the phases of three phase supply

Fig.5. indicates clearly the successful detection of swell in one of the phases accompanied by transient in one of the phase. Hence, the effectiveness of the algorithm in detection of both types of disturbances.

The following tables indicate the estimated and actual values of $|\vec{V}_{res}|$, obtained and the deviation from its nominal value during both balanced and un balanced conditions after simulation using Matlab / Simulink.

TABLE 1 for three phase balanced sag

Level of sag in %	V_{ref} in p.u	Positive Sequence Component in p.u.	$\lvert\vec{V}_{res}\rvert$ in p.u	$\lvert\vec{V}_{diff}\rvert$ in p.u	$\lvert\vec{V}_{trig}\rvert$ in p.u
10	1.5	0.9	1.35	0.15	0.15
20	1.5	0.8	1.20	0.30	0.30
30	1.5	0.7	1.05	0.45	0.45
40	1.5	0.6	0.90	0.60	0.60
50	1.5	0.5	0.75	0.75	0.75
60	1.5	0.4	0.60	0.90	0.90
70	1.5	0.3	0.45	1.05	1.05
80	1.5	0.2	0.30	1.20	1.20
90	1.5	0.1	0.15	1.35	1.35

TABLE 2 for sag in one phase

Level of sag in %	V_{ref} in p.u	Positive Sequence Component in p.u.	$\lvert\vec{V}_{res}\rvert$ in p.u	$\lvert\vec{V}_{di}\rvert$ in p.u	$\lvert\vec{V}_{trig}\rvert$ in p.u
10	1.5	0.9667	1.45	0.05	0.05
20	1.5	0.9333	1.399	0.101	0.10
30	1.5	0.9	1.35	0.15	0.15
40	1.5	0.866	1.299	0.20	0.20
50	1.5	0.8333	1.2499	0.25	0.25
60	1.5	0.8	1.20	0.30	0.30
70	1.5	0.7667	1.1500	0.35	0.35
80	1.5	0.7333	1.0999	0.40	0.40
90	1.5	0.70	1.05	0.45	0.45

TABLE 3 for swell in one phase

Level of sag in %	V_{ref} In p.u	Positive Sequence Component in p.u.	$\lvert\vec{V}_{res}\rvert$ in p.u	$\lvert\vec{V}_{diff}\rvert$ in p.u	$\lvert\vec{V}_{trig}\rvert$ in p.u
10	1.5	1.033	1.55	0.05	0.05
20	1.5	1.067	1.60	0.10	0.10
30	1.5	1.10	1.65	0.15	0.15
40	1.5	1.133	1.7	0.20	0.20
50	1.5	1.166	1.75	0.25	0.25
60	1.5	1.20	1.80	0.30	0.30
70	1.5	1.233	1.85	0.35	0.35
80	1.5	1.266	1.90	0.40	0.40
90	1.5	1.3	1.95	0.45	0.45

TABLE 4 for sag in two phases

Level of swell in %	V_{ref} in p.u	Positive Sequence Component in p.u.	$\lvert\vec{V}_{res}\rvert$ in p.u	$\lvert\vec{V}_{diff}\rvert$ in p.u	$\lvert\vec{V}_{trig}\rvert$ in p.u
10	1.5	0.933	1.40	0.10	0.10
20	1.5	0.8667	1.30	0.20	0.20
30	1.5	0.8	1.20	0.30	0.30
40	1.5	0.73	1.10	0.40	0.40
50	1.5	0.667	1.00	0.50	0.50
60	1.5	0.6	0.90	0.60	0.60
70	1.5	0.533	0.80	0.70	0.70
80	1.5	0.4667	0.70	0.80	0.80
90	1.5	0.40	0.60	0.90	0.90

6. SIMULATION RESULTS USING LABVIEW

The simulation was done using LABVIEW and the results are as indicated below for different conditions of balanced and unbalanced supply conditions.

6.1. NORMAL CONDITION OF BALANCED THREE PHASE SUPPLY: Fig.5. shows the case of a balanced three phase supply, the resultant space vector $|\vec{V}_{res}|$, which has a nominal value of 1.5p.u according to Eq(4),The deviation from the resultant which is measured by the trigger signal has a value of zero p.u. in this case which is shown in Fig.7

Fig.5. Balanced three phase supply(1.0 p.u.)under normal conditions

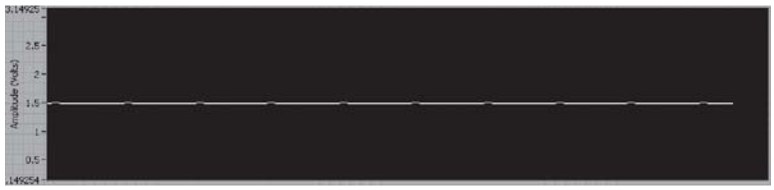

Fig.6. Magnitude of Vresultant(=1.5p.u.) under normal conditions

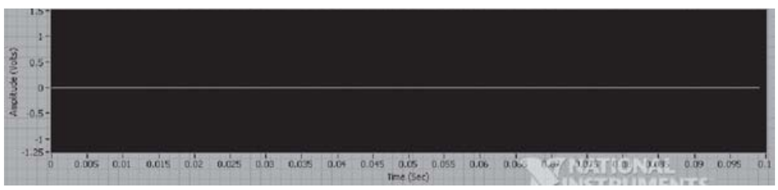

Fig.7. Magnitude of Trigger=0.0p.u. under normal conditions

6.2. BALANCED VOLTAGE SWELL IN ALL THE THREE PHASES The following Figs.8,9 and 10 shows the case of 40%swell in all the three phases. The magnitude of the resultant space vector in this case is 2.1p.u.as given by Eq(3). The trigger which indicates the deviation in the magnitude of $|\vec{V}_{res}|$, from the nominal value of 1.5p.u as given by Eq(4) is indicated in Fig.10.

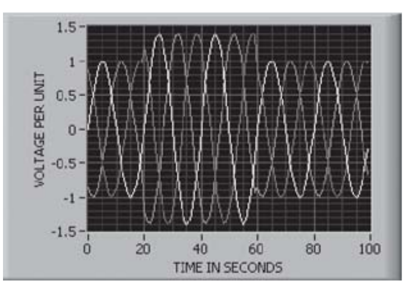

Fig.8. Balanced Voltage Swell of 40%

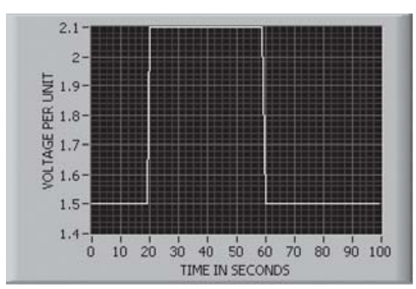

Fig.9. Magnitude of Vres(1.4x1.5=2.1V) during 40% swell

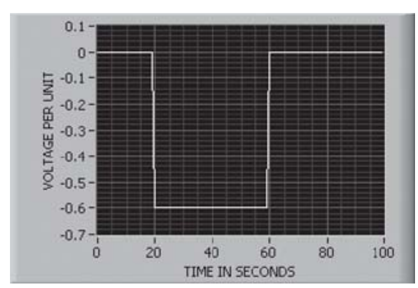

Fig.10. Trigger indicating the deviation of Vres

6.3. UNBALANCED SAG : The Fig.11,12 and 13, shows the detection of sag level in only Phase A, Equal sags in both Phase A and B and unequal sags in Phase A and Phase B.The positive sequence component for the same is obtained as shown in the fig. The trigger quantifies the deviation in the value of $|\vec{V}_{res}|$, of the balanced positive sequence component from the nominal value obtained during normal operating conditions.

50% Sag in Phase A

50% Sag in Phase A and Phase B

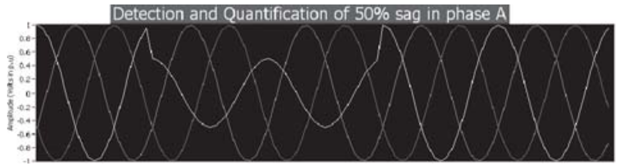

Positive Sequence Component **Positive Sequence Component**

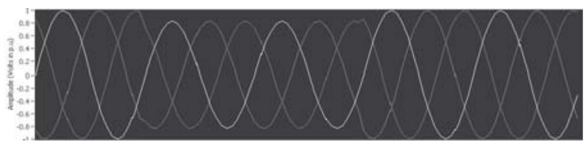

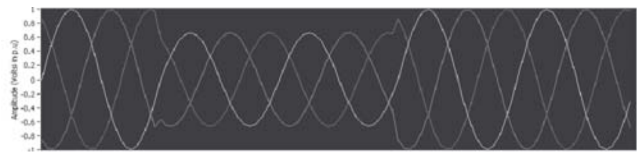

Trigger (0.25p.u.)Quantifying single phase sag level of 50% Trigger(0.5p.u.)quantifying two phase sag level of 50

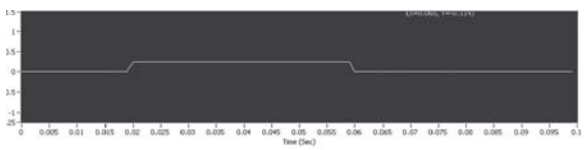

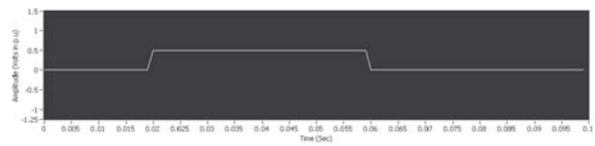

Fig.11. Detection and quantification of 50% Sag in A. Fig.12. Detection and Quantification of 50% Sag in A &B
70% Sag in Phase A and 50%in Phase B

Positive Sequence Component (0.6p.u.)

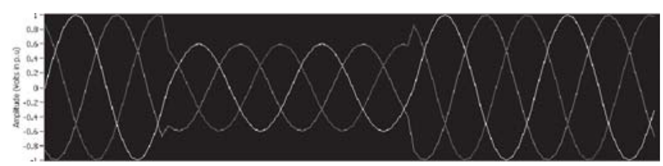

Trigger (0.6.p.u)

Fig.13. Detection and Quantification of 70%sag in A & 50% in B

7. EXPERIMENTAL SET-UP AND RESULTS

To test the algorithm real-time in hardware, the execution target for NI LabVIEW real-time applications,NI c-RIO ,real time controller was used.IT is a small and rugged embedded controller ,with 400 MHz Freescale MPC5200 real-time processor with -40 to 70 °C operating temperature range.It is reliable and deterministic in operation for stand-alone control, monitoring, and logging.It has full-speed USB host port for connection to USB flash and memory devices,10/100BASE-T ethernet port with embedded Web and file servers with remote-panel user interface,and a RS232 serial port for connection to peripherals; dual 9 to 35 VDC supply inputs.

The Block diagram of the set-up is as shown in Fig.14.The three phase disturbance signals of different types are generated using LAB VIEW code and transferred to the output port of the c-RIO. The target is configured through the ethernet connection .These signals are converted into analog signals by the NI9263 D/A module. The three phase disturbance signals are now available real-time at the analog out put ports .These are fed back into the real-time controller through the NI 9201 A/D module which has signal conditioning unit as well as anti aliasing filters built in The sampling frequency chosen is 1KHz.The algorithm which resides in the memory of the real time controller now acts on the signals and generates the trigger which is available at the output of the D/A module. The corresponding waveforms are observed using Tektronix Digital Oscilloscope TPS 2024B which has four channels ,200MHz band width with built in isolation.

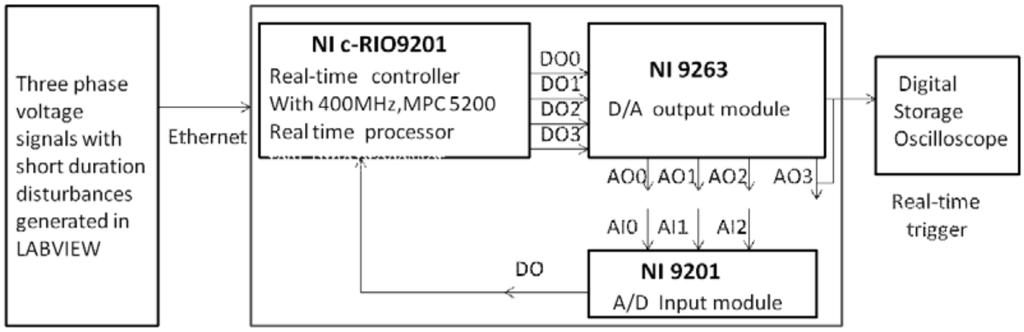

Fig.14. Block Diagram of the detection set up

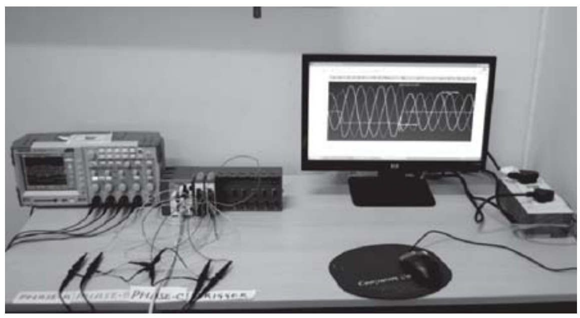

Fig.15. The experimental set-up for the real –time detection of the disturbances

7.1 Results recorded from the set –up real-time:

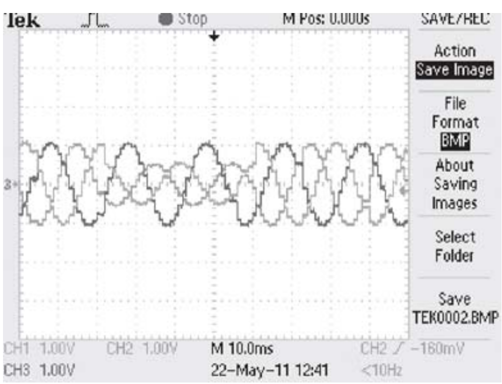

Fig.16. Real-time unbalanced sag of 50%

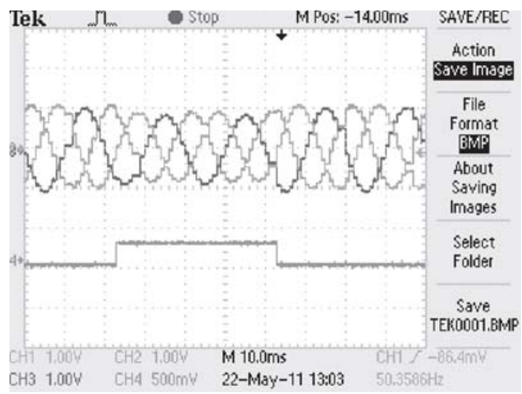

Fig.17. Positive sequence component and (0.5V) real-time trigger

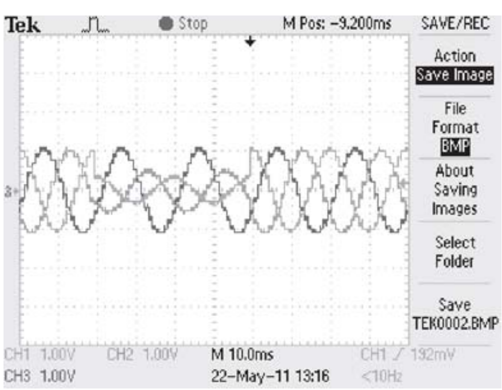

Fig.18. Unbalanced sag of 50% and 70% in Phase A&B

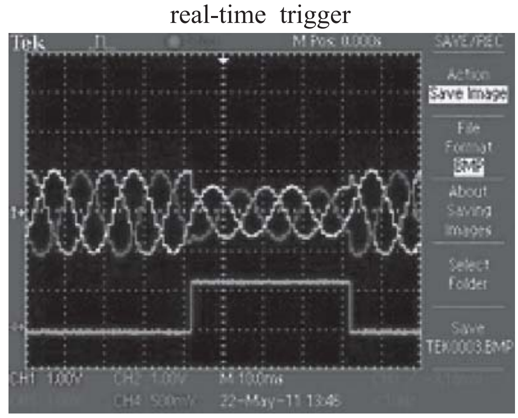

Fig.19. Positive sequence .component and trigger (0.6p.u) during 50% and 70% sag in Phase A&B

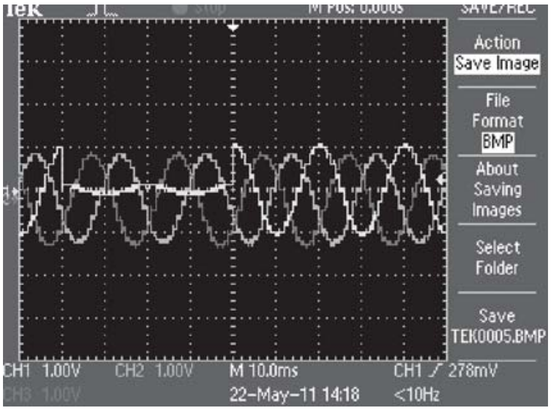

Fig.20. Interruption in One phase

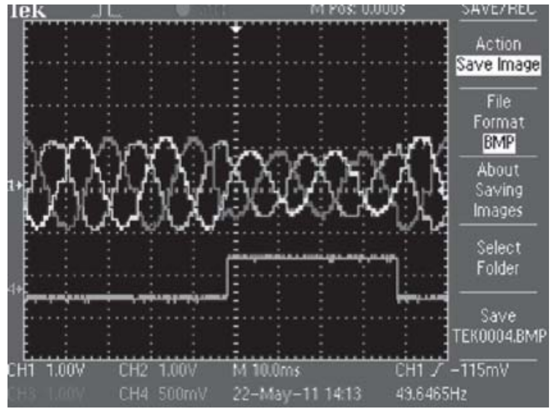

Fig.21. Positive Sequence component and quantified trigger(0.45p.u.) during interruption in one

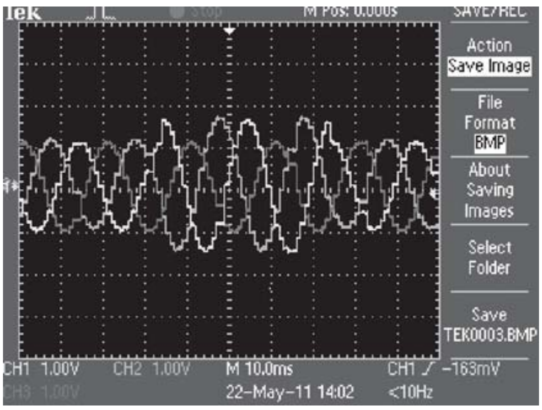

Fig.22. 60%Swell in Two Phases

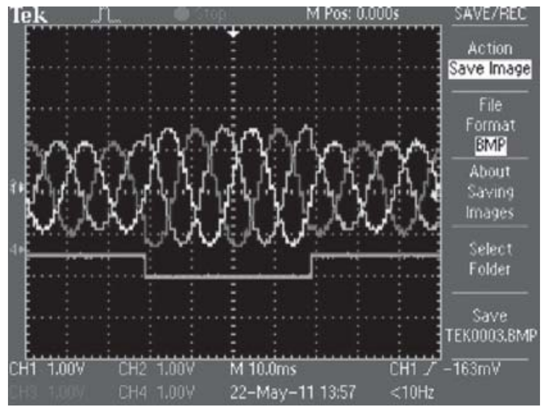

Fig.23. Positive Sequence Component and Quantified trigger of (0.6p.u.) during swell

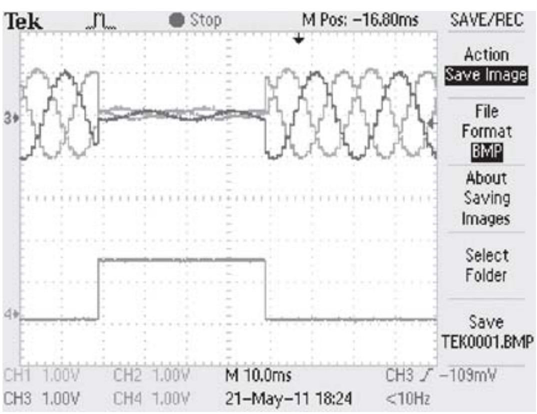

Fig.24. Balanced interruption in all three phases and quantified (1.35p.u.) trigger.

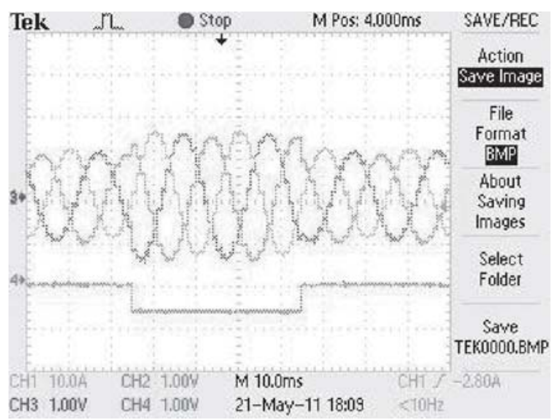

Fig.25. 40% Balanced Swell in all three phases and quantified (0.6p.u.)trigger

8. CONCLUSION

The trigger signal generated during the deviation of the resultant space vector from its nominal value, clearly indicates the type of disturbance as well as quantifies the magnitude of the disturbance. The algorithm has been successfully tested in simulation for detection of voltage sags, swells and interruptions in three phase system. The results obtained are indicative of its accuracy in detection as well as measurement in the levels of disturbance with no time delays. Therefore the trigger signal can also be directly used as a control signal for custom power devices to mitigate the disturbances. The algorithm has also been successfully tested for both balanced and unbalanced cases using LabVIEW and also has been implemented successfully real-time on Compact RIO, provided by National Instruments. The simplicity of the algorithm sugggests the use of it to initiate the operation of an inverter as a dynamic voltage restorer to maintain normal voltage across the load during the disturbance .Real-time testing of this set-up is in progress and would be published .

ACKNOWLEDGEMENTS

The authors acknowledge Mr.Visweswaran of National Instruments for the technical support provided by supplying the c-RIO board and accessories for testing the algorithm real –time.

REFERENCES

1. Math H. J. Bollen, Irene Y. H. Gu, Surya Santoso, Mark FMcGranaghan, Pete A..Crossley, Moisės V. Ribeiro, and Paulo F. Ribeiro, *Bridging the gap between signal and Power,* IEEE Signal Processing Magazine [12], July2009.

2. ITI. (CBEMA) Curve, Information Technology Industry Council(ITI) Washington, DC, [Online]. Available:http://www.itic.org.

3. "Voltage characteristics of electricity supplied by public distribution systems,"CENELEC, EN 50 160, 1994.

4. Oscar C. Montero-Hernández, and Prasad N Enjeti,*A Fast Detection Algorithm suitable for mitigation of numerous Power Quality Disturbances*, IEEE transactions on Industry Applications,Vol.41, NO.6,November/December 2005.

5. *IEEE Recommended Practice for Monitoring Electric Power Quality*,IEEE Standard 1159–1995, 1995.

6. "Electromagnetic compatibility (EMC), Part 3-2, Limits: Limitation of voltage fluctuations and flicker in low-voltage supply systems for equipment with rated current <= 16 A," IEC, IEC 61000–3–3, 1994.

7. "Electromagnetic compatibility (EMC), Part 3, Limits: Section 5—Limitation of voltage fluctuations and flicker in low- voltage power supply systems for equipment with rated current greater than 16 A," IEC, 61000–3–5, 1994.

8. "A Simple Method For Real-Time Detection Of Voltage Sags and Swells in Practical loads", P. Meena, K. Uma Rao, Ravishankar Deekshit, European Power Electronics and Drives Journal,Vol21,No.3, Sept 2011.

9. International Electrotechnical Commission, 2003, "IEC 61000-4-30.Part4:Testing and measurement techniques.Section 30:Power quality measurement methods".

10. Application of Abrupt Change Detection in Power Systems Disturbance Analysis andRelay Performance Monitoring, Abhisek Ukil, and Rastko ˇ Zivanovic´, IEEE Transactions On Power Delivery, Vol. 22, No. 1, January 2007.

11. "Phase-Space-Based Fault Detection in Distance Relaying", S. R. Samantaray, IEEE Transactions On Power Delivery, Vol. 26, No. 1, January 2011.

12. "*Modelling and Simulation Studies on Parameter Adaptation and Digital Controller Synthesis for Vector Controlled ACDrives"*, L. Umanand PhD dissertation, Centre for Electronics Design and Technology, Indian Institute of science , December 1994.

13. "A simple Algorithm for fast detection and Quantization of Voltage Deviations using Space Vectors", P. Meena, K. Uma Rao, Ravishankar Deekshit, IPEC Oct 2010, Singapore.

SECURE SECURITY ACCESS: AN APPROACH TO COUNTER HACKING

Rajesh Kumar
Global Logic India Pvt. Ltd.,
B 34/1, Sec 59, Noida 201301 (U.P.), India
E-mail: rajeshruhil@gmail.com, Contact No.: +919971706996

Neelam Ruhil
Gurgaon College of Engineering
Bilaspur-Tauru Road, Gurgaon (HR), India
E-mail: neelamruhil@gmail.com

ABSTRACT

An important aspect of information security is recognizing the value of data and information and defining appropriate procedures and protection requirements for the information. This paper defines a way to track unauthorized access on different shared folders in network. It identifies all the users and group who either are allowed or denied access on selected shared paths. This paper also defines a way to create security access utility; it will track access on shared physical paths. End result of the utility will be an excel report. This report is very well formatted and clearly displays the security details for the selected paths. The technologies used in this paper are VBA, EXCEL and VBS. It uses XCACLS.VBS to track access for all the physical paths defined in EXCEL Sheet. XCACLS.VBS is provided by Microsoft. It can also be used as command line using DOS prompt. XCACLS.VBS accepts several parameters and return access information. To identify and fetch details of all the domain users we used Active DS Type Library. It also fetches details of nested windows users group. We have used windows form to show details of user who belongs to any particular group or sub-group of the parent group.

Keywords: security access, folders security, windows security, information security, XCACLS.VBS.

1. INTRODUCTION

Most of the security problems are intentionally caused by malicious people to get attention, gain some benefit, or to harm someone [1]. Keeping network secure involves a lot more than just keeping it free of programming bugs. Authentication plays a big role in network security. Authentication is a technique by which a process verifies that a communication partner is who it is supposed to be and not an imposter. If any unauthorized person gets access of something that he is not supposed to access can create a big mess. Tracking unauthorized access is very important for every organization. Security Access Utility is a process to track unauthorized access and build report of access control list.

Security Access Utility is an excel workbook that generates a report. This report includes all the access permission for the specified paths in the Main sheet. The Main worksheet includes three columns (Sr#, Group, and Location). This worksheet also has a button with the name Get Access. Clicking on Get Access will call a macro, and it will generate a report. This report is printed in a new worksheet. The new worksheet name is current date and time in US format. The result worksheet contains all the access details on the location path that we want.

This utility mainly contains three worksheets. These worksheets are Main, Configure, and Process. Configure and Process worksheets are not visible. Main worksheet is visible to everyone. Main worksheet has two sections. First section is Report Execute section. And second is Data Entry section. Report Execute section includes a dropdown and a command button. Data Entry Section has three columns (Sr#, Group, and Location). Anytime we make an entry in the data entry section, that group entry is also made in the dropdown box of Report Execute section. This dropdown box contains unique group names.

To execute report select a group name in the dropdown and click on Get Access button. A new worksheet will be added with the name current date and time in US format. And the sheet includes Sr#, Group, Location, User/Group, Read, Write, Modify, Full Access, Special Access, This Folder Only, This Folder and Files, This Folder and Subfolders, This Folder, Subfolder and Files, Files Only, Subfolders Only, Subfolders and Files Only, and Comments. The records are shown only for the selected group name.

In this report Sr#, Group, and Location are same as in the Main sheet. User/Group contains the name of the user or Group that have access on that location. Read, Write, Modify, and Full Access are marked as "X" where the group or user has read, write, modify, and full access irrespectively. If any user or group has special access all these permission will be printed under Special Access. It would also print type of permission (Allowed or Denied). Inherited permissions will be marked as "X" under This Folder Only, This Folder and Files, This Folder and Subfolders, This Folder, Subfolder and Files, Files Only, Subfolders Only, and Subfolders and Files Only [4, 6]. If location path is not correct or user don't have administrator access on that path or user/group has other permission rather than listed above then it would be printed under Comments.

Double click on any of the group under User/Group will pop up a window including list of all the members in that group. This popup window contains a read only multiline textbox. That has list of all the members in that group. This popup window also has an Exit button. Clicking on Exit button will bring user back to the result sheet.

2. PRIME MODULES

This project consist three modules. These modules are Data Entry, Access Report, and Group Details.

(i) **Data Entry:** Data Entry is available in Main worksheet. This module has two sections.

a) Report Execute Section: First section is Report Execute section. This section includes a drop down to select a group. And a button to execute report for that selected group

.

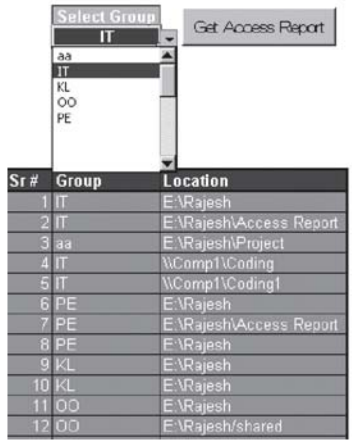

Sr #	Group	Location
1	IT	E:\Rajesh
2	IT	E:\Rajesh\Access Report
3	aa	E:\Rajesh\Project
4	IT	\\Comp1\Coding
5	IT	\\Comp1\Coding1
6	PE	E:\Rajesh
7	PE	E:\Rajesh\Access Report
8	PE	E:\Rajesh
9	KL	E:\Rajesh
10	KL	E:\Rajesh
11	OO	E:\Rajesh
12	OO	E:\Rajesh/shared

Figure 1

b) Data Entry Section: Second is Data Entry section. Data Entry section has three columns. These columns are Sr# (serial number), Group (name of the group), and Location (path). Anytime we make an entry in the Data Entry section, it runs a macro in background and enters the group in dropdown of Report Execute section. Group in the dropdown are unique.

```
On Error Resume Next
    If Not Intersect(Target, Range("B9:B65000")) Is Nothing Then
        Sheets("AccessConfigs").Visible = -1
        Sheets("Temp").Visible = -1
        AccessReport.getGroup
        Range(Target.Address).Select
        Sheets("AccessConfigs").Visible = 2
        Sheets("Temp").Visible = 2
    End If
```

Figure 2

To execute report select a group name in the dropdown and click on Get Access Report button. It runs a macro and a new worksheet is added, with the current date and time in US format. This macro creates a file system object and run csscript using xcacls.vbs.

```
'Create Object of FileSystemObject
Set ObjShell = CreateObject("WScript.Shell")
Set Fso = CreateObject("Scripting.FileSystemObject")
Set Fold = Fso.GetFolder(FoldPath)
'Execute csscript to fetch permission on folder using xcacls.vbs
Set OExec = ObjShell.Exec("cscript c:\xcacls.vbs " & Chr(34) & FoldPath & Chr(34))
Do While Not OExec.StdOut.AtEndOfStream
    Dim Str As String
    Str = OExec.StdOut.ReadAll
Loop
Set OExec = Nothing
```

Figure 3

(i) Access Report: Windows users have several permissions like Read, Write, Change, and Full etc [3]. Access Reports shows all the permission details for the select group. Access Report is available in new result sheet, with the name current date and time in US format. This report includes Sr#, Group, Location, User/Group, Read, Write, Modify, Full Access, Special Access, This Folder Only, This Folder and Files, This Folder and Subfolders, This Folder, Subfolder and Files, Files Only, Subfolders Only, Subfolders and Files Only, and Comments. The records are shown only for the selected group name. In this report Sr#, Group, and Location are same as in the Main sheet. User/Group contains the name of the user or Group that have access on that location. Read, Write, Modify, and Full Access are marked as "X" where the group or user has read, write, modify, and full access irrespectively. If any user or group has special access all these permission will be printed under Special Access. It would also print type of permission (Allowed or Denied). Inherited permissions will be marked as "X" under This Folder Only, This Folder and Files, This Folder and Subfolders, This Folder, Subfolder and Files, Files Only, Subfolders Only, and Subfolders and Files Only [4, 6]. If location path is not correct or user don't have administrator access on that path or user/group has other permission rather than listed above then it would be printed under Comments.

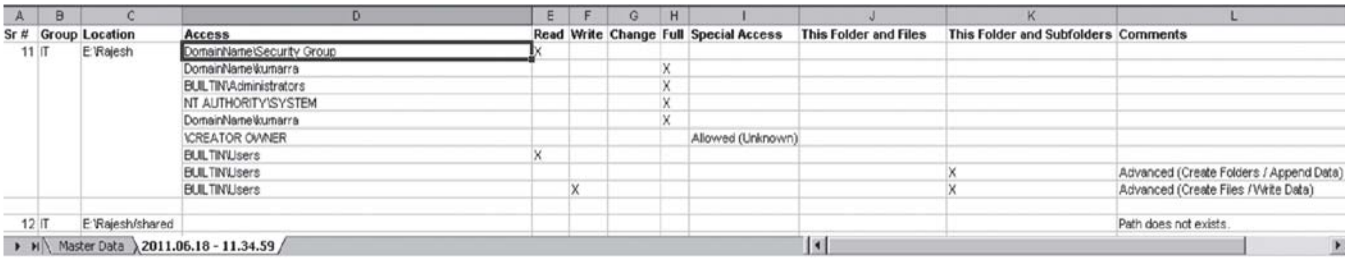

Sr #	Group	Location	Access	Read	Write	Change	Full	Special Access	This Folder and Files	This Folder and Subfolders	Comments
11	IT	E:\Rajesh	DomainName\Security Group	X							
			DomainName\kumarra				X				
			BUILTIN\Administrators				X				
			NT AUTHORITY\SYSTEM				X				
			DomainName\kumarra				X				
			\CREATOR OWNER					Allowed (Unknown)			
			BUILTIN\Users	X							
			BUILTIN\Users							X	Advanced (Create Folders / Append Data)
			BUILTIN\Users		X					X	Advanced (Create Files / Write Data)
12	IT	E:\Rajesh/shared									Path does not exists.

Master Data | 2011.06.18 - 11.34.59

Figure 4

(i) Group Detail is available when we double click on any of the user/Group. This popup window contains a read only multiline textbox. That has list of all members in that group. This popup window also has an Exit button. Clicking on Exit button will bring user back to the result sheet.

3. PROCEDURES OF MODULES

A. **Process Description:** The application is developed using excel macros. This application also uses xcacls.vbs [5]. This xcacls.vbs is provided by Microsoft at http://download.microsoft.com/download/f/7/8/f786aaf3-a37b-45ab-b0a2-8c8c18bbf483/XCacls_Installer.exe. Following references should be added in excel to use the application:

1.A.1. Visual Basic for Applications.

1.A.2. Microsoft Excel 11.0 Object Library.

1.A.3. OLE Automation.

1.A.4. Microsoft Office 11.0 Object Library.

1.A.5. Microsoft Forms 2.0 Object Library.

1.A.6. Active DS Type Library

B. **User Characteristics:**

1.B.1. To create this report user should have administrator access.

1.B.2. User can provide path and generate access report for that path.

1.B.3. Support multiple path at one go.

1.B.4. Display members of group, if permission is granted or denied to any specific group.

4. STRATEGY FOR COMPUTERIZATION

The strategy for implementing secure security access is a state-of-the-art excel based modular, integrated, scalable and networked System based on the following features: -

C. Language: VBA, VBS

D. Operating System: Window server 2003

E. Role: Administrator

F. Hardware & Networking: Servers, Desktops

The proposed system use XCACLS.VBS provided by Microsoft. As per the application requirement this file should be placed in C: drive. XCACLS.VBS can be downloaded from http://download.microsoft.com/download/f/7/8/f786aaf3-a37b-45ab-b0a2-8c8c18bbf483/XCacls_Installer.exe. For this application we are using version 5.2 of XCACLS.VBS [5].

Few code changes is required in XCACLS.VBS to support long user/ group name

5. PREPARATION OF DESIGN AND MODEL

This utility uses Microsoft Excel as a front end to track security permission for all the folders in network. VBA code is used with the help of XCACLS.VBS in the backend. XCACLS.VBS is modified to provide support for long File name.

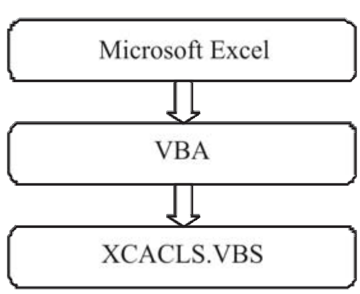

Xcacls.vbs can be executed from DOS prompt. It accepts several parameters to achieve the required functionality. To fetch folder security information it requires path of the folder to be passed as an argument [4, 6].

Xcacls returns permission in following way [4, 6]:

Table 1

Permissions…	
F	Full control
M	Modify
X	read & eXecute
R	Read
W	Write
Advanced…	
E	Synchronize
D	Take Ownership
C	Change Permissions
B	Read Permissions
A	Delete
9	Write Attributes
8	Read Attributes
7	Delete Subfolders and Files
6	Traverse Folder / Execute File
5	Write Extended Attributes
4	Read Extended Attributes
3	Create Folders / Append Data
2	Create Files / Write Data
1	List Folder / Read Data

6. CONCLUSION

Security is not just about keeping people out of your network. Security also provides access into your network in the way you want to provide it, allowing people to work together [2]. But tracking unauthorized access is very important. Information in wrong hand can create very big problem. We can use xcacls.vbs to track unauthorized access. Xcacls.vbs can also be used to grant and revoke access for any user or group on any particular path. It can be bundled with an application to develop a useful utility to trace unauthorized access. Thus it helps in securing network. xcacls.vbs can be used to set all file system security options those are accessible in windows explorer using command line.

REFERENCES

1. Andrew S. Tanenbaum: *Computer Networks, fourth edition*. Ch.8
2. Mark Rhodes-Ousley, Roberta Bragg and Keith Strassberg, *Network Security: The Complete Reference* Ch.1
3. Ed Tittel, Mary T. Madden and James M. Stewart, *Windows 2000 Server for Dummies* Ch. 16.
4. Microsoft Support: *How to use Xcacls.exe to modify NTFS permissions*, http://support.microsoft.com/kb/318754
5. Microsoft Download Center: *Extended Change Access Control List Tool*.
6. Microsoft TechNet. *File and Folder Permission.*
   http://technet.microsoft.com/en-us/library/bb727008.aspx

AN S-MESH BASED PROTOCOL FOR PEER – TO – PEER STREAMING TO SERVE DYNAMIC GROUPS

Mr. V. MARUTHI PRASAD
Asst. Professor, Dept of MCA,
Madanapalle Institute of Technology and Science, Madanapalle.
Email: maruthi_vv@yahoo.co.in, Mobile: 9885259496

Mr. V. RAGHAVENDRA PRASAD
HOD, Dept of CSE, MNR College of Engineering,
Sangareddy, Medak Dist.

ABSTRACT

Peer-to-peer (P2P) streaming has been widely deployed over the Internet. A streaming system usually has multiple channels, and peers may form multiple groups for content distribution. In this paper, we propose a distributed overlay framework (called SMesh) for dynamic groups where users may frequently hop from one group to another while the total pool of users remain stable. SMesh first builds a relatively stable mesh consisting of all hosts for control messaging. The mesh supports dynamic host joining and leaving, and will guide the construction of delivery trees. Using the Delaunay Triangulation (DT) protocol as an example, we show how to construct an efficient mesh with low maintenance cost. We further study various tree construction mechanisms based on the mesh, including embedded, bypass, and intermediate trees. Through simulations on Internet-like topologies, we show that SMesh achieves low delay and low link stress.

Keywords: *Peer-to-peer streaming, Dynamic group, Delaunay triangulation, Mesh.*

1. INTRODUCTION

In a P2P streaming system, the server (or a set of servers) usually provides multiple channels. A peer can freely switch from one channel to another. For example, one of the most popular P2P streaming systems, PPLive, has provided over 400 channels in September 2007 [4]. According to a measure-ment study from the Polytechnic University, the total number of peers in PPLive during a day in 2007 varies from around 50 thousand to 400 thousand, and the number of peers in a single channel, e.g., CCTV1, varies from several hundred to several thousand [5], [6]. We can see that there is a large pool of peers in the streaming network. Peers are divided into multiple small groups, each corresponding to a channel.

Peers in the same group share and relay the same streaming content for each other. In another study, a six-month 150-channel IPTV trace shows that people frequently change from one channel to another, with the median and mean channel holding time being 8 seconds and 14.8 minutes, respectively [7]. The trace also shows that a household (among those watching TV for the longest time) on average watches 2.54 hours and 6.3 distinct channels of TV a day.

In fact, there are many other similar applications over the Internet. In the application, the system contains multiple groups with different sources and contents. A user may join a specific group according to its interest. While the lifetime of users in the system is relatively long and the user pool is rather stable, users may hop from one group to another quite frequently. Examples include stock quotes, news on demand, and multisession conferencing. A more typical example is group chat of Skype [8]. Skype allows up to around 100 users to chat together. While millions of Skype users stay online and relay data for each other, the users may form multiple small groups for group chat. According to Rossi et al. [9], except for very short sessions, most Skype peers are alive for about one-third of a day. Generally such life time of a Skype peer is longer than the duration of a group chat.

In above applications, as peers may dynamically hop from one group to another, it becomes an important issue to efficiently deliver specific contents to peers. One obvious approach is to broadcast all contents to all hosts and let them select the contents. Clearly, this is not efficient in terms of bandwidth and end-to-end delay, especially for unpopular channels. Maintaining a separate and distinct delivery overlay for each channel appears to be another solution. However, this approach introduces high control overhead to maintain multiple dynamic overlays. When users frequently hop from one channel to another, overlay reformation becomes costly and may lead to high packet loss.

In this paper, we consider building a data delivery tree for each group. To reduce tree construction and maintenance costs, we build a single shared overlay mesh. The mesh is formed by all peers in the system and is, hence, independent of joining and leaving events in any group. This relatively stable mesh is used for control messaging and guiding the construction of overlay trees. With the help of the mesh, trees can be efficiently constructed with no need of loop detection and elimination. Since an overlay tree serves only a subset of peers in the network, we term this framework Subset-Mesh, or Smesh.

Our framework may use any existing mesh-based over-lay network. In this paper, we use Delaunay Triangulation (DT) as an example [10]. We propose several techniques to improve the DT mesh, e.g., for accurately estimating host locations and distributed partition detection. Based on the mesh, we study several tree construction mechanisms to trade off delay and network resource consumption. We investigate the following two important issues in SMesh.

1.1 MESH FORMATION AND MAINTENANCE: The mesh should be efficiently formed and maintained in order to reduce control and delivery overhead. We choose the DT mesh as an example. We then use the Global Network Positioning tool (GNP) [11] (or many other equally good ones [12], [13], [14]) to estimate host locations in the Internet in order to improve mesh efficiency. We further present a distributed algorithm on how to detect and recover mesh partitions. Our mesh has the following properties:

1.1.1 LOW DELIVERY DELAY: As mesh formation and message forwarding are based on hosts' net-work locations, the delay for data delivery is significantly reduced as compared to that in the traditional DT mesh.

1.1.2 DISTRIBUTED: Unlike the traditional DT mesh, SMesh does not require a central server for mesh maintenance. It is fully distributed and scalable.

1.2 CONSTRUCTION OF DATA DELIVERY TREES: Given the mesh, we study how source-specific overlay trees can be efficiently constructed and maintained. We consider three ways to construct a tree: a) Embedded tree, where tree branches are all mesh edges; b) Bypass tree, where tree nodes can only be group members and tree branches may not be mesh edges; and c) Intermediate tree, which is a trade-off between an embedded tree and a bypass tree. These trees have the following properties:

1.2.1 OVERHEAD REDUCTION: As compared to traditional tree-based protocols, SMesh achieves much lower control overhead for tree construction and maintenance. This is because the mesh has maintained enough host information and can efficiently deal with host hopping between different groups.

1.2.2 QOS PROVISIONING: SMesh provides QoS in the following senses: a) It limits the node stress of a host in a tree according to the host's capability. b) It aggregates long-delay paths and delegates data delivery to shorter paths. As a result, packets may take more hops to reach their destinations, and this trades off end-to-end delay with network resource consumption. SMesh does not rely on a static mesh. In the case of host joining or leaving, the underlying DT mesh can automatically adjust itself to form a new mesh. The trees on top of it will then accordingly adjust tree nodes and tree edges. Also note that in SMesh a host may join as many groups as its local resource allows. If a host joins multiple groups, its operations in different groups are independent of each other.

The rest of the paper is organized as follows: In Section 2, we review the GNP and DT protocols. In Section 3, we discuss how to form and maintain an efficient mesh. In Section 4, we study the tree construction mechanisms. In Section 5, we present illustrative simulation results on Internet-like topologies. We discuss related work in Section 6, and finally conclude the paper in Section 7.

2. REVIEW ON GNP AND DT

In this section, we briefly review the GNP and DT protocols. We will construct our SMesh system based on these building blocks.

2.1 REVIEW ON GNP ESTIMATION GNP estimates host coordinates in a multidimensional euclidean space such that the distance between two hosts in the euclidean space correlates well with the measured round-trip time between them [11]. In GNP, a few hosts are used as landmarks. Landmarks first measure the round-trip time between each other and forward results to one of them. The landmark receiving results uses the results to compute the landmark coordinates in the euclidean space. The coordinates are then disseminated back to the respective landmarks. More specifically, to estimate landmark coordinates, the following objective function is minimized[1]:

JlandmarkðL1; L2; . . . ;LM

Li;Lj2fL1 ;...;LM gji>j

where M is the number of landmarks, L_i and L_j are the coordinates of landmarks i and j in the euclidean space, and RTT ði; jÞ is the round-trip time between i and j. As shown, $J_{landmark}$ is the sum of the estimation error between the measured round-trip time and the logical distances in the euclidean space among the landmarks. Therefore, we seek a set of landmark coordinates such that the sum is mini-mized. If there are multiple sets of

fL$_1$; L$_1$; . . . ; L$_M$ g to minimize $J_{landmark}$, any one set can be used.

Given the landmark coordinates, a normal host estimates its coordinates by minimizing a similar objective function:

$$XJ_{host}ðH_uÞ ¼ ðkH_u ³ L_ik ³ RTT ðu; iÞÞ^2; \quad ð2Þ \; L_i2fL_1;...;L_M g$$

where H_u is the coordinates of host u, and RTT ðu; iÞ is the measured round-trip time between host u and landmark i.

Note that landmarks do not have to be permanent. It is easy to modify (2) to remove a failed landmark or add a new landmark. According to Ng and Zhang [11], GNP has shown good enough performance when the number of landmarks is a constant (9-15 as recommended in [11] and 20 in our simulations). Therefore, each host can obtain its coordinates by pinging Oð1Þ landmarks and using Oð1Þ messages. It is highly efficient and scalable.

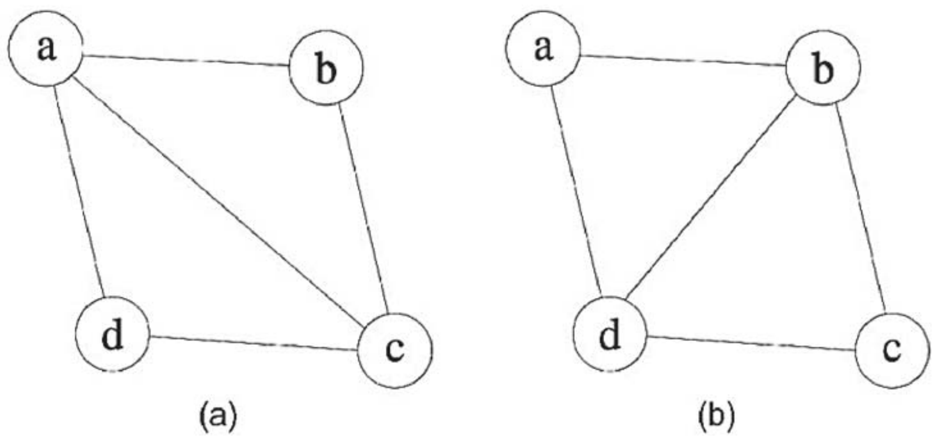

Fig. 1. (a) Two adjacent triangles in a convex quadrilateral (4abc and 4adc) violate the DT property and (b) restore the DT property by disconnecting a from c and connecting b and d.

2.2 REVIEW ON DELAUNAY TRIANGULATION In the traditional DT protocol, each host knows its geographic coordinates [10]. Hosts form a DT mesh based on their geographic coordinates. Compass routing, a kind of local routing, is then used to route a message along the mesh [15]. In this approach, a host only needs to know the states of its immediate neighbors to construct and maintain the mesh, and the mesh is adaptive to dynamic host joining or leaving.

DT protocol connects hosts together so that the mesh satisfies the DT property, i.e., the minimum internal angle of the triangles in the mesh is maximized [16], [17]. Here angles are computed according to the coordinates of hosts as in traditional geometry. It has been shown that a mesh formed in this way connects close hosts together. We illustrate the triangulation process in Fig. 1. Suppose that hosts a; b; c, and d form a convex quadrilateral abcd. Two possible ways to triangulate it are shown in Figs. 1a and 1b, respectively. Clearly, the minimum internal angle of 4abc and 4acd is smaller than that of 4abd and 4bcd. DT protocol then transforms the former configuration into the latter one. To achieve this, a host periodically sends HelloNeighbor messages to its neighbors to exchange their neighborhood information. It removes a host from its neighbor list if the connection to that host violates the DT property. Similarly, a host adds another host into its neighbor list only if the addition does not violate the DT property. Given a set of N hosts in the network, a DT mesh among them can be constructed with OðN log NÞ messages. The detailed construction mechanism and complexity analysis can be found in [16].

Compass routing works as follows. Host a forwards messages with destination t to b, if b, among all a's neighbors, forms the smallest angle to t at a. We show an example in Fig. 2. Hosts b; c, and d are neighbors of host a, and a needs to forward a message to destination t. Since ffbat is the smallest among ffbat; ffcat, and ffdat; b is chosen by a as the next hop for message forwarding.

In the traditional DT protocol, mesh partition is detected by a central server. In each connected DT mesh, a host is selected as the leader, which periodically exchanges control messages with the server. If the mesh is partitioned, more than one host will claim to be leaders. The server then requests them to connect to each other.

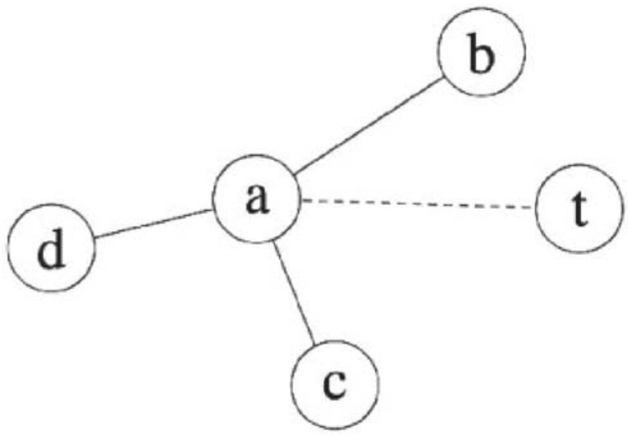

Fig. 2. An example of compass routing. The angle ffbat is smaller than angles ffcat and ffdat. Therefore, when a receives a message with destination t, it forwards the message to b.

2.2.1. INACCURACY IN ESTIMATING HOST LOCATIONS: DT estimates host locations based on their geographic coordinates. This may work well for wireless networks, but not for the Internet where the network delay between two hosts may not correlate well with their geographic distance. In other words, the traditional DT protocol may build a tree with a low geographic distance but a high end-to-end network delay.

2.2.2. SINGLE POINT OF FAILURE: Partition detection and recovery rely on a central server. This forms a single point of failure and is not scalable.

2.2.3. MESSAGE LOOPING: Compass routing in connected DT mesh does not result in loops [10], [15].

However, looping may persist in partitioned meshes. If the destination of a message is in another mesh, the message may loop in the current mesh for a long time.

3. MESH FORMATION AND MAINTENANCE

In this section, we discuss how SMesh forms and maintains an efficient mesh. SMesh addresses the above problems as follows:

- SMesh uses GNP to estimate host locations in the Internet space and builds a DT mesh based on the estimated host coordinates. Since GNP estimation is based on network distances between hosts, the resultant mesh can achieve lower end-to-end delay than the traditional DT mesh.
- SMesh uses a distributed algorithm to detect and recover mesh partition, thereby eliminating the need for a central server from the system.
- The distributed algorithm is able to detect whether a message destination is in a partitioned mesh or not, and hence solves the message looping problem.

3.1 DISTRIBUTED ALGORITHM FOR PARTITION DETECTION AND RECOVERY: We now present a distributed algorithm to detect and recover mesh partition. We define some notations as follows. Given a graph, define ff_pabc as the clockwise angle from edge ab to edge bc and ff_3abc as the counter-clockwise angle from edge ab to edge bc. They are both between 0 degree and 360 degrees (i.e., the angle is not negative). We further define the undirected angle ffabc as the smaller one of ff_pabc and ff_3abc, which is certainly between 0 degree and 180 degrees. We show the examples of ff_p; ff_3, and ff in Figs. 3a, 3b, and 3c, respectively.

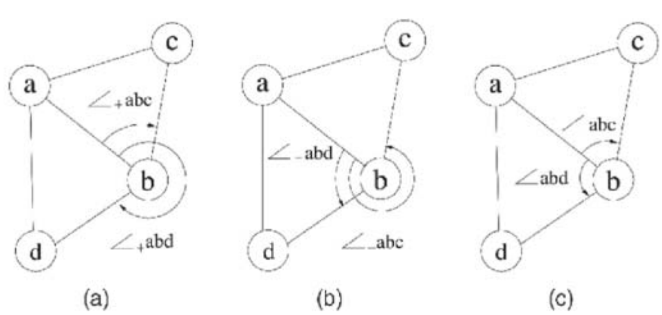

Fig. 3. Examples of (a) clockwise angles ff_p, (b) counterclockwise angles ff_s , and (c) undirected angles ff.

We further consider two connected hosts b and c, and another host a in the graph (whether a is a neighbor of b or c is irrelevant here). We say that c is the clockwise neighbor of b with respect to a if and only if $f_p$abc is less than 180 degrees and is the minimum among all the neighbors of b b (i.e., $f_p$abc f $f_p$abx; 8x 2 neighbors of b). In this case, we write $N_{b;a}^{þ}$ ¼ c (one can imagine that the edge ba with b fixed, when sweeping clockwise by less than 180 degrees, would first touch c among all b's neighbors). For example, in Fig. 3a, c is the clockwise neighbor of b with respect to a (i.e., $N_{b;a}^{þ}$ ¼ c). Similarly, we say that c is the counter-clockwise neighbor of b with respect to a, denoted as $N_{b;a}$ ¼ c, if and only if $f_3$abc is less than 180 degrees and is the minimum among all the neighbors of b. In Fig. 3b, d is the counterclockwise neighbor of b with respect to a (i.e., $N_{b;a}^{3}$ ¼ d). Note that host b may not have any clockwise neighbor (or counterclockwise neighbor) with respect to a. For example, in Fig. 3, host b does not have any clockwise neighbor with respect to c, since angles $f_p$cbd and $f_p$cba are larger than 180 degrees.

Theorem 1. Given the above definitions and host coordinates, a host u detects that a destination t is partitioned from the mesh if and only if one of the following conditions is satisfied:

1. $N_{u;t}^{þ}$ ¼;, or
2. $N_{u;t}^{3}$;, or ff
3. $N_{u;t}^{3}$ u$N_{u;t}$ > 180°, or ff
4. $N_{u;t}$ t$N_{u;t}^{3}$ > 180°.

Proof. There are two possible cases for t's location

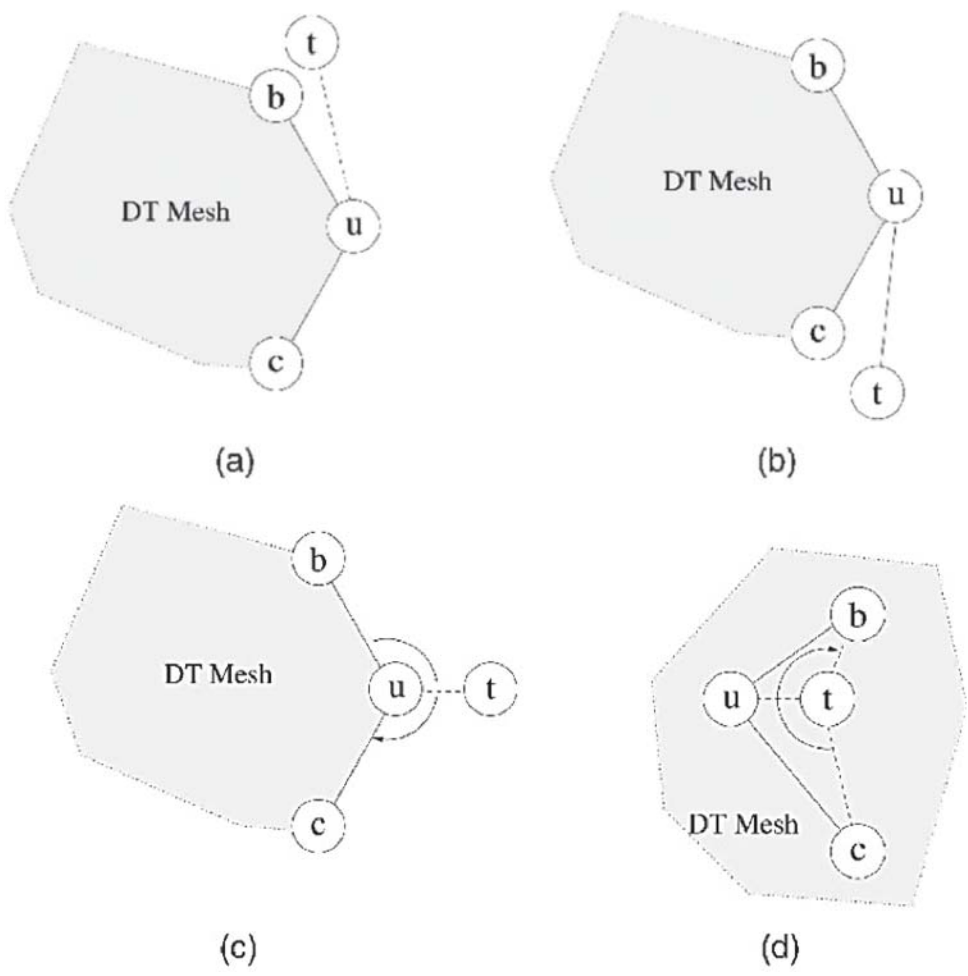

FIG 4. (a), (b), and (c) Host u is on the boundary of the overlay mesh, and host t lies outside the mesh. (d) u is an interior host of the mesh. Host t lies inside triangle 4ubc, but does not belong to the mesh.

- t is outside the mesh (see Figs. 4a, 4b, and 4c). By definition, a DT mesh is a convex polyhedron where only the external angles are larger than 180 degrees. As t falls outside the mesh, a message with destination t must be finally forwarded to a boundary host u in the mesh. The possible positions of t are given in Figs. 4a, 4b, and 4c, where hosts b and c are two neighbors of u on the boundary of the mesh. Fig. 4a corresponds to condition 1. Fig. 4b corresponds to condition 2. Fig. 4c corresponds to condition 3, where ffþN_u;tuNþu;t is as indicated.
- t is in the interior of the mesh (see Fig. 4d). If t is in the interior of the mesh, the position of t must fall inside a certain triangle 4ubc (as shown in Fig. 4d). When a host u receives a message with destination t, if it finds that ffþNþu;ttN_u;t > 180 degrees and there is no connection with t, it can conclude that t is not in the mesh. tu Therefore, a host u checks whether the

destination has been partitioned from its mesh before forwarding a message. If so, u directly forwards the message to t to avoid message looping, and asks t to join the mesh through itself (using the joining mechanism below) so as to recover the partition.

3.2 JOINING MECHANISM A joining host, after obtaining its coordinates, sends a MeshJoin message with its coordinates to any host in the system. MeshJoin is then sent back to the joining host along the DT mesh based on compass routing. Since the joining host is not a member of the mesh yet, it can be considered as a partitioned mesh consisting of a single host. The MeshJoin message finally triggers the partition recovery mechanism at a particular host in the mesh, which helps the new host join the mesh. We illustrate the host joining mechanism in Fig. 5. Suppose that u is a joining host. The following steps show how u joins the mesh (corresponding to Fig. 5):

a. u first retrieves the list of landmarks by querying a host b with a GetLandmark message.

b. Then u measures the round-trip time to the landmarks and estimates its coordinates.

c. After that, u sends a Mesh Join message to b.

d. The message is then forwarded from b to c based on compass routing.

e. Since u falls into Δacd; c knows that u is in another partitioned mesh. c then adds u into its neighbor listNc to recover the partition. Note that the minimum internal angle of Δauc and Δabc is less than that of Δbuc and Δabu. Therefore, the connection between c and a violates the DT property, and c will remove a from Nc and notify a to remove the connection. c then broadcasts its neighborhood information to its neighbors through HelloNeighbor messages. (In DT, each host needs to periodically send HelloNeighbor messages to its neighbors to exchange the neighborhood information.)

f. Upon receiving HelloNeighbor messages from c; b, and d discover u. They add u into their neighbor lists since such connections do not violate the DT property. In the meantime, u also discovers b and d and adds them into its neighbor list. Suppose that b is the next to broadcast HelloNeighbor messages. Upon receiving the message, a discovers u and adds u into its neighbor list.

g. The resultant overlay mesh after the joining of u still satisfies the DT property.

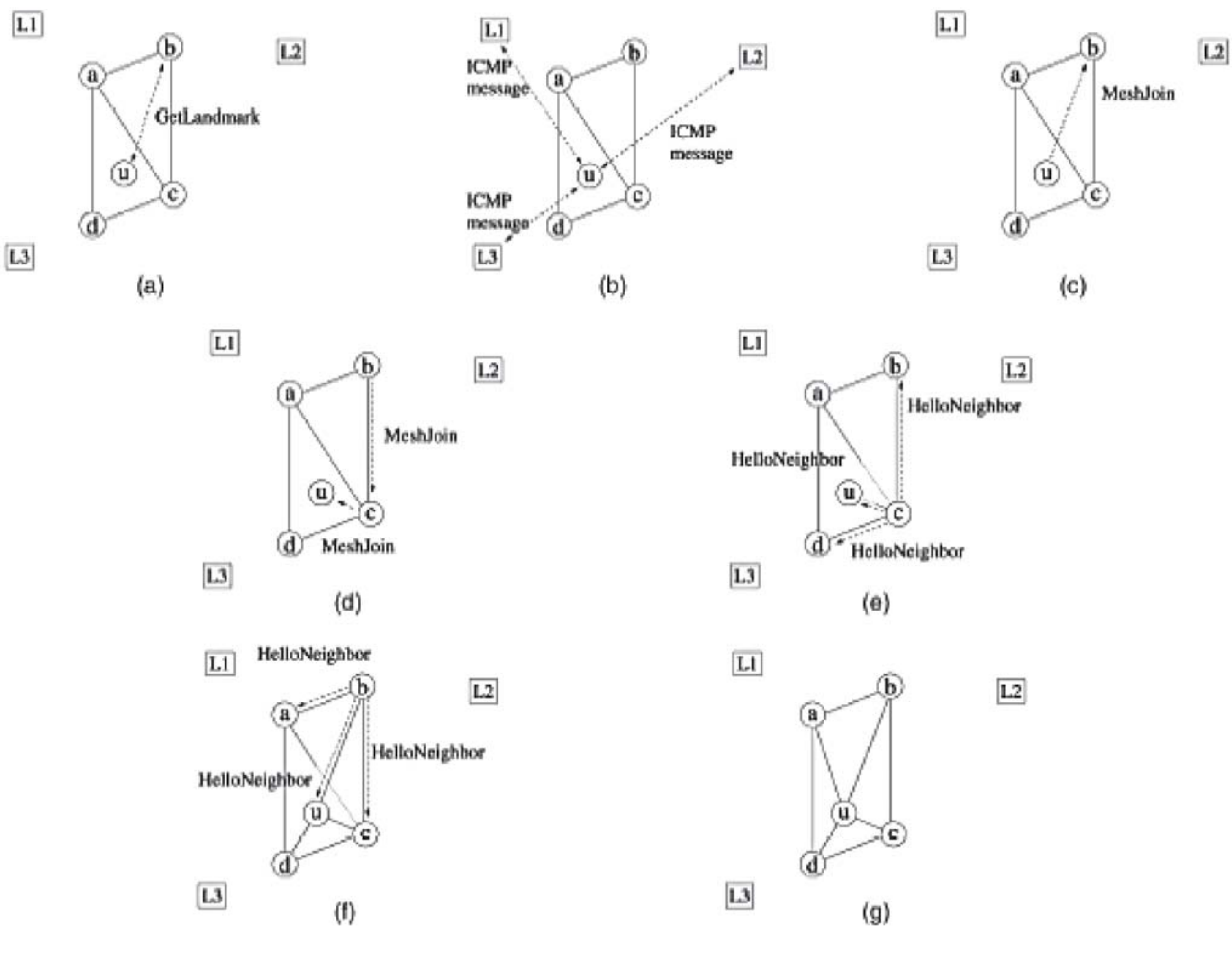

4. CONSTRUCTION OF DATA DELIVERY TREES

In this section, we discuss tree construction mechanisms in SMesh. In Section 4.1, we propose three algorithms to construct data delivery trees on top of the mesh. In Section 4.2, we present a path aggregation algorithm for QoS provisioning. In Section 4.3, we illustrate our algorithms with examples.

4.1 EMBEDDED, BYPASS, AND INTERMEDIATE TREES: We study three ways to build trees in SMesh. The first type of tree is called an embedded tree, where all tree edges are part of the overlay mesh. When forming the tree, nonmember hosts may be included. This is similar to Skype routing, where a Skype client may help relay packets that it is not interested in. The second one builds an overlay tree that covers only group members without having to use mesh edges. We call it a bypass tree. All tree nodes in a bypass tree are members of the group. This is similar to traditional overlay tree construction, where a node relays packets only for other members in its groups. However, the construction of a bypass tree has to rely on the underlying mesh. The third one is termed an intermediate tree, which lies between embedded and bypass trees. In the following, we call a nonleaf host in an overlay tree a forwarder, which needs to forward data messages to its children in the tree. We elaborate the details as follows:

- Embedded Tree: To join an embedded tree, a joining host first sends a TreeJoin message to the group source along the DT mesh using compass routing. All hosts along the message routing path become forwarders for the tree no matter whether they are group members. In Algorithm 1, we show how the TreeJoin message is handled by a host in the mesh: A host first adds the joining host into its children table for the specified group. Then, it checks whether itself is already a forwarder of the group. If so, the host has already started to forward messages for the tree and known the overlay path along the mesh to the group source. So, it suppresses the forwarding of the TreeJoin message and does nothing. Otherwise, it turns itself into a forwarder and relays the TreeJoin message to the group source. The TreeJoin message will eventually discover a path along the mesh to the group source.
- Bypass Tree: All forwarders in a bypass tree are the group members. Similarly, in order to join a bypass tree, a joining host needs to send a TreeJoin message to the group source using compass routing. We show the tree construction algorithm in Algorithm 2. A nonmember host receiving the TreeJoin message simply relays the message to the next hop without turning itself into a forwarder. Such a host will not forward data packets for the group in the future. On the other hand, if the host receiving the message is a member of the group, it accepts the joining host as its child by adding the joining host into its children table. Clearly, such a host has already joined the tree and known the path to the group source. So, it stops forwarding the TreeJoin message.

  Intermediate Tree: We observe that an embedded tree requires the participation of nonmember hosts, and a host may need to serve multiple hosts of different groups. As compared to a bypass tree, it consumes more network resources and suffers from higher delay, especially for sparse groups. On the other hand, a host in a bypass tree may have a high node stress and heavy load for data forwarding (e.g., a star-like topology rooted at the source for a sparse group). Therefore, we propose an intermediate tree which trades off between an embedded tree and a bypass tree. In an intermediate tree, a nonmember host is included in the tree if it receives more than a certain number of joining messages. Such a host resides in many routing paths, and we expect high delivery efficiency by including it in the tree. In Algorithm 3, we show how the TreeJoin message is handled by a host: A host handles the message as in a bypass tree if the number of received messages is less than a certain threshold. Otherwise, the host forwards the message as in an embedded tree.

Algorithm 1.

```
TREEJOINHANDLER_EMBEDDEDTREE (TreeJoin)
    Me.Child[TreeJoin.InterestGroup] Me.Child[TreeJoin.InterestGroup] [TreeJoin.JoinHost]
    if TreeJoin.InterestGroup 62 Me.InterestGroups
    then Me.InterestGroups Me.InterestGroups [TreeJoin.InterestGroup]
    TreeJoin.JoinHost Me
    CompassRoute(TreeJoin, TreeJoin.GroupSource);
```

Algorithm 2.

```
TREEJOINHANDLER_BYPASSTREE (TreeJoin)
    if TreeJoin.InterestGroup 2 Me.InterestGroups
    then Me.Child[TreeJoin.InterestGroup]
    Me.Child[TreeJoin.InterestGroup] [ TreeJoin.JoinHost
    else CompassRoute(TreeJoin, TreeJoin.GroupSource);
```

Algorithm 3.

```
TREEJOINHANDLER_INTERMEDIATETREE (TreeJoin)
    Received Message Received Message þ 1
    if Received Message _ Message Threshold
    then TreeJoinHandler_BypassTree (TreeJoin);
    else TreeJoinHandler_EmbeddedTree (TreeJoin);
```

4.2 PATH AGGREGATION FOR QOS PROVISIONING We note that the traditional DT protocol may result in high network resource consumption. For example, if host a belongs to domain A, and hosts b and b0 belong to domain B, usually the delays of interdomain paths ab and ab0 are much higher than that of intradomain path bb0. In other words, angle ffbab0 is small. As a result, using compass routing, if either b or b0 is a child of a, the other one is also likely to be a child of a. Therefore, two independent connections across domains A and B are set up, which leads to high usage of long paths and hence high network resource consumption. Furthermore, in the traditional DT protocol, a host may have many children. However, a host often has a node stress threshold K for each group depending on its resource. To address these problems, we require that the minimum adjacent angle between two children of a host should exceed a certain threshold T. If the condition on K or T is violated, SMesh modifies its overlay tree through aggregation and delegation. Consider a source s and a host u in the network. Once u accepts a child, u checks whether its node stress exceeds K or whether the minimum adjacent angle between its children is less than T. If so, it runs the path aggregation algorithm, as shown in Algorithm 4. It selects a pair of children with the minimum adjacent angle and delegates the child farther from the source to the other. Note that after aggregation, the overlay tree is still loop free because hosts are still topologically sorted according to their distances from the source. We show an example in Fig. 6, where ffbuc is the smallest angle among all u's children. If it is smaller than the threshold T and because ks _ bk < ks _ ck; u delegates c to b.

Algorithm 4.

PATHAGGREGATION(u)

1. ½c; c0_ a pair of children with the minimum adjacent angle
2. while ffcuc0 < T OR number of children > K
3. do if kc _ sk < kc0 _ sk
4. then delegate c0 to c
5. else elegate c to c0
6. ½c; c0_ a pair of children with the minimum adjacent angle

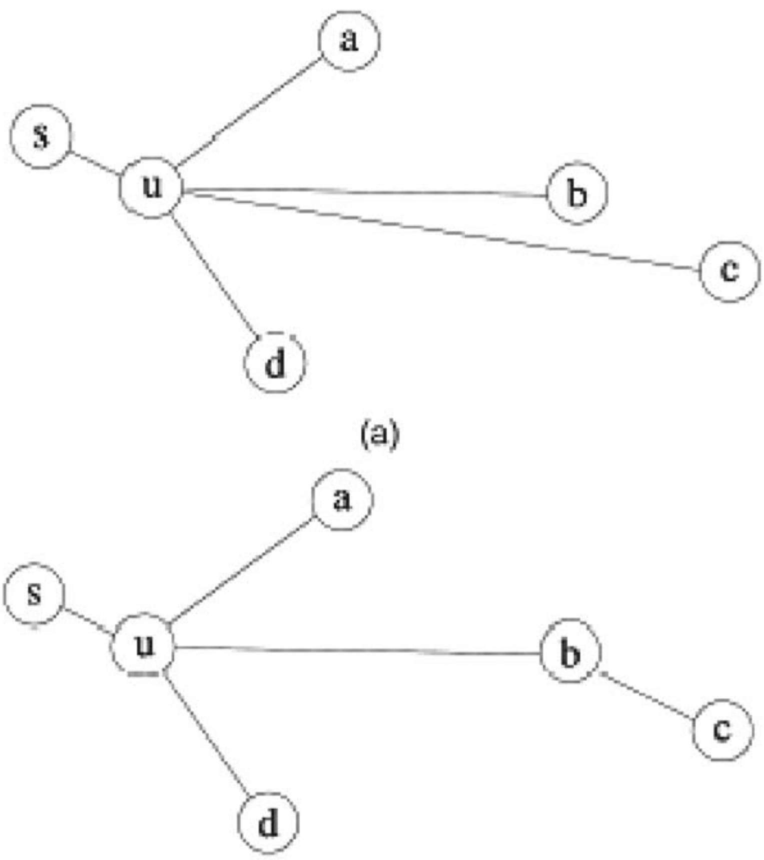

(b)

Fig. 6. Host u delegates its child c to child b, since ffbuc < T and ks _ bk < ks _ ck.

SMesh avoids tree partition during aggregation by temporarily setting up backup paths. If u delegates its child c to another child c_0; u would keep forwarding data to c unless it receives an acknowledgment from c_0. (This way, a backup path uc is set up.) Backup paths are also present when a host leaves its group. For example, in a bypass tree, a leaving host u sends a TreeLeave request to its parent p with the information of its children C ¼ fc_1; c_2; . . . ; c_Mg. p keeps forwarding data to u until p has handled (either accepted or delegated) all the hosts in C (i.e., backup paths uc_1; uc_2; . . . ; uc_M are set up).

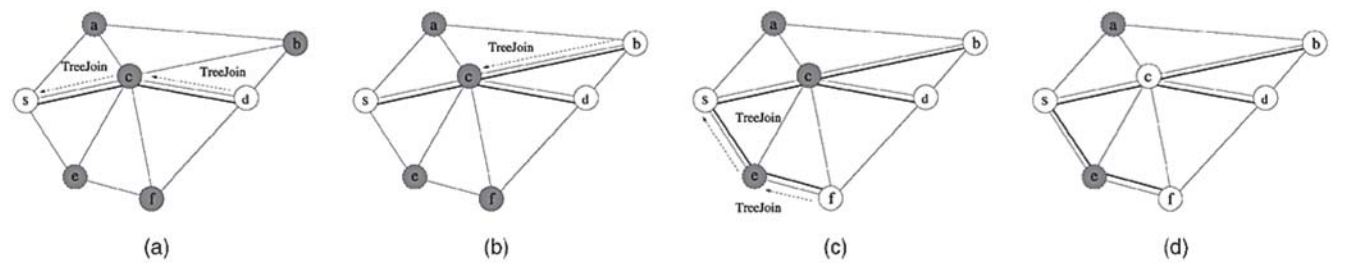

Fig. 7. An example of building an embedded tree. Tree branches are indicated by bold lines.

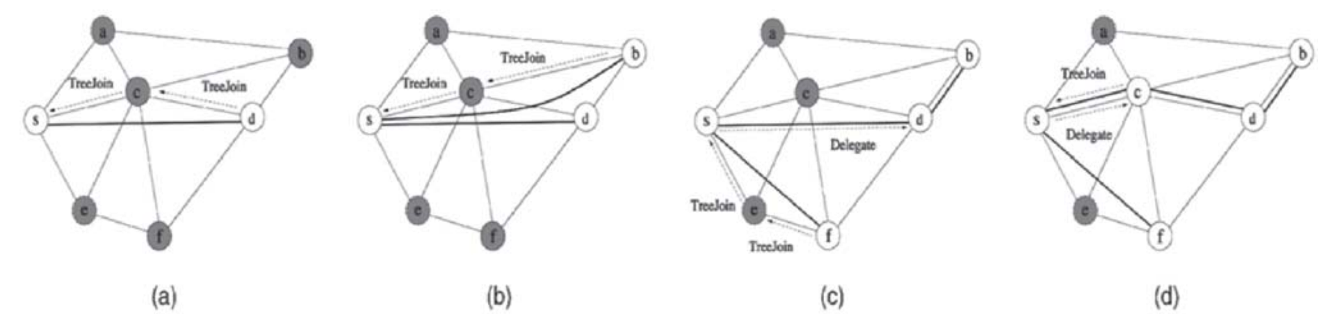

Fig. 8. An example of building a bypass tree. Tree branches are indicated by bold lines

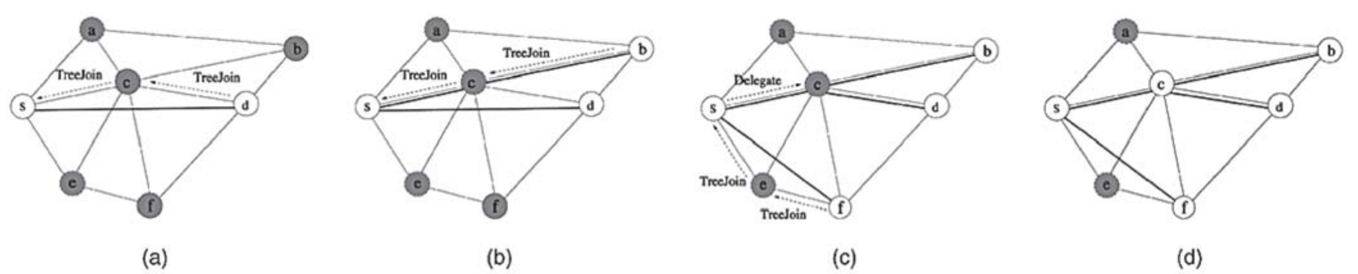

Fig. 9. An example of building an intermediate tree. Tree branches are indicated by bold lines.

4.3 ILLUSTRATIVE EXAMPLES We show in Figs. 7, 8, and 9 how embedded, bypass, and intermediate trees are constructed. White circles in figures denote hosts belonging to the same group. The joining sequence is fd; b; f; cg, and s is the source.

We first show the construction of an embedded tree in Fig. 7. When d joins, its TreeJoin message is first forwarded to c (Fig. 7a). Although c is a nonmember, the message turns it into a forwarder and it relays the message to s. Next, b joins the group and its TreeJoin message is also forwarded to c (Fig. 7b). Since c is a forwarder already, it only modifies its children table and does not relay the message again. Afterwards, when f joins, its TreeJoin message is first forwarded to e, and then to s (Fig. 7c). Finally, when c joins the group, it does not need to send a TreeJoin message since it is already a forwarder (Fig. 7d).

In Fig. 8, we show a bypass tree with forwarding delegation (K ¼ 2 without T threshold, i.e., T ¼ 360 degrees). When d joins, its TreeJoin message is first forwarded to c and then to s (Fig. 8a). Since c is a nonmember, s directly serves d. Later on, when b joins, its TreeJoin message is also forwarded to s through c. Similarly, s directly serves b (Fig. 8b). Note that at this moment, s has already had K children (K ¼ 2). Therefore, when f joins and becomes s's child, s has to delegate one of its children (d; b; and f) to others. It first selects a pair of children with the minimum adjacent angle, which are b and d. Then, it delegates the child farther from the source (i.e., b) to the other one, i.e., d (Fig. 8c). Finally, when c joins, s similarly delegates d to c (Fig. 8d).

We finally show an intermediate tree with K ¼ 2 and MessageThreshold ¼ 1 in Fig. 9. d is the first to join and its TreeJoin message is forwarded to c (Fig. 9a). Since this message is the first joining request c has received, c handles the message as in a bypass tree. That is, c relays the message to s without becoming a forwarder, and s directly serves d. Later on, when b joins, its

TreeJoin message goes through c to s (Fig. 9b). Now c has received two joining messages and this number exceeds its message threshold 1. Therefore, c handles the message as in an embedded tree and turns itself into a forwarder. Afterwards, when f joins, s directly serves f by skipping e. Now s has three children, i.e, c; d, and f. s then delegates d to c as ffdsc is the minimum among all angles formed by s's children (Fig. 9c). Finally, when c joins the group, it does not need to send any TreeJoin message since it is already a forwarder (Fig. 9d).

5. CONCLUSION

In P2P streaming networks, users may frequently hop from one group to another. In this paper, we propose a novel framework called SMesh to serve dynamic groups for Internet streaming. SMesh supports multiple groups and can efficiently distribute data to these dynamic groups. It first builds a shared overlay mesh for all hosts in the system. The stable mesh is then used to guide the construction of data delivery trees for each group. We study three ways to construct a tree, i.e., embedded, bypass, and intermediate trees. We also propose and study an aggregation and delegation algorithm to balance the load among hosts, which trades off end-to-end delay with lower network resource usage.

Through simulations on Internet-like topologies, we show that SMesh achieves low RDP and low link stress as compared to traditional tree-based protocols. In our simulations, a bypass tree performs better than an embedded tree in terms of RDP but not so for link stress. By adjusting message threshold, an intermediate tree can achieve performance between bypass and embedded trees.

ACKNOWLEDGEMENTS

This work was supported, in part, by the General Research Fund from the Research Grant Council of the Hong Kong Special Administrative Region, China (611107), and the Cisco University Research Program Fund, a corporate advised fund of Silicon Valley Community Foundation.

REFERENCES

1. X. Zhang, J. Liu, B. Li, and T.-S.P. Yum, “CoolStreaming/DONet: A Data-Driven OverlayNetwork for Peer-to-Peer Live Media Streaming,” Proc. IEEE INFOCOM '05, pp. 2102-2111, Mar. 2005.

2. X. Liao, H. Jin, Y. Liu, L.M. Ni, and D. Deng, “Anysee: Peer-to- Peer Live Streaming,” Proc. IEEE INFOCOM '06, Apr. 2006.

3. Y. Tang, J.-G. Luo, Q. Zhang, M. Zhang, and S.-Q. Yang, “Deploying P2P Networks for Large-Scale Live Video-Streaming Service,” IEEE Comm. Magazine, vol. 45, no. 6, pp. 100-106, June 2007.

4. PPLive, http://www.pplive.com, 2009.

5. X. Hei, Y. Liu, and K.W. Ross, “Inferring Network-Wide Quality in P2P Live Streaming Systems,” IEEE J. Selected Areas in Comm., vol. 25, no. 9, pp. 1640-1654, Dec. 2007.

6. X. Hei, C. Liang, J. Liang, Y. Liu, and K.W. Ross, “A Measurement Study of a Large-Scale P2P IPTV System,” IEEE Trans. Multimedia, vol. 9, no. 8, pp. 1672-1687, Dec. 2007.

7. M. Cha, P. Rodriguez, J. Crowcroft, S. Moon, and X. Amatriain, “Watching Television over an IP Network,” Proc. ACM Internet Measurement Conf. (IMC '08), pp. 71-83, Oct. 2008.

8. Skype, http://www.skype.com/, 2009.

9. D. Rossi, M. Mellia, and M. Meo, “A Detailed Measurement of Skype Network Traffic,” Proc. Int'l Workshop Peer-To-Peer Systems (IPTPS '08), Feb. 2008.

10. J. Liebeherr, M. Nahas, and W. Si, “Application-Layer Multicasting with Delaunay Triangulation Overlays,” IEEE J. Selected Areas in Comm., vol. 20, no. 8, pp. 1472-1488, Oct. 2002.

METRICS FOR MEASURING THE UNDERSTANDABILITY OF OBJECT-ORIENTED DESIGN QUALITY

Devpriya Soni
Associate Professor, Department of Computer Science and Engineering
Dronacharya College of Engineering, Greater Noida, India
Email: devpriyasoni@gmail.com

ABSTRACT

Software design quality directly affects the understandability of the software developed. The increase in size and complexity of software drastically affects quality attributes, especially understandability. The direct measurement of quality is difficult because there is no single model that can be applied in all situations. Researchers have developed quality models that attempt to measure quality in terms of attributes, characteristics and metrics. However these models are not comprehensive. Quantitative measurement of an operational system's understandability is desirable both as an instantaneous measure and as a predictor of understandability over time. This work proposes the method of measuring understandability using Logical Scoring of Preferences (LSP) method. I have also evaluated one design through this model.

Keywords: Software Quality, Quantitative Measurement ,LSP.

1. INTRODUCTION

The demand of the quality software is increasing at rapid pace due to the society's increasing dependence on software. Measuring quality in the early stage of software development is the key to develop high-quality software. False interpretations can lead to misunderstandings and to faulty development results. Without an understanding and the ability to articulate the processes in use, it is not likely that they can be managed and improved. Therefore, the readability and understandability of the software has a lot of influence on the factors that directly or indirectly affect software quality. Complex design may lead to poor testability, which in turn leads to ineffective testing that may result to severe penalties and consequences. It is well understood fact that flaws of design structure have a strong negative impact on quality attributes. But, structuring a high-quality design continues to be an inadequately defined process [1]. Therefore, software design should be built in such a way so as to make them easily understandable, testable, alterable, and preferably stable. This work focuses on the understandability assessment during the design phase to produce quality software.

Our methodology for the quantitative evaluation of software's understandability in the design phase is based on the core evaluation models and procedures are grounded in the LSP model and continuous preference logic as mathematical background [2]. Kumar and Soni [4] have proposed a hierarchical model of quality attributes. This is used to evaluate quality of human resource system design which was proposed by Kumar and Gandhi [3].

2. PREVIOUSLY PROPOSED QUALITY MODELS FOR OBJECT-ORIENTED SOFTWARE PRODUCTS:

One of the earliest software product quality model was suggested by McCall et.al.[5]. They defined software product qualities as a hierarchy of factors, criteria and metrics. The McCall's quality factors are correctness, reliability, efficiency, integrity, usability and maintainability. Boehm [6] described a set of quality characteristics. International bodies ISO/IEC came up with ISO9126 model for ensuring quality in software products. The ISO9126 [7, 17] model defines six quality attributes namely functionality, reliability, efficiency, usability, maintainability and portability. They are further subdivided into 26 sub-attributes (criteria) and nearly 100 sub-criteria or metrics. All these models were developed for structured methodology of software product development.

Even though there are many object-oriented analysis and design methodologies, languages, database management systems and tools, relatively less work has been done in the area of object-oriented design quality assurance [7, 8]. However, many metrics were developed to measure size and complexity of an object-oriented software system. One of the most popular set of metrics (commonly know as CK Metrics suite) was proposed by Chidamber and Kemerer [9]. The same suite was later refined and presented with empirical validation by Chidamber and Kemerer [10]. Basili et.al. [11, 12] also performed the empirical validation of CK metrics suite.

A framework for building product based quality models has been developed by Dromey [13,14]. The framework is a methodology for development of quality models in a bottom-up fashion, providing an approach that will ensure that the lower-level details are well specified and computable [12]. Bansiya et.al. [15] extended this methodology to develop the hierarchical

Quality-Model for Object-Oriented Design (QMOOD) assessment. In the Quality Model for Object-Oriented Design (QMOOD), Bansiya et.al [15] identified the initial set of design quality attributes as: functionality, effectiveness (efficiency), understandability (maintainability), extendibility (portability), reusability and flexibility.

Further, Keller and Cockburn [16] organized a workshop, in which one group agreed upon following list of perspectives, with each having substantial influence on the quality of design artifacts: maintainability, documentation, extensibility, cost, reliability, ease of use, internationalization, usability, market goals, performance, team structure.

The second group discussed design properties that are of interest for project participants (developers) and gave following attributes: clarity, simplicity, scalability, modifiability, extendibility, reusability, effectiveness, reliability, robustness, security, and cost.

The metrics proposed by Bansiya et.al. [15] are quite general in nature and they have not provided the methodology to measure these metrics. Keller and Cockburn [16] have observed that there was no consensus on the quality attributes. However, they prescribed attributes and metrics that are very broad in nature and are not in conformance with ISO/IEC 9126 standards.

The author in her previous work [3] has given a generic model which assesses quality of design in early stage of software product development life cycle. This hierarchical model is based on five factors, their sub-factors and metrics and shown in Figure 2.1. These five-factors for design quality assessment are: functionality (modifiability), effectiveness (efficiency), understandability (usability), extendibility (portability), reusability, and maintainability (flexibility).

3. STEPS FOR THE EVALUATION OF DESIGN QUALITY

Steps required for the evaluation of design quality are:

1. Consider a hierarchical model for quality characteristics and attributes (i.e. A1 …. An): here, evaluators should define and specify the quality characteristics and attributes, grouping them into a model. For each quantifiable attribute Ai, we can associate a variable Xi, which can take a real value: the measured value.

2. Defining criterion function for each attribute and applying attribute measurement: In this process, the evaluators should define the basis for elementary evaluation criteria and perform the measurement sub-process. An elementary evaluation criterion specifies how to measure quantifiable attributes. The result is an elementary preference, which can be interpreted as the degree or percentage of satisfied requirement. For each variable Xi , i = 1, ...,n it is necessary to establish an acceptable range of values and define a function, called the elementary criterion. This function is a mapping of the measured value in the empirical domain [18] into the new numerical domain. Then the final outcome is mapped in a preference called the elementary quality preference, EQi. We can assume the elementary quality preference EQi as the percentage of requirement satisfied by the value of Xi . In this sense, EQi = 0% denotes a totally unsatisfactory situation, while EQi = 100% represents a fully satisfactory situation [2]. Ultimately, for each quantifiable attribute, the measurement activity should be carried out.

3. Evaluating elementary preferences: In this task, the evaluators should prepare and enact the evaluation process to obtain an indicator of partial preference for design. For n attributes, the mapping produces n elementary quality preferences.

4. Analyzing and assessing partial quality preferences: In this final step, the evaluators analyze and assess the elementary, partial and total quantitative results regarding the established goals.

3.1 ESTABLISHING ELEMENTARY CRITERIA FOR UNDERSTANDABILITY: The significance of understandability is very obvious that can be perceived as 'If we can't learn something, we won't understand it. If we can't understand something, we can't use it - at least not well enough to avoid creating a money pit. We can't maintain a system that we don't understand - at least not easily. And we can't make changes to our system if we can't understand how the system as a whole will work once the changes are made. Understandability of software documents is thus important as 'the better we know what the thing is supposed to do, the better we can test for it'. A good software design with manageable complexity usually provides proper data abstraction; it reduces coupling while increasing cohesion that make them easily understandable. Researchers and Practitioners advocated that understandability aspect of software is highly desirable and significant for developing quality

1. Functionality
    - 1.1 Design Size
        - 1.1.1 Number of Classes (NOC)
    - 1.2 Hierarchies
        - 1.2.1 Number of Hierarchies (NOH)
    - 1.3 Cohesion
        - 1.3.1 Cohesion Among Methods of Class (CAM)
    - 1.4 Polymorphism
        - 1.4.1 Number of Polymorphic Methods (NOP)
    - 1.5 Messaging
        - 1.5.1 Class Interface Size (CIS)
2. Effectiveness
    - 2.1 Abstraction
        - 2.1.1 Number of Ancestors (NOA)
        - 2.1.2 Number of Hierarchies (NOH)
        - 2.1.3 Maximum Depth of Inheritance (MDIT)
    - 2.2 Encapsulation
        - 2.2.1 Data Access Ratio (DAR)
    - 2.3 Composition
    - 2.3.1 Number of aggregation relationships (NAR)

2.3.2 Number of aggregation hierarchies (NAH)
2.4 Inheritance
2.4.1 Functional Abstraction (FA)
2.5 Polymorphism
2.5.1 Number of Polymorphic Methods (NOP)
3. Understandability
3.1 Encapsulation
3.1.1 Data Access Ratio (DAR)
3.2 Cohesion
3.2.1 Cohesion Among Methods of Class (CAM)
3.3 Inheritance
3.3.1 Functional Abstraction (FA)
3.4 Polymorphism
3.4.1 Number of Polymorphic Methods (NOP)
4. Reusability
4.1 Design Size
4.1.1 Number of Classes (NOC)
4.2 Coupling
4.2.1 Direct Class Coupling (DCC)
4.3 Cohesion
4.3.1 Cohesion Among Methods of Class (CAM)
4.4 Messaging
4.4.1 Class Interface Size (CIS)
5. Maintainability
5.1 Design Size
5.1.1 Number of Classes (NOC)
5.2 Hierarchies
5.2.1 Number of Hierarchies (NOH)
5.3 Abstraction
5.3.1 Number of Ancestors (NOA)
5.4 Encapsulation
5.4.1 Data Access Ratio (DAR)
5.5 Coupling
5.5.1 Direct Class Coupling (DCC)
5.5.2 Number of Methods (NOM)
5.6 Composition
5.6.1 Number of aggregation relationships (NAR)
5.3.2 Number of aggregation hierarchies (NAH)
5.7 Polymorphism
5.7.1 Number of Polymorphic Methods (NOP)
5.8 Documentation
5.8.1 Extent of Documentation (EOD)

Figure 2.1 Hierarchical design quality assessment model

software. Literature survey reveals that there are various aspects of software, including understandability factor that either directly or indirectly influence testability of software [19], [20].

Therefore, out of the five factors of the hierarchical model [4] I have focused on the understandability aspect in this work. Understandability is further decomposed into four sub factors namely: encapsulation, cohesion, inheritance and polymorphism. However, I have measured only three sub-factors in this work and they are: encapsulation, cohesion and polymorphism.

For each attribute Ai we can associate a variable Xi which can take a real value by means of the elementary criterion function. The final result represents a mapping of the function value into the elementary quality preference, EQi. The value of EQi is a real value that 'fortunately' belongs to the unit interval. As stated by Dujmovic et al. in [2]:
“the elementary preference is interpreted as a continuous logic variable. The value 0 denotes that Xi does not satisfy the requirements and the value 1 denotes a perfect satisfaction of requirements. The values between 0 and 1 denote a partial satisfaction of requirements. Consequently, all preferences are frequently interpreted as a percentage of satisfied requirements, and defined in the range [0, 100%]”.

Further, the preference can be categorized in three rating levels namely: satisfactory (from 60 to 100%), marginal (from 40 to 60%), and unsatisfactory (from 0 to 40%). For instance, a marginal score for an attribute could indicate that a correction action to improve the attribute quality should be taken into account by the manager or developer. Figure 3.1, shows two elementary criteria for attributes of understandability. There are two major categories to classify elementary criteria, that is, absolute and relative criteria. Moreover, regarding the absolute elementary criteria, these are further decomposed in continuous and discrete variables.

The preference scale for the Data Access Ratio (DAR) metric is a multi-level discrete absolute criterion defined as a subset, where 0 implies ratio is less then 5%; 80% or more implies satisfactory (100%) ratio.

The resulting value of this discrete multivariable absolute criterion could be between 0 (completely unsatisfactory) and Xmax (completely satisfactory). If the measured value of X is above Xmax, the corresponding elementary preference X will be equal to Xmax. Similar criteria were followed for other metrics as well.

3.2 COMPUTING PARTIAL PREFERENCE FOR MAINTAINABILITY: In this process, the evaluators should define and prepare the evaluation process to obtain a quality indicator for each competitive system. Applying a stepwise aggregation mechanism, the elementary quality preferences can be accordingly structured to allow the computing of partial preferences. Thereby global preferences can be obtained through repeating the aggregation process at the end. The global quality preference represents the global degree of satisfaction of all involved requirements. Here I am computing partial preferences for understandability. In this study, we use a logical scoring of preferences model called LSP model. A broad treatment of LSP relationships and continuous Logic Preference (CLP) operators could be found in [2, 21], as well as the mathematical background.

The strength of LSP resides in the power to model different logical relationships to reflect the stakeholders' needs, namely:

- Simultaneity, when is perceived that two or more input preferences must be present simultaneously
- Replaceability, when is perceived that two or more attributes can be replaced (there exist alternatives, i.e., a low quality of an input preference can always be compensated by a high quality of some other input).
- Neutrality, when is perceived that two or more input preferences can be grouped independently (neither conjunctive nor disjunctive relationship)
- Symmetric relationships, when is perceived that two or more input preferences affect evaluation in the same logical way (tough may be with different weights)
- Asymmetric relationships, when mandatory attributes are combined with desirable or optional ones; and when sufficient attributes are combined with desirable or optional ones.

Figure 3.2, depicts the aggregation structure for understandability characteristic. The stepwise aggregation process follows the hierarchical structure of the hierarchical model from bottom to top. The major CLP operators are the arithmetic means (A) that models the neutrality relationship; the pure conjunction (C), and quasi-conjunction operators that model the simultaneity one; and the pure disjunction(D), and quasi-disjunction operators that model the replaceability one. With regard to levels of simultaneity, we may utilize the week (C-), medium (CA), and strong (C+) quasi-conjunction functions. In this sense, operators of quasi-conjunction are flexible and logic connectives. Also, we can tune these operators to intermediate values. For instance, C-- is positioned between A and C- operators; and C-+ is between CA and C operators, and so on. The above operators (except A) mean that, given a low quality of an input preference can never be well compensated by a high quality of some other input to output a high quality preference. For example at the end of the aggregation process we have the sub-characteristic coded 3.1 (called Encapsulation in the hierarchical Model, with a relative importance or weight of 0.3), and 3.2 sub- characteristic (Cohesion, 0.4 weighted), and 3.4 sub-characteristic (polymorphism, 0.3 weighted).

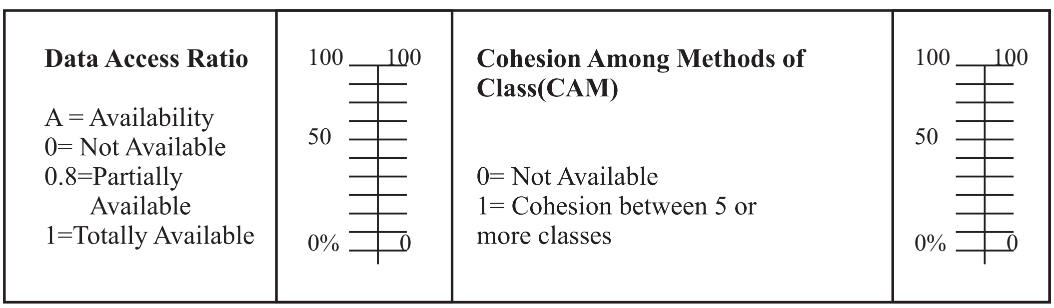

Figure 3.1 sample elementary criteria defined as preference scales taken from the hierarchical

All these sub-characteristic preferences are input to the C-+ logical function, which produce the partial global preference coded as 3, (called Understandability).

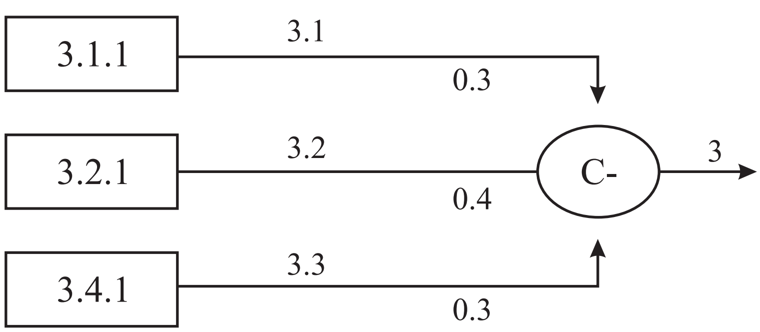

Figure 3.2 Structure of Partial Logic Aggregation for Understandability Factor

Similarly, we can also utilize the quasi-disjunction operators in a range of strong (D+), medium (DA), and week (D-) or polarization, and also their intermediate values. For instance, D-- is positioned between A and D- operators; and D-+ is between DA and D- operators; and D+- is between D+ and DA operators; and finally, D++ is between D+ and D operators. D operator represents the pure disjunction.

4. ASSESSING UNDERSTANDABILITY OF THE DESIGN SELECTED

Figure 4.1 shows the design of human resource management information system, which is developed to take care of the important function of the Human Resource Development. The system keeps record of the employees both regular and ad-hoc along with their qualification details, the designation at the time of joining the organization, the present designation and number of promotions any employee has been given since he joined the organization. It keeps the detailed record of employee family members, medical facilities along with his telephone number, job responsibilities of each and every employee and the reporting officer/person of each employee is also maintained and several other information as shown in Fig 4.1.
In the evaluation process, I decided the elementary criterion for each metric, as shown in fig 3.1. I then confronted partial preferences as shown the section 3.2 and fig 3.2.

The partial outcomes for each subfactor and the total outcome for understandability is shown in Table 1

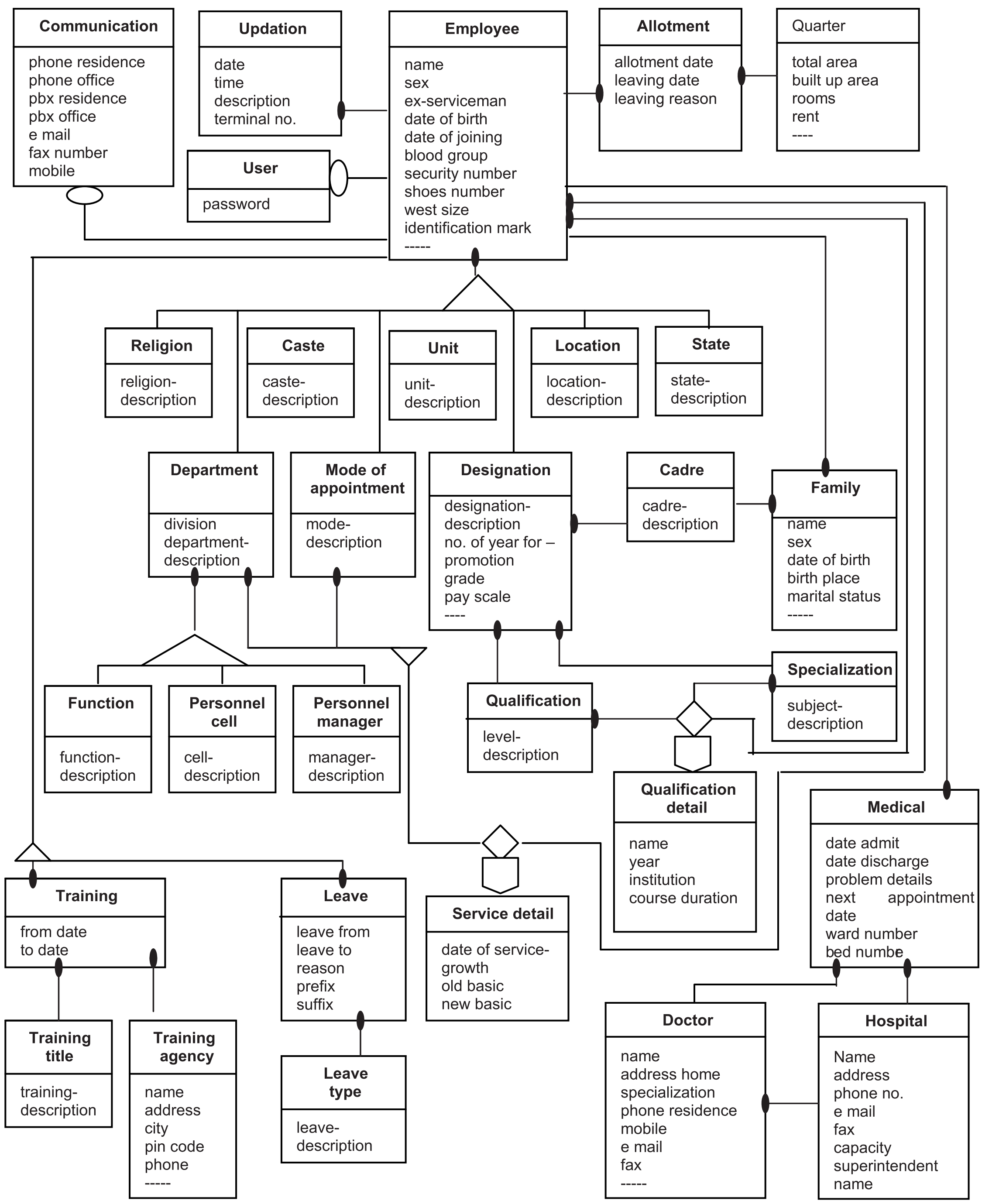

Figure 4.1 Class Diagram for Human Resource Information System

This shows that the design of the human resource information system is falling into a satisfactory level because it has 85.79% of the quality preference.

Table 1 Detailed result of partial quality preferences after computing the aggregated criteria function of the design

Characteristics and Sub-characteristics	Values
3. Understandability	
3.1 Encapsulation	
3.1.1 Data Access Ratio (DAR)	.8
3.2 Cohesion	
3.2.1 Cohesion Among Methods of Class (CAM)	.8
3.4 Polymorphism	
3.4.1 Number of Polymorphic Methods (NOP)	1
Partial Quality Preference	**85.79**

5. CONCLUSION

In this work we have proposed a methodology, for the quantitative evaluation of software's understandability in the design phase. The core evaluation model and procedures are grounded in the LSP model and continuous preference logic. The attributes and metrics of understandability are measured from the hierarchical model proposed by Kumar and Gandhi [3]. The weights assigned for preferences are arbitrary and can be changed according to the requirement. I have found that the understandability of design [3] came out to be 85.79 which means that the system will be easy to understand.

The method is suitable for comparing alternative designs of a system for understandability aspect. This will help choose a design that is most suited for understanding especially when the software has been deployed.

REFERENCES

1. C. Valdaliso, O. Eljabiri, F.P. Deek, Factors Influencing Design Quality and Assurance in Software Development: An EmpiricalStudy, Electronic Proceedings of the First International Workshop on Model-based Requirements Engineering (MBRE 01), San Diego, California, 2001, p.78-82.

2. J.J. Dujmovic, A Method for Evaluation and Selection of Complex Hardware and Software Systems, The 22nd International Conference for the Resource Management and Performance Evaluation of Enterprise CS. CMG 96 Proceedings, 1996, Vol. 1, p.368-378.

3. M.Kumar and S.K. Gandhi, Object-Oriented Modeling Design Approach to General Human Resource System, Journal of MACT, 2003-04, Vol.2, p. 34,35.

4. M.Kumar and D. Soni, Observations on Object-Oriented Design Assessment and Evolving New Model, Proc of The National Conference on Software Engineering, 2007, p. 161-164.

5. J.A. McCall, P.K. Richards, and G.F. Walters, “Factors in Software Quality”, National Tech. Information Service, Springfield, Va., vols. 1,2, and 3, AD/A-049-014/015/055, 1977.

6. B.W. Boehm, Characteristics of Software Quality, TRW Inc. 1978.

7. Software Product Evaluation - Quality Characteristics and Guidelines for Their Use, ISO/IEC Standard ISO-9126, http://www.cse.dcu.ie/essiscope/sm2/9126ref.html, 1991.

8. H.M. Olague, L.H. Etzkorn, S.L. Messimer, and H.S. Delugach, An Empirical Validation of Object- Oriented Class Complexity Metrics and their Ability to Predict Error-prone Classes in Highly Iterative, or Agile Software: a Case Study, Journal of Software Maintenance, , 2008, vol. 20, no. 3, p. 171 - 197.

9. S.R. Chidamber and C.F. Kemerer, Towards a Metric Suit for Object-Oriented Design, Proc of Sixth Object-Oriented Programming Systems, languages and Applications, 1991, pp. 197-211.

10. S.R. Chidamber and C.F. Kemerer, A Metrics Suite For Object-Oriented Design, IEEE Trans. Software Eng., June 1994, vol. 20, no. 6, p. 476-493.

11. Basili V., Briand L. and Melo W.: A Validation of Object-Oriented Design Metrics as Quality Indicators, IEEE Transactions of Software Engineering, 1996, vol. 22, no. 10, p. 751-761.

12. M.O. Elish and K.O. Elish, Application of TreeNet in Predicting Object-Oriented Softwar Maintainability: a

Comparative Study, Proc. of European Conference on Software Maintenance and Reengineering (CSMR'09), 24 - 27 Mar, 2009, p. 69 - 78.

13. G.R. Dormey, A Model for Software Product Quality, IEEE Trans. Software Eng., Feb. 1995, vol. 21, no. 2, p. 146-162.

14. G.R. Dormey, “Cornering the Chimera”, IEEE software, 1996, vol. 13, no. 1, p. 33-43

15. J. Bansiya and C.G. Davis, A Hierarchical Model for Object-Oriented Design Quality Assessment, IEEE Transactions on Software Engineering, 2002, Vol. 28, no. 1, p. 4-17.

16. R.K.Keller and A. Cockburn, “Object-Oriented Design Quality”, OOPSLA, workshop#12, Atlanta, Georgia, 1997, p. 63-67.

17. P. Antonellis, D. Antoniou, Y. Kanellopoulos, C. Makris, E. Theodoridis, C. Tjortjis, and N. Tsirakis, A Data Mining Methodology for Evaluating Maintainability According to ISO/IEC-9126 Software Engineering Product Quality Standard, Proc. 11th IEEE Conference on Software Maintenance and Reengineering (CSMR2007), 21 – 23 Mar. 2007, p. 35-42

18. N.E. Fenton, S.L. Pfleeger, “Software Metrics: a Rigorous and Practical Approach”, 2nd Edition, PWS Publishing Company, 1997.

19. J. Gao, S. Ming-Chih, A Component Testability Model for Verification and Measurement”, In Proceedings of the 29th Annual International Computer Software and Applications Conference, IEEE Computer Society, 2005, p. 211–218.

20. G. Jimenez, S. Taj, and J. Weaver, Design for Testability, in the Proceedings of the 9th Annual NCIIA Conference, 2005.

21. Luis Olsina Santos, Web-site Quality Evaluation Method: a case Study on Museums, ICSE 99 – 2nd Workshop on Software Engineering over the Internet, 1999.

ANALYTICAL STUDY OF AUTO RUN WORM KILLER: A STRATEGIC APPROACH

Aradhana Goutam *, Dr. Raj Kamal, Dr. (Mrs.) Maya Ingle
Fr. Conceicao Rodrigues College of Engineering, Mumbai 400050, Mahtraahara, India
aradhana.pande@gmail.com, Ph. No. 9004239967

ABSTRACT

The focus of the current paper lies on the AutoRun Worm killer. This is a buzz word in present era of Information technology and its related areas. The failures of the system and the hard drives destruction have led us to study the buzzword in the detail and atleast make a approach to protect the valuable data and information lying in our systems and laptops.

This specific area become more important for research due to the underlying fact that the files lying in the registry in our systems never gets manipulated due to the antivirus software. The above statement holds true for the fact because of collection of the files being stored in the registries and on manipulation of the same the system may crash. The presence of AutoRun worms in the registry files may crash the system. The registry files contain several useful information and data. The safety of registry files is of utmost concern for the seamless working of the system.

Keywords: *System, Security & Information technology*

1. INTRODUCTION

The concern and care for the registry files also lies in the fact to differ the effect of the virus and the worm. The differentiation between the virus and the worm is extremely important to study and analyze the effect of the both on the working of the system and the performance of the system. The virus (Vital Information Resources Under Seize) tries to attach itself to the programs (already existing) lying in the system.

The registry files mainly comprise of the core components of the system installed programs. (This essentially includes the address , validity of the programs etc). The AutoRun worm tries to attach itself to the registry files and hamper the performance of the system. The AutoRun Worm has a unique property of creating the multiple copies of itself. The copies getting multiplied in number put effect on the registries and this significantly reduces the operational efficiency of the system. The protective shield of the antivirus software may be hampered due to this. The antivirus software is extremely important for the system , as it protects the system from unauthorized access.

2. DEFINING TERMS

Vital Information Resources Under Seize (Virus) & its effects

Vital Information Resources Under Seize (Virus) can be termed as the dangerous and hazardous codes in the information technology area. The Virus have the ability to hide itself in the executable files or the booting sectors of our systems. The Virus may lead to the corruption of the files, if they attach to the files. This leads to the system failure or crash. This can be termed as the one of the most important and the frequent problems of the information technology era.

A computer virus can be termed as a program which have an ability to make a copy of itself. This affects the system performance and efficiency. We generally refer to other malware , spyware and adware as the virus , which is a wrong notation in itself. This is wrong because of the fact that these programs do not multiply on their own and cannot have the multiple copies of their own.

A virus can be transferred from the one system or laptop to the other very easily. This movement can be over the mediums like CDs, DVDs, floppy drives etc. These are the most common mediums of spreading of the virus from one system to the other. (This is most common in case of the college going students and the working professional having lot of the exchange and the interchange of the data and the information). The virus can also be spread on account of the transfer of its host to the other computer. The probability of the spread of the virus from one system to other is increased highly by the infecting files on the network and the files being accessed by the various systems in the network in the organization. This poses a threat to the organizational IT security and the specialists have a great concern for the same.

3. WORM AND ITS EFFECTS

The unique characteristic of the worm is that it makes the use of the network to transfer the multiple copies of itself. The multiple copies are transferred to the various nodes and this transfer cannot be realized easily , as this requires no user intervention. This is a spontaneous action and it is very fast in the nature.

The worm can also be termed as the computer program which as the property of replication on its own. The worm is different from the virus in the property that worm need not attach itself to the existing program. Worms pose serious threat to the organizational IT network and pose a risk on the security. Mostly the effect of the virus can be that the files may get corrupted or destroyed. The files can also get modified on the targeted system having the virus effect. The root directories and the registry files are also affected by the worm. The anti-virus present in the system never changes the data present in the registries and the root directories. This is because of the fact that these contains the lot of the data and information.

4. STUDYING THE AUTORUN WORM AND THEIR EFFECTS

Lot of research and development has been done in the present concerned area which has led to generation of lot of information. However more research needs to be in done on the same. The researchers and the scientists working for the various IT organizations has tried to study the effect of the AutoRun worms. The scientists working for MS tried to make a feature termed as AutoRun In windows 95. The higher version of the same contains a code which is stored in the root directory of the medium, which is having a extension file under name ".inf".

The structure of the INF files comprises of the different sections which specify the various files thos e are to be copied and the various changes in the registry files. The structure of INF file closely resembles to the structure of the INI file. The INF files have a particular structure that all the INF files essentially have a section termed as version section , which has a Signature value specifying the version of the windows that corresponds to the INF file. The other sections are mostly user defined in nature. The sections specifically contain the information of the component to be installed. The signature for windows 9X may be $CHICAGO $ (in common) and the signature for the Windows NT/2K/ XP may be $WINDOWS NTS in general.

The automatic access of the external hard drives may be allowed automatically. The latest version of the windows essentially possess the feature termed as Autoplay. This feature is being possessed by the versions like Windows XP and onwards. The feature Autoplay has been introduced to make the use of the peripheral devices simpler and easier than ever before. This is made simpler on account of the automatic start of the software needed to access and as result the devices contents can be viewed. The feature of autoplay can be enhanced by the usage of the compatible software and hardware.

The specific feature can be configured by the user so that the favorite applications may be associated with the autoplay events and the actions. The feature has been extensively used by the hackers by creating a code being termed as the AutoRun worms. The main and important aspect of the AutoRun worms is that they are executed automatically whiles the insertion and attachment of the hard drives. The automatic execution of the files malicious in nature is prevented on account tof the fact that they are executed automatically and spontaneously.

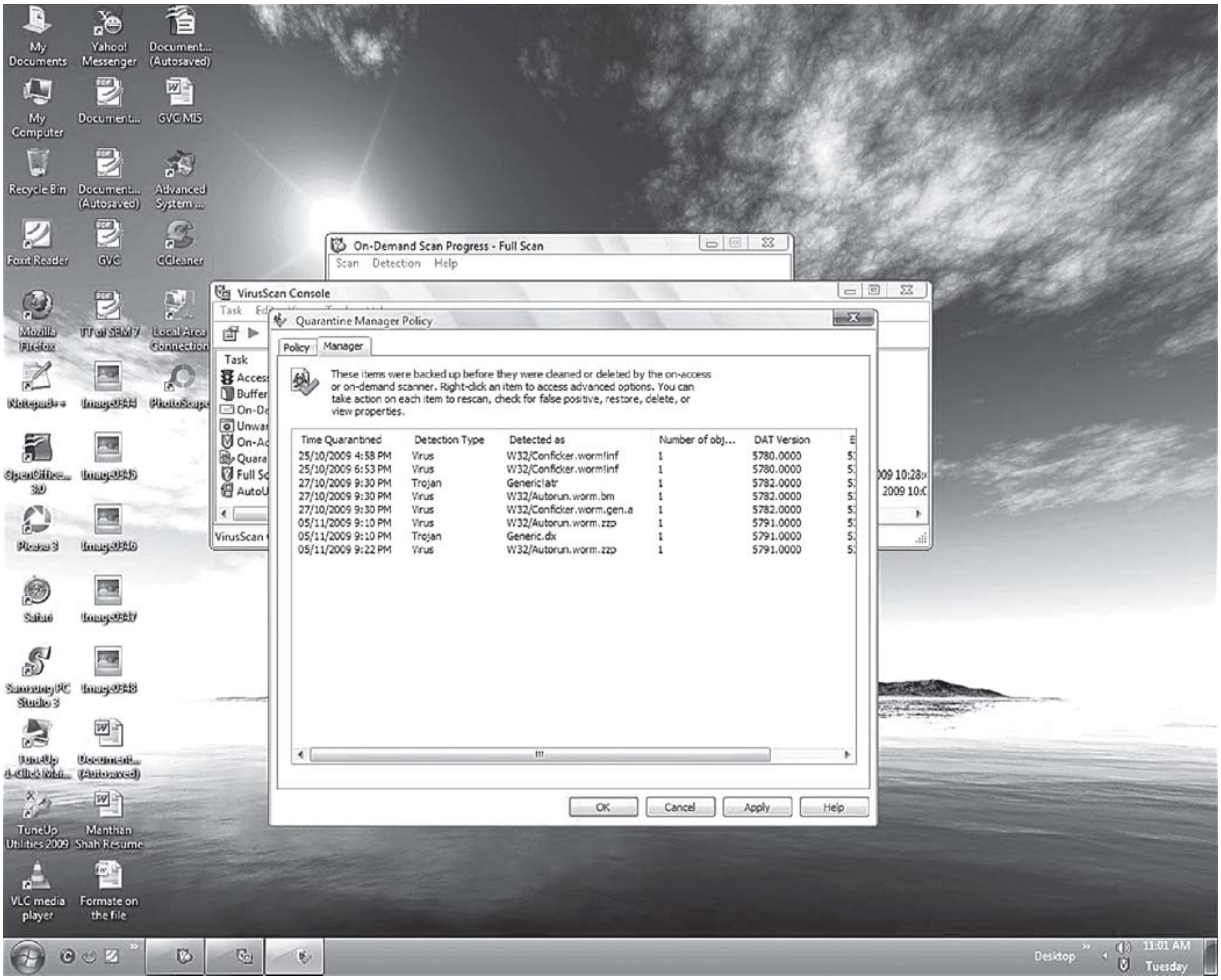

5. ANALYSIS OF AUTORUN WORMS

The AutoRun worms are the codes which possess the self replication property. The numerous copies of the codes are created. These numerous copies cause heavy load on the system registry files. This affects the system performance and reduces the system operational efficiency significantly. The registry file is one of the important components of the system and the registry files are mostly affected by the AutoRun worms.

Paged pool memory lies in the virtual memory. The registry size have been limited to the 25 %o f the paged pool memory. This is a general approximation. Since the paged pool memory has generally its size as of 32 MB so using the same equation the registry size comes approximately to the 8MB. The minimum size of the registry files can be 4 MB. The maximum extent in size to which the registry file can go is up to the 80 % of the size of the paged pool memory. In such a scenario the registry files cannot use the space reserved for the processes. The registry files are very important component in the system and are referred very frequently.

Most of the versions of the windows like MS Windows 98, Windows CE , Windows NT and windows 2000 uses windows registry in the central hierarchical database. The information contained in the registry is frequently referred by windows during the operations.

These worms multiply on their own and create numerous copies of themselves , thereby increasing the load significantly and finally resulting in the low operational performance of the system. The anti-virus software never eliminates the AutoRun Worms. The probability still lies that the worm may have mobility and move to attack the registry files unknown to the user.

These defects have to be removed from the system so as to increase the operational efficiency of the system. The AutoRun worm killer may kill and destroy the worms even before the entry of the worms in the system. The main objective of the project lies in implementing the automated process using a command prompt or C++.The command prompt (which is .cmd) is actually a command line interpreter on OS /2 , Windows CE.

Fig. 2 Flow Chart

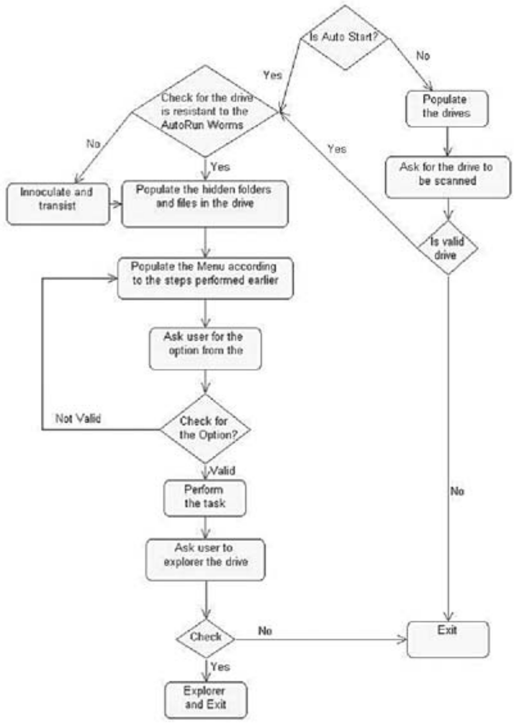

6. RESULT

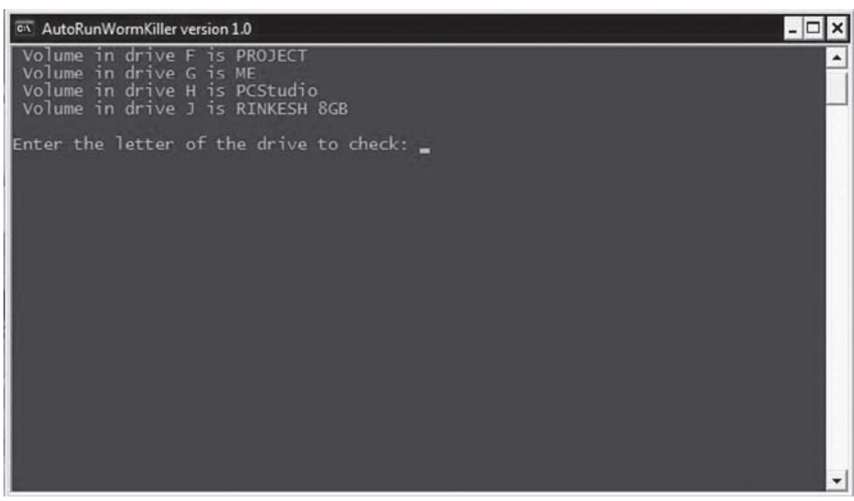

MANUAL START

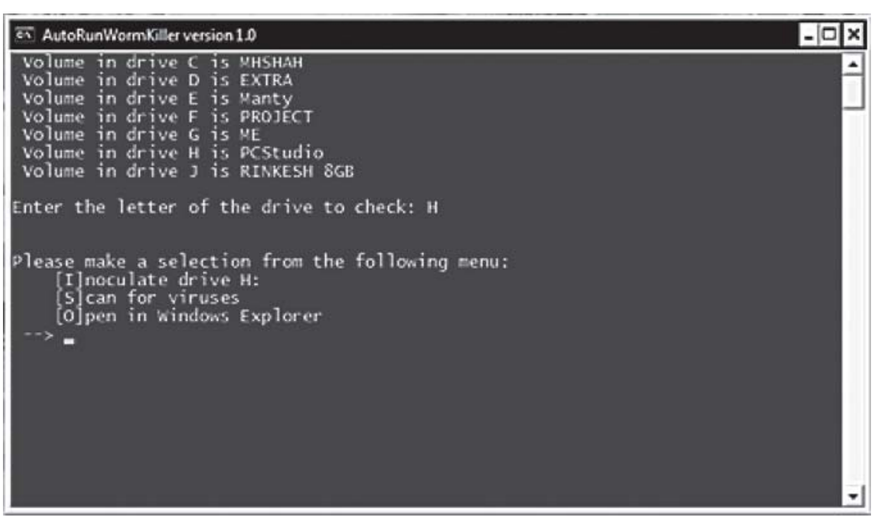

INNOCULATION OPTION

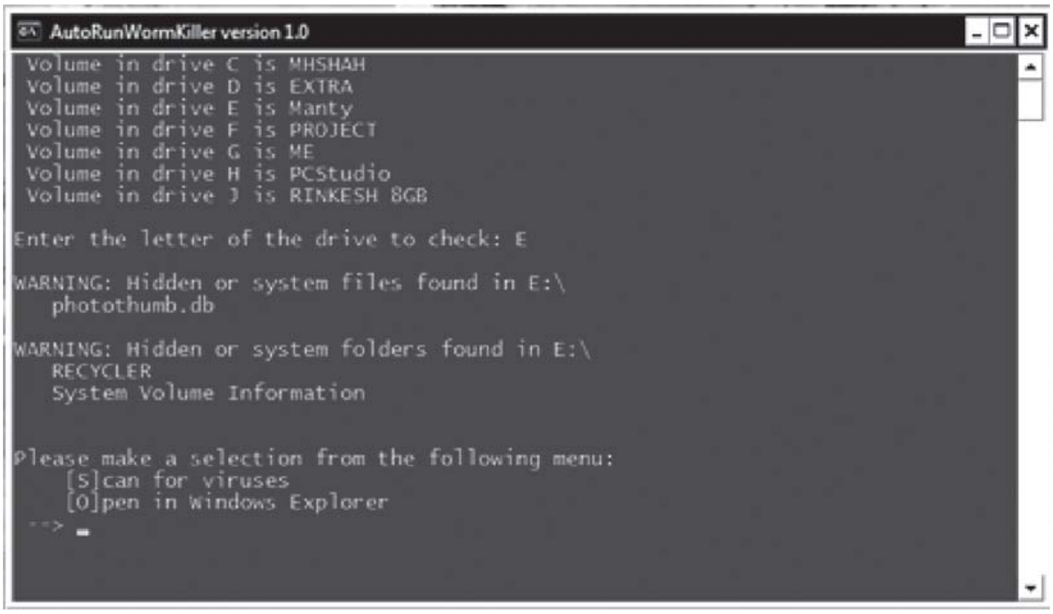

HIDDEN FILES AND FOLDERS DETECTION

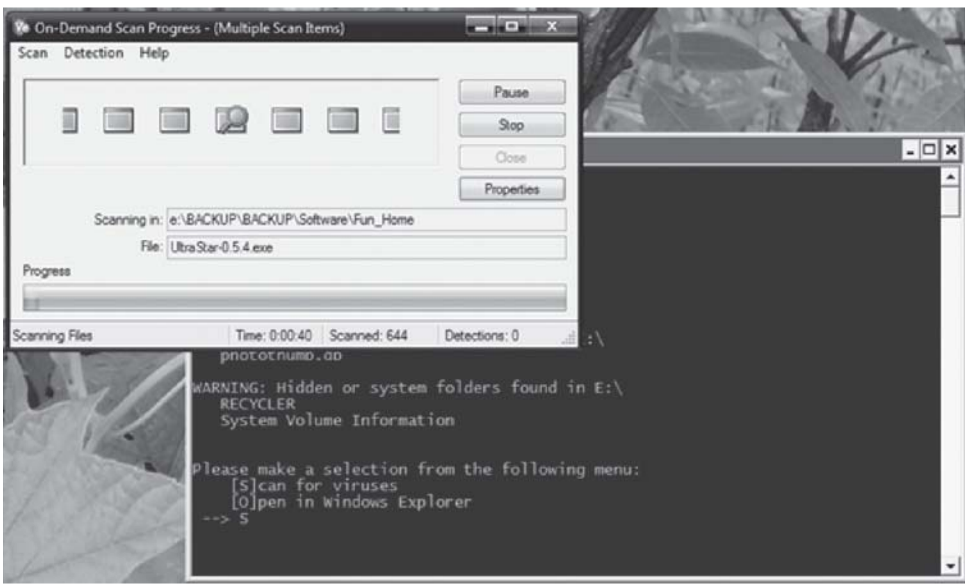

SCANNING WITH MANUALY OVER – RIDED SYSTEM ANTI – VIRUS

AUTO START

7. SCOPE OF FUTURE WORK

The scope for the future may be the detailed and functional study of the AutoRun Worms. This may lead to the software being more effective and user friendly which not only eliminates the worms present in the external drives but also destroys the existing worms present in the registries and internal hard drive.

8. CONCLUSION

The project execution goes successful by removal of the AutoRun worms. The software termed as AutoRun Worm killer is stable and hence can be patched with the antivirus installed in the system to make it more effective. This will increase the performance of the system and the operational efficiency of the system gets a boost.

REFERENCES

1. Computer Virus –Wikipedia http://en.wikipedia.org/wiki/Computer_virus, "Nov 2010"

2. WikiAnswers – What is paged pool memory?http://wiki.answers.com/Q/What_is_paged_pool_memory, "Nov 2010"

3. INF file –Wikipedia http://en.wikipedia.org/wiki/.inf, "Feb 2011"

4. Windows registry information for advanced users – Microsoft http://support.microsoft.com/kb/256986, "march 2011"

5. Command Prompt –Wikipedia http://en.wikipedia.org/wiki/Command_Prompt, "Feb 2011"

6. Nicholas Weaver and Vern Paxson and Stuart Staniford and Robert Cunningham," A Taxonomy of Computer Worms" , WORM '03 Proceedings of the 2003 ACM workshop on Rapid malcode, New York, NY, USA ©2003

7. Gupta, A.; DuVarney, D.C.; "Using Predators to Combat Worms and Viruses:", : Computer Security Applications Conference, 2004. 20th Annual, 6-10 Dec. 2004, page(s): 116 – 125, ISSN: 1063-9527

8. Cliff C. Zou, Don Towsley, Weibo Gong, "On the Performance of Internet Worm Strategies (2003) Elsevier Journal of Performance Evaluation" Journal Performance Evaluation archive, Volume 63 Issue 7, July 2006

9. An Environment for Controlled Worm Replication and Analysis (2000) by Or Internet-Inna-Box Ian , Ian Whalley, http://www.research.ibm.com/antivirus/SciPapers/VB2000INW.pdf

MODELS OF EMPLOYEE ENGAGEMENT-AN ELUCIDATION

G. Swetha
Assistant Professor, S.V.College of Engineering, Tirupati
Swetha_reddi84@yahoo.com

Dr. D. Pradeep Kumar
Professor & Head, Department of Management Studies, Madanapalle Institute of Technology & Science, Madanapalle
pradeep4a2@yahoo.co.in,

ABSTRACT

Employee engagement has emerged as a critical driver of business success in today's competitive marketplace. The models of Employee Engagement illustrate the factors that can affect engagement and how engagement impacts on the wider performance of the organisation. It is clear that there is no 'one-size fits all' model of engagement. However, what can be concluded is that the primary driving force behind engagement is the organisation, its view of engagement and how it acts to create an environment conducive to engaging employees. Important areas in which the organisation can work to improve engagement include training and career development, effective management, promoting a clear strategic vision, communication, fair treatment, pay and benefits, job satisfaction, cooperation and trust. These factors vary between those that tend to be taken as given, and written explicitly into the contract of employment (i.e. pay and benefits) and those that are organisational-dependent, cannot be taken for granted and require the organisation to take an initiative (i.e. ensuring two-way communication, promoting a strategic vision and building trust).

Secondary to this are some variations in individual employees, with different groups or individuals responding differently to the environment in which they work. This paper presents the periodic growth in the development of various employee Engagement models and interprets them for a more pragmatic implementation.

Keywords: *Burnout; Commitment; Engagement; Job Demands; Job resources.*

1. INTRODUCTION TO EMPLOYEE ENGAGEMENT

Employee engagement has emerged as a critical driver of business success in today's competitive marketplace. Further, employee engagement can be a deciding factor in organizational success. Not only does engagement have the potential to significantly affect employee retention, productivity and loyalty, it is also a key link to customer satisfaction, company reputation and overall stakeholder value. Thus, to gain a competitive edge, organizations are turning to HR to set the agenda for employee engagement and commitment. Employee engagement is defined as "the extent to which employees commit to something or someone in their organization, how hard they work and how long they stay as a result of that commitment."1 In fact, employees with the highest levels of commitment perform 20% better and are 87% less likely to leave the organization, which indicates that engagement is linked to organizational performance.2

2. IMPORTANCE OF EMPLOYEE ENGAGEMENT MODELS

This article throws light on the models of engagement. It was highlighted that from an employer's point of view, engagement is often about employees 'going the extra mile' or exerting 'discretionary effort'. It was also found that many of the factors that drive engagement are under the control of the organization. However, employees will place different emphasis on the extent to which they value each of these factors in exchange for their discretionary effort. This topic therefore examines the models of engagement in to determine what the key drivers of engagement are, and the extent to which employees value these, and what employees find connects them to the organisation, motivates them to perform above and beyond expectations and compels them to actively promote the interests and objectives of the organisation.

Although the organisation has primary responsibility for leading engagement, there are also secondary employee and job specific factors which can affect levels of engagement. The article provides a more comprehensive picture of the factors that determine engagement. The findings are presented under the following headings:

Modelling Employee Engagement – A series of the most relevant interpretative engagement models are presented.

Role of Employee Engagement in Organisational Outcomes – This section illustrates the mechanisms through which engagement can impact on organisational outcomes.

Employee Variations – An analysis of the extent to which engagement varies between employees.

2.1 MODELLING EMPLOYEE ENGAGEMENT As highlighted by CIPD (2007a), there is no definitive all-purpose list of engagement drivers. There are many individual and organizational factors that determine whether employees become engaged, and to what extent they become engaged. This section highlights the models that illustrate these factors and the importance that employees place on them in becoming engaged.

a) Gallup Model of Engagement Following the Gallup tradition, Harter, Schmidt and Keyes(2003)4 propose a model of engagement that is strongly influenced by Maslow's (1970)5 hierarchy of needs. In the model basic needs at work must be fulfilled before higher needs can be considered and this has implications regarding the antecedents of engagement. Starting at the bottom of the hierarchy (see Figure 1), basic needs involve clarity of expectations and the provision of basic materials (e.g., functioning PCs, faxes etc.) Moving beyond this, employees need to feel that they are contributing to the organisation, that they have opportunities to use their talents, and that they are receiving recognition and feedback for the work they do (Harter et al., 2003). In essence, this is akin to the notion of person environment fit, whereby the employee is matched to their organisation.

At the next level, employees need to feel a sense of belonging. This involves participative decision-making and having meaningful relationships with co-workers and supervisors. Such resources reinforce communication and creativity (Harter et al., 2003). The peak of this hierarchy – in line with Maslow's (1970) notion of self-actualisation – is self-development. For this to occur, employees need to be allowed to discuss their progress and to be given the opportunity to learn new skills and develop existing ones. When these factors come together, Harter et al. (2003) argue, they create the type of environment in which employees become engaged and, therefore, more productive.

Figure 1: Gallup Model of Engagement (Based on Maslow's [1970] Hierarchy of Needs.

b) A two-dimensional view of subjective well-being (Russell, 2003; see also Bakker Oerlemans, in press). A two-dimensional (2-D) model of affective experience as mapped by the circumplex model (e.g., Lang, Bradley, & Cuthbert6, 1998; Larsen & Diener7, 1992; Thayer8, 1989). Using the circumplex model of emotions, Bakker and Oerlemans9 (in press) positioned work engagement in the upper right quadrant of the circumplex model as it resemblances high levels of pleasure and activation (see also Parker & Griffin10, 2011). Burnout can be positioned in the lower left quadrant as it resemblances low levels of pleasure and activation. Whereas burned-out individuals are exhausted and cynical about work, engaged employees are full with energy and enthusiasm. The implication of this analysis is that, in order to facilitate work engagement and to prevent burnout, employers should work to create an organizational context where employees feel enthusiastic, energized, and motivated because their jobs are both "active" and "pleasurable".

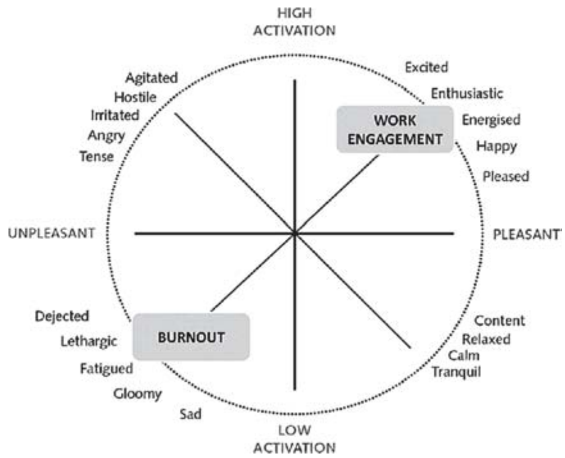

Figure 2: A two-dimensional view of subjective well-being (Russell, 2003; see also Bakker & Oerlemans, in press).

c) Robinson et al11 (2004) model of the drivers of employee engagement Although tested within the NHS, the authors suggest that many of the drivers of engagement will be common to all organisations, regardless of sector. engagement levels can vary according to demographic and job related factors. What is noted from the model above is that some of these factors are what would be fundamental or contractual requirements for the organisation (the 'hygiene' factors), such as pay and benefits and health and safety, whereas others are the areas where the organisation must 'go the extra mile' to ensure effective communication, management and cooperation.

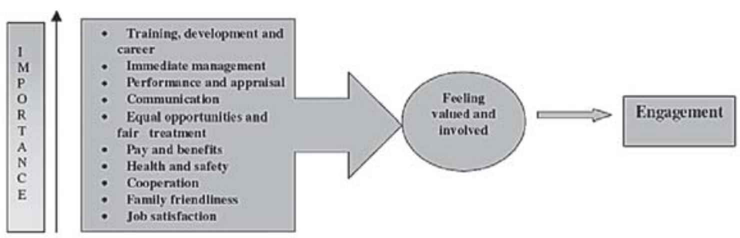

Figure 3: Robinson et al (2004) model of the drivers of employee engagement

d) Schmidt12 (2004) model of organisational dynamics in the public sector This model implies that the foundations of engagement lie in policies to recruit and retain the right workforce (i.e. in terms of employing specific competences, knowledge and experiences required for success as well as diversity) and to promote health, safety, and wellbeing.

Schmidt (2004) bases the model on a variety of studies and writings, implicit in which is the notion that it is WWB that drives engagement. CIPD (2007a) concurs with this view of the importance of well being, stating that engagement is 'wholly consistent' with an emphasis on employee well-being.

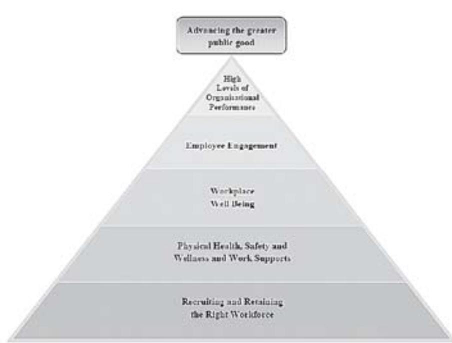

Figure 4: Schmidt (2004) model of organisational dynamics in the public sector

In Schmidt's (2004) discussion, WWB itself is driven by commitment and job satisfaction, which in turn are determined by a number of factors. It is a similar idea to the model presented by Robinson et al (2004) where 'feeling valued and involved' was the key driver of engagement, but in turn was influenced to a varying degree by a range of factors. As is the case throughout much of the literature, Schmidt (2004) does not present a definitive list of the drivers of commitment and satisfaction (as the drivers of engagement) but reviews several studies and reports. Concentrating here on the studies presented by Schmidt (2004) that appear to be based on a more robust approach (e.g. regression analysis as opposed to theorising) the following results are of interest:

Work USA (2000) - This survey used regression analysis to identify the key factors affecting employee commitment:

- Trust in senior leadership
- Chance to use skills
- Competitiveness of rewards
- Job security
- Quality of company's products and services
- Absence of workplace stress
- Honesty and integrity of company's business conduct

ERIN Research - The Region of Peel (a large municipality in Ontario, Canada) carried out an employee survey in 2002. Schmidt (2004) advocates the robustness of the results, from the Canadian public sector, due to the use of 'advanced statistical techniques' and 'excellent' return rates on the survey of 72%. The survey identified job satisfaction and commitment as the drivers for the engagement model, with the following factors found to be important to each:

Job satisfaction:

- A career path that offers opportunities for advancement;
- Fair pay and benefits;
- The perception that the municipality offers good value to customers;
- A satisfactory work environment, as defined by:
- A reasonable workload;
- Good relations with immediate supervisor;
- Smoothly functioning organisational dynamics;
- Good relationships with colleagues; and
- Effective internal communication.

Commitment:

- Job satisfaction;
- A career path that offers opportunities for advancement;
- A positive perception of senior management; and
- The perception that the municipality offers good value to customers.

The analysis of the survey found a correlation between satisfaction and commitment of 0.57 suggesting that the two concepts are related but deserve separate analysis. Further, what also emerges from these results is that satisfaction is a driver of commitment, but not vice versa, as commitment does not appear as a key factor in the analysis of what drives satisfaction.

e) RBC's new model of employee communication Moorcroft (2006)13 notes that the 'old' model was focused on developing tactics and methods by which to inform employees, or create awareness, of company news and objectives. However, the new model (see figure 5 above) is based on engaging employees in the communication process in order to achieve the desired outcomes and thus build the business value. This is achieved by helping employees have a better idea of how what they do impacts upon the organisation and by promoting behaviours that help achieve organisational objectives.

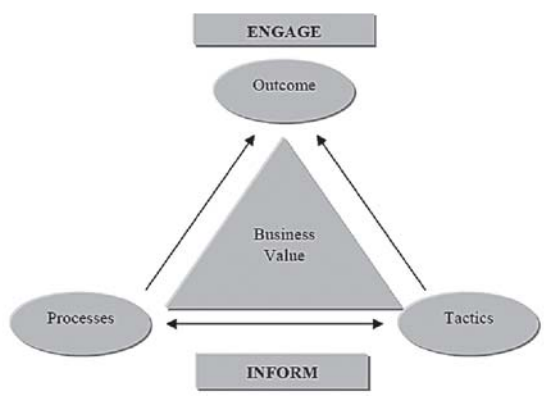

Figure 5: RBC's new model of employee communication (Source: Moorcroft (2006))

Moorcroft (2006) reports that the changes to employee communications are beginning to show solid results, with employee alignment and engagement scores improving. Interestingly, the communication budget has actually been reduced at the same time, illustrating that a more focused and thought through strategy can result in better value for money.

f) Kahn's model of engagement (2004) During two of Kahn□s14 qualitative studies (1990), he examined the psychological conditions of personal engagement and disengagement at work. Kahn interviewed employees of two different organizations about their moments of engagement and disengagement. The researcher stated that there are three psychological conditions that people experience at work, particularly, meaningfulness, safety, and availability. These psychological conditions are linked to personal engagement or disengagement. According to Kahn (ibid, p. 703), employees in each work situation unconsciously ask themselves three questions: "(1) How meaningful is it for me to bring myself into this performance? (2) How safe is it to do so? And (3) How available am I to do so?"

An empirical test of Kahn□s model (May et al. 2004)15 found that meaningfulness, safety, and availability have significant influence on engagement (Figure 6).

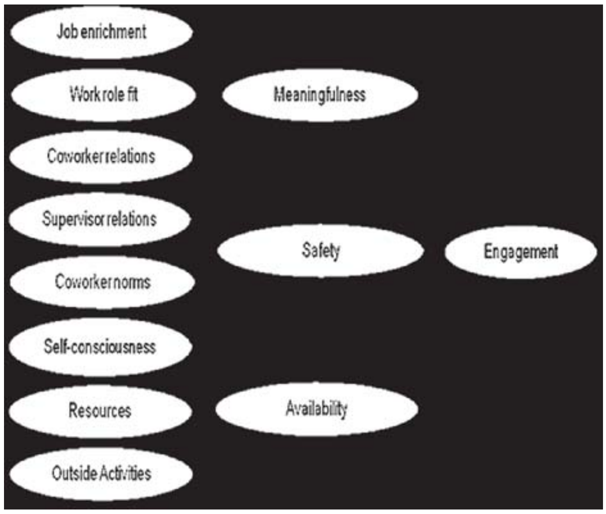

Figure 6: Path-analytic framework of engagement (adapted from May et al. 2004, p. 25)

There were also identified several important links (ibid, p. 30):

- Job enrichment, as an attempt to make work different and interesting, and also fit between the employee and his or her work role, are positive predictors of meaningfulness.
- Good relationships with workmates and supportive supervisor relationships are positive predictors of safety.
- Strict observance of co-worker norms (norms within the groups and organization) and self-consciousness are negative predictors of safety.
- Accessibility of physical, emotional and cognitive worker□s resources is a positive predictor of psychological availability.
- Participation in outside activities is a negative predictor of psychological availability.

The findings of Kahn (1990) and May et al. (2004) described engagement from the psychological point of view and identified the main factors that influence its level

2.2 THE ROLE OF ENGAGEMENT IN ORGANISATIONAL OUTCOMES This section discusses the models that illustrate the place of engagement in the wider operations of the organisation and the mechanisms through which engagement can impact on the wider context.

Heintzman and Marson (2006)16 use the private sector service-profit chain model as a basis for producing a public sector equivalent (see Fig 7). They base the model on research carried out in Canada on what the top public sector challenges are, namely;

- Human resource modernisation;
- Service improvement; and
- Improving the public's trust in public institutions.

Heintzman and Marson (2006) point out that the private sector has, for over a decade, documented the links between employee engagement and client satisfaction, and between client satisfaction and bottom line financial results. The authors note that the third element (the bottom line) cannot be transferred directly to the public sector but based on research on the link between public service outcomes and the public's rating of overall government performance, they suggest the following public service value chain:

Figure 7: Heintzman and Marson's (2006) public sector value chain(Source: Heintzman and Marson (2006)

Whilst Heintzman and Marson (2006) state that work is still underway to document the drivers of employee engagement with respect to this model they state that possible candidates (based on secondary research quoted within the paper) are:

- Support for the goals and mandate of the organisation;
- Effective leadership and management;
- Supportive colleagues and work unit;
- Tools, authority and independence to do the job;
- Career progress and development; and
- Workload.

Heintzman and Marson (2006) cite emerging Canadian evidence that supports this concept. They suggest that by understanding the drivers of engagement and the link between engagement and performance of the institution, this tool can be used across public sector management to make significant improvements in employees' work and in the overall performance and perception of the public sector.

g) The CIPD (2006c) model of employee engagement model A model produced by the CIPD (2006c)17 and presented in the organisation's Employee Attitudes and Engagement Survey' of 2006, brings various elements of employee engagement together in one overarching model (see figure 8). This then formed the basis of the survey, which was carried out across the private and public sectors.

The model, which illustrates the linkages and important factors in each of these elements, is provided below, with arrows indicating directions of influence:

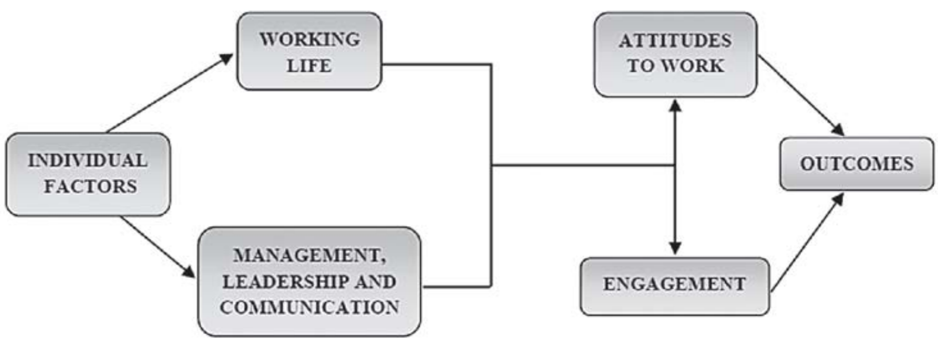

Figure 8: The CIPD (2006c) model of employee engagement model (Source: CIPD (2006c)

Individual factors are those such as gender, age, ethnicity and disability. Working life describes factors such as occupation, hours of work and pay, as well as important issues such as bullying or workplace harassment.

Management, leadership and communication refers to how employees view their managers and leaders, how much opportunity they have to participate in organizational decision making and levels of trust. As CIPD (2006c) highlights, these factors have been found in research to be very important in determining levels of engagement. This is also the area where managers can have an important influence.

An attitude to work refers to employees' perceptions of their jobs and includes levels of well-being, satisfaction, enthusiasm, commitment and loyalty. It is important to note here the two-way interaction in this model between attitudes to work and engagement. Whilst satisfaction, commitment, stress and loyalty factors feed into levels of engagement, it follows from the model that organisations that successfully engage their employees will engender greater levels of job satisfaction and loyalty.

The engagement box itself refers to the CIPD's (2006c) three types of engagement – cognitive, emotional and physical. Finally, in the model above, engagement and attitudes to work lead to outcomes for the organisation, in terms of individual performance, intent to quit and absence levels. The model was used by CIPD in their annual attitude and engagement survey, with the finding that there is in fact a lot that managers and leaders can do to drive up engagement. Levels of trust and confidence in senior management and line managers were found to be 'disappointingly low' in the survey, however CIPD (2006c) cites this as an opportunity for managers to evaluate how their own organisation compares with the national sample and to consider how best to harness the engagement levels of their own workforce.

h) The Model of the Antecedents and Consequences of Employee Engagement Saks did a study that aimed to test a model of the antecedents and consequences of job and organization engagements (Figure 9). The model was developed based on principles of Social Exchange Theory (SET)

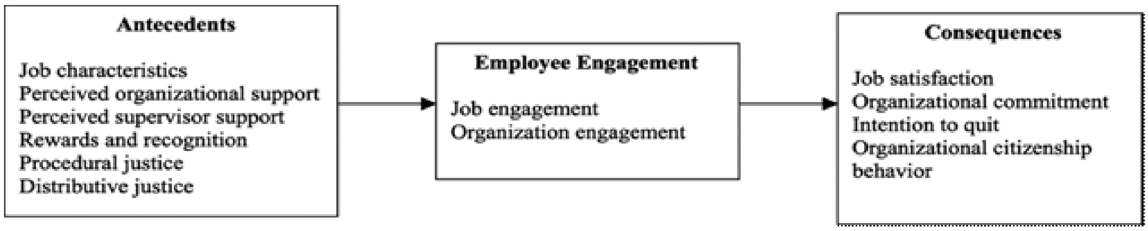

Figure 9: A model of the antecedents and consequences of employee engagement (Saks 2006, p. 604)18

Results of tests done by Saks (ibid, p. 613) showed that: There is a distinction between the constructs of job engagement and organization engagement.

- Support provided by an organization is a positive predictor of both job and organization engagement.
- Job characteristics considerably predict job engagement.
- Procedural justice is an important predictor of organization engagement.
- Job and organization engagement are significant predictors of job satisfaction, organizational commitment, intentions to quit, and organizational citizenship behaviour directed to organization.

Saks asserted that employee engagement is a meaningful construct that should be studied more. Identification of other potential predictors of the phenomenon and possible effects of experimental interventions on employee engagement were offered by the researcher as issues for further studies. (Ibid, p. 613–614)

i) Extending the Value-Profit Chain to Engagement With regard to how employee engagement is operationalized to translate into increased business performance, the concept of the "service-profit chain" (Heskett, Jones, Loveman, Sasser, Jr., & Schlesinger, 1994)19 is key. Under this model, employee satisfaction is viewed as critical to inspiring the productivity and service necessary to secure business success and drive growth and profitability. The service-profit chain begins with management practices that achieve the goal of providing employees with what they need to best serve customers of the firm. When employees receive this support, they are more likely to be satisfied and thus, exhibit loyalty to the firm as well as improved productivity. These increased levels of commitment and productivity function to increase the value proposition of a firm's services or products to customers, which itself creates customer satisfaction. Satisfied customers become loyal to the firm and, finally, the repeat business generated by these customers drives overall profitability and growth (Heskett, et al., 1994).

Recently, Carrig & Wright20 (2006:18-19) further elaborated on the model in order to better describe the process by which employees create value. Employees are seen to drive customer satisfaction by achieving operational excellence with regard to everyday tasks and innovating to capitalize on business opportunities as they become available. Carrig & Wright also recognize additional factors—employee characteristics, core capabilities, valued customer outcomes, and revenues and costs—as interacting with the inputs along what they refer to as the "value-profit chain".

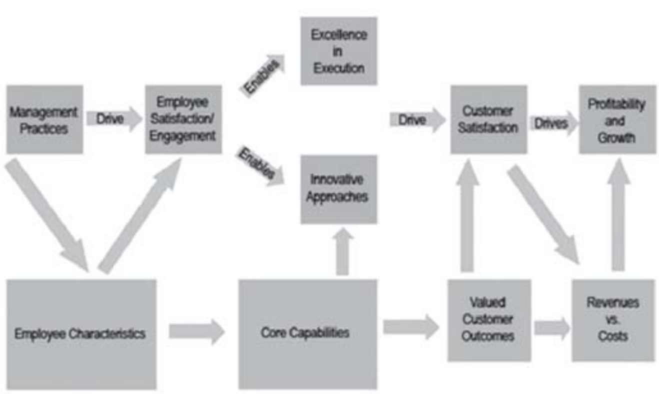

Figure 10: (Adapted from Carrig & Wright, 2006: 19.)

Extending the application of this expanded model to the concept of employee engagement, it becomes clear that engagement is but one of several interacting factors that influence firm performance—i.e., it is a necessary, but not sufficient, condition for profitability and growth. If the foundations upon which the value-profit chain rests are absent, employees, even if they are engaged, will be unable to leverage their commitment and abilities to positively affect the bottom line.

Perhaps more important, the framework laid out by Carrig & Wright takes notice of the many interactions that can potentially effect the progression from an engaged workforce to superior firm performance and highlights the possibility of multi-directional causes and effects. For instance, the authors (2006: 22) identify people (or employee) characteristics as consisting of skill and demographic mix of employees needed by the firm, the commitment workers feel to their organization, and behavioral components. These characteristics are influenced by the actions of managers and, in turn, influence the core capabilities of the firm and, in keeping with the work of Kahn (1990), employee satisfaction/engagement levels. From here, engagement comes to influence various other components of the model as its effects travel through the multiple linkages within the firm. Thus, the complex path that engagement takes before its eventual effect on profit and growth is realized begins to be borne out.

j) Digital Opinion Engagement Model(2007)21

Digital Opinion's define employee engagement as follows:

"Engaged employees enjoy their work and are proud to tell people that they work for the Company. They go the extra mile to help their customers and colleagues, and they want to stay and develop a career with the Company. In the long run they are the real contributors."

This definition forms the basis for our model, which reduces the inherent complexity to measurable proportions.

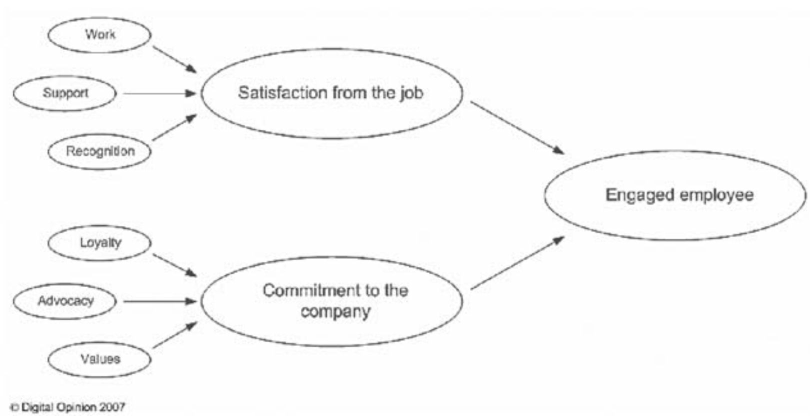

Figure 11: Engagement model

In the model, employee engagement has two dimensions: the first relates to the satisfaction that people get from the individual jobs that they do. The second relates to the commitment and loyalty they feel towards their employer.These two dimensions leads to engaged employee.

k) Penna (2007)22 model of hierarchy of engagement Penna (2007) presents a hierarchical model of engagement factors (see figure 12), which illustrates the impact each level will have on the attraction, engagement and retention of talent. They propose a model with "meaning at work" at the apex, which they maintain is borne out by the research carried out into meaning at work. In this context, Penna (2007) defines meaning at work as the situation where a job brings fulfillment for the employee, through the employee being valued, appreciated, having a sense of belonging and congruence with the organization and feel like they are making a contribution. In this model, as the hierarchy ascends and the organisation successfully meets each of these engagement factors, the organization becomes more attractive to new potential employees and becomes more engaging to its existing staff.

Figure 12: Penna (2007) model of hierarchy of engagement (Source: Penna (2007)

Interestingly in this model the 'hygiene' factors appear at the foundation of the model, indicating the nature of these factors as a necessary, but not sufficient, building block upon which the organisation must further develop in order to engage staff.

l) The JD-R Model of Work Engagement (based on Bakker & Demerouti, 2007)23. The JD-R model of work engagement is graphically depicted in Figure 13. As can be seen, job resources and personal resources independently or combined predict work engagement. Further, job and personal resources particularly have a positive impact on engagement when job demands are high. Work engagement, in turn, has a positive impact on job performance. Finally, employees who are engaged and perform well are able to create their own resources, which then foster engagement again over time.

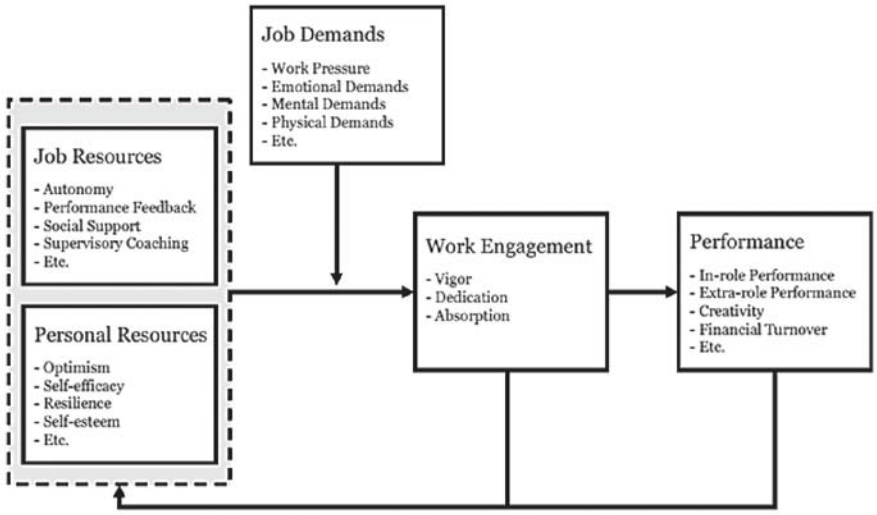

Figure 13:. The JD-R Model of Work Engagement (based on Bakker & Demerouti, 2007)

m) DDI's engagement value proposition Figure 14 shows DDI's engagement value proposition24, which includes four sequential components. Top of the model, engagement drivers are the levers that organizations can use to build a more engaging work environment. Engagement does not just materialize. Organizations must hire employees who fit the job requirements, develop leaders with the right skills, and provide support through strong systems and strategies. Together, these three drivers lead to the formation of an engaging work environment. Once created, the engaging work environment has a positive impact on employee behaviors and attitudes. In particular, an engaging environment builds loyalty in employees by meeting their personal and practical needs, thus encouraging them to stay with the organization. In addition, an engaging work environment taps into employees' motivation to try harder and put forth the extra effort that differentiates organizations from their competitors. Finally, when organizations have engaged employees, the long-term benefits appear in the bottom line. Organizations have more satisfied and loyal customers, increased profits, better-quality products or services, and greater growth potential.

Figure 14: DDI's Engagement Value Proposition

n) Right Management's Employee Engagement Model25 The four components of the model describe the emotional and behavioral aspects of engagement. When people positively evaluate their experience of the job and organization, they are more likely not only to feel satisfied, committed and proud, but also to be advocates for the company and engage in behaviors that enhance both job and organizational performance

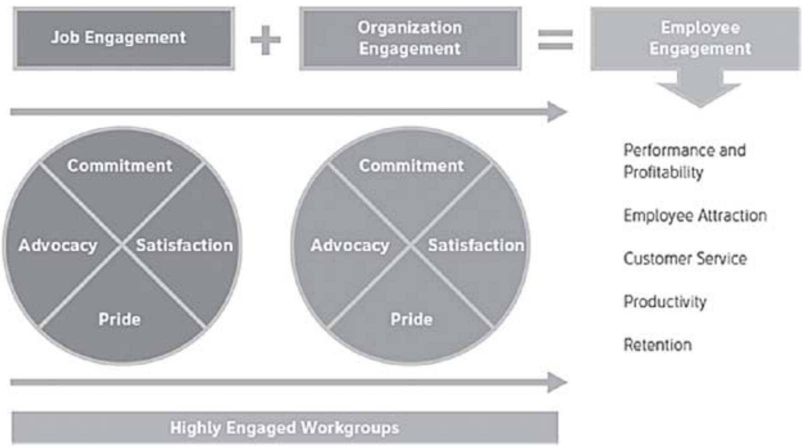

Figure 15. Right Management's Employee Engagement Model

o) Proposed Model of Engagement Developing from the research on burnout, extensive academic work has been carried out by Schaufeli and his colleagues (e.g. Schaufeli & Bakker, 2003)26. This angle focuses more on the employees' feelings and attitudes, and considers the broader picture by viewing engagement as a process rather than simply a state. Both perspectives are loosely rooted in the following hypothesised model: employee engagement – a combination of cognitive and emotional antecedents – generates higher frequency of positive affect such as satisfaction and commitment, which in turn results in efficient application of work. As of yet, the directionality of such a model has not been confirmed empirically but a suggested diagram of how that model might appear is provided in Figure 16. In fact, it is likely that such a model would be circular in nature. While the former perspective seems to place a greater emphasis on how engagement affects productivity, the second framework places a stronger emphasis on employee well-being

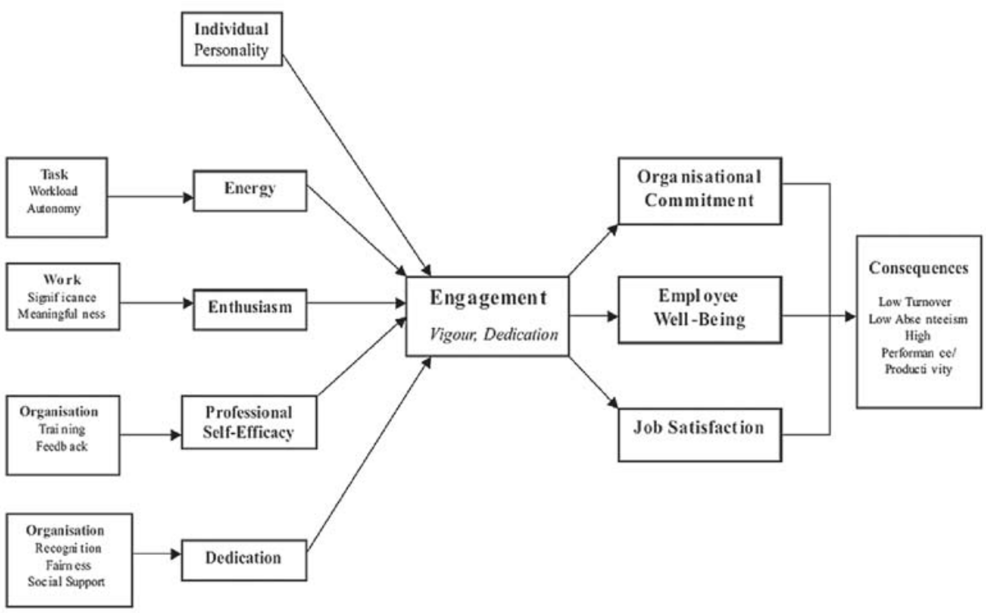

Figure 16: Proposed Model of Engagement

Developing from the research on burnout, extensive academic work has been carried out by Schaufeli and his colleagues (e.g. Schaufeli & Bakker, 2003)26. This angle focuses more on the employees' feelings and attitudes, and considers the broader picture by viewing engagement as a process rather than simply a state. Both perspectives are loosely rooted in the following hypothesised model: employee engagement – a combination of cognitive and emotional antecedents – generates higher frequency of positive affect such as satisfaction and commitment, which in turn results in efficient application of work. As of yet, the directionality of such a model has not been confirmed empirically but a suggested diagram of how that model might appear is provided in Figure 16. In fact, it is likely that such a model would be circular in nature. While the former perspective seems to place a greater emphasis on how engagement affects productivity, the second framework places a stronger emphasis on employee well-being.

p) Linking Employee Engagement to Financial Performance Figure 17 draws on our Linkage Framework to show the strength of the direct and indirect relationships among company programs, employee behavior, customer focus and financial results. While. it's important to recognize that thereare many variables that affect business outcomes, our analysis nonetheless shows a clear relationship between increased engagement, improved retention of talent and better financial performance.

Here's how to understand this picture.

On the extreme left are the 10 workplace attributes that, as we've seen, help drive employee engagement. The stronger these attributes are in the workplace, the stronger the level of employee engagement. As engagement rises, we see two important outcomes: a decline in the likelihood of leaving the company and a stronger orientation around meeting customer needs. Put simply, the more highly engaged employees are, the more likely they are to put customers at the heart of what they do and how they think about their jobs, and the less likely they are to leave their company.

The right side of the picture addresses financial results where, not surprisingly, there's a relationship between customer focus and revenue growth (as well as one between engagement itself and revenue growth). There's also an inverse relationship between engagement and the cost of goods sold (COGS). In other words, we found that the cost of production tends to drop as employees become more engaged in their work.

Rounding out this picture is the relationship between turnover, turnover costs (which can average about 40% of an employee's salary), and sales, general and administrative expense (SG&A). SG&A, in turn, along with COGS and revenue growth, are key mathematical components of operating margin — a significant bottom-line measure of a business's financial health.

Basically, what we're seeing here is the power of discretionary effort on multiple levels. In a service business, for instance, the relationship is readily apparent: An engaged employee focuses on customer service, giving the customer a reason to return to the store or business and buy more goods and services. Such employees build customer loyalty and retention over time. But even in a business where there is little direct contact between employees and customers, engaged employees can still indirectly affect revenue growth; for instance, by supporting other employees who do have direct contact or by pioneering an innovation that boosts sales.

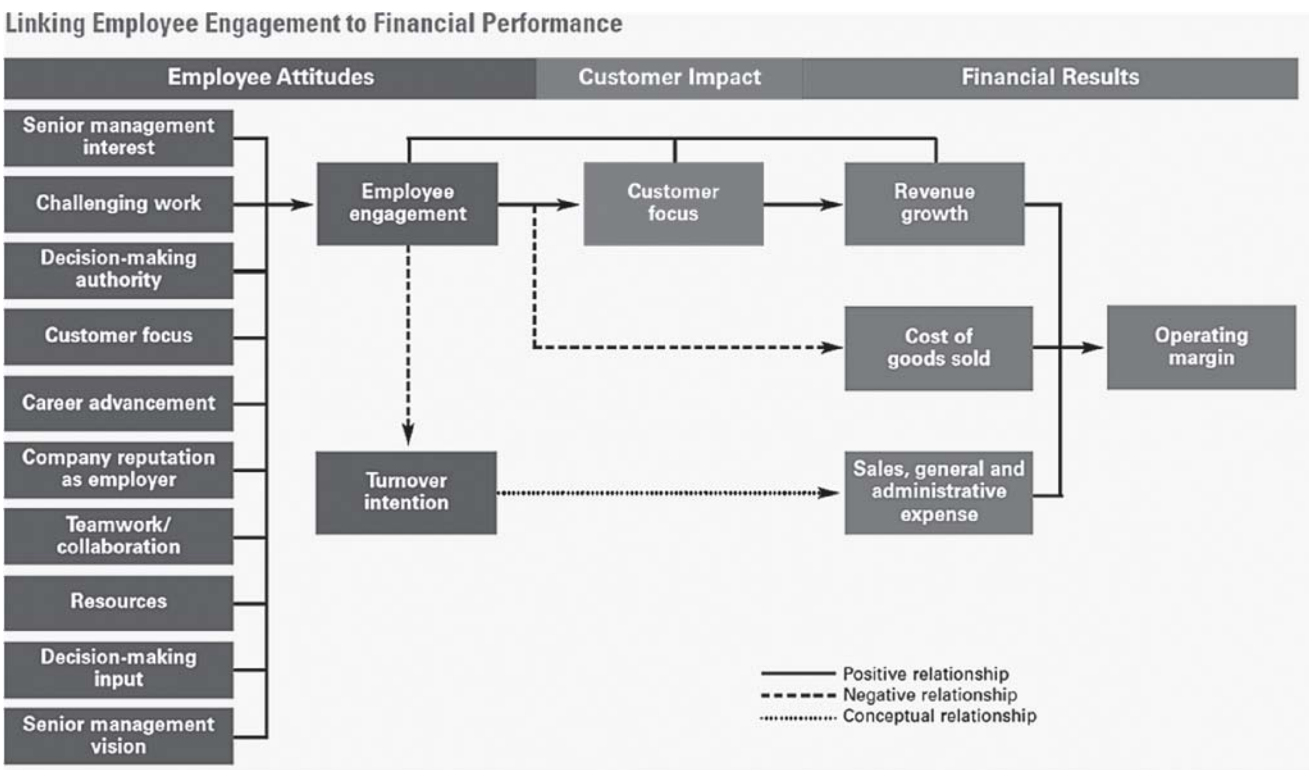

Figure 17: Linking Employee Engagement to Financial Performance Model

q) Factors Leading to Employee Engagement27 Studies have shown that there are some critical factors which lead to Employee engagement. Some of them identified are

Figure 18: Factors Leading Employee Engagement

3. MANAGEMENT AND COMMUNICATION

The importance of good management and effective communication has been highlighted as key vehicles through which employee engagement can be implemented. As Robinson et al (2004) highlight, organisations must work to engage employees and establish a two-way relationship between the employer and employee. Michelman (2004)28 notes that the defining contribution of great managers is that they boost the engagement levels of the people who work for them. Michelman (2004) suggests that they achieve this through concentrating on four core areas of managing people:

- Selection;
- Expectation setting;
- Motivation; and
- Development

Michelman (2004) points out that in leading engagement, great managers will seek the right fit for a person's talent, they work to see that employees are rewarded for their performance and they endeavour to ensure that talent is developed through progressively more challenging and meaningful assignments.

A research report into employee engagement by Melcrum Publishing29 (2005) based on a global survey of over 1,000 multinationals concluded that from an organisation's point of view it is the senior executives that 'set the tone' of engagement in an organisation, whatever the size. There are a number of actions and strategies that senior management can make use of to inspire engagement among employees and motivate them to go the extra mile. The six top drivers of engagement from the senior management perspective were found to be:

- Communicating a clear vision of the future
- Building trust in the organisation
- Involving employees in decision making that will affect them
- Demonstrating commitment to the organisation's values
- Being seen to respond to feedback
- Demonstrating genuine commitment to employee's well being

The same Melcrum Publishing (2005) report also examined the role of line managers in encouraging engagement. In this regard, the survey results imply that 'creating a climate of open communication' is the single most important action for line managers in affecting levels of employee engagement, with 60% of those surveyed claiming it is the most important element.

Regarding the importance of communication, Moorcroft (2006)30 discusses the restructuring that took place at the Royal Bank of Canada (RBC) in 2004. It was noted at that time that there was a need to engage rather than inform employees and thus better align their performance with the organisation's vision and business goals. Formerly, communication strategies had focused on informing employees and creating awareness. However a new strategy was designed by the company in order to engage employees (and thus generate desired behaviours) that would help create outcomes (measurable effects) in support of the organisation's objectives.

The strategy has four key objectives:

- Help employees develop a better understanding of how what they do relates to the organisation's vision, strategies and goals;

- Create a more dynamic and interactive communication environment that involves employees in thinking about and understanding how they can influence business results;
- Ensure employees are getting the information they need to help frame and guide their day-to-day decisions;
- Promote and recognise the desired behaviours and outcomes in communication.
-

2.3 Employee variations The final variable impacting on employee engagement relates to employees themselves. A number of studies have produced quantitative research findings that demonstrate the impact that biographical and job characteristics can have on employee engagement. One of the most in-depth was conducted by the Institute for Employment Studies (IES) (as analysed by Robinson et al 2004) which analysed attitude survey data for 2003 from 14 organisations in the NHS (>10,000 completed questionnaires). The key findings were:

4. BIOGRAPHICAL CHARACTERISTICS

- **Gender** – The difference in engagement scores between men and women was not significant (although note that some surveys (see CIPD 2006c discussed below) find that females are generally more engaged than males
- **Ethnicity** – Minority ethnic employees have higher engagement levels than their White colleagues. Black, Chinese and Asian employees have higher scores than those in Mixed and White groups.
- **Age** – Engagement levels go down slightly as employees get older – until they reach the oldest group, 60 and over.
- **Work-life balance** – Those in their 40s and 50s have the highest levels of workplace stress and are likely to find it difficult to balance work and home life. Robinson et al (2004) therefore suggest that attention to family friendly policies could increase the engagement levels for this group.
- **Caring responsibilities** – Employees with caring responsibilities for children have significantly lower engagement levels than those who have no caring responsibilities.
- **Medical** – Those with a disability/medical condition have lower engagement levels than those who do not have such a condition.

CIPD (2006c)31 in their national survey of 2,000 employees across a wide spectrum of public and private sector employers found broadly similar findings to the NHS survey, although several disparities are noted:

- **Gender** – women were found, in general, to be more engaged than men, but they also tend to be doing different kinds of jobs.
- **Age** – workers aged 55+ are more engaged with their work than younger employees, and they are also happier with their work-life balance, working shorter hours than others. Employees aged under 35 are significantly less engaged with their work than older workers.
- **Disability** – employees with a disability are less engaged due to a range of negative factors including: bullying and harassment, not being listened to, the stress of work, a feeling of less control over their work, and higher levels of anxiety.
- **Managers** – they find their work more important and more meaningful than nonmanagers do. Their responses on communication and involvement are much more positive than those of non-managers, and managers feel that they have more support and recognition and are listened to more than non-managers are.
- **Flexible contracts** –Those on flexible contracts tend to be more emotionally engaged, more satisfied with their work, more likely to speak positively about their organisation and least likely to quit than those not employed on flexible contracts.

However, it is particularly important to point out that demographic variables should not be seen in isolation as predictors of performance or engagement. CIPD (2006c) stresses the following:

"…what we have found is that good management practice and a conducive working environment can lead to high levels of engagement and performance amongst all groups of workers."

CIPD (2006c) also note the following regarding job characteristics:

- **Job group** – The nature of the job makes a big difference to engagement levels. In general, managers and professionals have higher levels of engagement than do their colleagues in supporting roles.
- **Working pattern/hours** – Full-timers are significantly more engaged than part timers, while employees who work days are more engaged than their colleagues on shifts or on a rota.
- **Length of service** – Engagement levels go down as length of service increases – an indication to employers that they need to ensure that longer-serving employees continue to be exposed to new and interesting challenges.

5. FINDINGS AND CONCLUSION

The key points that emerge from an examination of the models of engagement are:

- There is no one-size fits all definitive explanation of what drives engagement. Each of the models and research studies discussed present a range of different factors and place varying importance on each. What can be concluded is that the organisation first and foremost has the power of influence over a range of factors (contractual and extra-contractual) and employees place a varying degree of importance on these.

- Harter, Schmidt and Keyes (2003) propose a model of engagement that is strongly influenced by Maslow's (1970) hierarchy of needs. In the model basic needs at work must be fulfilled before higher needs can be considered and this has implications regarding the antecedents of engagement

- A two-dimensional (2-D) model of affective experience as mapped by the circumplex model (e.g., Lang, Bradley, & Cuthbert, 1998; Larsen & Diener, 1992; Thayer, 1989) explained clearly that in order to facilitate work engagement and to prevent burnout, employers should work to create an organizational context where employees feel enthusiastic, energized, and motivated because their jobs are both "active" and "pleasurable".

- Kahn's model (May et al. 2004) found that meaningfulness, safety, and availability have significant influence on engagement

- Feeling valued and involved is the key to the Robinson et al (2004) model of engagement, although other factors such as training and development, communication and job satisfaction are important in determining the extent to which employees feel valued and hence engaged.

- The Penna (2007) model of engagement noted that pay and benefits were at the foundation of the model but ranked lowest on the extent to which they would retain staff if other factors were lacking. In that model value and meaning at work are at the apex, with leadership and learning and development also cited as important factors in driving engagement from the employee's point of view.

- The RBC model of communication was also highlighted, and it was noted that it succeeded as it strived to engage employees rather than just inform. The organisation realised that the previous model of informing employees, rather than engaging them, was not helping to promote the 'line of sight' from employee actions to the overall objectives and outcomes for the organisation. This model highlights an important element of engagement – that communication is more effective as a two-way process that involves the employee, as opposed to merely presenting them with information.

- Management and communication were highlighted in particular in several models (i.e. Robinson et al (2004) and Penna (2007) as being key organisational drivers of engagement. Here it was found that promoting a clear vision of the future, being seen to respond to feedback and demonstrating a genuine commitment to the employees' well-being are all important actions at an organisational/managerial level.

- Several models that illustrate the overall impact of engagement and the mechanisms through which factors feed into engagement and how in turn engagement affects the overall organisational outcomes were also presented. What Schmidt (2004) points out as the overarching goal of public organisations – advancing the greater public good – can be affected by engagement levels through an overall mechanism that involves various elements from the 'right' workforce through workplace well-being, engagement, organisational performance and finally advancing the public good.

- Finally the CIPD (2006c) model of engagement was presented, which presents an overall picture of the place of engagement within a wider scope of individual factors, aspects of working life, management, attitudes to work and outcomes for the organisation. This demonstrates that engagement should not be considered in isolation, and these other factors should be taken on board when measuring engagement and considering engagement strategies.

- Secondary to the organisational lead in driving engagement are several demographic and job-related factors that highlight variations in engagement. It was noted from several studies that those in their 40s and 50s have the highest levels of workplace stress and are most likely to find it difficult to achieve a work/home life balance. Further, those with caring responsibilities for children are less likely to be engaged. These results tie in with the Robinson et al (2004) model which highlighted family friendly policies as an important organisational driver of engagement.

REFERENCES

1. Corporate Leadership Council. (2004). Driving performance and retention through employee engagement. Washington, DC: Corporate Executive Board.

2. Ibid

3. Chartered Institute of Personnel and Development (CIPD) (2007a) Employee engagement.Available online at http://www.cipd.co.uk/subjects/empreltns/general/empengmt.htm?IsSrchRes=1 [retrieved on 6 March 2007]

4. Harter, J.K., Schmidt, F.L & Keyes, C.L.M. (2003). Well-Being in the workplace and its relationship to business outcomes: A review of the Gallup studies. In C.L.M. Keyes & J.Haidt (Eds.), Flourishing: Positive psychology and the life well-lived (pp. 205-224).Washington, DC: American Psychological Association.

5. Maslow, A. (1970). Motivation and personality.New York: Harper and Row.

6. Lang, P. J., Bradley, M. M., & Cuthbert, B. N. (1998). Emotion, motivation, and anxiety: Brain mechanisms and psychophysiology. Biological Psychiatry, 44, 1248–1263.

7. Larsen, R. J., & Diener, E. (1992). Promises and problems with the circumplex model of emotion. In M. S. Clark (Ed.), Review of personality and social psychology (Vol. 13, pp. 25–59). Newbury Park, CA: Sage.

8. Thayer, R. E. (1989). The origin of everyday moods: Managing energy, tension and stress. NewYork, NY: Oxford University Press.

9. Bakker, A. B., & Oerlemans, W. (in press). Subjective well-being in organizations. In K. Cameron & G. Spreitzer (Eds.), Handbook of positive organizational scholarship. New York, NY: Oxford University Press.

10. Parker, S. K., & Griffin, M. A. (2011). Understanding active psychological states: Embedding engagement in a wider nomological net and closer attention to performance. European Journal of Work and Organizational Psychology, 20(1), 60–67.

11. Robinson, D., Perryman, S. and Hayday, S. (2004) The drivers of employee engagement. Brighton: Institute for Employment Studies.

12. Schmidt, F (2004) Workplace well-being in the public sector – a review of the literature and the road ahead for the Public Service Human Resources Management Agency of Canada. Ottawa: PSHRMA. Available online at http://www.hrma-agrh.gc.ca/hr-rh/wlbpseeoppfps/documents/WorkplaceWell-Being.pdf [retrieved on 6 March 2007]

13. Moorcroft, D Realising RBC's new vision for employee communications, IN Strategic Communication Management Volume 10, Issue 6, October/November 2006. Available online at http://www.melcrum.com/articles/vision_at_RBC.shtml [retrieved on 6 March 2007]

14. Kahn, W.A. 1990. Psychological conditions of personal engagement and disengagement at work. Academy of Management Journal, Vol. 33, Issue 4, pp. 692–724.

15. May, D.R., Gilson, R.L., and Harter, L.M. 2004. The psychological conditions of meaningfulness, safety and availability and the engagement of the human spirit at work. Journal of Occupational and Organizational Psychology, Vol. 77, pp. 11–37.

16. Heintzman, Ralph and Marson, Brian (June/July 2006) People, service and trust: links in the public sector service value chain. Canadian Government Executive. Available online at http://www.hrma-agrh.gc.ca/veo-bve/publications/atricle_e.asp [6 March 2007]

17. Chartered Institute of Personnel and Development (CIPD) (2006c) Working Life: Employee attitudes and engagement 2006 Research Report.

18. Saks, A.M. 2006. Antecedents and consequences of employee engagement. Journal of Managerial Psychology, Vol. 21, Issue 7, pp. 600–619.

19. Heskett, J.L., Jones, T.O., Loveman, G.W., Sasser, Jr., W.E., & Schlesinger, L.A. (1994). Putting the service-profit chain to work. Harvard Business Review, 72(2): 164.

20. Carrig, K. & Wright, P.M. (2006). Building profit through people: making your workforce the strongest link in the value-profit chain. Alexandria, Virginia: Society for Human Resource Management.

21. http://www.digitalopinion.co.uk/employeeengagement-our_insight-how.html

22. Penna (2006). Meaning at Work Research Report. Available online fro http://www.epenna.com/newsopinion/research.aspx [retrieved on 6 March 2007]

23. Bakker, A.B., Van Emmerik, IJ.H., Demerouti, E., & Geurts, S. (2007). Recovery turns job demands into challenges: A diary study on work engagement and performance. Working paper, Erasmus University Rotterdam.

24. WWW.DDIWORLD.COM

25. www.right.com

26. Schaufeli, W.B. & Bakker, A.B. (2003). Utrecht Work Engagement Scale: Preliminary manual (Version 1). Unpublished manuscript, Occupational Health Psychology Unit, Utrecht University, The Netherlands.

27. www.siescoms.edu.

28. Michelman, Paul (2004) Methodology – how great managers manage people. Harvard Management Update. 1 August 2004 Boston: Harvard Business School Publishing.

29. Melcrum Publishing (2005) Employee Engagement: How to build a high- performance workforce. An independent Melcrum Research Report Executive Summary.

30. Moorcroft, D Realising RBC's new vision for employee communications,IN Strategic Communication Management Volume 10, Issue 6, October/November 2006. Available online at http://www.melcrum.com/articles/vision_at_RBC.shtml [retrieved on 6 March 2007]

31. Chartered Institute of Personnel and Development (CIPD) (2006c) Working Life: Employee attitudes and engagement 2006 Research Report.

INTERNATIONAL JOURNAL OF ENGINEERING SCIENCES AND MANAGEMENT

International Journal of Engineering Sciences and Management (IJESM)
is a bi-annual journal of Dronacharya College of Engineering, Greater Noida, UP, India.

SCOPE OF THE JOURNAL

To publish full-length research papers in any one or more of the following disciplines:
Computer Science & Engineering, Information Technology, Electrical, Electronics & Communication Engineering, Mechanical Engineering, Civil Engineering, Physics, Mathematics, Economics, and Management.

PURPOSE OF THE JOURNAL

To keep the academic community abreast of the research and technical scenario in the stated disciplines in the world.

CHERISHED AIM OF THE JOURNAL

To excite and ignite the young minds and to motivate them for involving themselves in research and development activities. This will empower our manpower in the context of fast changing technologies across the globe.

GUIDELINES FOR AUTHORS

SUBMISSION OF MANUSCRIPTS: Soft copy of the manuscript for consideration of publication should be sent (as MS Word Windows 2007 attachment) by Email to the Executive Editor at advisor.r&d@gnoida.dronacharya.info.

There are “no page charges” for the publication of papers in IJESM.

All papers, received for publication and complying with the below-mentioned format will be sent for review to at least two referees. In accepting the paper for publication, the Editors and reviewers will give special weight to readability and interest value for a wide readership besides the originality and the high-standard of its content.

The Executive Editor's decision is final in case of non-unanimity of opinion of referees. Under normal circumstances, the contributors of papers will be informed about the status of their papers by the Executive Editor within eight weeks of their submission.

PREPARATION OF MANUSCRIPTS

- Manuscript: Manuscript should be in English, the preferred spelling being that of the Concise Oxford Dictionary. It should be in 'Times New Roman', single-spaced and typed on 8.5" x 11" or A4-size paper with margins of 1" (25 mm) on each side. Manuscript should be typed in single column only (and not in double or triple columns).
- Title of Paper: Font size 16, ALL CAPITALS, bold, centered, and not underlined. The title must be 12.5 mm below the top of the page (in addition to the standard 25 mm margin). The Title should adequately describe the content of the paper.
- Full names of all Authors, with * as superscript with corresponding author's name and his/her Email ID (Font size 12, centered). A blank line should be left between the title and the author's name(s).
- Full postal address along with affiliations (Font size 10, centered). Contact number may preferably be given along with this.
- Abstract: All papers must have a non-mathematical abstract of not more than 200 words. The abstract should indicate the general scope of the paper, the important findings and the conclusions drawn. The abstract should include only text. It should be specific about the methodologies used and the conclusion drawn of the work reported. Please avoid the use of abbreviations and references. (Font size 9, single-space, justified).
- Keywords: Include up to six keywords that describe your paper for indexing and for web searches. The more discriminating your keywords are, the greater is the likelihood that your article will be found and cited. (Font size 9, italics, centered).
- Short Title: The manuscript should also include a short title of maximum fifty characters (to be used in the subsequent pages of the manuscript). The short title should provide a broad indication of the content of the paper. (Font size 9, left-justified).
- Text: (Font size 10, Justified). The paper must be divided into sections starting preferably with "Introduction" and ending with "Conclusion". The main sections should be numbered 1, 2, 3 etc and subsections 2.1, 2.2 etc.Main headings should be typed in capitals, subheadings in lower case. Both types of heading should be underlined and left-justified. Footnotes should be avoided. Equations should be typewritten and with the number placed in parentheses at the right margin. Reference to the equation should use the form 'Eq. (3)'. Use extra line spacing between equations, illustrations, figures and tables. The use of SI units is strongly recommended.
- Tables and Figures: Tables and Figures should be integrated with the text (and not sent separately at the end of the manuscript) and numbered consecutively in the order in which reference is made to them in the text of the paper. All captions must be centrally located above a Table and below a Figure. All tables must be numbered consecutively in Arabic numerals (not Roman) (e.g., Table 3) in the order of appearance in the text. Tables & Figures should be reproduced in the exact format and at the exact place as desired to appear in the journal.
- Conclusion: A conclusion section must be included and should indicate clearly the advantages, limitations and possible applications of the paper. Authors may also discuss about the scope of future work.
- Acknowledgements: An acknowledgement section may be presented after the conclusion.
- References: References should be placed at the end of the text, should be numbered consecutively in order of their citation in the text and be indicated by superscripts. Examples of different citations as References are given below:

(i) In case of referring to an Article in a Journal
Kuebel, D.; Lahiri, M. & Wolf, E. *An Inverse Problem in the Theory of Stochastic Electromagnetic Beams*, Opt. Commn., 282, 2009, p.141.

(ii) In case of referring to a Book/Monograph
Rao, C.N.R. & Raveau, B. (Eds.). *Transition Metal Oxides*, Wiley-VCH, 2nd Edition, 1998, Ch. 2.

(iii) In case of referring to a Conference Paper
Ctvrtnickova, T.; Mateo, M; Yanez, A. & Nicolas, G. *Characterization of Coal Fly Ash Components by Laser-Induced Breakdown Spectroscopy*. Presented at the Fifth International Conf. on Laser-Induced Breakdown Spectroscopy, Berlin, Adlershof, Germany. Sep 22-26, 2008, CP-15, p. 67-68.

(iv) In case of referring to a Report
Marine, R.E. & Iliff, K.W. *Application of Parameter Estimation to Aircraft Stability and Control.* NASA, USA, 1986, Report No. NASA-RP-1168.

UNDERTAKING

Authors must include, in the initiating Email that their paper has not been published/ presented or submitted to or accepted for publication/presentation in any form in any other journal/conference and the work submitted by them is their own and original. The same undertaking should also be attached along with the manuscript. This ethical policy of the Journal will be strictly adhered to.

A GURUKUL COMBINING TRADITION AND MODERNITY

DCE, A flagship Institution reputed for its disciplined environment
Where faculty development, career-consciousness & merits are a tradition
Where academia, placement and industry face are in sync.
Where infra-structural growth is an offshoot of the institution growth
Where aspirants can dare to dream to ascend to the highest aptitude of success

Approved by
All India Council for Technical Education, New Delhi

Affiliated To:
Mahamaya Technical University, Noida

Corporate Office:
76P, Part-III, Sector-5, Gurgaon, 122001, Haryana (India)
Phone: 0124-2251602, 2253144, Email: info@dronacharya.info

www.dronacharya.info

design: www.studio1-india.com